GEOLOGY OF MESOPROTEROZOIC ANORTHOSITE INTRUSIONS IN THE VICINITY OF NAIN, LABRADOR

RONALD JAAP VOORDOUW

Geology of Mesoproterozoic Anorthosite Intrusions in the vicinity of Nain, Labrador

By

Ronald Jaap Voordouw

A thesis submitted to the School of Graduate Studies
in partial fulfillment of the requirements for the
degree of Doctor of Philosophy

Department of Earth Sciences
Memorial University of Newfoundland
May 2006

St John's Newfoundland

To my time in St John's, Newfoundland

"I was going to…become again that most limited of all specialists, the "well-rounded man"."

from The Great Gatsby by F.Scott Fitzgerald

Abstract

This thesis investigates aspects of the 'anorthosite problem' through geological mapping and petrographic study of Proterozoic anorthositic rocks in the Nain batholith (NB), Labrador. The aspects of this problem to be investigated include the tectono-magmatic setting of this batholith, and the controls on ascent, emplacement and crystallization of the anorthositic rocks. Secondary emphasis is placed on the mineral and whole rock chemical evolution of these anorthositic rocks over time. Brief descriptions of Mesoproterozoic gabbronoritic, Fe-rich gabbroic, Fe-rich dioritic rocks and granitoid rocks that are spatially associated with anorthositic rocks are also presented, as well as descriptions of Paleoproterozoic and Archean country rock.

The main findings of the thesis are based on 1:20 000 scale geological mapping over a 400 km^2 area that was previously covered only at reconnaissance scale. This area comprises four belts of Paleoproterozoic and/or Archean country rock and three Mesoproterozoic 'centered intrusive complexes'. These intrusive complexes are here referred to as 'centered' because each consists of a 'core' that is enveloped by a 'margin'. The core is sub-horizontally oriented and consists of anorthositic rocks, whereas the margin is sub-vertically oriented and consists of anorthositic, gabbronoritic +/- monzonitic, troctolitic and Fe-rich gabbroic rocks. The centered intrusive complexes in the study area are referred to as Tikkoatokak, Sophie and Kikkertavak.

The four belts of country rock are here referred to as the Anaktalik Brook, Kangilialuk Lake, Nain Hill and Kauk Harbor country rock belts. Each of these belts contains gneiss and granulite that is of Paleoproterozoic +/- Archean age and structures

that strike parallel to Paleoproterozoic structures of the Torngat orogen. Compositional layering in the Nain Hill country rock belt shows an arcuate strike that is interpreted as a Paleoproterozoic structure that was rotated into a Mesoproterozoic east-west shear zone. This Mesoproterozoic shear zone was active during emplacement of the Nain batholith. This interpretation contrasts with previous work that suggested the arcuate strike was formed by a pre-Mesoproterozoic episode of folding or by the intrusion of Mesoproterozoic anorthositic rocks.

The margins of all intrusive complexes in the study area were deformed in sub-vertical, north-south striking, shear zones and/or sub-vertical, east-west striking, shear zones. Field relations and compiled U-Pb ages indicate that this deformation was synchronous with emplacement of the Nain batholith (1365-1270 Ma). Map compilation is used to show that these shear zones continue north of the study area. Field relations of strongly and weakly deformed plutonic rocks in these shear zones indicate that Mesoproterozoic deformation on individual shear zones was episodic, which is consistent with new and compiled U-Pb ages that show north-south deformation occurred between 1351 and 1313 Ma and east-west deformation occurred between 1340 and 1311 Ma.

Mesoproterozoic plutonic rocks in the study area were deformed in Mesoproterozoic north-south and east-west shear zones. The north-south striking shear zones lie adjacent to and strike parallel to Paleoproterozoic structures in the country rock, and it is suggested that the shear zones developed on re-activated Paleoproterozoic structures. The east-west striking shear zones strike parallel to the orientation of Mesoproterozoic faults in the Gardar Province of western Greenland, which comprised

part of Mesoproterozoic Laurentia with the rocks in the study area. In addition to previous work on the tectono-magmatic setting of the Nain batholith, the findings indicate that emplacement of this batholith was contemporaneous with: (a) development of north-south shear zones, (b) development of east-west shear zones, (c) lithospheric thinning, graben development, and (d) back-arc extension. These findings are in contrasts to a mantle plume-related setting that has been proposed for petrogenesis of the Nain batholith.

The margins of Mesoproterozoic intrusive complexes in the study area are: (a) composite, (b) bound by shear zones, (c) elongate parallel to shear zones, (d) are structurally controlled at shear zone intersections, and (e) contain xenoliths of strongly deformed plutonic rocks. These features are all characteristic of shear zone assisted melt transport and emplacement. These findings contrast with the widely held belief that the emplacement of anorthositic magmas is diapiric, and suggests a liquid-state rheology for anorthositic magmas during ascent and emplacement.

The Tikkoatokak centered intrusive complex contains the oldest plutonic rocks in the study area. This intrusion shows a sub-rectangular and bell-jar form that suggests emplacement into a ductile crust that was controlled by sub-vertical and north-south striking shear zones. The northwestern part of the Kikkertavak centered intrusive complex contains the youngest plutonic rocks in the study area. This intrusion shows a sub-rectangular and convex down form that suggests emplacement into a dilating brittle crust that was controlled by steeply dipping, east-west striking, shear zones. The Sophie centered intrusive complex is intermediate in age with respect to the Tikkoatokak and

NW Kikkertavak centered intrusive complexes and contains plutonic rocks that were deformed in both north-south and east-west shear zones. These findings suggest that over the time span that covers emplacement of the Tikkoatokak (>1333 Ma), Sophie and NW Kikkertavak (between 1318 and 1311 Ma) centered intrusive complexes, the rheology of the crust changed from ductile to brittle and the structural controls on emplacement changed from north-south to east-west shear zones. These findings contrast with previous studies that suggested crustal uplift occurred in the waning stages (<1290 Ma) of emplacement of the Nain batholith.

Anorthositic rocks in the study area show granular and/or poikilitic textures and microstructures that indicate high-T deformation and/or recrystallization. In addition, anorthositic rocks show relatively high variation in whole rock Mg/(Mg+Fe) in comparison to the range in normative plagioclase compositions, and are cut by ferrodiorite dikes that show sharp to gradational contacts. These characteristics are used to suggest that the crystallization of anorthositic magmas involved the formation of crystal frameworks and the compaction of these frameworks. Compaction may have been related to tectonic activity on the same shear zones that controlled the ascent and emplacement of magmas into intrusive complexes. It is suggested that this compaction also formed mottled rocks, primary layering and foliated rocks. In addition, compaction may also have produced planar aggregates of pyroxene crystals, calcic rims on plagioclase crystals and elevated wt% Al_2O_3 in the orthopyroxenes of anorthositic rocks. These findings indicate that the textures and structures in anorthositic rocks were produced in magmas that exhibited solid-state rheology and contrasts with previous work

that suggests liquid-state processes (convection, crystal sedimentation) formed textures and structures during the crystallization of anorthositic magmas.

Anorthositic rocks in the Tikkoatokak centered intrusive complex contain high abundances of Na-rich plagioclase, wt% K_2O, ppm Ba and ppm Sr in comparison to anorthositic rocks in the Sophie and Kikkertavak centered intrusive complexes. In contrast, the Sophie and Kikkertavak centered intrusive complexes contain high wt% CaO and Mg/(Fe+Mg). All anorthositic and gabbronoritic rocks in the Tikkoatokak centered intrusion lack olivine, whereas minor abundances of anorthositic and/or gabbronoritic rocks in the Sophie and NW Kikkertavak centered intrusive complexes contain olivine. These findings indicate that relatively Na-, K-, Ba- and Sr-rich anorthositic rocks were emplaced prior to Ca-rich, high Mg/(Fe+Mg) +/- olivine-bearing anorthositic rocks. These characteristics are used to suggest that anorthositic rocks with a greater crustal component were emplaced prior to anorthositic rocks with a lower crustal component.

Mineral and whole rock chemistry of anorthositic rocks from this study were compared to previous mineral chemistry, whole rock chemistry and geochronology studies. The mineral and whole rock chemistry characteristics of NB noritic anorthosite and NB troctolitic anorthosite are summarized, and follow a sub-division presented by Xue and Morse (1993). The result of this compilation is used to divide emplacement of the Nain batholith into four episodes. Episode 1 (1365 – 1330 Ma) involved the emplacement of NB noritic anorthosite and episode 2 (1330 – 1310 Ma) involved the emplacement of NB troctolitic anorthosite +/- NB noritic anorthosite. Episode 3 (1310 –

1290) involved the emplacement of troctolitic rocks in the northeastern part of the Nain batholith and emplacement of anorthositic and granitic rocks in the southern part of the Nain batholith. Episode 4 (1290 – 1270 Ma) involved the emplacement of peralkaline volcanic rocks and basaltic dikes.

This study shows that anorthositic rocks in a Proterozoic batholith were generated and emplaced during a localized period of tectonic activity. This activity was accommodated on sub-vertically oriented and north-south, or east-west, striking shear zones, which also controlled the transport and emplacement of the magmas. The magmas that formed anorthosite were likely 'leucogabbroic' (65-90% plagioclase, 10-35% pyroxene + olivine + Fe-Ti oxide) in composition, and the crystallization of anorthosite from such magmas involved compaction and the removal of interstitial liquid. These findings suggest a positive correlation between tectonic activity and the petrogenesis of Proterozoic batholiths with anorthositic rocks, and it is hoped that this study will inspire further research of this correlation.

Acknowledgements

The Memorial University of Newfoundland (MUN), the Voisey's Bay Nickel Company (VBNC), and my supervisor John Myers made this study possible. Many thanks to the faculty and staff of the MUN Earth Sciences Department, especially my committee members Aphrodite Indares and Paul Sylvester, and the head of department John Hanchar. The students in the MUN Labrador Research Group; Owen Gaskill, Tanya Tettelaar, Don Wright, Marianne Mader, Cory Furlong and Clare Goddard; are thanked for their camaraderie. The VBNC is thanked for providing essential logistical support in the field. I would especially like to thank VBNC's Dawn Evans-Lamswood, Dan Lee and Robert Wheeler for sharing their expertise. Lastly, I would very much like to thank John Myers for acting as my supervisor, and for teaching me much about geology.

My examining committee; Carol Frost, Toby Rivers and Bob Wiebe; is thanked for their helpful comments. Thanks to Warren Brown, Johan Voordouw and Cory Furlong for their generous help in the field. Many thanks for help with the analytical work go to Marc Poujol, Pam King, Maggie Piranian and Mike Schaeffer. Bruce Ryan is thanked for writing an extensive critique of this thesis.

Many thanks to my family for bringing me home, and for keeping me home away from home. My friends are thanked for the same reasons.

All research was funded by NSERC and VBNC through a CRD project grant (CRDPJ 233669-99) to John Myers. Other funding was provided by an NSERC post-graduate fellowship, the Estate of Alfred K. Snelgrove and the School of Graduate Studies.

Table of contents

List of Figures

List of tables

List of abbreviations (mostly from Kretz, 1983)

ab:	albite
aggr:	aggregate
alt:	altered
an:	anorthite
anor:	anorthosite
ap:	apatite
bt:	biotite
cpx:	clinopyroxene
crn:	corundum
defm:	deformed
di:	diopside
dio:	diorite
en:	enstatite
ex:	exsolution
fa:	fayalite
Fe-di:	ferrodiorite
Fe-gb:	ferrogabbro
fo:	forsterite
fs:	ferrosilite
gb:	gabbro
gn:	gabbronorite

gran:	granite
hbl:	hornblende
hy:	hypersthene
ilm:	ilmenite
lgn:	leucogabbronorite
ln:	leuconorite
ltr:	leucotroctolite
mgn:	melagabbronorite
ne:	nepheline
ol:	olivine
or:	orthoclase
opx:	orthopyroxene
ox:	Fe-Ti oxide
pl:	plagioclase
px:	pyroxene
qtz:	quartz
tr:	troctolite
wo:	wollastonite

Chapter 1: Proterozoic anorthositic rocks

This thesis investigates aspects of the 'anorthosite problem' through geological mapping and petrographic study of Proterozoic anorthositic rocks in the vicinity of Nain, Labrador. The so-called anorthosite problem refers to the many questions that surround the origins, transport, emplacement and crystallization of anorthositic magmas. This study will show that the emplacement of anorthositic magmas in the Nain area was associated in space and time with movement and deformation in an orthogonal set of crustal-scale structures. This study suggests that these structures controlled the transport and emplacement of anorthositic magmas, and that these structures also influenced textural and structural development.

The study area is located near Nain, Labrador, which is world-renowned for its high quality and high abundance of exposed Proterozoic anorthositic rock. The main obstacle to investigating rocks in this area is their remote location. About 6 years before the start of this project, however, a large Ni-Cu-Co deposit was found in troctolitic rocks about 40 km south of Nain. The ensuing exploration boom led to the granting of research funds for a regional investigation of the intrusive rocks that surround Nain, and provided project members such as myself with unparalleled accessibility into a traditionally inaccessible area. This unique opportunity is reflected in the strong emphasis on fieldwork in this thesis.

The bulk of the world's anorthosite volume resides in Proterozoic batholiths that were emplaced into continental crust. The anorthosites in these batholiths are referred to as Proterozoic massif anorthosite (see Ashwal, 1993, p. 82), and are here referred to as

'Proterozoic anorthosite'. This chapter reviews: (a) the petrogenesis and physical properties of the magmas that formed these rocks, (b) the intrusive forms, textures and structures of anorthositic rocks, and (c) the origins of recrystallized anorthositic rocks in regionally undeformed intrusions.

1.1 General occurrence

Proterozoic anorthositic rocks consist mostly of intermediate plagioclase ($An_{50+/-10}$) (Ashwal, 1993, p. 83), orthopyroxene (Barton, 1996) and olivine (Scoates and Mitchell., 2000). Clinopyroxene is present in lesser abundances relative to orthopyroxene and olivine (see Ashwal, 1993). These rocks crystallized from magmas that formed large batholiths in the middle to upper continental crust (Ashwal, 1993, p. 100). These batholiths also contain large abundances of granitic and monzonitic rocks, and lesser abundances of troctolitic, gabbronoritic, Fe-rich gabbroic and/or Fe-rich dioritic rocks (see Wiebe, 1992, p. 215; Ashwal, 1993, p. 162; Emslie et al., 1994; Hall, 1996, p. 487), as well as broadly contemporaneous high-Fe and/or -Al basaltic rocks (see Wiebe, 1985b; Olson and Morse, 1990; Scoates and Mitchell, 2000). Mesoproterozoic plutonic rocks in the study area consist mostly of anorthositic and gabbronoritic rocks, and minor abundances of Fe-rich gabbroic, Fe-rich dioritic and monzonitic rocks.

1.2 Petrogenesis and physical properties of anorthositic magmas

It is generally accepted that the main physical components of the magmas that formed anorthositic rocks were (a) Fe-rich basaltic liquid and (b) plagioclase crystals.

Furthermore, it is generally accepted that this mixture of liquid and crystals was formed by the accumulation of plagioclase crystals into a basaltic liquid that was undergoing fractional crystallization at the boundary between the mantle and the crust (see Buddington, 1969; Phinney, 1969; Emslie, 1978; Wiebe, 1985a; 1990a; Ashwal, 1993,p. 209; Emslie et al. 1994; Mitchell et al., 1995; 1996; Bhattacharya et al., 1998; Dempster et al., 1999). An alternative is that the anorthositic magmas were derived through partial melting of the lower crust (see Longhi et al., 1999). The anhydrous mineralogy of Proterozoic anorthositic rocks suggests that H_2O contents were low (Ashwal, 1993, p. 203; Hall, 1996, p. 501), although there is some H_2O-enrichment of residual melts (Wiebe, 1992, p. 238; Ashwal, 1993, p. 134). The plagioclase crystals may have remained in the magma throughout the transport, emplacement and crystallization history of the rock (see Buddington, 1969; Ashwal, 1993, p. 210; Mitchell et al., 1996; Bhatthacharya et al., 1998; Dempster et al., 1999), or they may have been partially resorbed at the instant of ascent (see Wiebe (1990a).

The rheology of magma depends partly on the viscosity (Spera, 2000). Magma viscosity increases with solid content (Fig. 1.1) as crystals impinge on each other to form crystal frameworks. These frameworks promote a change from liquid- to solid-state rheology (see Marsh, 1981; Philpotts and Carroll, 1996; Takeda and Mosaki, 2003). Studies related to crystal frameworks in magma have suggested a change from liquid- to solid-state occurs at ~35% crystals (Philpotts and Carroll, 1996), ~55% crystals (Marsh, 1981; Vigneresse et al., 1996) and at ~65-70% crystals under a shear rate of 10^{-5}/s (van der Molen and Paterson 1979 in Longhi et al., 1993). All of these studies suggest that

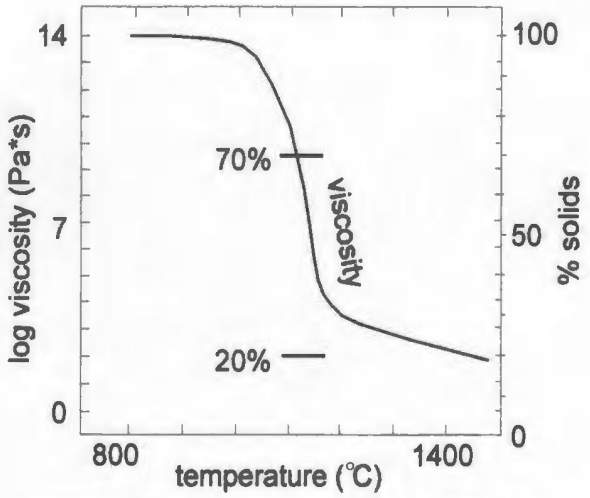

Figure 1.1: Apparent viscosity of magma as a function of temperature and solid content (from Leitch, 2003). Lines on the graph indicate solid contents of 20% and 70%.

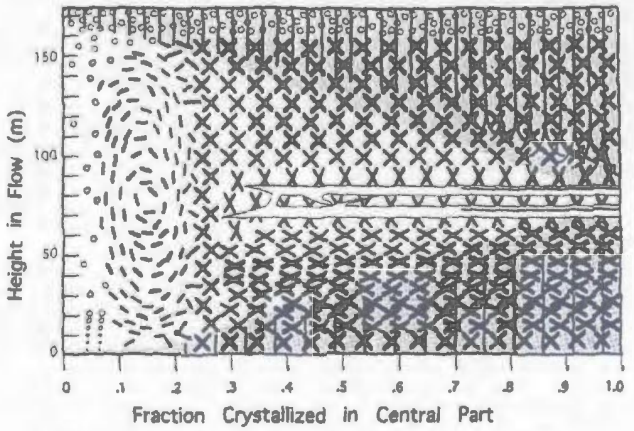

Figure 1.2: Time-elapsed cross-section for the crystallization of a flood basalt. Magmatic convection occurs only below 0.2 fraction crystallized. Rigid crystal frameworks are formed by 0.35 fraction crystallized, although magma convection was probably inhibited prior to that (from Philpotts et al., 1996).

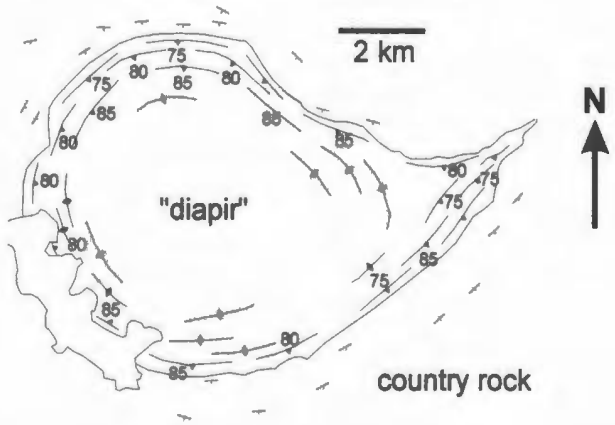

Figure 1.3: Example of a pluton that may be interpreted as diapiric following Hall (1996, p. 85). The pluton is domical in form and shows intrusive contacts that strike parallel to layering in country rock (figure from Hall, 1996, p. 85).

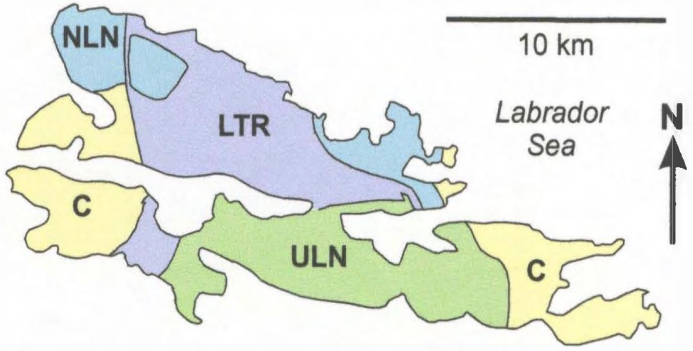

Figure 1.4: Geological map of anorthositic (LTR; lower leucotroctolite, ULN; upper leuconorite, NLN; northern leuconorite) and country rocks (C) on Paul Island, Labrador. Anorthositic rocks are interpreted to have formed by the incremental emplacement of hyper-feldspathic magma pulses (from Wiebe, 1990a).

there exists a critical point at which the rheology of magma changes from liquid- to solid-state. In contrast, a study by Takeda and Mosaki (2003) found that the viscosity of granitic rock is reduced rapidly and continuously with melt fraction. Takeda and Mosaki (2003) suggested that liquid- and solid-state rheology are end-members at 0% and 100% solids, respectively, and that any magma with an intermediate solid content exhibits an intermediate rheology.

Previous studies have suggested that the plagioclase crystal content of anorthositic magmas ranged up to 20% (Wiebe, 1990a), 40% (Buddington, 1969) and 65 – 70% (Longhi et al., 1993). Magmas with 20 – 70% crystals will show rheology that is transitional between liquid- and solid-state behaviors (see van der Molen and Paterson, 1979; Marsh, 1981; Philpotts and Carroll, 1996; Vigneresse et al., 1996). Philpotts and Carroll (1996) suggested that frameworks of crystals inhibit the ability of magma to convect and promote stagnant crystallization (Fig. 1.2). Similarly, anorthositic magmas that consist of fractionated basaltic liquid and 20 – 70% plagioclase crystals would have shown a rheology that is transitional between liquid- and solid-state behaviors. In this study, field mapping shows that the form of anorthositic intrusions is compatible with liquid-state rheology during ascent and emplacement, whereas the textures and structures of anorthositic rocks are compatible with more solid-state rheology during crystallization.

1.3 Ascent and emplacement of anorthositic magmas

The rheology of magma affects ascent and emplacement mechanisms. These mechanisms may be investigated through field-based studies of intrusive forms. The

various forms of Proterozoic anorthositic intrusions have been ascribed to emplacement mechanisms and/or externally imparted tectonic stress (see Wiebe, 1992, p. 217; Ashwal, 1993, p. 101). A classification scheme by Wiebe (1992, p. 225) describes three types of forms: diapir, layered intrusion and massive bodies. Proterozoic anorthositic dikes have also been found (see Wiebe, 1979; 1990a).

Diapirs have been invoked as a possible means by which anorthositic magmas were transported and emplaced (see Woussen et al., 1981; Duchesne, 1984; Scoates, 1990; Wiebe, 1990a; 1992, p. 228; Mitchell et al., 1995; 1996; Bhattacharya et al., 1998; Barnichon et al., 1999; Dempster et al., 1999; Mukherjee et al., 1999). The type-example of a diapiric intrusive form comprises a sub-spherical and domical core that is enveloped by a layered and/or foliated margin (Fig. 1.3). This margin strikes parallel to layering in the country rock. Cruden (1990) suggested that the internal circulation of magma during diapiric ascent leads to strong, sub-vertical, penetrative foliation at the margins. In addition, Barnichon et al. (1999) used finite element modeling to show that sub-horizontal stresses in the margin of an anorthositic intrusion developed in response to extensional stresses at the tip of an ascending diapir. These studies suggest that sub-vertical and sub-horizontal foliations may be integrated with diapiric ascent models. There is one pluton in the study area (Lister pluton) that exhibits a form similar to the diapir form of Wiebe (1992, p. 228), although a section in chapter 8 of this thesis will suggest that it was unlikely the Lister pluton was emplaced as a diapir.

Layered anorthositic intrusions show a layered interior and gently dipping and/or funnel-shaped floors (Wiebe, 1990a; 1992, p. 230). The ascent and emplacement of some

of these intrusions is inferred to have occurred in pulses (Fig. 1.4) (Berg, 1980; Wiebe, 1990a; 1992, p. 231) and/or involved magmas that showed liquid-state rheology (Longhi et al., 1993). Like massive intrusions, the margins of these intrusions are also relatively fine-grained and mafic in composition as compared to the bulk of the intrusion (Wiebe, 1992, p. 230). The layered anorthositic intrusions as described by Wiebe (1992; which are mostly leucotroctolitic in composition) are not present in the study area.

Massive anorthositic bodies typically lack the magmatic structures of layered bodies the and strongly deformed margins of diapiric bodies (Wiebe, 1992, p. 232). Wiebe (1992, p. 232) suggested that in some cases, these massive anorthositic rocks represent stagnant accumulations of plagioclase near the roofs of magma chambers that produced layered anorthositic rocks on the floor. The margins of some massive anorthositic intrusions are fine-grained and comprise a wide range of anorthositic, massive mafic and layered mafic rocks (Wiebe, 1992, p. 232). Most of the anorthositic rocks in the study area are similar to the massive bodies described by Wiebe (1992). Fine-grained and weakly to strongly deformed mafic rocks were found along the margins of these massive intrusions and, in the following sections, are used to propose an emplacement model that includes shear-zone assisted melt transport and emplacement.

Anorthositic dikes are known from several Proterozoic anorthositic-granitic batholiths (Wiebe, 1979; 1990a; Fram and Longhi, 1992; Ashwal, 1993, p. 112). The emplacement of such dikes suggests that anorthositic magmas behaved as rheological liquids. Royse and Park (2000) used a density contrast of 0.14 g/cm^3, magma viscosity of 10^6 pa*s and critical dike width of 2 – 18 m to calculate an ascent rate of 0.09 – 7.56 cm/s

for fracture-controlled flow of anorthositic magmas. This liquid-state ascent of anorthositic magmas is 6 – 9 order of magnitudes faster than diapiric ascent (Royse and Park, 2000). A conclusion of the present study is that Mesoproterozoic centered intrusive complexes are bound by shear zones of broadly similar age, which is compatible with a liquid-state rheology for magmas during ascent and emplacement.

1.4 Crystallization of anorthositic magmas

The rheology of anorthositic magmas during crystallization may be investigated through observations of primary textures and structures. The crystallization of most anorthositic magmas resulted in massive cumulate rocks and lesser abundances of layered and foliated cumulate rocks (Ashwal, 1993, p. 108). This section summarizes the types and possible origins of textures and structures in Proterozoic anorthositic rocks. In the study area, anorthositic rocks are massive (i.e. lack structures), layered or foliated.

Massive anorthositic rocks are coarse- to very coarse-grained and show textures that are often described as adcumulate (Isachsen and Moxham, 1969; Morse, 1969b; Wiebe, 1975; Emslie, 1978; Ranson, 1981; Ashwal, 1993, p. 115; Martignole et al., 1993; Xue and Morse, 1993; Hall, 1996, p. 490), clotted or oikocrystic (Ryan, 2000a; 2000b; 2001a), sub-ophitic (Ryan, 1997; 2000b), mottled (Emslie in Berg et al., 1994, p. 55), seriate (Ryan, 2001a), diabasic (Wheeler, 1942), saccharoidal (Wheeler, 1942), pegmatoidal (Wheeler, 1942; Ryan, 2000a; 2000b; 2001a) and granular aplitic (Ryan, 2000b). Wiebe (1992, p. 235) suggested that the overall homogeneity of some anorthositic rocks is "consistent with the crystallization of a stagnant mush". Studies by

Morse (1972a) and Ranson (1981) found a limited range of plagioclase mineral chemistry in anorthositic rocks and attributed this to adcumulus growth. The development of adcumulate texture, following Wager et al. (1960), involves the isothermal growth of cumulus crystals at the interface between a crystal pile and a liquid. The terms clotted, oikocrystic, sub-ophitic and mottled describe the distribution of poikilitic and sub-poikilitic minerals (pyroxene, Fe-Ti oxide) among larger cumulus crystals of plagioclase. The terms saccharoidal and granular aplitic suggest granular textures, whereas pegmatoidal refers to the extremely large grain size of some anorthositic rocks. In this study, the terms granular and poikilitic are used describe the textures of anorthositic rocks.

Primary layering is found in most anorthositic intrusions (Emslie, 1980; Wiebe, 1990a; Wiebe, 1992, p. 223; Ashwal, 1993, p. 108; Hall, 1996, p. 498; Scoates, 2000), although it is of minor abundance in comparison to massive rocks. The development of layering has been linked to gravitational settling or floor accumulation of plagioclase (Berg, 1972; 1973; Morse, 1972b; Ranson, 1975; 1981), flotation or roof accumulation of plagioclase (Morse, 1969b; 1972b; Davies, 1973a), downward flow of dense plagioclase crystal-liquid packages (Morse, 1972b; congelation cumulates in Berg, 1973; two-phase convection in Scoates, 2000) and differential flow of solidifying anorthosite (Wiebe, 1980b). Several workers (Morse, 1969b; 1972b; Ranson, 1981; Scoates, 2000) have noted that the density of cumulus plagioclase (2.55 – 2.65 g/cm^3) is lower than the residual liquid (2.95 – 3.0 g/cm^3, in Royse and Park, 2000), suggesting that the flotation of plagioclase during fractional crystallization is most likely. Wiebe (1992, p. 232)

suggested that some massive anorthositic rocks were formed as a stagnant plagioclase accumulation near the roof of a magma chamber, whereas concurrent gravitational settling at the bottom of the same chamber formed layered anorthositic rocks. Phinney (1969) also described evidence for both the settling and flotation of plagioclase, and suggested this contrasting behavior may be related to the intersection of density and temperature curves and/or minor element content. This study will suggest that primary layering formed during the partial compaction of cumulus plagioclase frameworks.

Primary foliation in anorthositic rocks has been linked to gravitational settling (Morse, 1972b; Ryan, 2000a), magmatic flow (Morse, 1969b, Olmsted, 1969; Letteney, 1969; Higgins, 1991) late-magmatic compaction (Ryan, 2000a), sub-solidus deformation (Ryan, 2000a) and perpendicular growth of feldspars from the floor (Berg and Briegel, 1981). Higgins (1991) suggested that foliated anorthositic rocks developed from periodic changes in flow velocities and that these changes were also related to the folding of layering and segregation of interstitial melt. Buddington (1969) suggested that foliated anorthositic rocks were formed by flow differentiation, and he related this differentiation to the segregation of residual liquid from plagioclase crystals. This study will suggest that foliated rocks developed from the crystallization of intercumulus liquid in strained frameworks of cumulus plagioclase.

1.5 Recrystallization and deformation of anorthositic rocks

There are numerous studies (Wheeler, 1942; Morse, 1969b; Morse and Wheeler, 1973; Duchesne, 1984; Scoates, 1990; Wiebe, 1978; 1992, p. 230; Scoates and

Chamberlain, 1995; Lafrance et al. 1996; Bhattacharya et al., 1998; Barnichon et al., 1999; Hinchey et al., 1999; Royse and Park, 2000; Ryan, 2000a; 2001a) that describe recrystallized and/or deformed plagioclase in regionally undeformed anorthositic intrusions. Numerous studies (Duchesne, 1984; Scoates, 1990; Wiebe, 1992, p. 230; Scoates and Chamberlain, 1995; Bhattacharya et al., 1998; Barnichon et al., 1999) have linked this high-T recrystallization and/or deformation of plagioclase to diapiric ascent. Recrystallization and deformation have also been linked to tectonic activity (shearing, extension, tilting) during and/or shortly after the ascent and emplacement of anorthositic magmas (Morse and Wheeler, 1973; Ranson, 1975; Morse, 1981b; Royse and Park, 2000), the buoyant ascent of residual granitic magmas through anorthositic cumulates (de Waard, 1972), and relative movement of adcumulates, orthocumulates and liquid during crystallization (Wiebe, 1974).

Several workers (Buddington, 1969; Wiebe, 1978; Lafrance et al. 1996; Mitchell et al., 1996; Bhatthacharya et al., 1998) have also suggested that the crystallization of anorthositic magmas involved cumulate compaction and the removal of interstitial melts. La France et al. (1996) linked high-T recrystallization of cumulus plagioclase to the compaction of anorthositic magmas and the removal of interstitial melt. Mitchell et al. (1996) and Bhattacharya et al. (1998) suggested that small intrusive bodies of Fe-rich dioritic rocks in anorthositic intrusions were segregated during post-emplacement compaction of anorthositic diapirs. Morse (1972a) suggested that narrow ranges in plagioclase composition could be attributed to prolonged autometamorphism and annealing under rotational stress. This study will also propose that plagioclase was

recrystallized during compaction of cumulus plagioclase frameworks. A possible driving force for these compactions are the shear zones that bound each intrusive complex in the study area.

1.6 Summary

Anorthositic rocks crystallized from magmas that consisted of (a) fractionated basaltic and/or hyperfeldspathic liquid, (b) plagioclase crystals and (c) low abundances of H_2O. Previous work on intrusive forms suggests that the transport of anorthositic magmas may have been (a) diapiric or (b) fracture-controlled, which corresponds to a more solid- or liquid-state rheology of the parental anorthositic magma. Likewise, previous work on igneous textures and structures suggests that the rheology of anorthositic magmas during crystallization was either more (a) solid-state (massive rocks) or (b) liquid-state (layered and foliated rocks). Plagioclase crystals could have been recrystallized and/or deformed (a) during diapiric ascent, (b) during crystallization and/or (c) after crystallization. This study found that the form of anorthositic intrusions suggests more liquid-state rheology during the ascent and emplacement of magmas, and more solid-state rheology during the development of textures and structures.

Chapter 2: Overview of regional geology

The study area lies in a Mesoproterozoic anorthosite-granite batholith that is formally known as the Nain Plutonic Suite. The term 'suite', however, is ambiguous. As defined by Christie et al. (1981) a 'suite' refers to a collection of two or more lithodemes and is also used to name highly deformed and/or highly metamorphosed rocks. In addition, Bates and Jackson (1984) define suite as comprising a collection of rock specimens: (a) from a single area, or (b) of a single kind. In contrast, the term 'batholith' refers exclusively to a large mass of plutonic rocks and is thereby more specific in comparison to 'Plutonic Suite'. Hence, in this thesis the large mass of Mesoproterozoic plutonic rocks exposed in the vicinity of Nain is referred to by the informal name 'Nain batholith'. This name and its abbreviation (NB) are used in the remainder of the thesis.

The Mesoproterozoic Nain batholith was emplaced across the Paleoproterozoic Torngat orogen. This orogen separates the North Atlantic craton in the east from the Rae craton in the west. Locally, the North Atlantic craton is known as the Nain Province and the Rae craton is referred to as the Core zone. This chapter summarizes the main sub-divisions of Archean and Paleoproterozoic rocks that lie adjacent to the Nain batholith, and summarizes the main sub-divisions of Mesoproterozoic plutonic rock in the Nain batholith.

2.1 Archean and Paleoproterozoic rocks

The North Atlantic craton of Labrador is divided into the Archean Saglek and Hopedale blocks (see Connelly and Ryan, 1996) and was intruded by the

Paleoproterozoic Arnanunat Plutonic Suite (see Ryan and James, 2003) and The Bridges layered intrusion (see Ashwal et al., 1992). The Rae craton of western Labrador contains Archean rocks that are flanked, in the east, by Paleoproterozoic Tasiuyak paragneiss and Paleoproterozoic calc-alkaline orthogneiss. These Paleoproterozoic units were deformed in the Torngat orogeny shortly after they formed. This section reviews the main rock types and ages of these aforementioned units, and also describes the structures that mark the Torngat orogen.

2.1.1 Archean rocks

The main components of the Saglek block (Fig. 2.1) consist of tectonically interleaved Uviak gneiss, Nulliak supracrustal remnants, Nanok plutonic rocks and Upernavik gneiss (James et al., 2002). Uviak gneiss consists of tonalitic, trondhjemitic and granodioritic rocks that range in age from 3.7 – 3.3 Ga (Wendt and Collerson, 1999). Nulliak supracrustal rocks contain metakomatiites that show a Pb-Pb age of 3845 +/- 160 Ma (Wendt and Collerson, 1999). Upernavik gneiss consists of metavolcanic and metasedimentary rocks that range in age from 3260 – 3200 Ma (Schiötte et al., 1993). Most of the Saglek block was metamorphosed at granulite grade between 2780 – 2740 Ma (Schiötte et al., 1993; James et al., 2002). The western margin of the Saglek block was also reworked during the Torngat orogeny (Mengel and Rivers, 1989; 1997; Bertrand et al., 1993).

The Hopedale block (Fig. 2.1) is an Archean granite-greenstone terrane that includes the Maggo gneiss, Hunt River Group, Florence Lake Group and Kanairiktok

Plutonic Suite (James et al., 2002). The Maggo gneiss (>3.1 Ga) consists of metamorphosed granitoid rocks that predate the Hunt River and Florence Lake groups (James et al., 2002). The Hunt River and Florence Lake groups consist of mafic to felsic metavolcanic rocks, komatiite flows and metasedimentary rocks (James et al., 2002). The Hunt River group contains felsic volcanics that crystallized at 3105 +/- 3 Ma, whereas the Florence Lake group contains felsic metavolcanic rocks that crystallized at 2990 +/- 2 Ma and 2979 +/-1 Ma (James et al., 2002). The Hunt River group was metamorphosed at amphibolite-facies, whereas the Florence Lake group was metamorphosed at greenschist- to amphibolite-facies (James et al., 2002). The Kanairiktok Plutonic Suite consists of granitic rocks that were emplaced at 2890 – 2825 Ma (James et al., 2002). The northern part of the Hopedale block collided with the southern part of the Saglek block at 2580 – 2550 Ma (Connelly and Ryan, 1996). This collision is marked by metamorphism and the intrusion of granites and mafic dikes (Connelly and Ryan, 1996).

The Rae craton of western Labrador (Fig. 2.1) consists of tonalitic and granitic gneiss, amphibolite gneiss, two-pyroxene granulite and metasedimentary gneiss (see Ryan et al., 1997; Wardle et al., 2002). Tonalitic and granitic gneiss yields ages of 2.7 – 2.6 Ga and a minor component at 3.0 Ga (Wardle et al., 2002). Amphibolite gneiss and two-pyroxene granulite were derived from layered intrusions, whereas the metasedimentary rocks are older then some granitoids (Ryan et al., 1987).

2.1.2 Paleoproterozoic rocks

The Saglek block was intruded by a Paleoproterozoic anorthositic-granitic batholith that is referred to as the Arnanunat Plutonic Suite (in Ryan and James, 2003) (Fig. 2.1). Anorthositic and granitic rocks are superficially similar to those of the Nain batholith (Connelly and Ryan, 1998) and occur along the northern margin of the Nain batholith. U-Pb dating of zircons from granitic rocks, some of which contain xenoliths of anorthositic rocks, indicate crystallization at 2109 +/- 3, 2052 +/- 4 and 2025 +/- 7 Ma (Connelly and Ryan, 1998). Ryan and James (2003) suggested that the Arnanunat Plutonic Suite was emplaced between 2130 – 2040 Ma. The juxtaposition of Proterozoic anorthositic-granitic batholiths is also known from Wyoming (USA), where ca. 1.4 Ga anorthosite (Laramie complex) was emplaced adjacent to ca. 1.7 Ga anorthosite (Horse Creek complex) (Scoates and Chamberlain, 1997). The western part of the Arnanunat Plutonic Suite was deformed during the Torngat orogeny, whereas the eastern part is relatively undeformed (Ryan and James, 2003).

The Tasiuyak paragneiss (Fig. 2.1) consists of parallel-layered gneiss that is defined by alternations of garnet-sillimanite-biotite-graphitic pelitic gneiss and up to 80% leucogranite (Wardle et al., 2002). The Tasiuyak paragneiss is structurally continuous for over 1300 km and contains detrital zircons that crystallized between 1940 and 1895 Ma (Scott, 1998). As well, the Tasiuyak paragneiss was strongly deformed during the Paleoproterozoic Torngat orogeny (Mengel and Rivers, 1989; 1997). Deformation produced a steeply dipping foliation and north-northwest trending structures (Mengel and

Rivers, 1989) under maximum P-T conditions of 6 – 7 kb and 650° – 750°C (Rivers et al., 1996).

Calc-alkaline orthogneiss (Fig. 2.1) consists of dioritic, quartz dioritic and tonalitic gneiss (Rawlings-Hinchey et al., 2003). Calc-alkaline orthogneiss occurs in a sub-vertical, north-south striking belt that is more-or-less continuous from the northern tip of Labrador to the Nain area (Rawlings-Hinchey et al., 2003). Geochemistry and isotopic characteristics indicate that rock types were generated by crustal contamination of partial melts derived from the mantle wedge, or partial melting of the subducted crust and its sedimentary cover sequence (Rawlings-Hinchey et al., 2003). The protoliths were emplaced between 1910 – 1865 Ma (Scott, 1998), after which they were deformed in the Torngat orogeny. About 40 km southwest of Nain, calc-alkaline orthogneiss was deformed at amphibolite- to granulite-facies grade (Rawlings-Hinchey et al., 2003).

The Bridges layered intrusion, located at the southeast corner of the study area (Fig. 2.1), consists of layered olivine gabbro that occurs among undeformed intrusions of the Nain batholith (Palansky, 1972; Ashwal et al., 1992; Ryan, 2000, 2001a). Rock types contain plagioclase (An_{60-80}), olivine (Fo_{66-71}), clinopyroxene ($Mg/(Fe+Mg)_{75-82}$) and orthopyroxene (En_{71-75}) (in Ashwal et al., 1992). A Sm-Nd isochron age of 1667 +/- 75 Ma (in Ashwal et al., 1992) suggests the Bridges intrusion preceded emplacement of the Nain batholith by ~300 m.y. Relict magmatic structures consist of channel scours, troughs, slumps, modally graded layers, plagioclase lamination, poikilitic olivine and poikilitic pyroxene (Ashwal et al., 1992), whereas deformation structures consist of asymmetrical folds, thrusts, boudins, shear zones, granulation and recrystallization

(Ashwal et al., 1992). Ashwal et al. (1992) suggested that deformation of The Bridges intrusion occurred during emplacement of the Nain batholith.

2.1.3 Torngat orogen

The Torngat orogen is marked by amphibolite- and granulite-facies grade terranes (Mengel and Rivers, 1989). The orogen is 130 km wide, steeply dipping and north-northwest striking (see Mengel and Rivers, 1989; Van Kranendonk, 1996). Van Kranendonk (1996) suggested that the orogen evolved during (1^{st}) crustal thickening at ca. 1860 Ma, (2^{nd}) sinistral transpression shear at ca. 1845 – 1822 Ma and (3^{rd}) west-directed exhumation at ca.1794 – 1740 Ma. The largest of the structures associated with the Torngat orogen is the Abloviak shear zone (Fig. 2.1). The Abloviak shear zone is marked by a sub-vertical mylonitic foliation and a very strongly developed sub-horizontal stretching lineation (Rivers et al., 1996). The shear zone contains shear bands and local inclusion trails in rotated garnets that indicate sinistral strike-slip displacement that was parallel to the sub-horizontal stretching lineation.

2.2 Mesoproterozoic plutonic rocks of the Nain batholith

The Nain batholith is one of several Mesoproterozoic anorthosite-granite batholiths that occur in northern Labrador (see Fig. 2.1). These batholiths are referred to as the Mistasin Lake batholith, Harp Lake intrusive suite and Michikamau intrusion.

Wheeler (1942, 1960, 1969) was the first to conduct extensive geological mapping in the Nain area. Over time, these plutonic rocks have been referred to as the

anorthosite-adamellite complex of Nain (Wheeler, 1960), Nain anorthosite massif (Rubins and de Waard, 1971), Nain anorthositic complex (de Waard, 1976; de Waard et al., 1976; Wiebe, 1980a; 1985b; 1987; 1988; Wiebe and Snyder, 1993), Nain complex (de Waard, 1976; Berg, 1977a; 1977b; Wiebe, 1978; 1979; 1990a; 1990b; Berg, 1980; Ranson, 1981) and the Nain Plutonic Suite (Ryan, 1991b; Emslie and Loveridge, 1992; Emslie and Stirling, 1993; Yu and Morse, 1993; Xue and Morse, 1993; 1994; Berg et al., 1994; Emslie, 1996; Ryan, 1997; 2000b; Li et al., 2000; Royse et al., 1999; Royse and Park, 2000). Xue and Morse (1993) suggested that intrusive bodies are of batholithic size. Ryan (1997) referred to the Nain Plutonic Suite as a batholithic assemblage of plutonic rocks. Ryan (2001a, p. 127) also suggested that "the igneous processes that contributed to the construction of this batholith are similar to those advocated for batholiths worldwide". These plutonic rocks are informally referred to as the Nain batholith (NB) in this study.

2.2.1 Rock types

In a summary of units in the Nain area, Wheeler (1942) described an anorthosite-gabbro-diorite group, an adamellite group, a tonalite group, a monzonite group, dike rocks, ultrabasic rocks and gneisses associated with anorthositic rocks. A geological map by Wheeler (1969) divided plutonic rocks into adamellite and minor related intrusives, Kiglapait layered intrusive and minor basic intrusives, and anorthosite complex. De Waard (1973) suggested that the Nain batholith be divided into anorthositic, gabbroic, troctolitic, monzogabbroic and adamellitic rocks. A map by Ryan (1990) divides the Nain

batholith into anorthositic, troctolitic, granitic and monzonitic, and Fe-rich gabbroic and Fe-rich dioritic members (Fig. 2.2). This section will review rock types of the Nain batholith following sub-divisions on the map by Ryan (1990), although members are here referred to as rocks. As well, occurrences of basaltic dikes and deformed gabbronoritic rocks that occur in the margins of anorthositic intrusions ('mafic granulite') are also summarized.

2.2.1.i Anorthositic rocks

Wheeler (1960, 1969) divided the anorthositic rocks into an olivine-bearing dark-facies, hypersthene-bearing pale-facies and inverted pigeonite bearing buff-facies. Morse (1969b) found that dark-, pale- and buff-facies correspond to average plagioclase compositions of An_{52}, An_{46} and An_{40}, respectively.

Morse (1981b) used field relations to divide magmatism of the Nain batholith into an old anorthosite event, main anorthosite event and a troctolite intrusive event. Yu and Morse (1993) used $^{40}Ar/^{39}Ar$ dating to show that plagioclase ages in anorthositic rocks of the old event (1260 – 1284 Ma) are generally older in comparison to those of the main event (1232 – 1254 Ma). The old anorthosite event includes the Pearly Gates intrusion (Bird Lake massif and Susie Brook Slab in Yu and Morse, 1993), Lister pluton (Lister massif in Yu and Morse, 1993) and the Port Manvers Run intrusion (Fig. 2.2). The main anorthosite event includes the Paul Island, Kikkertavak and Jonathon intrusions (Yu and Morse, 1993). The troctolitic intrusive event includes the Kiglapait, Tigalak, Newark Island and Hettasch intrusions (Yu and Morse, 1993).

A study by Xue and Morse (1993) used whole rock geochemistry to divide anorthositic rocks into a noritic and troctolite facies. Whole rock element abundances for noritic anorthosite, in comparison to troctolitic anorthosite, are high in SiO_2, K_2O and Sr, and low in CaO/Al_2O_3 and Ba/K (Xue and Morse, 1993). A follow-up mineral chemistry study (Xue and Morse, 1994) found that the noritic anorthosite group contains andesine plagioclase (An_{42-54}) whereas the troctolitic anorthosite group contains labradorite plagioclase (An_{51-61}). Xue and Morse (1993; 1994) grouped the Pearly Gates and Lister intrusions into the noritic anorthosite group, whereas the Kikkertavak and Port Manvers Run intrusions were grouped into the troctolitic anorthosite group.

Table 2.1: U-Pb ages of anorthositic rocks in the Nain batholith (* indicates not shown on Fig. 2.2)

Intrusion	Rock type	Age (Ma)	Analysis	Reference
Fraser Canyon*	anorthosite	1356 +/- 2	U-Pb	Tettelaar, 2004
Pearly Gates	anorthosite	1344 +/- 2	U-Pb	Tettelaar, 2004
Akpaume*	leuconorite	1331 +/- 2	U-Pb	Hamilton et al., 1994
Ikadlavik Brook	leuconorite	1322 +/- 1	U-Pb	Hamilton et al., 1994
Pyramid Pass	leuconorite, leucotroctolite	1322 +/- 1	U-Pb	Hamilton, 1997
Paul Island	anorthosite	1319 +/- 1	U-Pb	Hamilton et al. 1994
Kikkertavak	anorthosite, leuconorite	1311 +/- 2	U-Pb	Hamilton et al., 1994
Tabor Island*	anorthosite, leuconorite	1311 +/- 2	U-Pb	Hamilton et al., 1994
Port Manvers Run	leucotroctolite	1308 +/- 2	U-Pb	in Ryan, 2001a
Koliktalik Island*	anorthosite	1305 +/- 2	U-Pb	Hamilton et al., 1994
Sango Bay	leucotroctolite	1294 +/- 1	U-Pb	Hamilton et al., 1994

Studies by Hamilton et al. (1994) and Hamilton (1997) found zircons in anorthositic rocks that crystallized between 1331 +/- 2 and 1294 +/- 1 Ma (Table 2.1). A study by Tettelaar (2004) found zircons in anorthositic rocks that crystallized at 1356 +/- 2 Ma. These results indicate a time span of ~62 m.y. (1356 – 1294 Ma) for the crystallization of zircons in NB anorthositic rocks.

2.2.1.ii Troctolitic rocks

Wheeler (1942; 1960) described ultrabasic and olivine gabbroic rocks that he felt were likely related to the anorthositic rocks. A geological map by Wheeler (1969) shows the Kiglapait layered intrusion and other smaller basic intrusions as comprising part of the Nain batholith. Subsequent studies examined troctolitic rocks and related differentiates (olivine gabbro, ferrodiorite, ferrosyenite) in the Kiglapait intrusion (see Morse, 1969a), Hettasch intrusion (see Berg, 1980), Barth Island layered structure (see de Waard and Mulhern, 1972), Newark Island layered intrusion (see Wiebe, 1987, 1988), Mushua intrusion (Reid Brook in Ryan, 1990; Li et al., 2000), Voisey's Bay intrusion (Reid Brook in Ryan, 1990; Li et al., 2000) and Jonathon intrusion (see Berg and Briegel, 1981). A regional map by Ryan (1990) groups all of these intrusions into a troctolitic member (Fig. 2.2). This member consists predominantly of troctolitic, melatroctolitic, leucotroctolite and olivine-bearing gabbroic rocks (Ryan, 1990). Recent work on the Pants Lake intrusion (Smith et al., 2001; Kerr, 2003) described rock types and U-Pb ages (Table 2.2) that overlap with the troctolitic rocks of the Nain batholith.

Morse (1981b) suggested that a troctolite intrusive event occurred after the old anorthosite and main anorthosite events. De Paolo (1985) used a Sm-Nd isochron to show that the Kiglapait intrusion crystallized at 1305 +/- 5Ma. Amelin et al. (1999) found zircons and baddeleyite in the Voisey's Bay intrusion that crystallized at 1333 +/- 1. Smith et al. (2001) found zircons and baddeleyite in troctolitic rocks of the Pants Lake intrusion that crystallized at 1337 +/- 2 and 1322 +/- 2 Ma. These studies show that U-

bearing minerals in troctolitic rocks of the Nain batholith crystallized between 1337 – 1305 Ma (Table 2.2).

Table 2.2: U-Pb ages of troctolitic rocks in the Nain batholith.

Intrusion	Rock type	Age (Ma)	Analysis	Reference
Pants Lake south	troctolite	1337 +/- 2	U-Pb	Smith et al., 2001
Voisey's Bay	troctolite	1333 +/- 1	U-Pb	Amelin et al., 1999
Barth Island	troctolite	1330 +/- 1	U-Pb	Gaskill, 2005
Pants Lake north	troctolite	1322 +/- 2	U-Pb	Smith et al., 2001
Mushua	troctolite	1313	U-Pb	Li et al., 2000
Jonathon Island	leuconorite, leucotroctolite	1311 +/- 2	U-Pb	Hamilton et al., 1994
Kiglapait	troctolite, leucotroctolite	1306 +/- 2	U-Pb	in Yu and Morse, 1993
Newark Island	troctolite	1305 +/- 5	U-Pb	Simmons et al. in Ryan, 1997

2.2.1.iii Granitic rocks

Wheeler (1942) described a widely distributed adamellite group and lesser abundances of tonalite and monzonite in the vicinity of Nain. The adamellite group includes granite through to adamellite, and granodiorite (Wheeler, 1942). Subsequent work by Wheeler (1960) suggested that the adamellite group is divided into a fayalite facies that is succeeded westwards by a hornblende facies. A regional map by Wheeler (1969) outlines much of the presently known extent of granitic rocks in the Nain area. Ryan (1990) includes the Umiakovik batholith, Makhavinekh pluton, Notakwanon batholith, Iviksuak pluton and the Tessiarsuyungoakh pluton into the granitic member (Fig. 2.2). This member consists predominantly of hornblende +/- biotite +/- fayalite +/- clinopyroxene +/- fluorite-bearing granite, quartz monzonite, monzonite, syenite, monzodiorite and quartz monzodiorite (Ryan, 1990). Peralkaline granitic volcanic rocks occur in the Flowers River area (Hill, 1982).

Table 2.3: U-Pb ages of granitic rocks in the Nain batholith (* not shown on Fig. 2.2)

Intrusion	Rock type	Age (Ma)	Analysis	Reference
Tessiarsuyungoakh	monzonite	1364 +/- 3.5	U-Pb	Tettelaar, 2004
Hare Hill	monzonite	1351 +/- 3	U-Pb	in Ryan and James, 2003
Lister margin*	monzonite	1343 +/- 3	U-Pb	Hamilton, 1997
Anaktalik*	monzonite	ca. 1326	U-Pb	in Ryan and James, 2003
Makhavinekh	granite	1322 +/- 1	U-Pb	Ryan et al., 1991
Barth Island*	monzonite	1322 +/- 2	U-Pb	Hamilton et al., 1994
Umiakovik	monzonite	1319 +/- 2	U-Pb	Emslie and Loveridge, 1992
Umiakovik	granite	1316 +/- 3	U-Pb	Emslie and Loveridge, 1992
Goodnews*	granite	1305 +/- 10	U-Pb	Simmons and Simmons, 1987, in Miller et al., 1997
Ivaksuak	monzonite	1296	U-Pb	Krogh and Davis, 1973, in Miller et al., 1997
Notakwanon	granite	1292 +/- 4	U-Pb	Ryan et al., 1991
Flowers River	peralkaline granite	1289	U-Pb	in Miller et al., 1997

Ryan et al. (1991a) found zircons in granite of the Notakwanon batholith that crystallized at 1292 +/- 4 Ma. Emslie and Loveridge (1992) found zircons in monzonitic rocks in the Umiakovik batholith that crystallized at 1319 +/- 2, and zircons in granitic rocks that crystallized at 1316 +/- 3 Ma (Table 2.3). Hamilton (1997) found zircons in monzonitic rocks that crystallized at 1343 +/- 3 Ma. Miller et al. (1997) report an age of 1289 Ma for a peralkaline ash flow tuff from the Flowers River area. Monzonite in the Hare Hill intrusion crystallized at 1351 +/- 3 Ma (in Ryan and James, 2003). Tettelaar (2004) found zircons in monzonitic rocks of the Tessiarsuyungoakh intrusion that crystallized at 1364 +/- 3 Ma. These studies indicate that granitic and monzonitic rocks contain zircons that crystallized between 1364 – 1289 Ma.

2.2.1.iv Fe-rich gabbroic to dioritic rocks

Wheeler (1942) described gabbro and diorite that occurs in dikes and as gneisses associated with plutonic rocks in the vicinity of Nain. Morse (1969a) described Fe-rich

gabbroic-dioritic rocks that are differentiates of troctolitic magmas in the Kiglapait intrusion. De Waard and Hancock (1973) described a curved dike of gabbroic to granodioritic rocks that is presently referred to as the Satorsoakulluk dike (see Ryan, 2000a; 2001a). Wiebe (1974) describes diorite and adamellite in the Goodnews complex, and suggested that anorthosite and diorite were related by differentiation of an unknown parental magma. Ryan (1990) included the Cabot Lake sheet, Goodnews complex, Akpaume intrusion and Tigalak intrusion into a Fe-rich gabbroic-dioritic member. This member consists of ferrogabbro, ferrodiorite, monzogabbronorite, monzogabbro, monzodiorite and monzonite (Ryan, 1990).

Table 2.4: U-Pb ages of Fe-rich gabbroic and dioritic rocks of the Nain batholith (* not shown on Fig. 2.2)

Intrusion	Rock type	Age (Ma)	Analysis	Reference
Tessiarsuyungoakh	ferrodiorite	1356 +/- 2	U-Pb	Tettelaar, 2004
Apkaume	ferrodiorite, hybrid	1333 +/- 2	U-Pb	Hamilton et al., 1994
Barth Island	ferrodiorite, monzonite	1322 +/- 2	U-Pb	Hamilton et al., 1994
Satossuakuluk	ferrodiorite, monzonite	1315 +/- 2	U-Pb	Hamilton et al., 1994
Jonathon Island	ferrodiorite	1312 +/- 3	U-Pb	Hamilton et al., 1994
Tigalak	ferrodiorite	1306 +/- 3	U-Pb	Hamilton et al., 1994
Satossuakuluk	ferrodiorite, monzonite	1301 +/- 2	U-Pb	Hamilton et al., 1994
Cabot Lake	ferrodiorite	1298 +/- 2	U-Pb	Hamilton et al., 1994

A study by Hamilton et al. (1994) found zircons in Fe-rich gabbroic and dioritic rocks that crystallized between 1333 +/- 2 and 1298 +/- 2 Ma (Table 2.4). A study by Tettelaar (2004) found zircons in ferrodiorite that crystallized at 1356 +/- 2 Ma. These studies indicate that the zircons in Fe-rich gabbroic to dioritic rocks crystallized between 1356 – 1298 Ma.

2.2.1.v Basaltic dikes

Two studies (Upton, 1973; Wiebe, 1985b) have suggested that basaltic dikes that cut the Nain batholith are similar to the Gardar dikes of southwestern Greenland. Wiebe (1985b) found that these dikes are of alkali to transitional basaltic composition and divided them into high-P_2O_5 (HP) and low-P_2O_5 (LP) groups. Basaltic dikes contain plagioclase (An_{49-63}), olivine (Fo_{47-51}), clinopyroxene (En_{30-36}) and oxide minerals (Wiebe, 1985b). Carlson et al. (1993) used a Rb-Sr isochron to determine that basaltic dikes that cut the Nain batholith were emplaced at 1276 +/- 23 Ma.

2.2.1.vi 'Marginal granulites'

Wheeler (1960, p. 630) described a group of "highly banded gabbroic and dioritic gneisses" that are best developed near the margins of anorthositic intrusions and within the country rock belts that lie within the Nain batholith. Wheeler (1960) noted that these gneisses are of similar composition to the anorthositic rocks and grouped these gneisses into the marginal facies of anorthositic intrusions. However, Wheeler (1960) also noted that similar gneisses occur distal to any known exposures of anorthositic rocks, and ultimately referred to these as 'granulites of uncertain origin' (see Davies, 1973b).

A study by Davies (1973b) described a group of pyroxene granulites that "field relations suggest...should be classified with basement rocks; however, its persistence adjacent to the anorthositic margins... leaves the origin of these rocks unresolved at this time". Davies (1973b) refers to these rocks as 'marginal granulites'. A study by Brand (1974) described a ~50 – 190 m wide zone of biotite-, pyroxene- and plagioclase-bearing

marginal granulite that also occurred next to an anorthositic intrusion. Brand (1974) linked these 'marginal granulites' with a unit of paragranulite in the country rock.

A study by Berg and Briegel (1981) found several generations of marginal granulites in country rock adjacent to the Jonathon intrusion and suggested that some of these generations were intruded at an early stage in the development of the Nain batholith. A study by Royse et al. (1999) also suggested that these granulites (marginal mafic granulites in Royse et al., 1999) are related to the Jonathon intrusion, and that they indicate emplacement of the Jonathon intrusion into cool Archean crust (Royse and Park, 2000).

The 'marginal granulites' of the Nain batholith therefore comprise a group of rocks that have been grouped with both the country rocks (see Davies, 1973b; Brand, 1974) and the margins of anorthositic intrusions (see Wheeler, 1960; Berg and Briegel, 1981; Royse et al., 1999). In the study area, the margins of anorthositic intrusions were found to contain strongly deformed gabbronoritic rocks that may be analogous to these 'marginal granulites'. This study uses field mapping, petrography, mineral chemistry, whole rock chemistry and/or geochronology to suggest that these strongly deformed gabbronoritic rocks comprise the outer-most parts of anorthositic intrusions. In addition, these strongly deformed rocks are used to interpret the tectono-magmatic setting of plutonic rocks in the study area.

2.2.2 Tectono-magmatic setting

Compiled U-Pb ages for plutonic rocks of the Nain batholith (see Tables 2.1 – 2.4) suggest that it was emplaced between 1365 – 1270 Ma. This magmatic event has been related to crustal extension, underplating of basaltic magma and/or impingement of a mantle-plume at the base of the crust. Wheeler (1960) suggested a westward direction for the migration of intrusion.

Berg (1977a; 1977b) suggested that the Nain batholith was emplaced into a crustal-scale graben during north-south directed extension. Morse (1981b) suggested that the old anorthosite event was emplaced during rifting and associated north-south extension (also in Berg and Briegel, 1981). Morse (1981b) also suggested that north-south extension was re-newed, and accompanied with east-west, left-lateral, motion that post-dated the troctolite intrusive event. Yu and Morse (1993) suggested that the Nain batholith was emplaced into an aborted rift zone.

Hill (1982) mapped peralkaline granite volcanics in the southern part of the Nain batholith and suggested that the crust must have been lifted upwards shortly after emplacement of the Nain batholith. Wiebe (1985b) made a similar suggestion on the basis of basaltic dikes that cut the Nain batholith. Royse and Park (2000) found that older anorthosite plutons were emplaced and deformed in ductile shear zones whereas younger intrusions were emplaced into more brittle crust.

Emslie et al. (1994) used a Sr and Nd isotopic study to suggest that magmatism in the Nain batholith was penecontemporaneous with a basaltic underplating episode. This episode of underplating helps to account for the mantle-like isotopic signatures of most

plutonic rocks in the Nain batholith, including the granites (see Emslie et al., 1994). Ryan (1997) suggested that the impingement of a mantle-plume at the base of the crust would have caused the crust that hosts the Nain batholith to extend at middle- and upper-crustal levels.

2.3 Summary

The Mesoproterozoic (1365 – 1270 Ma) Nain batholith was emplaced across the Torngat orogen, which is a Paleoproterozoic orogen that separates the North Atlantic and Rae cratons. Other large units of country rock occur in the Arnanunat Plutonic Suite and the Bridges layered intrusion. Rocks of the Nain batholith have been divided into anorthositic (1356 – 1294 Ma), troctolitic (1337 – 1305 Ma), granitic (1364 – 1289 Ma) and Fe-rich gabbroic to dioritic rocks (1356 – 1298 Ma). The margins of anorthositic intrusions contain 'marginal granulites' that may or may not be Mesoproterozoic in age. All of these plutonic rocks were generated during a Mesoproterozoic episode of extension and/or underplating of basaltic magma.

Chapter 3: Methods

The bulk of the results and interpretations presented in this study are derived from field mapping and petrographic observations. This chapter summarizes the criteria used to sub-divide the geological map produced in this study (Map 1), and the terms used to describe rock types, textures, structures and indicators of deformation. The methods used to obtain and process mineral chemistry, whole rock chemistry and U-Pb isotope data are also described.

3.1 Geological mapping and outcrop observations

Geological mapping comprises the most important facet of this study and was done in the vicinity of Nain, Labrador (Fig. 3.1), between longitude 61°38' to 62°12' W and latitude 56°35' to 56°25' N. This study area covers parts of topographic map sheets NTS 14C/12, 14C/5, 14D/9 and 14D/2. Elevation in the study area ranges from sea level to 600 m. Exposure is excellent on ridge tops and along shorelines, and fairly good along ridge flanks. Dense vegetation occurs mostly in valleys below an altitude of 100 m.

A geological map was made of a 400 km^2 study area at a scale of 1:20 000 (Map 1). Simplified excerpts of this map are presented in Chapters 4 through 7. This area was previously only covered at reconnaissance scale (see Fig. 3.1, Wheeler, 1969; Rubins and de Waard, 1971; Rubins, 1973; Ryan, 1990; 2000a; 2001a). Geological contacts, structural measurements, observation stations and sample locations were noted on sheets of Mylar that were overlain on air photos. Structural measurements were taken with a Suunto compass and photographs of outcrops were taken with 35 mm film for color

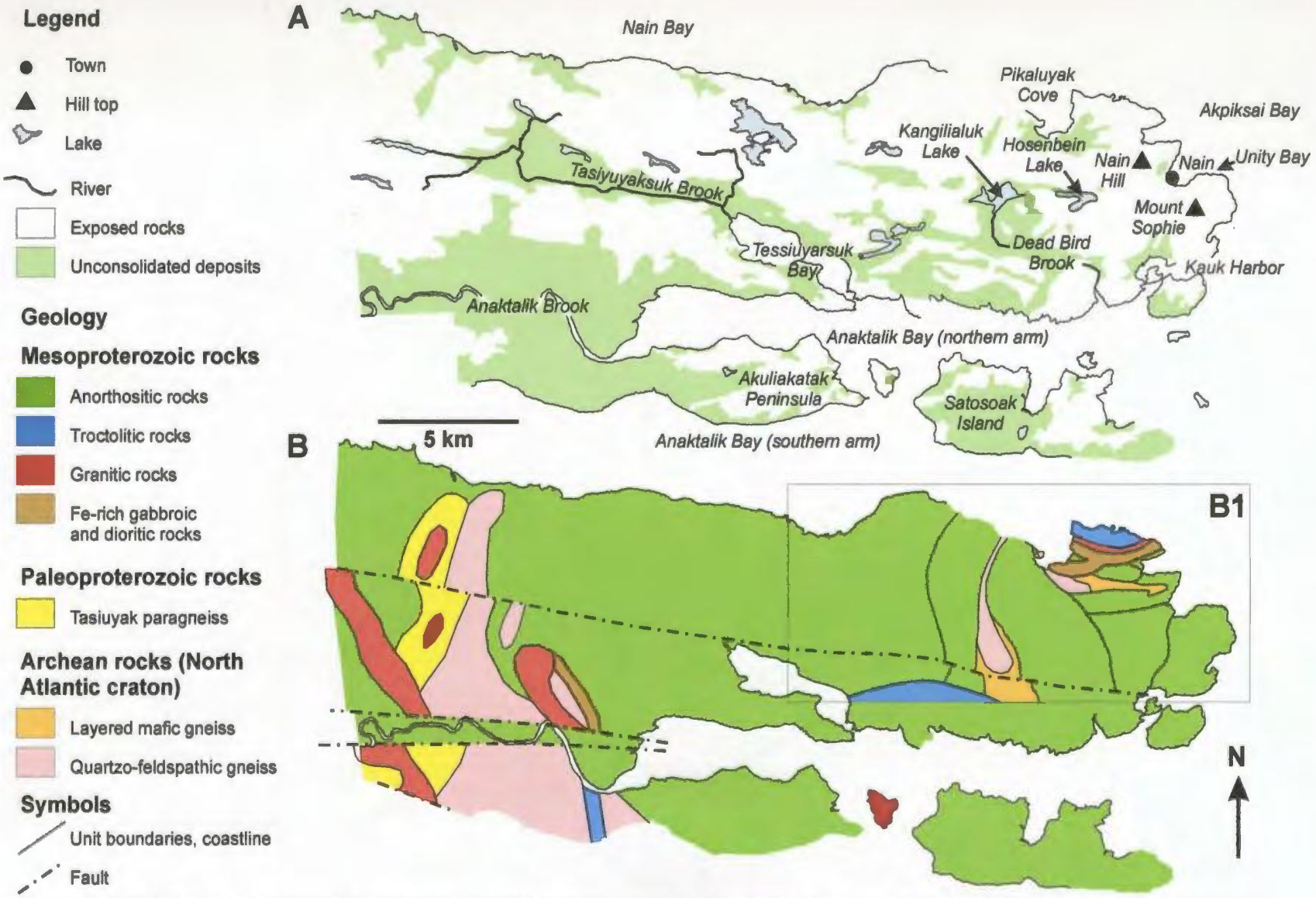

Figure 3.1: (A) Simplified topographic map and (B) solid geological map of the study area. Place names in (A) were compiled from maps by Ryan (2000a; 2001a; 2001b). Geology in (B) was compiled from Ryan (1990) and (B1) from Ryan (2001a), both of which comprise the most recently published geological maps for the study area.

slides. Mylar sheets were digitized and compiled on a 1:50 000 scale topographic map in Corel Draw 8. All structural map units, structural measurements and sample localities are shown on Map 1.

3.1.1 Naming of map units

Geological mapping built on regional scale (1:500 000) maps by Wheeler (1969) and Ryan (1990), and more detailed maps (1:50 000) in the vicinity of Nain by Rubins and de Waard (1971), Rubins (1973) and Ryan (2000a; 2001a). Newly identified units are named after geographical localities (Fig. 3.1) that were compiled from maps made by Ryan (2000a; 2001a; 2001b). In most cases, the geographical feature included in the geographical name (Mount, Lake, Hill, Brook) was dropped from the geological name when naming the units of plutonic rocks (e.g. Kangilialuk sheet after Kangilialuk Lake). For belts of country rock, and due to a shortage of available place names, the geographical feature was included in the geological name (e.g. Kangilialuk Lake country rock belt).

Maps by Ryan (1990; 2000a; 2001a) show that the study area contains Mesoproterozoic intrusions and Archean country rock. These maps show that Archean country rock forms elongated exposures that are referred to as 'country rock belts' in this study. The term 'belt' refers to the relatively high length to width aspect ratios that typify country rock exposures in the study area. Simplified maps of country rock belts are presented in chapter 4.

In this study, the terms 'pluton' and 'sheet' are used to describe intrusive bodies. A pluton consists mostly of sub-horizontally oriented and massive plutonic rocks. A sheet shows a length to width ratio that is high in comparison to a pluton, and is generally sub-vertically oriented.

Some plutons are divided into an 'inner zone' and a 'border zone'. The inner zone is sub-horizontally oriented and/or massive, whereas the border zone is moderately dipping to sub-vertically oriented, layered and separates the inner zone from country rock.

In this study, plutons and sheets are grouped into 'centered intrusive complexes'. Each centered intrusive complex contains one pluton that comprises the spatial center of the intrusive complex, and one or more spatially associated plutons and sheets that are: (a) structurally concordant with the spatial center, and (b) broadly contemporaneous (within 10's of m.y.) with the spatial center. In addition, each intrusive complex is divided into a core and a margin. The core consists of plutons and/or pluton inner zones, whereas the margin consists of pluton border zones and/or sheets. Maps of intrusive complexes are presented in chapters 5, 6 and 7.

In summary, all rock units in the study area are grouped into: (a) a country rock belt, or (b) a centered intrusive complex (Fig. 3.2). Each centered intrusive complex is divided into: (a) a core that consists of plutons and/or pluton inner zones, and (b) a margin that consists of pluton border zones and/or sheets.

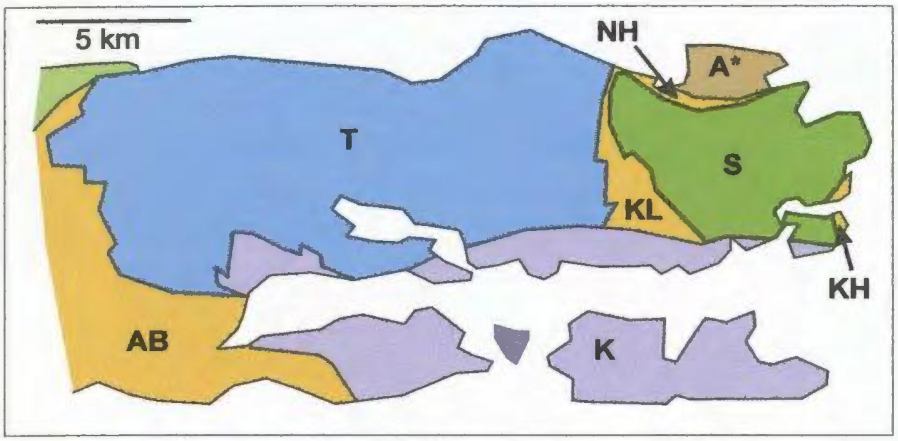

Figure 3.2: Simplified solid geological sketch map of the study area. The area is divided into country rock belts (AB: Anaktalik Brook, KL: Kangilialuk Lake, NH: Nain Hill, KH: Kauk Harbour) and centered intrusive complexes (T: Tikkoatokak, S: Sophie, K: Kikkertavak, A: Ametok). * The Ametok complex is not described in this study.

3.1.2 Terminology used to name rocks

Rocks are named with the gabbroic and Quartz-Alkali feldspar-Feldspathoid-Plagioclase (QAFP) plutonic rock classifications that follow Streckeisen (1976, in Le Maitre, 2002) (Fig. 3.3, 3.4). Some workers (see Vander Auwera and Longhi, 1994; Nielsen et al., 1996; Vander Auwera et al., 1998; Bolle et al., 2003) have used the charnockite classification to name granitoid rocks associated with Proterozoic anorthosite. The charnockite classification is avoided in this study because it is also used, in other studies (e.g. Kroener and Williams, 1993; Perchuk and Gerya, 1993; Harlov, 2000), to name high-grade metamorphic rocks. This study uses the QAFP classification to name granitoid rocks in order to emphasize the igneous origin of these rocks.

Some exceptions are made in use of the gabbroic plutonic rock classification. These exceptions concern the range of plagioclase compositions used to distinguish gabbro from diorite, and are discussed in section 3.2.3.

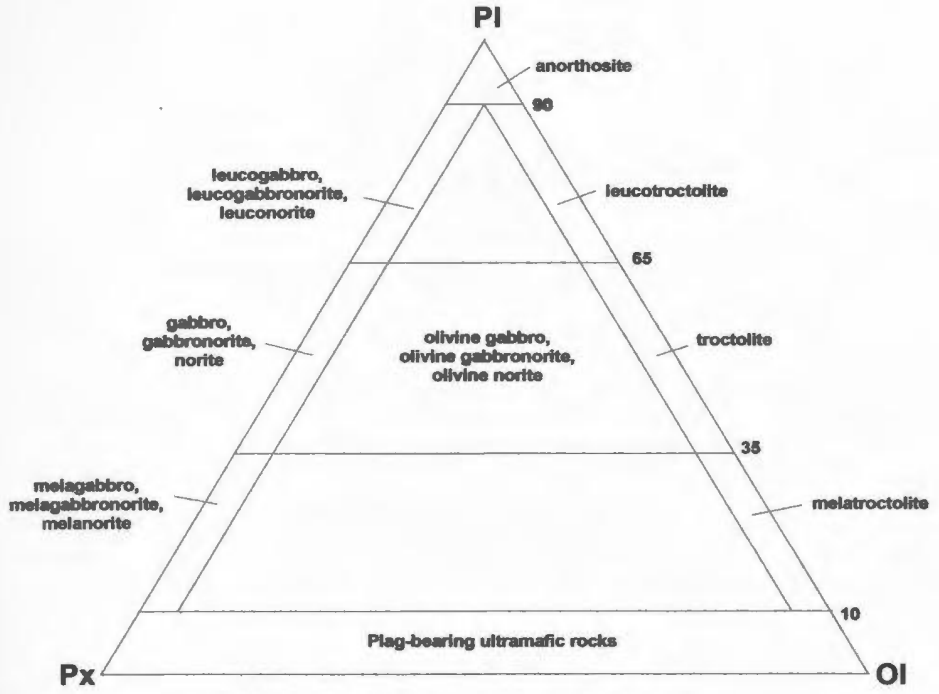

Figure 3.3: Streckeisen classification of gabbroic (plagioclase (Pl), pyroxene (Px), and/or olivine (Ol) bearing) plutonic rocks (after Streckeisen, 1976, in Le Maitre, 2002, p. 25). In this study, this classification scheme is used for gabbroic rocks with plagioclase compositions $>An_{40}$.

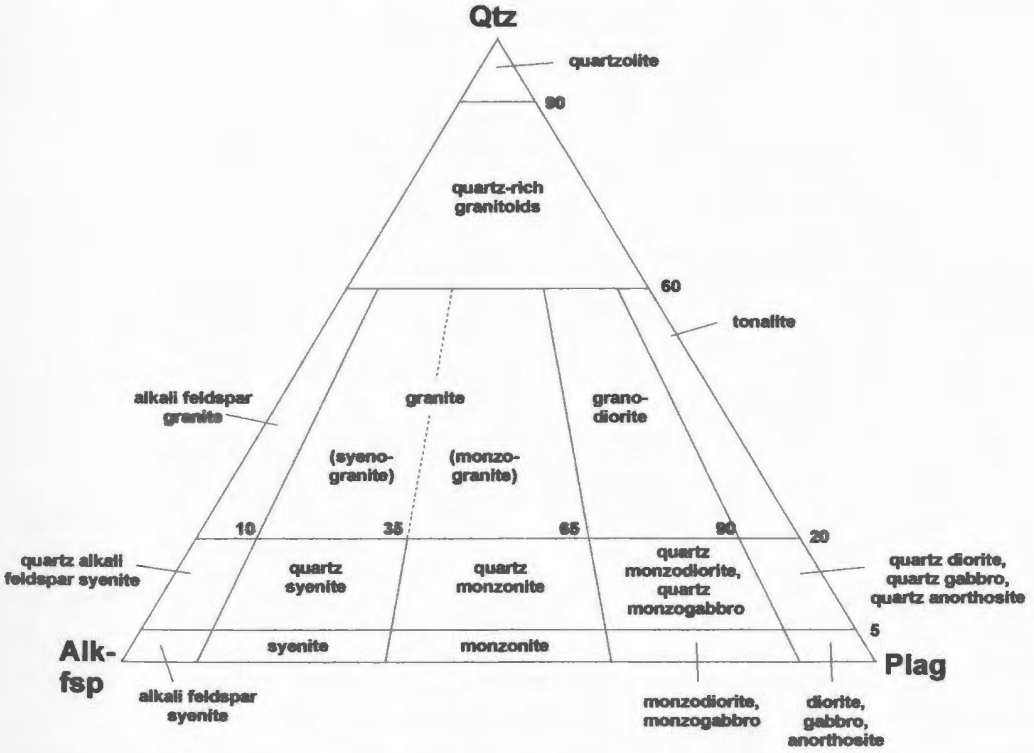

Figure 3.4: Streckeisen classification of felsic (plagioclase (Pl), quartz (Qtz), and/or alkali feldspar (Alk-fsp) bearing) plutonic rocks (after Streckeisen, 1976, in Le Maitre, 2002, p. 22). In this study, this classification scheme is used for rocks with plagioclase compositions $<An_{40}$.

3.1.3 Naming of textures and structures

Standard ranges (see Philpotts, 1990, p. 92) for fine- (<0.1 cm) and medium-grained (0.1 – 0.5 cm) plutonic rocks are applied to both country rocks and plutonic rocks in the study area (Table 3.1). In this thesis, coarse-grained refers to rocks with a mean average grain size diameter of 0.5 – 2 cm. Very coarse-grained refers to rocks with a mean average grain size diameter of >2 cm. For the description of individual crystals, the terms small (<0.1 cm), medium-sized (0.1 – 0.5 cm) and large (>0.5 cm) correspond to rocks that are the equivalent of fine-, medium-, and coarse- to very coarse-grained, respectively.

Table 3.1: Summary of size ranges and terms used to describe grain sizes

Mean size of grains (cm)	Rock	Mineral
<0.1	fine-grained	small
0.1 - 0.5	medium-grained	medium-sized
0.5 - 2	coarse-grained	large
>2	very coarse-grained	(range given)

This study uses the following terms to describe the texture of plutonic rocks in the study area; (a) granular, (b) poikilitic and (c) porphyritic. The use of these terms is adapted from the definitions of Bates and Jackson (1984) and Hunter (1996). Granular texture indicates a holocrystalline igneous rock that is made up of grains of nearly the same size. Poikilitic texture indicates an igneous rock in which an interstitial mineral is irregularly scattered in between larger crystals of another mineral. Porphyritic texture indicates an igneous rock of any composition that contains conspicuous phenocrysts in a finer-grained groundmass.

This study considers structures to comprise "a megascopic feature of a rock, generally best seen on the outcrop rather than in hand specimen" (Bates and Jackson, 1984, p. 499). 'Primary structures' refer to structures that are inferred to have formed during the crystallization of magma. Following this definition, structures of anorthositic rocks in the study area consist of (a) mottling, (b) layering and (c) foliation. These structures are described in terms of the textures they comprise (i.e. granular, poikilitic and/or porphyritic).

In this study, many plutonic rocks are described as 'weakly deformed' whereas all of the country rocks and some of the plutonic rocks are described as 'strongly deformed'. Weakly deformed rocks show: (a) preserved primary structures, and (b) petrographic indicators of high temperature deformation and/or recrystallization (see section 3.2.1). In contrast, strongly deformed show: (a) deformation structures such as folds, boudins and/or bedding plane faults, (b) shear indicators such as rotated porphyroclasts and/or sigmoidal foliation, (c) granular or gneissic texture, and/or (d) moderately dipping to sub-vertical, relatively thin (<20 cm on average) compositional layers. This study found that most of the country rock is strongly deformed, whereas there are also strongly deformed plutonic rocks in the margins of centered intrusive complexes. The strongly deformed country rocks are here referred to as: (a) gneiss if approximately >20% of minerals show a preferred orientation, and (b) granulite if approximately <20% of minerals show a preferred orientation. The strongly deformed plutonic rocks, which may be analogous to the 'granulites of uncertain origin' and 'marginal granulites' of previous workers (see Davies, 1973b; Brand, 1974; Berg and Briegel, 1981; Royse et al., 1999), are simply

referred to as strongly deformed. The terms gneiss and granulite are avoided for these strongly deformed plutonic rocks because they are here used to refer to strongly deformed rocks formed by regional metamorphism.

3.2 Thin section analysis

Thin section analysis consisted of petrographic analysis and electron microprobe (EMP) analysis. This section presents some comments on petrographic analysis, petrographic interpretations, methods for mineralogical analysis, precision and accuracy determinations for mineralogical analysis, and the context within which mineralogical analyses are interpreted.

3.2.1 Some comments on petrographic analysis

Rick Soper made the thin sections in the lapidary lab at the Memorial University of Newfoundland (MUN). These thin sections were examined with transmitted and reflected light using an Olympus microscope at MUN. Photographs were taken with a digital camera attached to the microscope.

Modal abundances of 'major', 'minor' and 'accessory' minerals were visually estimated. Major and minor minerals are silicates or oxides formed by the main rock forming elements, and range from 5 – 100% to <5% of the mode respectively. Accessory minerals are stabilized by trace elements and also comprise <5% of the mode. The visual estimates are used to name rocks using the Streckeisen classifications (see Figs. 3.3, 3.4).

Petrographic analysis as part of this study demonstrates that many plagioclase crystals exhibit (a) serrated and/or (b) interlobate grain margins. Several workers (see Lafrance et al., 1996; Rosenberg and Stuenitz, 2003) have suggested that these types of grain margins form by subgrain rotation and associated grain boundary migration at 'high temperatures'. Lafrance et al. (1996) suggested that these high temperatures range from 600 – 800 °C. In addition, it was also observed that many plagioclase crystals exhibit: (a) deformation twins, (b) deformation bands, and/or (c) undulose extinction. These features result from insertion and climbing of dislocations in the crystal lattice, and from intragranular diffusion. Both of these processes are facilitated by high temperatures (see Lafrance et al., 1996). In this study, the presence of serrated grain margins, interlobate grain margins, deformation twins, deformation bands and/or undulose extinction is used to suggest that plagioclase crystals were recrystallized and/or deformed at high temperatures.

Petrographic study shows that secondary mineral assemblages in plagioclase-pyroxene +/- olivine rocks consist of: (a) sericite, saussurite, chlorite, uralite and/or serpentine or (b) amphibole. Deer et al. (1992) suggested that the alteration of plagioclase to sericite (p. 443) and saussurite (p. 94), alteration of pyroxene to uralite (p. 257) and chlorite (p. 342), and the alteration of olivine to serpentine (p. 351), are commonly the result of pneumatolytic or hydrothermal alteration. The replacement of pyroxene with amphibole may also be related to hydrothermal alteration or retrogression at upper greenschist to lower granulite facies conditions (Deer et al., 1992, p. 256).

3.2.2 Electron microprobe analysis

Mineral chemistry data for plagioclase, pyroxene and/or olivine were obtained for country rocks and plutonic rocks. Full results are presented in Appendix 1 and are summarized in chapters 4 through 7. Minerals selected for analysis were circled with a pen prior to probe work. Mineral chemistry data are used in this study to calculate mineral compositions in terms of end-members. These mineral compositions are used to: (a) name rock types, (b) characterize units, (c) support the grouping of strongly deformed rocks with intrusive complexes, and (d) distinguish 'evolved' from 'primitive' plutonic rocks in the same pluton. In the last case, evolved rocks refer to those with relatively Fe-rich pyroxene +/- Na-rich plagioclase and primitive rocks refer to those with relatively Mg-rich pyroxene +/- Ca-rich plagioclase.

Mineral chemistry data were collected on a Cameca SX-50 microprobe at the Memorial University of Newfoundland and a JEOL JXA-8200 microprobe at the University of Calgary. Maggie Piranian and Michael Shaffer provided assistance at Memorial University, whereas Dr. Robert Marr provided assistance at the University of Calgary.

Analyzed minerals consist of plagioclase, orthopyroxene, clinopyroxene and olivine. Within each thin section, 4 – 7 grain cores and margins of each mineral were analyzed. Analyses with oxide totals < 98 wt% or >102 wt% were omitted when calculating mineral compositions. Obtaining a major element spectrum during microprobe analysis helped to identify Fe-Ti oxides and accessory phases.

Plagioclase was analyzed under a de-focused beam (~10 microns wide), a beam current of 10.00 amps and an accelerating voltage of 15.0 kvolts. Wavelength-dispersive spectrometry (WDS) was used to analyze Na, Al, Si, K, Ca and Fe, under peak time counts of 10 seconds. Pyroxene was analyzed under a focused beam (1 micron wide) and a beam current of 20.00 amps and accelerating voltage of 15.0 kvolts. WDS was used to analyze Na, Mg, Al, Si, Ca, Ti, Mn and Fe. Peak time counts were 10 seconds for Mg, Al, Si and Fe and 20 seconds for Na, Ca, Ti and Mn. Olivine was analyzed under a beam current of 20.00 amps and accelerating voltage of 15.0 kvolts. WDS was used to analyze Mg, Si, Mn and Fe. Peak time counts were 10 seconds for Mg, Si and Fe and 20 seconds for Mn.

Standards used for analyses consist of AN95 (anorthite, Ca, Al, Si), ALBI (albite, Na, Al, Si), ORTH (orthoclase, K, Si), ALMA (almandine, Mg, Fe, Si, Mn), FASY (fayalite, Fe) and JTHY (hypersthene, Mg, Si, Mn). Sample analysis was initiated when the condition:

$$0.98 < X_{element\ measured}/X_{element\ given} < 1.02$$

was met for the standard. These standards were analyzed intermittently to every 6 – 8 thin sections analyzed. This procedure ensured that the precision and accuracy of all electron microprobe analyses were within +/- 2%.

Conversion from wt% to stoichiometry was done using the method of Deer et al. (1992, p.678). In chapters 4 – 7, mineral compositions for plagioclase are expressed in terms of the end-member anorthite (An = An/(An + Ab)), pyroxene is expressed in terms of the end-member enstatite (En = En/(En + Fs)) and olivine is expressed in terms of the

end-member forsterite (Fo = Fo/(Fo + Fa)). The compositions presented for each sample comprise the mean of 4 – 6 core analyses. Compositional differences between the rims and cores are only noted if the difference is >2% end-member.

3.2.3 Considerations in naming of rock types and context for interpretation

The gabbroic plutonic rock classification of Streckeisen (1976, in Le Maitre, 2002) (Fig. 3.2) was used to name many rocks in this study and requires that plagioclase compositions are $>An_{50}$. However, many predominantly plagioclase- and pyroxene-bearing rocks collected during this study contain plagioclase that ranges from An_{40-50} in composition. In this thesis, all plagioclase-pyroxene-olivine rocks that show plagioclase compositions between An_{40-100} are named with the gabbroic plutonic rock classification of Streckeisen (1976, in Le Maitre, 2002). In the authors' opinion, use of the gabbroic rock classification in this way provides more continuity when naming anorthositic and related gabbronoritic rocks.

Le Maitre (2002, p. 80) stated that a ferrogabbro is "a variety of gabbro in which the pyroxenes and olivines are Fe-rich varieties…(and) plagioclase (is)…more calcic than An_{50} ". In addition, a ferrodiorite is a "rock of gabbroic appearance containing Fe-rich pyroxenes and olivines but with plagioclase more sodic than An_{50}" (Le Maitre, 2002, p. 79). In this study, the plagioclase composition that separates a ferrogabbro from a ferrodiorite is An_{40}. Furthermore, Fe-rich pyroxene compositions are herein defined as Fs>En.

The mineral chemistry of strongly deformed plagioclase-, pyroxene- +/- olivine-bearing rocks in the margins of centered intrusive complexes is here compared to the mineral chemistry of plagioclase-, pyroxene- +/- olivine-bearing rocks that comprise part of the: (a) country rock, and (b) cores of centered intrusive complexes. The purpose of these comparisons is to provide additional criteria (besides field relations, textures and structures) for grouping some strongly deformed rocks into the margins of centered intrusive complexes. These strongly deformed rocks may be analogous to the 'granulites of uncertain origin' and 'marginal granulites' of previous workers (see Davies, 1973b; Brand, 1974; Berg and Briegel, 1981; Royse et al., 1999).

Table 3.2: Summary of facies, event and chemistry classifications (see Xue and Morse, 1993; 1994; Yu and Morse, 1993) of anorthositic rocks in the Nain batholith, and U-Pb ages compiled from previous work (sources in chapter 2)

Intrusion	Facies	Event	Chemistry	Age (Ma)
NB noritic anorthosite				
Pearly Gates	pale	old anorthosite	noritic	1344 +/- 2
Lister	pale	old anorthosite	noritic	>1333 +/- 2
NB troctolitic anorthosite				
Paul Island	dark, pale	main anorthosite	Troctolitic, noritic?	1319 +/- 1
Kikkertavak	dark	main anorthosite	troctolitic	1311 +/- 2
Port Manvers Run	dark	old anorthosite	troctolitic	1308 +/- 2

Mineral chemistry data obtained for anorthositic rocks in this study are compared to 'NB noritic anorthosite' and 'NB troctolitic anorthosite' (Table 3.2). The 'NB noritic anorthosite' group is equivalent to pale-facies anorthosite of Wheeler (1960), old anorthosite event of Morse (1981b) and Yu and Morse (1994) and noritic anorthosite group of Xue and Morse (1993; 1994). The 'NB troctolitic anorthosite' group is equivalent to dark-facies anorthosite of Wheeler (1960), main anorthosite event of Morse

(1981b) and Yu and Morse (1993) and/or the troctolitic anorthosite group of Xue and Morse (1993; 1994). The data compiled from previous studies are compared to new data by direct comparison of plagioclase and orthopyroxene compositions (Table 3.3).

Table 3.3: Mineral composition data compiled from previous studies that are used to characterize NB noritic and troctolitic anorthosite.

Intrusion	Pl	Opx	Compiled from
	An	En	
NB noritic anorthosite			
Pearly Gates	40 - 43		in Berg et al., 1994
Noritic anorthosite	42 - 54	57 - 67	Xue and Morse, 1994
range	40 - 54	57 - 67	
NB troctolitic anorthosite			
Paul lower leucotroctolite	64 - 68		Wiebe, 1990a; Wiebe, 1992
Paul northern leuconorite	58		Wiebe, 1992
Paul upper leuconorite	54 - 60		Wiebe, 1990a; Wiebe, 1992
Port Manvers Run	45 - 60		Wiebe, 1992; in Berg et al., 1994
Troctolitic anorthosite	51 - 61	66 - 73	Xue and Morse, 1994
range	51 - 68	66 - 73	

Emslie (1975) subdivided orthopyroxene in anorthositic rocks of the Nain batholith into two types; those that crystallized at depth (type 1) and those that crystallized at the emplacement level (type 2). Type 1 orthopyroxene shows abundant exsolution of plagioclase and contains 4 – 9 wt% Al_2O_3 (Emslie, 1975). Type 2 orthopyroxene lacks exsolved plagioclase (Emslie, 1975). Pyroxenes with exsolved plagioclase and/or high wt% Al_2O_3 are also referred to as Al-rich pyroxene megacrysts (see Ashwal, 1993, p. 137) and high-Al orthopyroxene megacrysts (see Wiebe, 1992, p. 237; Ashwal, 1993, p. 139). These pyroxenes are referred to as 'high-Al pyroxene' in this study.

3.3 Whole rock chemistry

This section describes the analytical methods used to obtain whole rock geochemical data, precision and accuracy determinations, and the context within which these results are interpreted. Full results for whole rock chemistry are presented in Appendix 2, and summarized results are presented in chapters 4 through 7.

3.3.1 Whole rock geochemical analysis

Whole rock major and trace element data were obtained for samples that were collected in the field. These samples were selected to: (a) further characterize map units, and (b) aid in distinguishing strongly deformed gabbroic country rocks from plutonic rocks. Samples were cut into chips that contain no weathered surfaces and veinlets. Chips were rinsed with water and left to air-dry, after which they were crushed to gravel sized material. This material was placed in a tungsten-carbide casing and powdered within a centrifuge. The total weight of powders for individual samples ranges from 75 – 300 grams, with more rock crushed for coarser-grained samples.

For X-Ray Fluorescence (XRF) analysis, powders were dried in a furnace at 1050°C for 7 hours and then mixed with lithium metaborate and lithium tetraborate. The mixture was poured into a platinum crucible and a few drops of lithium bromide were added as a wetting agent. These crucibles were then placed in a Leco Fluxer and heated at ~850°C for 8.5 minutes and fused at ~1050°C for 11.5 minutes. The mixture was then poured into a platinum casting dish and left to cool. The cooled rock powder was weighed and mixed with phenolic resin binder. After mixing, this powder was placed in a

Herzog Pellet Press and pressed for 10 seconds at a pressure of 20 ton/in^2. The pellet was then baked at 200°C for 15 minutes. Pam King performed the analyses at the Memorial University of Newfoundland (see Appendix 2).

For Inductively Coupled Plasma-Mass Spectrometry (ICP-MS) analysis, 0.2 g of rock powder was sintered with sodium peroxide following procedures described in Longerich et al. (1990). The sintered powder was then dissolved in a rare earth element (REE) hydroxide-bearing precipitate. Pam King performed the analyses at Memorial University (see Appendix 2).

Standards for major elements consist of SY-2-G (Na, Al, Si, P, K, Mn) and MRG-1-G (Mg, Ca, Ti, $Fe^{3+}T$). Each standard was analyzed four times for every 20 samples analyzed. The mean wt% of major elements obtained in these four runs was compared to values provided by Govindaraju (1989). In all cases, the mean wt% of the four analyses was the same as the values provided by Govindaraju (1989).

Standards for trace elements consist of DTS-1 (Ni), BHVO-1 (Cu, Zn), MRG-1-G (Sc, V, Cr), SY-2 (Ga, Rb, Sr, Y, Zr, Ba, Pb, Th, U), PACS-1 (As) and SY-3 (Nb, Ce). Each standard was analyzed four times for every 20 samples analyzed. The means of these four analyses were compared with values given by Govindaraju (1989). The accuracy for Ni, Cu, As, Sr and Ce analyses were within 1% of the concentrations given in Govindaraju (1989); Zn, Ga, Rb, Ba, U and Pb analyses were within 1.38 – 3.81 %; Y, Zr and Th analyses were within 5.71 – 8.44%; and Nb analyses were within ~70%. In this study, only trace elements that are accurate within 4% are compared with results from previous studies (i.e. Ni, Cu, As, Sr, Ce, Zn, Ga, Rb, Ba, U, Pb).

The precision of these analyses was calculated by:

(standard deviation of element over 4 runs/

measured ppm of element in 1 run)*100

and ranged between 0.00 – 3.33% of the standard deviation. The high precision of all analyses indicates that the abundances of all trace elements in the samples from this study may be compared to each other. The trace elements that are of particular interest in this study are those that are abundant in plagioclase (Sr, Ba) and those that are abundant in the intercumulus minerals (pyroxene, Fe-Ti oxide) of anorthositic rocks (Sc, V, Zr).

3.3.2 Context used in interpretation

The whole rock chemistry of strongly deformed rocks in the margins of intrusive complexes is compared to the whole rock chemistry of country rocks. The purpose of this comparison is similar to that for the mineral chemistry comparison, namely to provide additional criteria (besides field relations, textures and structures) for grouping some strongly deformed rocks into the margins of centered intrusive complexes. As noted, these strongly deformed rocks may be analogous to the 'granulites of uncertain origin' and 'marginal granulites' of previous workers (see Davies, 1973b; Brand, 1974; Berg and Briegel, 1981; Royse et al., 1999).

Whole rock chemistry data obtained for anorthositic rocks in this study are compared to data for 'NB noritic anorthosite' and 'NB troctolitic anorthosite' (see Table 3.2). Comparative data are presented in Table 3.4 and closely follow a study of anorthositic whole rock geochemistry by Xue and Morse (1993), which found that noritic

Table 3.4: Compiled whole rock chemistry data and ranges for NB noritic and troctolitic anorthosite. Data compiled from (1) Berg et al., 1994, (2) Wiebe, 1990a, (3) Wiebe, 1992 and (4) Xue and Morse, 1993

Intrusion	Rock type	SiO_2	Al_2O_3	CaO	Na_2O	K_2O	Rb	Ba	Sr	Source
		wt%	wt%	wt%	wt%	wt%	ppm	ppm	ppm	
NB noritic anorthosite										
Lister	anorthosite	57.36	26.64	8.79	5.45	0.84	3.4	506	932	4
Pearly Gates	anorthosite	57.26	25.55	7.69	5.71	1.21	6.2	614	776	4
Pearly Gates	anorthosite	58.16	26.04	8.21	5.95	0.97	3.1	445	771	4
Pearly Gates	anorthosite	55.27	24.77	7.87	5.51	0.88	3.4	377	719	4
Pearly Gates	anorthosite	56.85	26.11	8.63	5.71	0.84	3.0	392	769	1
Pearly Gates	anorthosite	57.13	26.75	8.94	5.71	0.82	3.0	412	790	4
Pearly Gates	anorthosite	56.63	26.91	9.01	5.53	0.95	4.0	419	805	1
Pearly Gates	anorthosite	55.82	27.53	9.73	5.37	0.70	2.4	310	812	4
Pearly Gates	anorthosite	54.80	26.52	9.21	5.01	0.78	3.3	254	707	4
Pearly Gates	leuconorite	51.94	19.24	7.88	4.55	1.24	5.3	966	568	4
Pearly Gates	leuconorite	55.30	24.03	7.84	5.08	1.01	4.4	463	718	4
Pearly Gates	leuconorite	55.89	27.03	9.58	5.14	0.71	2.9	301	804	4
Pearly Gates	leuconorite	55.10	27.15	10.16	5.03	0.63	1.5	333	754	4
Pearly Gates	leuconorite	55.81	22.76	7.66	4.86	0.72	2.5	352	609	1
mean		55.95	25.50	8.66	5.33	0.88	3.5	439	752	
range		52 - 58	19 - 27	7.6 - 10.2	4.5 - 6.0	0.6 - 1.2	1.5 - 6.2	254 - 966	568 - 932	
NB troctolitic anorthosite										
Kikkertavak	anorthosite	54.94	27.68	10.66	5.04	0.43	1.4	278	705	4
Kikkertavak	anorthosite	54.08	27.81	11.15	4.71	0.34	2.0	217	735	4
Kikkertavak	leuconorite	53.60	26.48	10.89	4.51	0.41	1.5	296	734	4
Kikkertavak	leuconorite	53.63	24.56	9.90	4.18	0.32		221	647	4

Table 3.4 cont. (Paul I LTR is Paul Island lower leucotroctolite; Paul I ULN is Paul Island upper leuconorite; PMR is Port Manvers Run)

Intrusion	Rock type	SiO_2	Al_2O_3	CaO	Na_2O	K_2O	Rb	Ba	Sr	Source
		wt%	wt%	wt%	wt%	wt%	ppm	ppm	ppm	
Kikkertavak	leuconorite	53.41	24.15	9.70	3.70	0.30	1.3	190	609	4
Kikkertavak	leucotroctolite	52.16	25.04	10.25	4.06	0.29	1.5	187	625	4
Kikkertavak	leucotroctolite	51.25	24.75	10.30	3.86	0.24		154	592	4
Kikkertavak	leucotroctolite	50.34	24.47	10.34	3.65	0.19	0.5	121	560	4
Paul I LTR	leucotroctolite	50.52	27.03	11.59	3.66	0.20		126	597	3
Paul I LTR	leucotroctolite	50.30	23.77	10.40	3.20	0.24		148	553	2
Paul I LTR	leucotroctolite	52.02	28.43	12.38	3.77	0.26		174	617	3
Paul I LTR	leucotroctolite	48.87	24.59	10.81	3.15	0.24		146	533	3
Paul I LTR	leucotroctolite	49.12	25.26	11.28	2.99	0.18		120	520	2
Paul I ULN	leuconorite	53.66	24.50	10.15	4.30	0.44		230	603	2
Paul I ULN	leuconorite	52.46	22.31	9.79	3.80	0.38		252	599	2
Paul I ULN	leuconorite	53.69	24.91	9.99	4.23	0.37		221	656	3
Paul I ULN	leuconorite	52.67	25.09	10.49	3.88	0.29		190	626	3
Paul I ULN	leuconorite	52.61	27.12	11.42	4.15	0.30		181	582	3
PMR	anorthosite	54.35	26.91	10.45	4.97	0.47	2.9	307	672	4
PMR	anorthosite	54.08	26.30	10.55	4.66	0.43	4.0	268	672	1
PMR	anorthosite	53.59	28.43	11.61	4.59	0.39	4.0	192	685	4
PMR	leuconorite	54.69	24.18	9.84	4.53	0.55	3.6	320	630	4
PMR	leucotroctolite	50.02	21.00	8.86	3.69	0.41	3.6	235	511	4
PMR	leucotroctolite	48.57	21.37	9.06	3.42	0.36	4.3	196	514	4
PMR	leucotroctolite	48.57	21.37	9.06	3.42	0.36				4
mean		52.13	25.10	10.44	4.00	0.34	2.6	207	616	
range		48 - 55	21 - 29	8.8 - 12.4	2.9 - 5.1	0.1 - 0.6	0.5 - 4.3	120 - 320	511 - 735	

anorthosite shows high wt% SiO_2, wt% K_2O and ppm Sr, whereas troctolitic anorthosite shows high CaO/Al_2O_3 and Ba/K (Table 3.4). In this thesis, the whole rock chemistry of anorthositic rocks is described in terms of wt% SiO_2, wt% K_2O, Ba/K, Sr/Ca, Ca/Al and Mg/(Fe+Mg).

The Cross, Iddings, Pirsson and Washington (CIPW) norms were calculated using Igpet 2000 (Carr, 2000) and with all Fe expressed as wt% FeOt (wt% FeOt = wt% FeO + 0.8998*(wt% Fe_2O_3)). A written description of the CIPW norm calculation is given in Philpotts (1990, p. 89). These norms are presented in Appendix 3, and were used to calculate abundances of normative plagioclase (albite + anorthite), normative pyroxene (hypersthene + diopside + wollastonite) and normative olivine. Normative plagioclase compositions were calculated by dividing normative anorthite by normative plagioclase abundance (An/(An+Ab).

3.4 U-Pb isotope analysis

Thermal Ionization Mass Spectrometry (TIMS) analysis was done on zircons separated from four samples of plutonic rock. These samples were split with a hydraulic press, crushed into gravel with a jaw crusher and powdered with a disc mill. First order separation of light and heavy minerals was done on the Wilfley table, after which samples were rinsed with ethanol and dried using a hot plate. The heavy fraction was sieved to remove large grains and then exposed to a hand magnet to remove highly magnetic minerals. The nonmagnetic fraction was then separated into light and heavy fractions using methylene iodide. Both fractions were rinsed with acetone and dried using

a hot plate. Magnetic minerals in the heavy fraction were removed with a Frantz isodynamic magnetic separator. Magnetic separation was done at an angle of 10° and 0.5, 1.0 and 1.7 amps, after which the angle was progressively reduced to 5°, 3°, 1° and 0°. Zircons were handpicked out of the final nonmagnetic fraction. The morphology and internal structures of these zircons were examined with a binocular microscope and by backscatter electron imaging with a scanning electron microscope. Handpicked zircons were abraded following the method of Krogh (1982). Dissolution and isotopic analysis were done by Dr Marc Poujol at the Memorial University of Newfoundland and are described in Appendix 4.

The samples were measured on a Finnigan MAT262 mass spectrometer equipped with an ion-counting secondary electron multiplier. The calculation of common Pb was made by subtracting blanks and then assuming that the remaining common Pb has a Proterozoic composition determined from the model of Stacey and Kramers (1975). Data were reduced using PbDat (Ludwig, 1993). Analytical uncertainties are listed at 2σ and age determinations were processed using Isoplot/Ex (Ludwig, 2003).

3.5 Outline of the thesis

The remainder of this thesis is divided into 6 chapters. The next four chapters describe the geology of country rock (chapter 4) and centered intrusive complexes (chapters 5, 6, 7). Chapter 8 is the discussion and chapter 9 presents conclusions and recommendations for future work.

The chapter on country rocks (4) is divided into three sections. The first section (4.1) describes the structure and composition, petrography, mineralogy and geochemistry of the types of country rock in the study area, and suggests regional correlations. The second section (4.2) describes how the different types of country rock form belts and suggests structural correlations of these belts to regional deformation. The third section (4.3) is a chapter summary.

The chapters on centered intrusive complexes (5, 6, 7) are divided into sections that: (1^{st}) describe the form, contacts, petrography, textures, structures, mineral chemistry, whole rock chemistry and/or geochronology of plutons or sheets, (2^{nd}) describe the tectonic overprint, and (3^{rd}) summarize the overall structure of the centered intrusive complex in terms of a core, margin and tectonic overprint.

Chapter 8 is a discussion that describes (8.1) the origin of strongly deformed rocks in the margins of centered intrusive complexes, (8.2) the tectono-magmatic setting of magmatism in the Nain batholith, (8.3) the emplacement of centered intrusive complexes, (8.4) the origin of textures and structures in anorthositic rocks, and (8.5) the compositional evolution of anorthositic magmas in the study area and in the Nain batholith as a whole. Chapter 9 presents the conclusions of this study and provides some directions for future research in the study area.

Chapter 4: Country rock

The geological maps of Wheeler (1969) and Ryan (1990) show that the study area consists of Mesoproterozoic Nain batholith (NB) plutonic rocks that are interspersed with belts of Archean and Paleoproterozoic country rock (see Fig. 3.1). These belts of country rock are described in this chapter and consist of granitoid and amphibolite gneiss, gabbroic granulite, metasedimentary gneiss and enderbitic gneiss. The first part of the chapter describes the structure, mineralogy and/or whole rock chemistry for these units of country rock and proposes correlations through comparison to previous studies on the areas Archean and/or Paleoproterozoic rocks. The second part of this chapter describes how these different units of country rock form structural belts (here referred to as Anaktalik Brook, Kangilialuk Lake, Nain Hill, Kauk Harbour) and how these belts relate to the regional structures in Archean and/or Paleoproterozoic rocks.

4.1 Units of country rock

4.1.1 Granitoid and amphibolite gneiss

Geological mapping by Wheeler (1969; 1972a) showed that a unit of basement granulite occurs in the southwestern part of the study area. Mapping by Ryan and Lee (1986) and Ryan (1996) in the same area found banded grey gneiss and amphibolite (Ryan and Lee, 1986) and grey migmatite (Ryan, 1996) that they grouped into Archean rocks of the North Atlantic craton (Nain Province in Ryan and Lee, 1986; Ryan, 1996).

The southwestern part of the present study area contains a unit of layered granitoid and amphibolite gneiss (Fig. 4.1). This unit is absent from country rock belts in

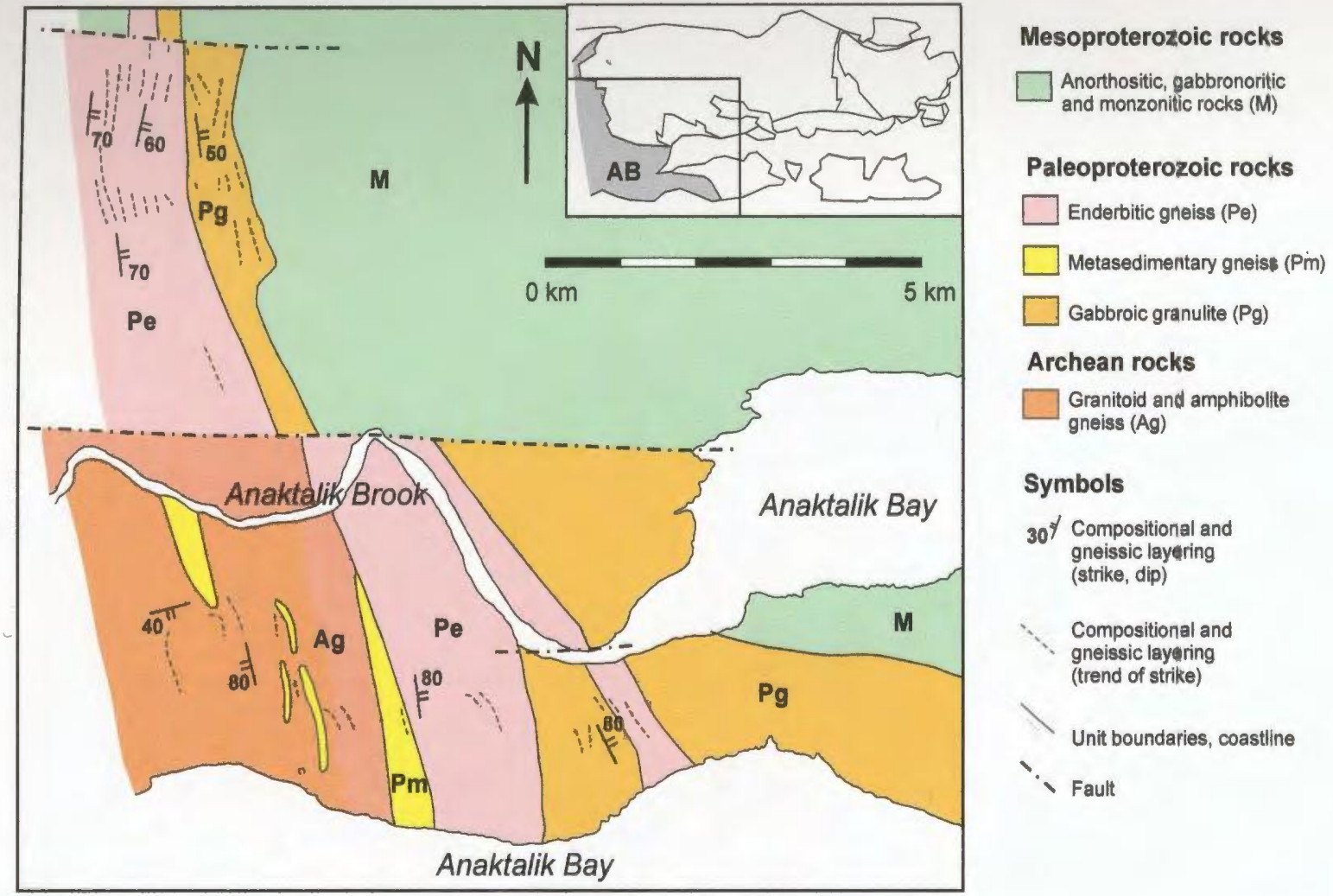

Figure 4.1: Solid geological map for the southern part of the Anaktalik Brook country rock belt (AB). The Mesoproterozoic rocks comprise part of the Nain batholith. The northern part of this belt is shown in Fig. 5.4.

the eastern part of the study area (Fig. 4.2). The granitoid and amphibolite gneisses were cut by enderbitic gneiss (Fig. 4.3). This unit of enderbitic gneiss is described in a later section of this chapter.

Granitoid layers weather pale grey to white and consist of small feldspar and purple quartz grains. Amphibolite layers consist of small plagioclase, hornblende and pyroxene grains. Preferred mineral orientations are shown by lens-shaped quartz crystals in granitoids, and lens-shaped hornblende crystals in amphibolites.

Alternations of granitoid gneiss and amphibolite gneiss comprise a compositional layering that is sub-vertical and north-south striking. In the southwestern-most outcrops of the study area, this compositional layering swings around into an orientation that is moderately (40°) south dipping and east-west striking (see Fig. 4.1). This swing in orientation suggests a regional synform. Individual layers are 0.1 – 10 cm thick (see Fig. 4.3), were folded and were disrupted into boudins. Some layers show elliptical forms (10 – 30 cm long axis) that indicate fold-interference patterns.

This unit of granitoid and amphibolite gneiss is similar to the descriptions in Ryan and Lee (1986) of Archean banded grey gneiss and amphibolite of the North Atlantic craton. An Archean age is also suggested by the relatively high abundance of poly-deformed structures, which contrasts with the single planar fabric found in most Paleoproterozoic country rocks (see below).

The mineralogy and poly-deformed structures of these rocks are distinct from the plagioclase-pyroxene mineralogy and single-phase deformed structures that characterize deformed rocks of the Mesoproterozoic Nain batholith.

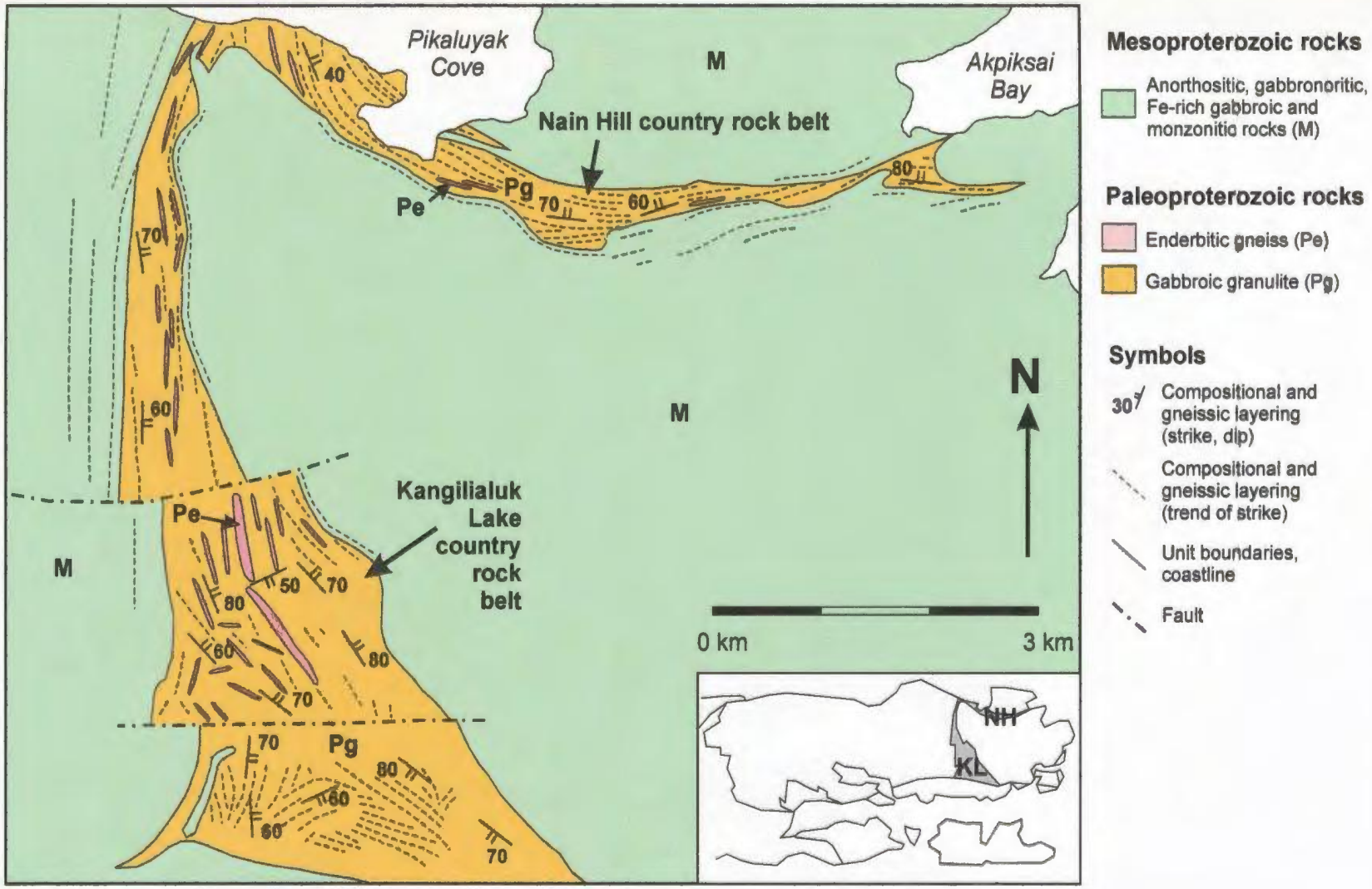

Figure 4.2: Solid geological map of the Kangilialuk Lake (KL) and Nain Hill (NH) country rock belts. The Mesoproterozoic rocks comprise part of the Nain batholith, and the map also shows the trend of strongly deformed compositional layers in these Mesoproterozoic rocks. The Nain Hill country rock belt is also shown in Fig. 6.3.

4.1.2 Gabbroic granulite

Previous geological mapping has identified units of Archean and/or Paleoproterozoic gabbroic granulite in the northeastern and southwestern parts of the study area, and ~6 km east of the study area on Paul Island. In the northeastern part of the study area (Fig. 4.2), geological mapping by Rubins and de Waard (1971) described two zones of layered norite and olivine-pyroxene granulite. Subsequent mapping in the same area by Ryan (2000a; 2001a) grouped these rocks into a unit of Archean layered mafic gneiss. In the southwestern part of the study area (Fig. 4.1), geological mapping by Wheeler (1972a) described a unit of stretched anorthositic rocks. Subsequent mapping in the same area by Ryan and Lee (1986) and Ryan (1991b; 1996) found meta-anorthosite and meta-leucogabbro that they grouped into Archean gneiss of the North Atlantic craton. East of the study area, geological mapping by Palansky (1972) described granular gabbroic rocks in the Bridges layered intrusion. This intrusion lies ~6 km east of the study area. A study by Ashwal et al. (1992) established a Sm-Nd isochron age for this intrusion at 1667 +/- 75 Ma. Subsequent mapping by Ryan (2000a; 2001a) found that this intrusion overlies an older anorthositic unit. This older anorthositic unit was named the Quarry intrusion by Ryan (2001a).

Several workers (see Wheeler, 1960; Berg and Briegel, 1981; Royse et al., 1999) have described gabbroic granulites in other parts of the Nain batholith that are possibly Mesoproterozoic in age. These granulites are generally localized along the margins of anorthositic intrusions and may be gradational into adjacent anorthositic rocks.

In this study, gabbroic granulite refers to a unit of country rock that is: (a) predominantly plagioclase-, pyroxene- and/or olivine-bearing, (b) strongly deformed, and (c) granular in texture. This section provides an overview of the structure, petrography, mineral compositions and whole rock chemistry for these gabbroic granulites. The geology and chemistry of these rocks is contrasted with strongly deformed, plagioclase- and pyroxene-bearing rocks that were here grouped into the margins of centered intrusive complexes. The end of this section suggests some regional correlations for gabbroic granulite in the country rock.

Structure and texture

Gabbroic granulite contains various abundances of small to medium-sized plagioclase, pyroxene and/or olivine grains. Small hornblende grains occur in minor abundances. Tabular plagioclase and poikilitic pyroxene grains are of relatively minor abundance and are interpreted as relict igneous grains. The overall texture of these rocks is granular, and the overall compositions include gabbronorite, melagabbronorite, olivine gabbro, olivine melagabbronorite, leucogabbronorite and anorthosite. All of these rock types occur as xenoliths in enderbitic gneiss (Fig. 4.4) and NB rocks (Fig. 4.5).

Gabbroic granulite is compositionally layered and foliated. Compositional layers are mostly steeply (60° – 80°) east dipping to sub-vertical and north-south to northwest-southeast striking. In the Kangilialuk Lake country rock belt, gabbroic granulite forms an antiform with a broadly northwest to southeast trending fold axis, and a synform with an arcuate fold axis that ranges in trend from broadly north-south in the northwest to east-

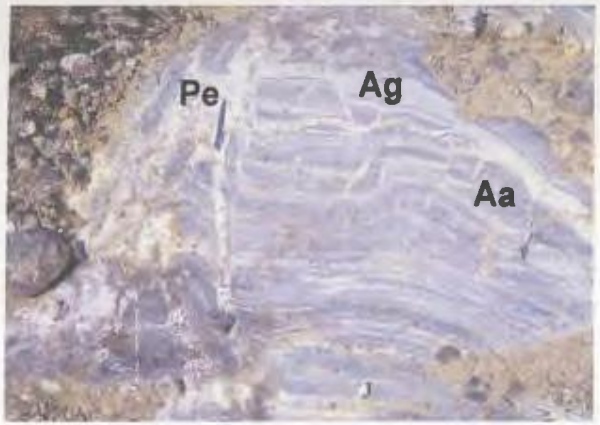

Figure 4.3: Gneissic layering in granitoid (Ag) and amphibolite (Aa) gneiss of the Anaktalik Brook country rock belt. This photo shows sub-vertical and north-south striking compositional layers that were cut by veins of enderbitic gneiss (Pe). Photo taken west of the Akuliakatak Peninsula.

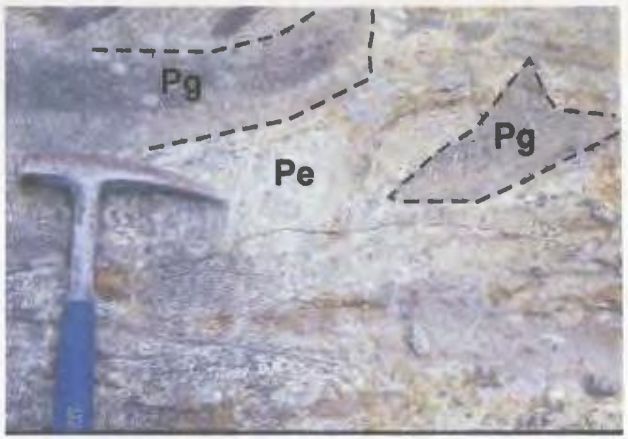

Figure 4.4: Angular xenoliths of gabbroic granulite (Pg) in enderbitic gneiss (Pe) of the Kangilialuk Lake country rock belt. Dashed lines show the outlines of the xenoliths. Photo taken northwest of Kangilialuk Lake.

Figure 4.5: Angular xenolith of gabbroic granulite that has weathered out of Mesoproterozoic anorthositic rocks of the Sophie centered intrusive complex. Photo taken northwest of Kangilialuk Lake.

Figure 4.6: Elliptical layer of anorthositic rock in gabbroic granulite of the Kangilialuk Lake country rock belt. This elliptical form is a fold-interference pattern that indicates poly-deformation. Photo taken south of Kangilialuk Lake.

west in the southeast. In the vicinity of Pikaluyak Cove and Akpiksai Bay (Fig. 4.2), compositional layers are steeply north dipping (60° – 80°) and east-west striking. Individual layers are 0.01 – 20 m thick. As well, these layers were folded and disrupted into boudins that indicate that they were deformed. Some compositional layers show elliptical forms (Fig. 4.6) that indicate fold interference patterns. Foliated rocks contain lens-shaped pyroxene grains that strike parallel to compositional layering.

Petrography and mineralogy

Plagioclase, orthopyroxene, clinopyroxene and/or olivine are small to medium-sized and granular in form. These grains meet at triple junctions that indicate the grain margins were equilibrated at high-T. Plagioclase grains show deformation twins, undulose extinction and fractures that indicate they were deformed. Likewise, orthopyroxene and clinopyroxene grains show abundant fractures and kink bands that also indicate they were deformed. Both types of pyroxene are rimmed by brown hornblende that suggests equilibration under amphibolite-facies conditions. Olivine grains show fractures and alteration to serpentine, indicating they were deformed and hydrothermally altered.

Mineral compositions were obtained for a wide range of rock types in order to establish additional context in distinguishing strongly deformed gabbroic granulites in the country rock from those in the margins of centered intrusive complexes. For gabbroic granulite in the country rock, mineral compositions range from An_{51-81} in plagioclase,

En_{58-85} in orthopyroxene and Fo_{63-83} in olivine (Table 4.1). This range in mineral compositions is shown on Fig. 4.7, and is used in chapters 5, 6 and 7 to compare the

Table 4.1: Mineral compositions for gabbroic granulite (Pg) and comparative data for NB gabbronoritic rocks (NB gn), NB anorthositic rocks (NB anor), and the Paleoproterozoic Bridges intrusion (*data from this study, ** data from Ashwal et al., 1992)

Rock type	Sample	Pl	Opx	Ol
		An	En	Fo
Gabbroic granulite (Pg)				
gn	01-16-26	51		
gn	01-14-18	52	58	
gn-mgn	00-22-14	81	69	
mgn	00-27-25	60	74	
mgn	00-4-4d	62		
ol gb	02-27-5	78		63
ol mgn	01-14-16		82	79
ol mgn	01-16-16		85	83
ol mgn	01-29-7a	62	77	72
range		51 - 81	58 - 85	63 - 83
Comparative data				
NB gn*		35 - 64	47 - 72	
NB anor*		43 - 64	31 - 71	
Bridges**		60 - 80	71 - 75	66 - 71

mineral compositions of gabbroic granulite to those gabbroic rocks that occur in the margins of centered intrusive complexes. Plagioclase compositions fall in the range shown by olivine gabbro in the Paleoproterozoic Bridges layered intrusion and are Ca-rich in comparison to most of the NB rocks in the study area (Fig. 4.7). Orthopyroxene compositions for gabbroic granulite fall in the range shown by the olivine-bronzite granulite of Rubins and de Waard (1971, En_{83}), olivine gabbro in the Bridges layered intrusion (En_{71-75}, in Ashwal et al., 1992) and are Mg-rich in comparison to most of the NB rocks of the study area. Orthopyroxene in gabbroic granulite contains 1.39 – 2.35 wt% Al_2O_3, which is high in comparison to orthopyroxene in NB rocks of the study area

(0.23 – 2.26 wt% Al_2O_3). Olivine compositions fall in the range shown by olivine-bronzite granulite of Rubins and de Waard (1971, Fo_{84}) and olivine gabbro in the Bridges layered intrusion (Fo_{66-71}, in Ashwal et al., 1992). In contrast, olivine is mostly absent from NB rocks of the study area.

Whole rock chemistry

Whole rock chemistry was obtained for several gabbroic granulites in the country rock in order to establish additional context to distinguish strongly deformed gabbroic granulite in the country rock from those in centered intrusive complexes. The whole rock chemistry presented here is described for groups that consist of: (1) pyroxene-rich gabbroic granulite, and (2) olivine-rich gabbroic granulite.

Pyroxene-rich gabbroic granulite consists of gabbronorite and melagabbronorite. Whole rock chemistry of pyroxene-rich gabbroic granulite comprises a sum of 94 – 96 wt% SiO_2 + MgO + FeOt + CaO + Al_2O_3 (Table 4.2), reflecting high abundances of pyroxene and Ca-rich plagioclase. In comparison to NB gabbronoritic rocks in the study area, pyroxene-rich gabbroic granulite shows relatively high wt% MgO and CaO/Al_2O_3, and relatively low wt% SiO_2, wt% Na_2O, ppm Sr and ppm Ba (see Fig. 4.11). Trace element abundances for pyroxene-rich gabbroic granulite are high for Cr (419 – 1875 ppm), V (166 – 255 ppm) and Sc (27 – 41 ppm). CIPW norms consist mostly of plagioclase, pyroxene and olivine, which contrasts with the predominantly pyroxene- and plagioclase-bearing norms obtained for the NB gabbronoritic rocks in the study area.

Olivine-rich gabbroic granulite consists of olivine gabbro and olivine melagabbronorite. Whole rock chemistry of olivine-rich gabbroic granulite comprises a sum of 96 – 98 wt% SiO_2 + MgO + FeOt + Al_2O_3 + CaO (Table 4.2), reflecting high abundances of olivine and Ca-rich plagioclase. In comparison to gabbronoritic plutonic rocks in the study area, olivine-rich gabbroic granulite shows relatively high wt% MgO and CaO/Al_2O_3, and relatively low wt% SiO_2, wt% Na_2O, ppm Sr and ppm Ba (see Fig. 4.11). Trace element abundances for olivine-rich gabbroic granulite are high for Cr (188 – 2008 ppm) and Sc (11 – 26 ppm). CIPW norms consist mostly of plagioclase, pyroxene and olivine, which contrasts with the predominantly pyroxene- and plagioclase-bearing norms found for NB gabbronoritic rocks in this study.

Table 4.2: Whole rock chemistry for pyroxene- and olivine-rich gabbroic granulite (Pg), and comparative data for NB gabbronoritic rocks and the Paleoproterozoic Bridges intrusion (*data from this study, ** data from Ashwal et al., 1992)

Rock type	Sample	SiO_2	TiO_2	Al_2O_3	FeOt	MgO	CaO	P_2O_5
		wt%	wt%	wt%	wt%	wt%	wt%	wt%
Pyroxene-rich Pg								
gn	01-16-26	48.08	0.78	14.57	11.44	6.84	13.24	0.08
gn	01-30-12b	46.91	0.51	10.08	12.58	17.15	9.54	0.01
gn	02-22-8b	45.94	0.39	15.31	10.63	13.81	10.73	0.03
mgn	00-27-25	48.87	0.51	5.01	11.69	16.45	13.57	0.03
range		46 - 49	0.4 - 0.8	5 - 15	11 - 13	7 - 17	10 - 14	<0.1
Olivine-rich Pg								
ol gb	02-27-5	44.03	0.45	16.92	11.71	10.71	13.09	0.02
ol mgn	02-22-8a	45.76	0.39	3.05	11.90	27.97	7.31	0.01
ol mgn	01-16-16	44.14	0.44	1.73	12.98	30.53	8.26	0.00
ol mgn	01-29-7a	45.33	0.35	8.15	12.96	22.53	7.33	0.02
range		44 - 46	0.4 - 0.5	2 - 17	12 - 13	11 - 31	7 - 13	<0.1
Comparative data								
NB gn*		42 - 53	0.1 - 4.9	11 - 18	10 - 19	3 - 14	8 - 12	0.0 - 2.2
Bridges**		43 - 49	0.1 - 1.1	6 - 24	3 - 13	6 - 18	11 - 17	<0.1

Regional correlations

The mineralogy of gabbroic granulite in the study area correlates with: (1) Archean layered mafic rocks (see Ryan and Lee, 1986; Ryan, 2000a, 2001a), (2) Paleoproterozoic olivine gabbro (see Palansky, 1972; Ashwal et al., 1992), and (3) Mesoproterozoic 'marginal granulites' (see Berg and Briegel, 1981; Royse et al., 1999). In the study area, gabbroic granulite was cut by enderbitic gneiss. Later in this chapter (see section 4.1.4), it is proposed that enderbitic gneiss is related to Paleoproterozoic (1910 – 1865 Ma, in Scott, 1998) unit of enderbitic (calc-alkaline) gneiss. These relations suggest that the gabbroic granulite unit in the study area is older than ~1910 Ma.

An Archean age for these country rocks was favoured by Ryan and Lee (1986) and Ryan (1996; 2000a; 2001a). Ryan (2001a, p. 131) states, however, that these rocks are "unusual within the Archean of northern Labrador". An Archean age remains a possibility in light of this study as well.

A Paleoproterozoic age for these rocks is somewhat precluded by the 1667 +/- 75 Ma Sm-Nd isochron age (in Ashwal et al., 1992) of the Bridges layered intrusion, which comprise the only known example of Paleoproterozoic gabbroic granulite in the study area. However, the large error on the isochron and the lack of U-Pb isotope data suggest that a lack of correlation between these units is still a tentative conclusion. This conclusion is especially tentative in light of the spatial association and the similarity in rock types between the unit of gabbroic granulite and The Bridges intrusion.

An alternative Paleoproterozoic association is that gabbroic granulite comprises part of the Arnanunat Plutonic Suite (2130 – 2040 Ma in Ryan and James, 2003). This

Plutonic Suite consists of AMCG suite rocks, which are known to be associated with layered gabbroic intrusions in some cases (ex. Nain batholith). In addition, the U-Pb ages show that the Arnanunat Plutonic Suite pre-dates enderbitic gneiss by ~300 m.y.. On the other hand, gabbroic rocks have not been reported as comprising part of the Arnanunat Plutonic Suite.

With respect to NB rocks in the study area, gabbroic granulite in the country rock: (a) is older, (b) is poly-deformed, (c) contains relatively abundant olivine, (d) shows more Ca-rich plagioclase compositions, (e) shows more Mg-rich pyroxene compositions, (f) shows higher whole rock wt% MgO, wt% CaO, ppm Cr and ppm Sc, and (g) contains relatively abundant normative olivine. These characteristics of gabbroic granulite in the country rock are used in the remainder of this thesis to provide additional criteria in distinguishing gabbroic granulite in the country rock from strongly deformed NB rocks in the margins of centered intrusive complexes. For comparative purposes, the gabbroic granulite in the country rock is referred to as 'Paleoproterozoic gabbroic granulite' in chapters 5 through 7.

4.1.3 Metasedimentary gneiss

Wheeler (1972a, 1973) described a unit of cordierite- and garnet-bearing paragranulite that lies in the southwestern part of the study area. Ryan and Lee (1986) describe these rocks as comprising Archean magnetite-bearing quartzite, sillimanite-bearing psammite and marble/calc-silicate rock. A geological map by Ryan (1990) shows that the Paleoproterozoic Tasiuyak paragneiss occurs immediately south of the study

area. Wardle et al. (2002) stated that the Tasiuyak paragneiss comprises garnet-sillimanite-biotite-graphitic pelitic gneiss and up to 80% leucogranite.

Geological mapping as part of this study outlined a unit of layered metasedimentary gneiss in the southwestern part of the study area (see Fig. 4.1). This unit consists of meta-pelite and meta-quartzite. Pelite layers contain small to large feldspar grains, biotite laths, muscovite laths, rectangular sillimanite porphyroblasts, round garnet porphyroblasts and quartz grains. Quartzite layers contain mostly small to medium-sized quartz grains. Pelite and quartzite are interleaved and form gneissic layers that are 0.1 – 50 m thick, sub-vertical and north-south striking. These compositional layers were folded and disrupted into boudins (Fig. 4.8). Veins of granitic rock are common throughout the metasedimentary gneiss unit and comprise up to 20% of some exposures.

Metasedimentary gneiss in the study area is similar to the description of Paleoproterozoic Tasiuyak paragneiss in Wardle et al. 2002, in that: (1) it is garnet-sillimanite-biotite bearing, and (2) contains veins of granitic rocks. Hence, in this study the metasedimentary gneiss is tentatively considered to be Paleoproterozoic in age. However, an Archean age is not ruled out for these rocks since Ryan and Lee (1986) and Ryan (1996) found that these metasedimentary rocks are similar to those that occur in Archean rocks ~100 km northeast of the study area.

4.1.4 Enderbitic gneiss

Rubins and de Waard (1971) described a unit of enderbitic rock that cut gabbroic granulite to the west of Nain. This unit occurs in the northeastern part of the study area.

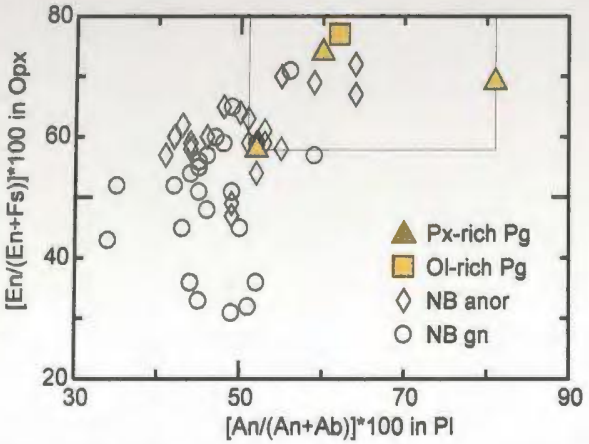

Figure 4.7: Comparison of mineral compositions in pyroxene- and olivine-rich gabbroic granulite (Pg), with NB anorthositic and gabbro-noritic rocks from this study. The box outlines the range of mineral compositions obtained for gabbroic granulite in this study and is used for further comparison in chapters 5 through 7.

Figure 4.8: Compositional layering between pelite (pe) and quartzite (qz) in metasedimentary gneiss of the Anaktalik Brook country rock belt. Photo taken west of the Akuliakatak Peninsula.

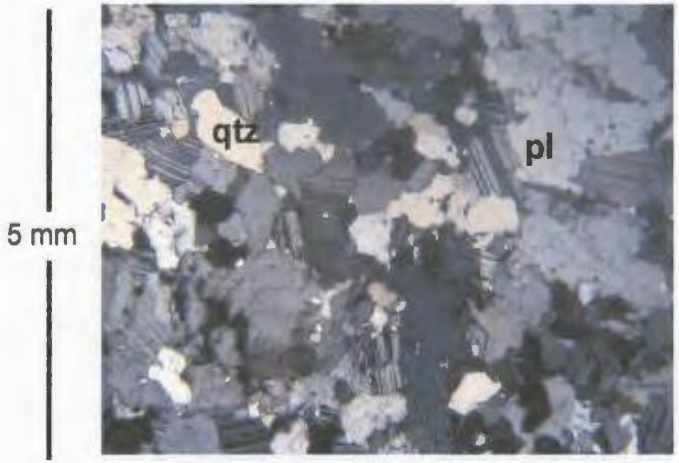

Figure 4.9: Thin section photo (XPL) of quartz diorite in the Kangilialuk Lake country rock belt. Plagioclase (pl) and quartz (qtz) show serrated and interlobate grain margins.

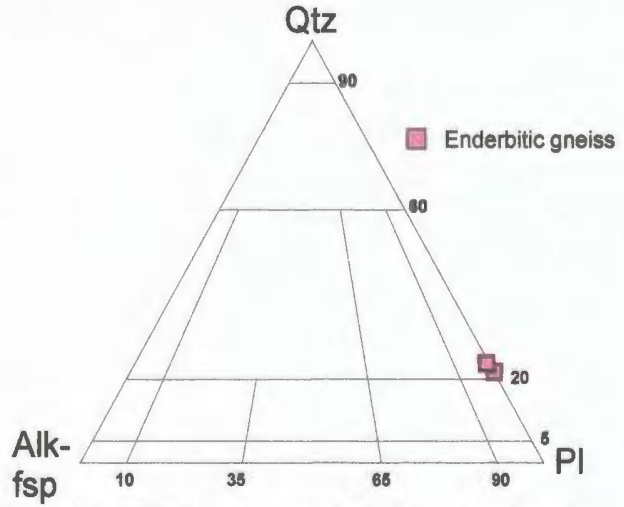

Figure 4.10: CIPW norms of enderbitic gneiss plotted on an QAFP diagram that follows Streckeisen (1976, in Le Maitre, 2002, p. 22). The norms show a mode that indicates the samples are tonalites.

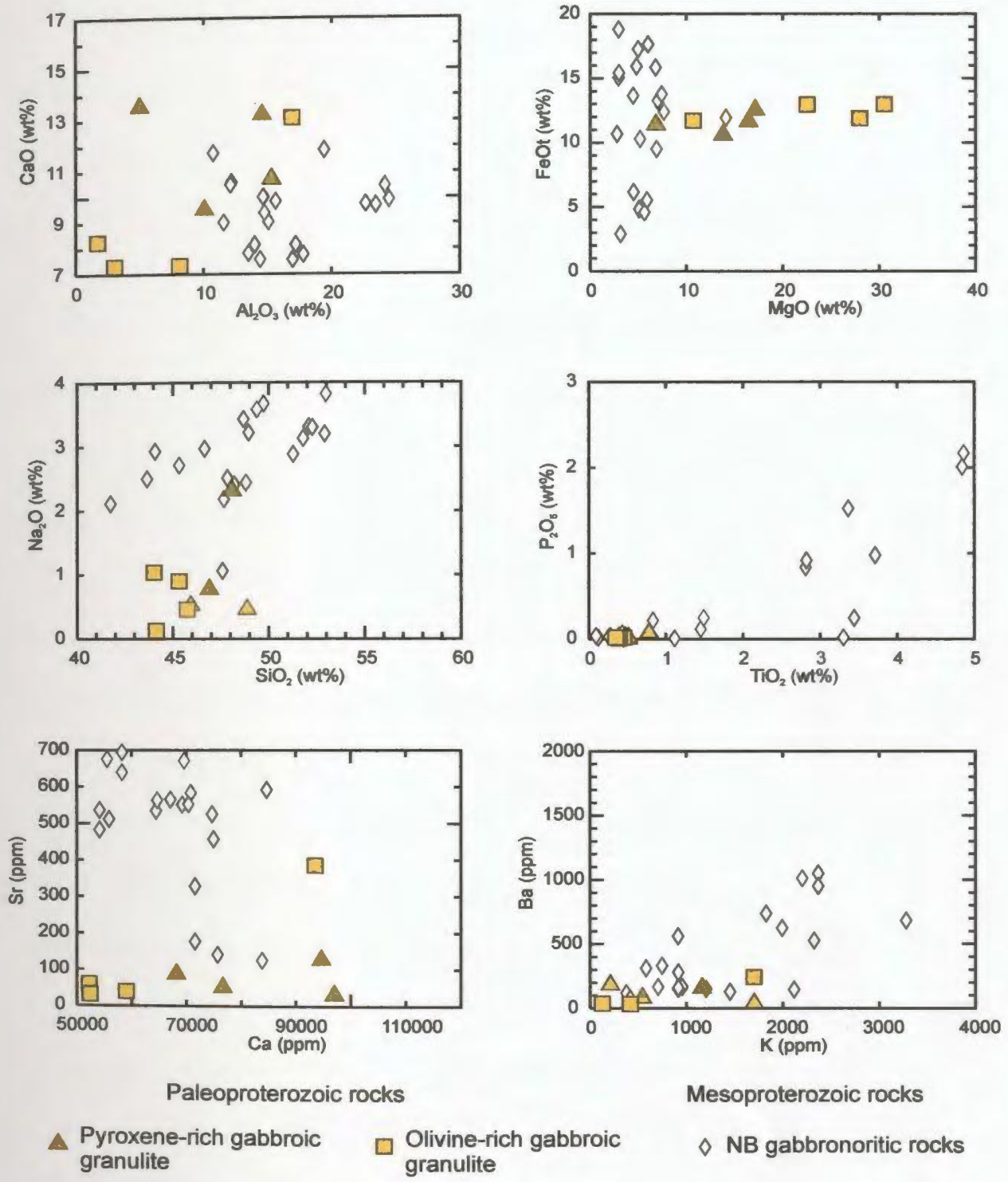

Figure 4.11: Whole rock chemistry of Paleoproterozoic gabbroic granulite and comparative data for Mesoproterozoic Nain batholith (NB) gabbronoritic rocks.

Ryan (2000a; 2001a) grouped this same unit of enderbitic rock into Archean quartzo-feldspathic gneiss. Wheeler (1973) described a unit of enderbitic paragranulite that is located in the southwestern part of the study area. Mapping by Ryan (1996) described a unit of Paleoproterozoic (1909 +33/-21 Ma in Ryan, 1996) enderbite that is located in the western-most part of the study area. Mapping and geochronology studies by Rawlings-Hinchey et al. (2003) found a unit of Paleoproterozoic enderbitic gneiss ~4 km south of the study area.

Structure and texture

Enderbitic gneiss is fine- to medium-grained and has the composition of quartz diorite and pyroxene diorite. Enderbitic gneiss cuts gabbroic granulite (see Fig. 4.4). This gneiss is pale pink to green weathering in the western part of the study area and chalky white weathering in the eastern and northern parts of the study area.

Enderbitic gneiss consists of small to medium-sized plagioclase grains, purple colored quartz grains and lenses, and pyroxene grains. Gneissic layers are formed by alternations in the abundance of quartz lenses and pyroxene grains. These layers are steeply dipping and 0.1 – 5 cm thick. In the Anaktalik Brook (Fig. 4.1) and Kangilialuk Lake (Fig. 4.2) country rock belts these enderbitic rocks are steeply (60 – 70°) east-dipping to sub-vertical and broadly north-south striking. To the northwest of Nain (Fig. 4.2), this unit of enderbitic gneiss is steeply north dipping and east-west striking. Foliated rocks contain lenses of quartz that strike parallel to gneissic layering.

Petrography and mineralogy

Plagioclase and quartz grains show interlobate grain boundaries (Fig. 4.9) that indicate they were recrystallized at high-T. Plagioclase in chalky white weathering enderbitic rocks shows more abundant alteration to sericite in comparison to plagioclase in pale pink to green weathering rocks. Orthopyroxene grains are fractured and are altered to uralite along grain fractures and grain margins.

Table 4.3: Mineral compositions (*) and whole rock chemistry for enderbitic gneiss (Pe), and comparative data for NB gabbronoritic rocks (NB gn)

Rock type	Sample	Pl*	Opx*	SiO_2	Al_2O_3	CaO	Na_2O	K_2O
		An	En	wt%	wt%	wt%	wt%	wt%
Enderbitic gneiss (Pe)								
qtz di	00-25-12	33	60					
qtz di	00-4-6b			63.35	16.11	5.3	3.92	0.36
qtz di	02-23-4			64.29	15.15	5	3.56	0.62
qtz di	01-19-5	30						
qtz di	01-29-7b	29						
range		29 - 33	60	63 - 64	15 - 16	5	3.5 - 4.0	0.4 - 0.6
Comparative data								
NB gn		35 - 64	47 - 72	42 - 53	11 - 25	8 - 12	1.1 - 3.8	0.1 - 0.8

Mineral compositions in enderbitic gneiss range from An_{29-33} in plagioclase and average En_{60} in orthopyroxene (Table 4.3). These plagioclase compositions are Na-rich in comparison to those in gabbronoritic plutonic rocks. Accessory minerals consist of small clinopyroxene (En_{35-40}), biotite, amphibole and zircon grains.

Whole rock chemistry

Quartz diorite in the Anaktalik Brook and Kangilialuk Lake gneiss belts show similar whole rock abundances of SiO_2, Al_2O_3, FeOt, CaO, Na_2O, (Table 4.3) Ba (452 and 659 ppm) and Sr (430 ppm), suggesting that they are correlated. Whole rock

abundances of SiO_2 (~64 wt%) and K_2O (~0.5 wt%) fall in the range shown by Paleoproterozoic calc-alkaline orthogneiss (46 – 77 wt% SiO_2, 0.15 – 4.31 wt% K_2O) as described by Rawlings-Hinchey et al. (2000). CIPW norms indicate a quartz diorite mode and 15 – 16% pyroxene (Fig. 4.8).

Regional correlations

Enderbitic gneiss in the study area may be correlated with: (1) Archean quartzo-feldspathic gneiss (see Ryan, 2000a; 2001a), or (2) Paleoproterozoic calc-alkaline orthogneiss (see Rawlings-Hinchey et al., 2000). The spatial distribution, rock types and whole rock chemistry of enderbitic gneiss in the study area are similar to those described for Paleoproterozoic calc-alkaline orthogneiss by Rawlings-Hinchey et al. (2003). For these reasons, the enderbitic gneiss in the study area is grouped with Paleoproterozoic calc-alkaline orthogneiss.

4.2 Country rock belts

Archean and Paleoproterozoic country rocks are spatially associated with each other in larger structures that are located near Anaktalik Brook, Kangilialuk Lake and Nain Hill (see Fig. 3.1). Country rock near Anaktalik Brook (see Fig. 4.1) extends for 13.8 km in a north-south direction and 0.5 – 10.3 km in an east-west direction. Country rock near Kangilialuk Lake (see Fig. 4.2) extends for 7.8 km in a north-south direction and 0.3 – 2.6 km in an east-west direction. Country rock near Nain Hill (see Fig. 4.2) extends for 6.9 km in a northwest-southeast to east-west direction and 0.3 – 0.5 km in a

north-south direction. The term 'belt' is used to name these larger structures of country rock. The three country rock belts in the study area are referred to as the Anaktalik Brook, Kangilialuk Lake and the Nain Hill country rock belts. A small exposure of gabbroic granulite in the eastern-most part of the study area (see Fig. 6.1) is referred to as the Kauk Harbour country rock belt.

The Anaktalik Brook country rock belt contains units of Archean granitoid and amphibolite gneiss, Paleoproterozoic or Archean gabbroic granulite, Paleoproterozoic or Archean metasedimentary gneiss and Paleoproterozoic enderbitic gneiss (see Fig. 4.1). Compositional and gneissic layers in all of these units are predominantly sub-vertical and north-south striking and strike parallel to sub-vertical and north-south striking structures in the Paleoproterozoic Torngat orogen (see section 2.1.3). Since the deformation associated with the Torngat orogen (<1860 Ma in Van Kranendonk, 1996) is younger than the youngest unit of country rock in the study area (enderbitic gneiss, >1865 Ma from Scott, 1998) it is suggested that the Anaktalik Brook country rock belt is a Paleoproterozoic structure.

The Kangilialuk Lake country rock belt contains units of Paleoproterozoic or Archean gabbroic granulite and Paleoproterozoic enderbitic gneiss (see Fig. 4.2). Compositional and gneissic layers in both units are predominantly sub-vertical and north-south striking, suggesting that the Kangilialuk Lake country rock belt is also a Paleoproterozoic structure.

The Nain Hill country rock belt consists of Paleoproterozoic or Archean gabbroic granulite and Paleoproterozoic enderbitic gneiss (see Figs. 4.2, 6.2). Compositional and

gneissic layers in the western part of this belt are moderately to steeply east-dipping and north-south striking, suggesting that this part of the belt is a Paleoproterozoic structure. In contrast, layering in the eastern part of this belt is steeply north dipping and east-west striking. This part of the belt may represent: (1) rocks that escaped Paleoproterozoic deformation, or (2) rocks that were re-worked after the Torngat orogen (<1740 Ma in Van Kranendonk, 1996) and before or during emplacement of the Nain batholith (1365 – 1270 Ma, see chapter 2). In chapter 8, it is suggested that the eastern part of the Nain Hill country rock belt was rotated into a sub-vertical, east-west striking, Mesoproterozoic shear zone.

The Kauk Harbour country rock belt consists only of Archean or Paleoproterozoic gabbroic granulite. Compositional layers are moderately east dipping and north-south striking. The rock types in the Kauk Harbour country rock belt were correlated with those in the Paleoproterozoic Quarry intrusion during a field trip taken by the author in the summer of 2002. It is possible that compositional layers represent a Paleoproterozoic overprint related to the Torngat orogen, although the dip is relatively shallow.

4.3 Summary

Country rock in the study area consists of Archean granitoid and amphibolite gneiss, Paleoproterozoic or Archean gabbroic granulite ('Paleoproterozoic gabbroic granulite' from hereon), Paleoproterozoic or Archean metasedimentary gneiss and Paleoproterozoic enderbitic gneiss. These units of country rock are spatially associated in the Anaktalik Brook, Kangilialuk Lake, Nain Hill and Quarry country rock belts. The

Anaktalik Brook, Kangilialuk Lake and western Nain Hill country rock belts strike parallel to Paleoproterozoic structures that are related to the Torngat orogen. The western part of the Nain Hill country rock belt is oriented perpendicular to these Paleoproterozoic structures. In chapters 5 – 7, the geology, mineral compositions and whole rock chemistry of Paleoproterozoic gabbroic granulite are contrasted with strongly deformed gabbronoritic rocks that are grouped into the centered intrusive complexes of this study.

Chapter 5: Tikkoatokak centered intrusive complex (T)

The Tikkoatokak centered intrusive complex (T) is a name that is here proposed for ~700 km^2 of spatially associated anorthositic, gabbronoritic and monzonitic rocks in the central part of the Nain batholith (Fig. 5.1). The southern part of this centered intrusive complex is exposed in the study area and consists of the Tasiyuyaksuk sheet (TY), Kangilialuk sheet (TK), Lister pluton (TL), Bird sheet (TB) and Anaktalik sheets (TA) (Fig. 5.2, 5.3). The Lister pluton is divided into an inner zone and a border zone, and the Anaktalik sheets are divided into lower and upper sheets. This chapter describes the contact relations, form, petrography, textures, structures, mineral compositions and whole rock chemistry for each of these units. U-Pb isotope data are presented for zircons from the Kangilialuk sheet. The order in which these units are described is from oldest to youngest based on field relations. A section entitled 'tectonic overprint' describes the strongly deformed plutonic rocks that occur in the margin of the Tikkoatokak centered intrusive complex.

Anorthositic rocks of the Lister pluton comprise the bulk and the spatial center of the Tikkoatokak centered intrusive complex (Fig. 5.2). The Tasiyuyaksuk sheet, Kangilialuk sheet, Bird sheet and Anaktalik sheet are included with the Lister pluton in the Tikkoatokak centered intrusive complex for reasons given later in this chapter. This chapter also describes the tectonic overprint on the margin of the Tikkoatokak centered intrusive complex.

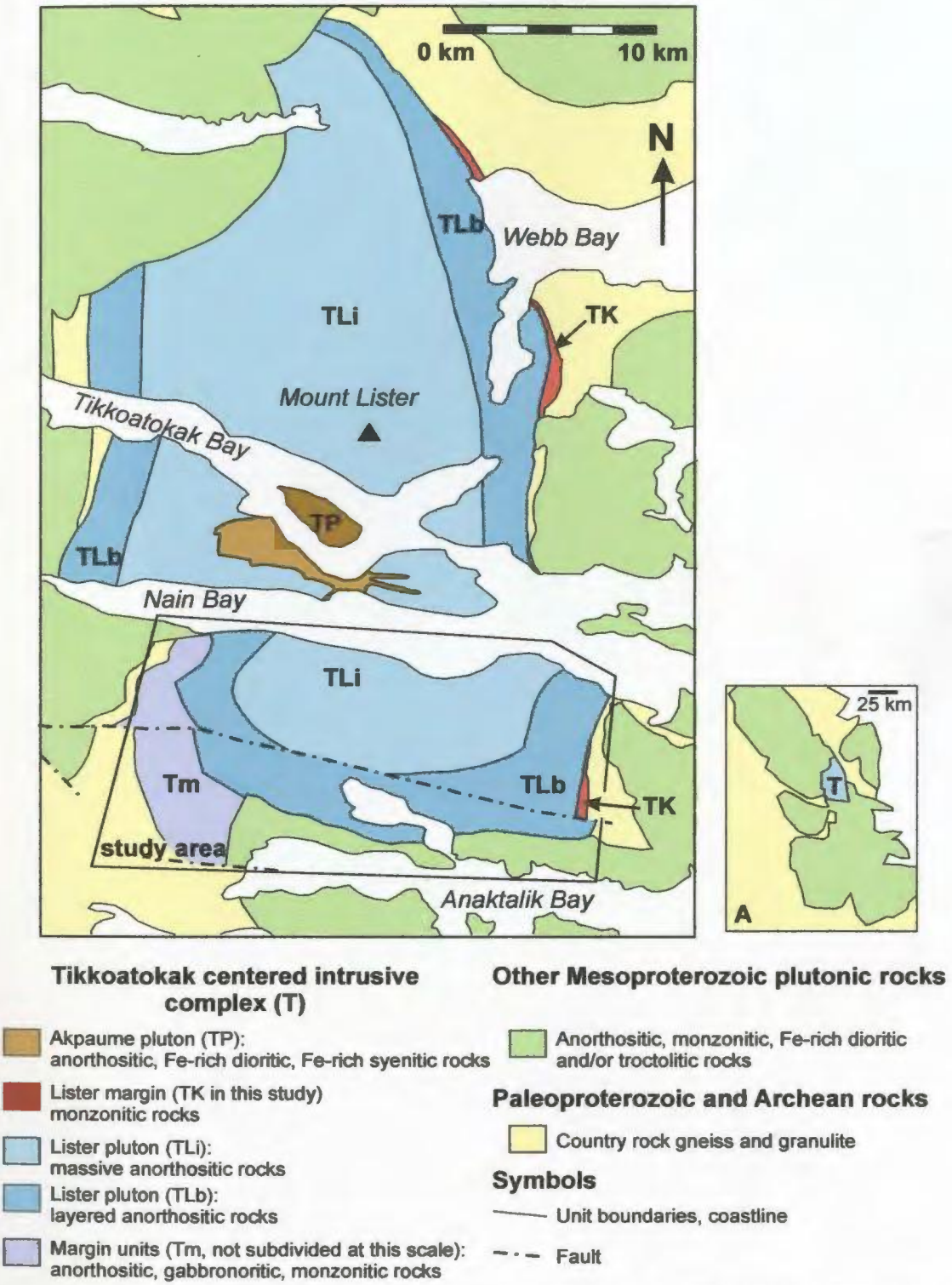

Figure 5.1: Solid geology map compiled from previous work (Ryan, 1990; 1993; 2000a; 2001a) that shows the units that comprise the Tikkoatokak centered intrusive complex in this study. The part examined in this study lies south of Nain Bay. Inset (A) shows the location of the Tikkoatokak centered intrusive complex in the Nain batholith.

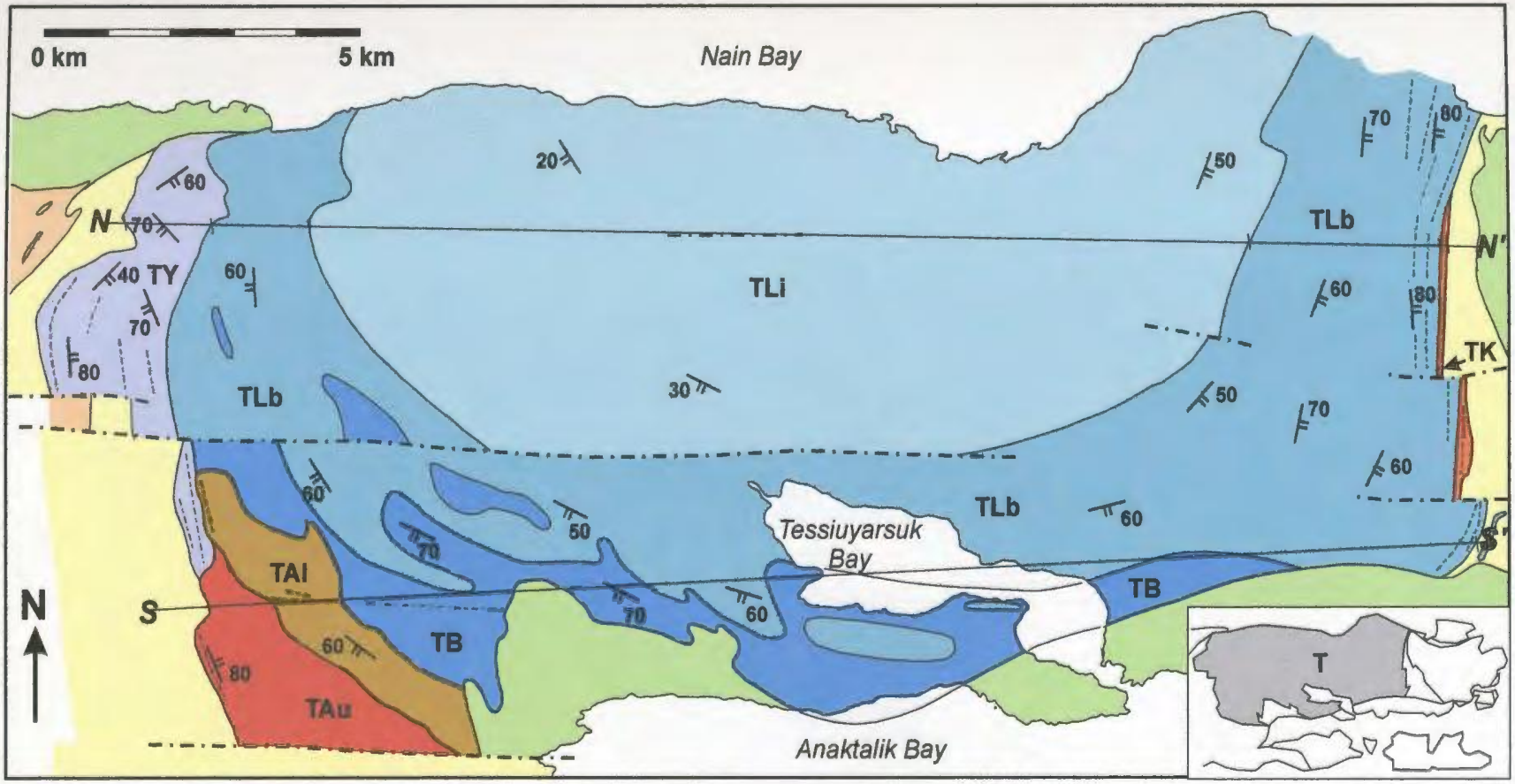

Figure 5.2: Solid geological map for the southern part of the Tikkoatokak centered intrusive complex. Cross-sections N- N' and S-S' are shown in Fig. 5.3

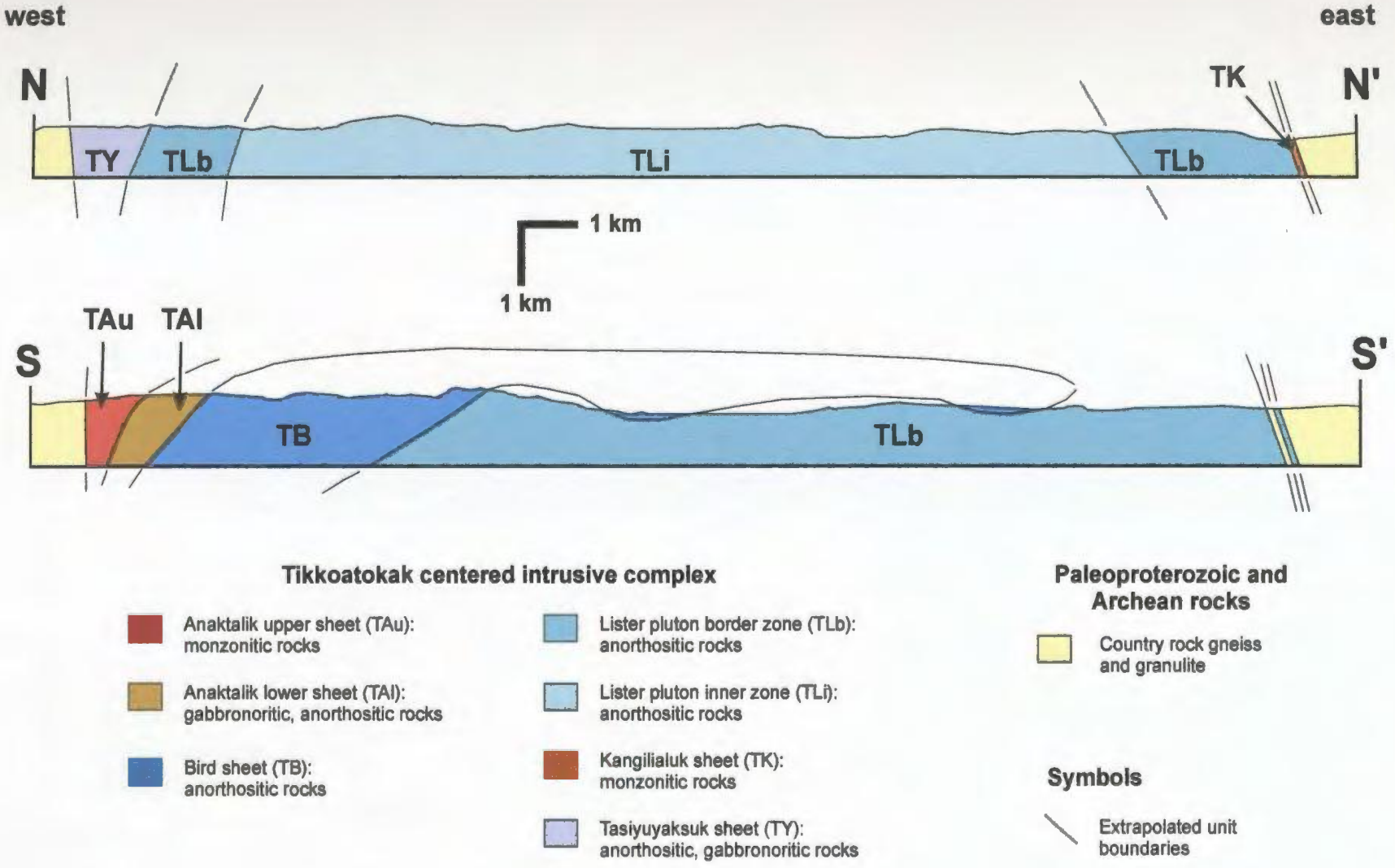

Figure 5.3: East-west cross-sections through the Tikkoatokak centered intrusive complex. Cross-sections are located on Figure 5.2.

5.1 Tasiyuyaksuk sheet (TY)

A geological map by Ryan (1996) shows a unit of recrystallized norite along the western margin of what is here referred to as the Lister pluton. A geological map by Myers (2000, unpubl.) in the same area sub-divided anorthositic rocks into four unnamed units and the Lister pluton. The full extent of the recrystallized norite of Ryan (1996) and one of the unnamed anorthositic intrusions of Myers (2000, unpubl.) was mapped as part of this study and is here named the Tasiyuyaksuk sheet (after Tasiyuyaksuk Brook, Fig. 3.1).

Form and contacts

Geological mapping as part of this study outlined a unit of steeply dipping, layered, strongly deformed, norite, leuconorite and lesser abundances of melanorite that is here named the Tasiyuyaksuk sheet (Fig. 5.4). The western side of this unit shows a sharp and concordant to discordant intrusive contact with Paleoproterozoic gabbroic granulite in the Anaktalik Brook country rock belt, and cuts sharply across unnamed anorthositic rocks to the north (Fig. 5.5). These unnamed anorthositic rocks were not traversed during this study, but are included with Mesoproterozoic anorthositic rocks in maps by Ryan (1990; 1996). The Lister pluton was intruded into the eastern part of the Tasiyuyaksuk sheet (Fig. 5.6).

The southern part of the Tasiyuyaksuk sheet is 0.4 – 2.2 km thick, 5.3 km long, moderately (50°) to steeply (70° – 80°) east dipping and north-south striking. The northern part is exposed over 1.5 km in an east-west direction and 1.9 km in a north-south

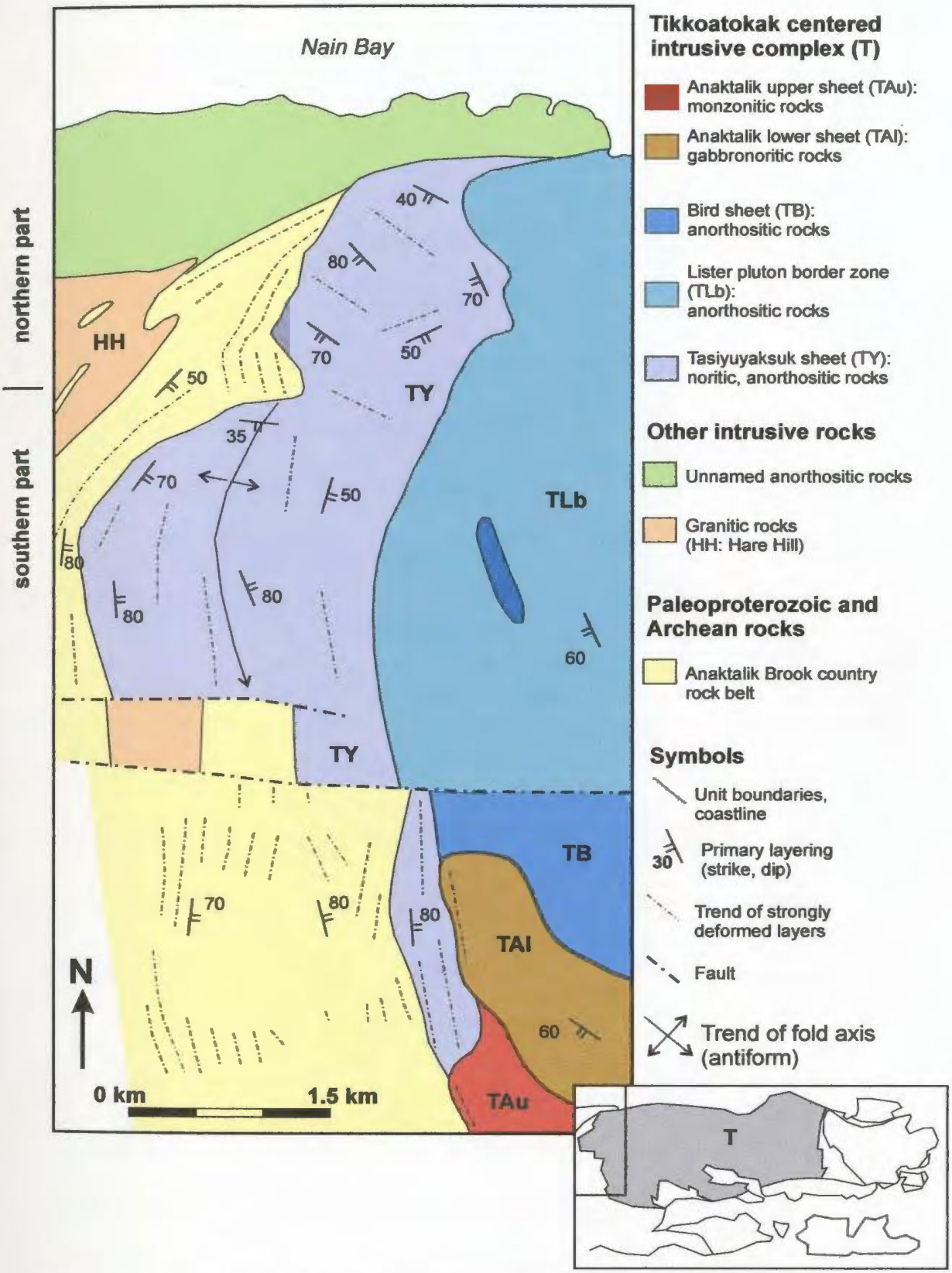

Figure 5.4: Solid geological map for the western part of the Tikkoatokak centered intrusive complex

direction, and is moderately (40°) to steeply (70° – 80°) southwest dipping and northwest to southeast striking.

Petrography

Norite contains orthopyroxene and plagioclase crystals that are of medium size and show granular to tabular habits. The tabular habits suggest that both of these minerals crystallized on the liquidus. Plagioclase crystals show deformation twins, equilibrated geometry and undulose extinction that indicate they were deformed and recrystallized at high-T. Tabular orthopyroxene grains are fractured and kinked, indicating they were also deformed. Melanorite contains orthopyroxene grains and interstitial plagioclase crystals, suggesting that plagioclase crystallized out of the intercumulus liquid.

Leuconorite contains plagioclase that is abundant, of large grain size and with granular to tabular habits, suggesting that plagioclase is cumulus. These cumulus crystals show deformation twins, deformation bands and undulose extinction (Fig. 5.7) that indicate they were deformed at high-T. Orthopyroxene crystals are of relatively low abundance and exhibit poikilitic to sub-poikilitic texture, suggesting that they crystallized out of the intercumulus liquid.

Textures and structures

Norite, leuconorite and melanorite are fine- to medium-grained and show an overall texture that is granular. Rocks that contain laths and/or poikilitic crystals show an overall texture that is porphyritic or poikilitic, respectively.

Figure 5.5: Unnamed anorthositic rocks (ua) cut by norite of the Tasiyuyaksuk sheet (TY). Dashed line marks the intrusive contact. Photo taken on hills above the northern shoreline of Nain Bay.

Figure 5.6: Norite in the Tasiyuyaksuk sheet (TY) cut by massive anorthosite of the Lister pluton border zone (TL). Photo taken on hills above the northern shoreline of Nain Bay

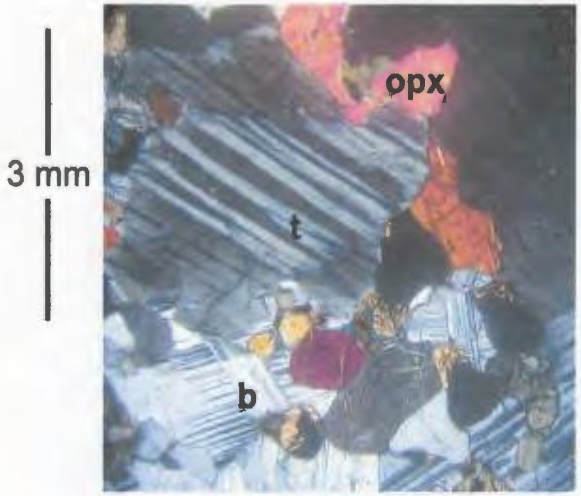

Figure 5.7: Thin section photo (XPL) of TY leuconorite. Plagioclase shows deformation twins (t), deformation bands (b) and undulose extinction. Orthopyroxene (opx) is sub-poikilitic.

Figure 5.8: Strongly deformed primary layers of norite (n) and leuconorite (ln) in TY. Layering is sub-vertical. Photo taken north of Tasiyuyaksuk Brook.

Norite, leuconorite and melanorite show primary layering and foliation. Primary layering comprises alternations of granular-, poikilitic- and/or porphyritic-textured leuconorite, norite and melanorite (Fig. 5.8). Individual layers are ~0.1 – 20 cm thick and were overprinted by a layer-parallel deformation (see below). Foliated rocks are either porphyritic-textured and contain plagioclase and pyroxene laths that are aligned parallel to the plane of layering, or poikilitic-textured and contain lens-shaped sub-poikilitic pyroxene crystals that are also aligned parallel to the plane of layering.

Leuconorite also contains planar aggregates of medium-sized, poikilitic, clinopyroxene crystals. These aggregates, which are 0.5 – 5 cm thick and 10's to 100's of cm's long, strike parallel to layering and foliation.

Primary layering in the Tasiyuyaksuk sheet is moderately dipping to sub-vertically oriented (Fig. 5.9), shows predominantly granular texture and was locally stretched into boudins. In addition, the orientation of layers in this sheet suggests that they comprise an antiform. These structures indicate that the Tasiyuyaksuk sheet was strongly deformed parallel to primary layering.

Mineral compositions and whole rock chemistry

Mineral compositions in norite and leuconorite range from An_{55-64} in plagioclase and En_{69-72} in orthopyroxene. These compositions fall in the range shown by Paleoproterozoic gabbroic granulite, and are Ca-rich for plagioclase and Mg-rich for orthopyroxene in comparison to the Lister pluton (Table 5.1, see Fig. 5.10). Plagioclase grains show rims that are Ca-rich (An_{59-68}) in comparison to cores and indicate a reverse

zoning. Orthopyroxene grains are homogeneous in composition and contain <2.3 wt% Al_2O_3. Exsolved lamellae of clinopyroxene (En_{42}) in orthopyroxene are of similar composition to clinopyroxene in planar aggregates (En_{41-42}).

Whole rock chemistry of leuconorite shows wt% SiO_2, wt% Na_2O and Sr/Ca that are high in comparison to Paleoproterozoic gabbroic granulite (Table 5.1, Fig. 5.13). Ratios of Ca/Al in Tasiyuyaksuk leuconorite are low in comparison to Paleoproterozoic gabbroic granulite, and reflect the relatively high proportions of clinopyroxene relative to plagioclase in Paleoproterozoic gabbroic granulite. In comparison to anorthositic rocks of the Lister pluton, anorthositic rocks of the Tasiyuyaksuk sheet show a similar range in Ca/Al, whereas wt% SiO_2, wt% Na_2O and Sr/Ca are low. CIPW norms consist mostly of plagioclase and pyroxene, which is similar to CIPW norms obtained for anorthositic rocks of the Lister pluton. In contrast, CIPW norms of Paleoproterozoic gabbroic granulite also contain olivine. Normative plagioclase compositions fall in the range shown by Paleoproterozoic gabbroic granulite.

Table 5.1: Mineral compositions (*) and whole rock chemistry of TY leuconorite, and comparative data for anorthositic rocks in the Lister pluton (TL) and for Paleoproterozoic gabbroic granulite (Pg)

Rock type	Sample	Pl*	Opx*	SiO_2	Na_2O	Ca/Al	Sr/Ca x 10	Mg/(Mg+Fe)	An/(An+Ab)
		An	En	wt%	wt%				CIPW
Tasiyuyaksuk sheet (TY)									
defm In	02-6-12i			52.08	3.31	1.16	0.10	0.45	0.62
defm In	02-6-12ii	55	70	51.79	3.13	1.65	0.07	0.45	0.59
defm In	02-6-14	64	72	51.26	2.88	1.12	0.08	0.49	0.66
defm In	02-20-7b	59	69						
defm In	02-20-30			52.97	3.82	1.09	0.08	0.45	0.60
Comparative data									
TL		41 - 47	57 - 62	53 - 55	4.1 - 5.1	0.9 - 1.2	0.13 - 0.15	0.14 - 0.35	0.47 - 0.51
Pg		51 - 81	58 - 85	44 - 49	0.1 - 2.3	1.9 - 12.9	0.00	0.32 - 0.65	0.56 - 0.89

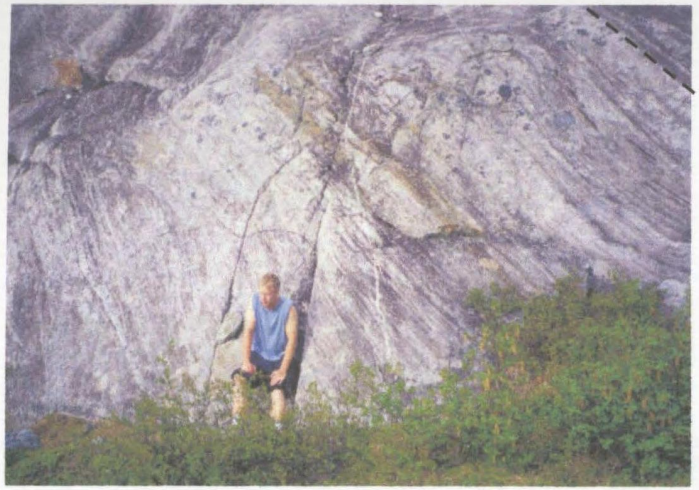

Figure 5.9: Steeply dipping and strongly deformed primary layers of leuconorite and norite in the Tasiyuyaksuk sheet. Photo taken on hills above the northern shoreline of Nain Bay.

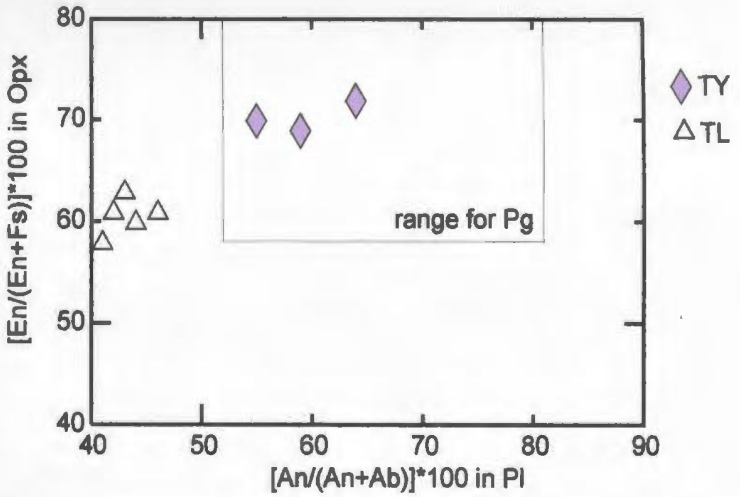

Figure 5.10: Comparison of orthopyroxene and plagioclase compositions in Tasiyuyaksuk leuconorite (TY) with those in Lister pluton anorthositic rocks (TL) and Paleoproterozoic gabbroic granulite (Pg).

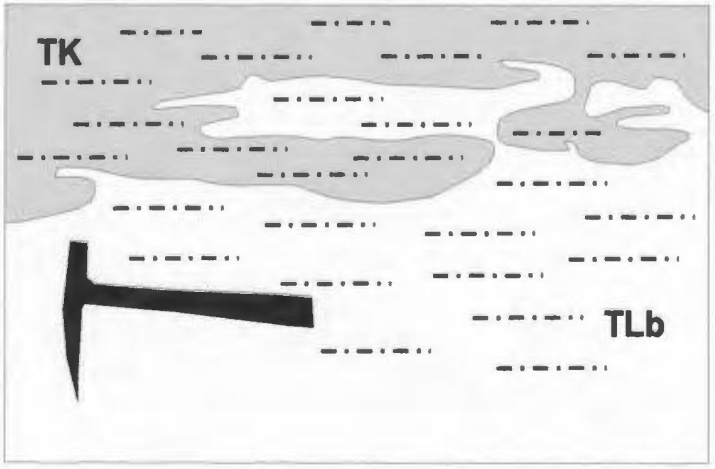

Figure 5.11: Field sketch of the contact between the Kangilialuk sheet monzonite (TK) and Lister pluton border zone anorthositic rocks (TLb) . Dashed lines indicate a strongly deformed compositional layering that is sub-vertical and north-south striking.

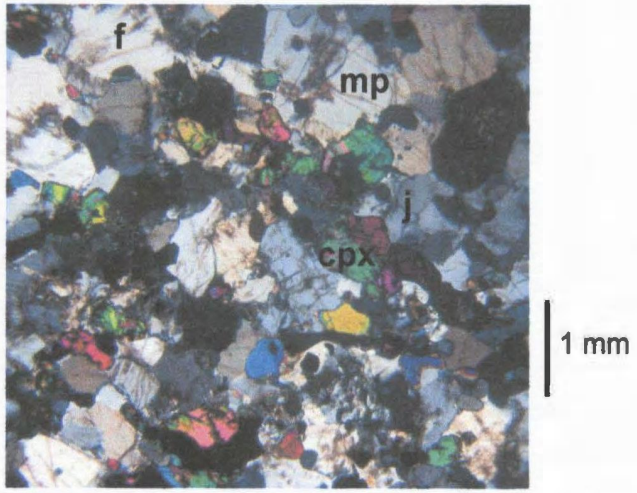

Figure 5.12: Thin section (XPL) photo of monzonite in TK. Crystals of mesoperthite (mp) and clinopyroxene (cpx) are granular to tabular and show triple junctions (j) and grain fracturing (f). Fe-Ti oxides are black.

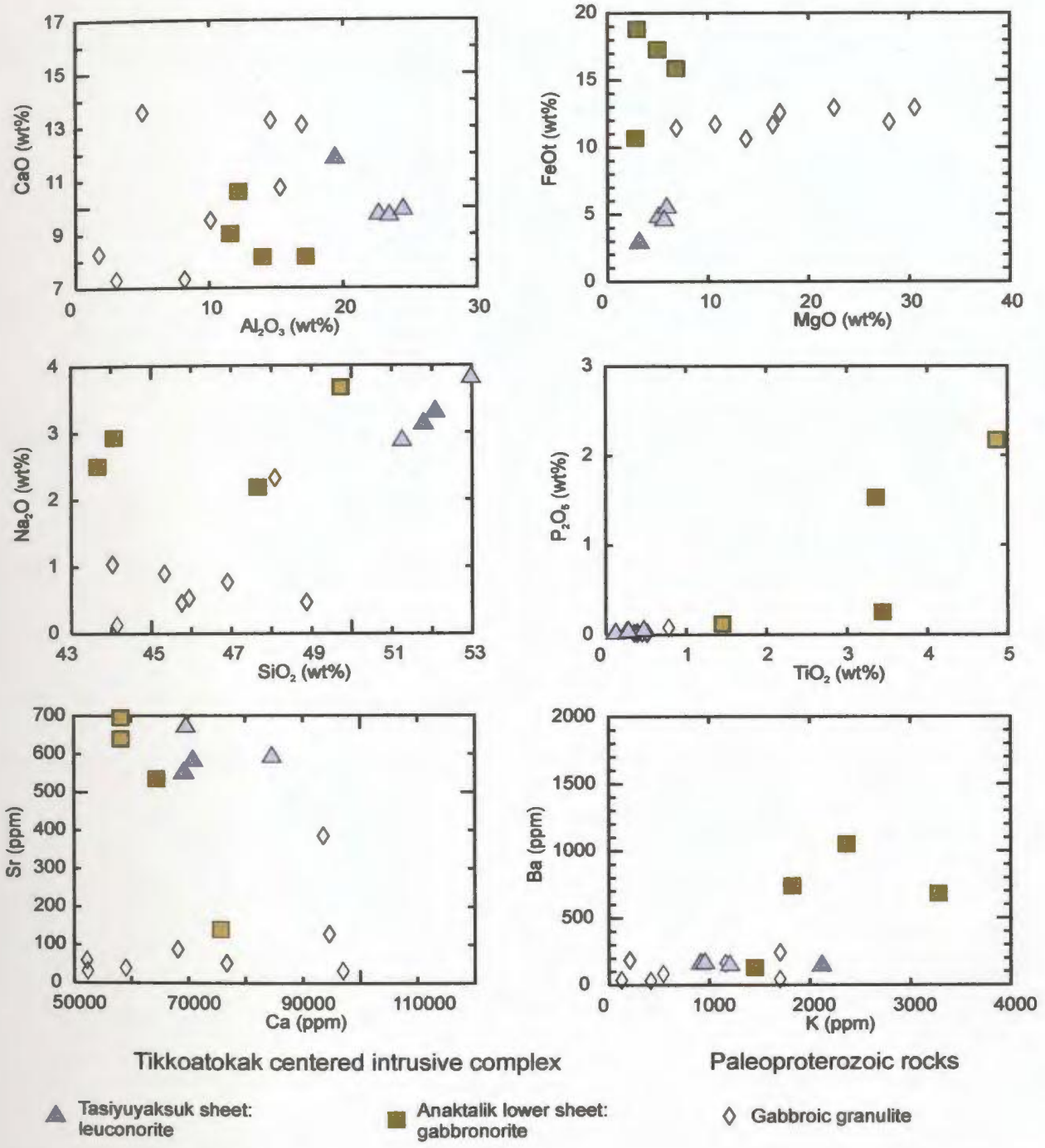

Figure 5.13: Whole rock chemistry for leuconorite in the Tasiyuyaksuk sheet and gabbronorite in the Anaktalik lower sheet, and comparative data for Paleoproterozoic gabbroic granulite. The Tasiyuyaksuk sheet is described in section 5.1 and the Anaktalik lower sheet is described in section 5.5.1.

One sample of Tasiyuyaksuk leuconorite (02-6-12ii) contains a planar aggregate of poikilitic clinopyroxene crystals. This sample shows high Ca/Al (1.65), and also contains relatively high whole rock abundances of TiO_2, FeOt, MnO, MgO, CaO, V, Sc, Ba and Zr.

Summary

Mineral compositions and whole rock chemistry show that noritic and anorthositic rocks in the Tasiyuyaksuk sheet are more similar to Paleoproterozoic gabbroic granulite in comparison to anorthositic rocks of the Lister pluton. On the other hand, the Tasiyuyaksuk sheet shows: (a) a form that parallels that of the Lister pluton border zone, (b) a relative age that is younger than gabbroic granulite and an unnamed unit of anorthositic rocks (Mesoproterozoic in Ryan, 1996), and (c) contains planar pyroxene aggregates that were not found in any gabbroic granulites. These rocks are here included as part of the Tikkoatokak centered intrusive complex and may be analogous to the 'marginal mafic granulites' of other workers (see Berg and Briegel, 1981; Royse et al., 1999).

5.2 Kangilialuk sheet (TK)

Geological maps by Ryan (2000a; 2001a; 2001b) show granitic rocks along the eastern margin of the Lister pluton. These rocks form a semi-continuous sheet that is included in the eastern margin of the Tikkoatokak centered intrusive complex, and which separates the Lister pluton from country rock. The sheet consists of strongly foliated,

fayalite- and augite-bearing, porphyritic monzonite and quartz monzonite (Ryan, 2001a). Ryan (2001a) found that the contact of this monzonite sheet and adjacent rocks was tectonically modified. The southern extent of this unit was mapped in this study (Fig. 5.14).

Form and contacts

Geological mapping as part of this study outlined a unit of steeply dipping, massive to layered, strongly deformed, fine- to medium-grained, monzonite and quartz monzonite that is here named the Kangilialuk sheet (after Kangilialuk Lake, see Fig. 3.1). This name is favored over Lister margin (see Miller et al., 1997) because the name Lister is used in this study to refer to a pluton of anorthositic rocks. The bottom and top of this unit are in sharp and concordant contact with the top of the Lister pluton and gabbroic granulite in the Kangilialuk Lake country rock belt, respectively.

The Kangilialuk sheet is 10 – 250 m thick, 4500 m long, steeply (70° – 80°) east dipping to sub-vertical and north-south striking. Geological maps by Ryan (1993; 2000, 2001a) shows that the Kangilialuk sheet is present up to ~30 km north of the study area as well, indicating that the total length of the Kangilialuk sheet is in excess of 34 km. The contact between the Kangilialuk sheet and the Lister pluton consists of strongly deformed, interleaved, monzonitic and anorthositic rocks (see Fig. 5.11), indicating that these two units were deformed together.

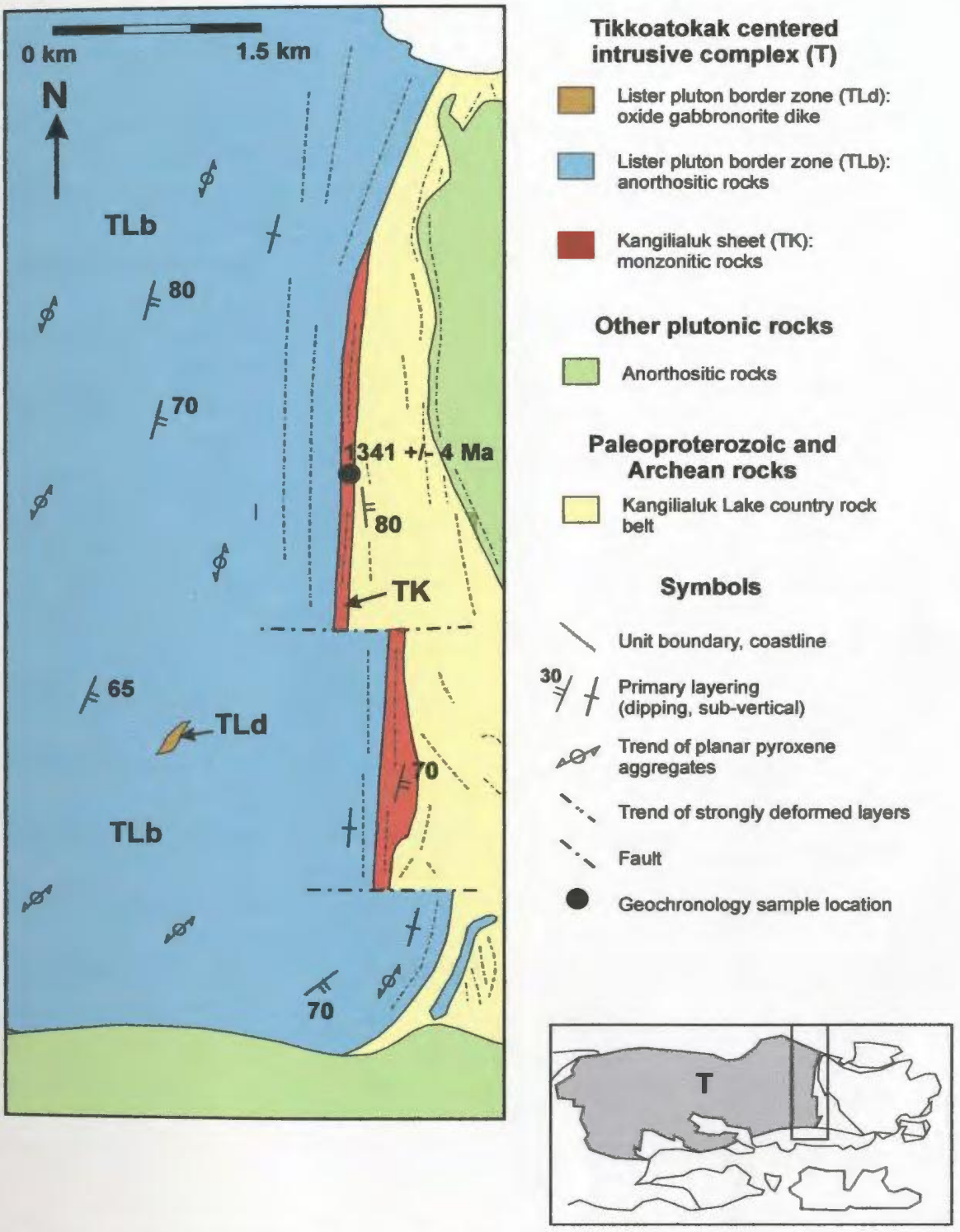

Figure 5.14: Solid geological map for the eastern part of the Tikkoatokak centered intrusive complex.

Petrography

Mesoperthite and clinopyroxene grains are medium-sized and tabular to granular in form. The tabular forms suggest that both of these minerals crystallized together on the liquidus. Both minerals show triple junctions and equilibrated geometries that indicate the grain margins were equilibrated at high-T (see Fig. 5.12). Both minerals also show grain fracturing that indicate they were deformed at lower-T as well. Fe-Ti oxide and quartz are of relatively smaller size and are interstitial with respect to mesoperthite and clinopyroxene. Minor and accessory minerals consist of Fe-rich olivine, apatite and zircon.

Textures and structures

Monzonite and quartz monzonite is fine- to medium-grained and shows an overall granular texture. Rocks with notable abundances of laths and interstitial Fe-Ti oxide crystals show an overall porphyritic or sub-poikilitic texture, respectively.

Most of the monzonitic rocks in the Kangilialuk sheet show granular texture and are massive. The sheet also contains minor abundances of layered and foliated rocks. Layered rocks comprise alternations of monzonite and quartz monzonite that show only granular texture. Individual layers are 1 – 10 cm thick, steeply dipping and north-south striking. These layered rocks are interpreted as strongly deformed on the basis of field and petrographic observations (deformed contacts, high-T recrystallization), and indicate that the Kangilialuk sheet was overprinted by deformation. Foliated rocks contain lens-shaped, sub-poikilitic, Fe-Ti oxide crystals that strike parallel to the orientation of layers.

Geochronology

U-Pb analysis of zircon was done on a sample of clinopyroxene-bearing monzonite that was collected from north of Kangilialuk Lake (see Fig. 5.10). This sample was analyzed because the strong deformation that occurs in the Kangilialuk sheet and the adjacent Lister pluton is cut by the Satosoak pluton to the south.

Zircon forms elongated crystals (Fig. 5.15) that are interstitial to mesoperthite and clinopyroxene. Individual grains are homogeneous or show a patchy zoning (Fig. 5.16). Some zircons contain small inclusions of apatite. The form and internal structures of these zircons suggest that they are igneous.

Table 5.2: Description and chemistry of zircons separated from TK pyroxene monzonite

Grain	Zr 1	Zr 2	Zr 3	Zr 4	Zr 6
Color	yellow	yellow	yellow	clear	clear
Translucent	yes	yes	yes	yes	yes
Shape	elongate	elongate	elongate	prismatic	prismatic
Weight (ug)	9	17	37	11	12
Com. (Pb pg)	4	2	5	2.2	9.4
U (ppm)	22	16	15	5	6
Th/U	0.6	0.95	1	1.1	1
$^{206}Pb/^{204}Pb$	765	1991	1788	392	140
Pb (ppm)	5.5	4.7	4.6	1.3	1.8
$^{206}Pb/^{238}U$	0.2262	0.2321	0.2249	0.2295	0.2314
% error	0.8	1.8	13.4	0.9	0.9
$^{207}Pb/^{235}U$	2.687	2.756	2.673	2.703	2.758
% error	0.8	1.8	13.4	1.9	2.4
$^{207}Pb/^{206}Pb$	0.0862	0.0861	0.0862	0.0854	0.0865
% error	0.3	0.4	1.1	1.6	2.1
$^{206}Pb/^{238}U$ (Ma)	1315	1345	1308	1332	1342
$^{207}Pb/^{235}U$ (Ma)	1325	1344	1321	1329	1344
$^{207}Pb/^{206}Pb$ (Ma)	1342	1341	1342	1325	1348
+/- m.y.	5	9	21	31	40
Conc. (%)	98	100	98	100	100

Five single zircon grains were analyzed for U and Pb isotope chemistry. Three of these zircons (Zr 1 – 3, Table 5.2) are yellow, elongate and contain relatively high abundances of U (15 – 22 ppm) and Pb (4.6 – 5.5 ppm). The other two zircons (Zr 4, 6) are clear, prismatic and contain relatively low abundances of U (5 – 6 ppm) and Pb (1.3 – 1.8 ppm). The yellow and clear zircons may represent two different populations, although the $^{207}Pb/^{206}Pb$ ages for all these zircons overlap within error (Table 5.2).

The $^{207}Pb/^{206}Pb$ ages of all five zircons overlap within error and lie on or within 2% of concordia. A concordia age was calculated by anchoring the lower intercept at 0 +/- 50 Ma. The % error on $^{206}Pb/^{238}U$ and $^{207}Pb/^{235}U$ measurements ranges from 0.8 – 2.4 for four of these grains, and one grain shows 13.4% error. The concordia age for the zircons with <2.4% error yields a concordant upper intercept age of 1341 +/- 4 Ma, whereas the concordia age for all five zircons is the same (Fig. 5.17). This age overlaps, within error, with a 1343 +/- 3 Ma age obtained by Connelly and Ryan (1994) for monzonitic rocks that are located ~30 km north of the study area (see Fig. 5.1).

Summary

The Kangilialuk sheet: (a) is spatially associated with the Lister pluton, (b) shows a form that strikes parallel to the Lister pluton, (c) shows the same Mesoproterozoic tectonic overprint as the Lister pluton, and (d) contains Mesoproterozoic zircons. The occurrence of deformed plutonic rocks at the margin of an anorthositic intrusion (Lister pluton in this case) is reminiscent of descriptions of 'marginal granulites' in the Nain batholith (see Davies, 1973b; Brand, 1974; Berg and Briegel, 1981; Royse et al., 1999),

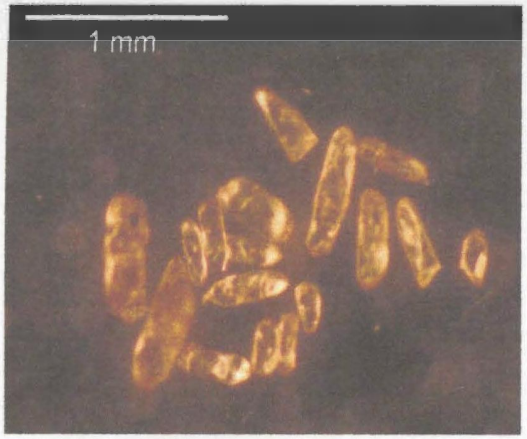

Figure 5.15: Binocular microscope photo of zircon grains from monzonite in TK. Zircons show elongate form and generally lack inclusions.

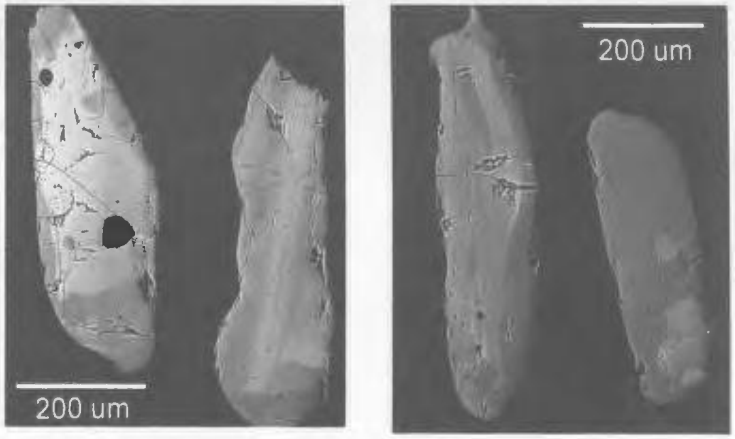

Figure 5.16: Electron backscatter images of zircons from monzonite in TK. Zircons show patchy zoning and inclusions of apatite.

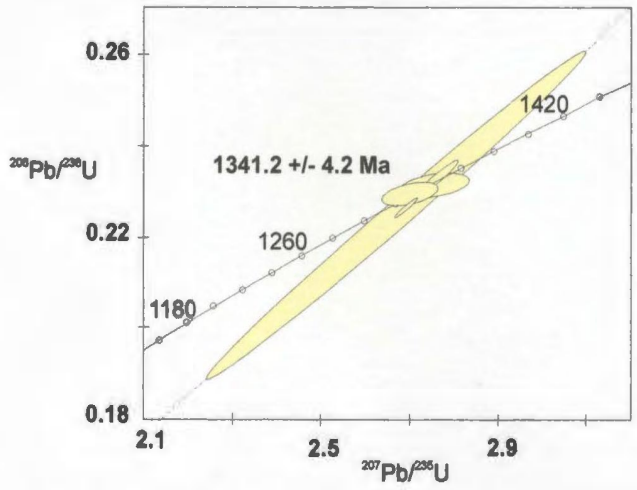

Figure 5.17: Concordia diagram for five zircon grains separated from monzonite in TK. Zircons define a concordia age of 1341 +/- 4 Ma when the lower intercept is anchored at 0 +/- 50 Ma. The mean square weighted deviate is 0.29.

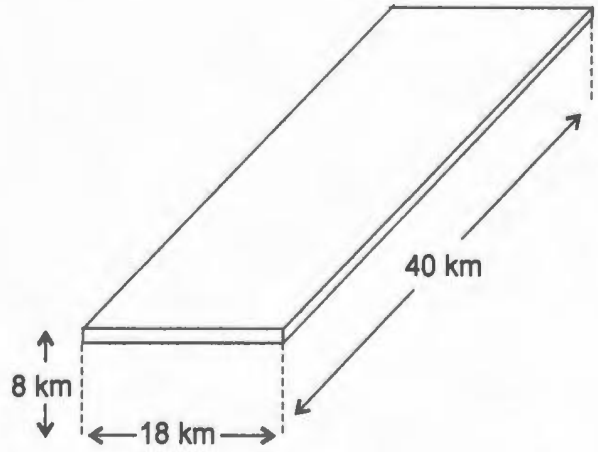

Figure 5.18: Box diagram that shows the approximate dimensions for the exposed part of the Lister pluton inner zone. The exposed dimensions comprise a sub-horizontal sheet-like form. Dashed line indicates the depth of the Nain batholith to the south of the study area (8 km in Funck et al., 2000).

although the monzonitic composition of these rocks is in contrast to the plagioclase-pyroxene modes that typify the 'marginal granulites'. For these reasons, the Kangilialuk sheet is included in the Tikkoatokak centered intrusive complex.

5.3 Lister pluton (TL)

A geological map by Wheeler (1969) shows a large (~640 km^2) exposure of pale-facies anorthositic rocks that spans Nain Bay and is bound by country rock along the eastern and western sides (see Fig. 5.1). Morse and Wheeler (1973) grouped these pale-facies rocks into the 'Lister massif'. Geological mapping by Ryan (2000a; 2001a) in the eastern part of this massif proposed the names Mount Lister pluton (Ryan, 2000a) and Mount Lister intrusion (Ryan, 2001a). This unit is here named the Lister pluton. Ryan (2001a; 2001b) sub-divided this pluton into: (a) an inner pegmatoidal anorthosite and leuconorite, and (b) a marginal foliated leuconorite and anorthosite.

The full extent of the pegmatoidal anorthosite and leuconorite unit of Ryan (2001a; 2001b) that occurs south of Nain Bay was mapped during this study, and is here named the Lister pluton inner zone. The foliated leuconorite and anorthosite unit was mapped south and west of the exposures mapped by Ryan (2001a; 2001b), and is here named the Lister pluton border zone. Mapping as part of this study found that the Lister pluton border zone envelops the entire inner zone, but varies from strongly deformed in the east to weakly deformed in the west.

North of the study area, the Lister pluton inner zone was cut by the Akpaume intrusion (see Fig. 5.1). This intrusion consists of Fe-rich dioritic rocks (1333 +/- 2 Ma,

Hamilton et al., 1994), anorthositic rocks (1331 +/- 2 Ma, Hamilton et al., 1994) and Fe-rich syenitic rocks (Emslie in Berg et al., 1994). Deuring (1975, p. 49) summarized the relationship between the Apkaume pluton and host rocks of the Lister pluton as an "injection of an iron-enriched magma into hot anorthosite", suggesting the Lister and Apkaume intrusions may be of similar age.

5.3.1 Lister pluton inner zone (TLi)

Form and contacts

Geological mapping as part of this thesis outlined a unit of massive to sub-horizontally layered, coarse to very coarse-grained anorthosite that is here named the Lister pluton inner zone. This unit also includes lesser abundances of leuconorite and leucogabbronorite. The base of this unit is unexposed. The top of this unit shows a gradational increase in the abundance of moderately dipping, layered, leuconorite and leucogabbronorite that mark the base of the Lister pluton border zone.

In the study area, the Lister pluton inner zone is exposed over 15 km in an east-west direction and 5 km in a north-south direction (see Fig. 5.2, 5.3). The exposed vertical thickness in the study area is up to 600 m. From the maps of Ryan (2000a; 2001a) and Ryan and James (2003) it was determined that the regional extent of the Lister pluton inner zone is 18 – 22 km in an east-west direction and 40 km in a north-south direction (Fig. 5.18). As well, the inner zone is up 1000 m thick in the area of Mount Lister.

Petrography

Plagioclase crystals are abundant, large to very large in size (0.1 – 100 cm) and tabular to granular in form, suggesting that they are cumulus. These crystals also show deformation twins, deformation bands, triple junctions, undulose extinction, equilibrated geometries, hairline fractures and/or serrated grain boundaries (Fig. 5.19) that indicate they were recrystallized and/or deformed at high-T. Plagioclase crystals also contain blebs of exsolved alkali feldspar. Orthopyroxene shows relatively low abundance and poikilitic to sub-poikilitic texture, suggesting that it crystallized out of the intercumulus liquid. In some cases, small pyroxene grains form aggregates that comprise large, relict, poikilitic pyroxene crystals. These relict crystals indicate that some of the intercumulus orthopyroxene was recrystallized. Orthopyroxene also shows rims and/or exsolved lamellae of clinopyroxene, and passes into sheath-like forms (Fig. 5.20) that also suggest intercumulus crystallization. Some of these pyroxene crystals show exsolved lamellae that contain very small exsolved plagioclase and oxide grains. This exsolved plagioclase suggests that the pyroxene originally was relatively Ca- and Al-rich. Fe-Ti oxide shows sub-poikilitic texture that suggests it also crystallized out of the intercumulus liquid.

Secondary minerals are widespread and replaced up to 5% plagioclase and 10% pyroxene. Altered plagioclase contains sericite +/- saussurite that suggest hydrothermal alteration. Rims and grain fractures in pyroxene contain uralite that also suggest hydrothermal alteration. Fe-Ti oxide shows partial coronas of very small biotite laths.

Textures and structures

Anorthositic rocks are medium- to very coarse-grained and show an overall texture that is granular. Minor abundances of anorthositic rocks contain ~10 – 20% poikilitic pyroxene and/or Fe-Ti oxide crystals and show an overall texture that is poikilitic (Fig. 5.21).

Anorthositic rocks are generally massive, but some are mottled and layered. Massive rocks show only granular texture. Mottled rocks comprise granular texture with patches of poikilitic texture. These patches are sub-spherical in form and range from 0.1 – 100 m in diameter. Primary layering comprises rhythmic alternations of granular and poikilitic texture. Individual layers are 0.1 – 10 m thick, 100's of m's in lateral extent and sub-horizontal to moderately (20° – 50°) dipping. Layers dip east on the eastern side of the inner zone and west on the western side, thereby defining a broadly convex upward form (domal attitude in Ryan, 2001a) for the inner zone.

Anorthositic rocks also contain pods that consist almost entirely of medium-sized to very large, poikilitic, pyroxene crystals (Fig. 5.22). These pods are sub-spherical in form and range from 10 – 200 cm in diameter, and pass into planar aggregates that also contain high abundances of poikilitic pyroxene crystals.

The Lister pluton inner zone also contains pink- to red-weathering granitic dikes that are fine- to medium-grained, granular-textured and layered (Fig. 5.23). These dikes are sub-vertically oriented and east-west striking (see Fig. 5.2). Individual layers are 0.1 – 2 cm thick and strike parallel to the trend of these dikes. The granular texture and thin compositional layering of these dikes suggests that they were strongly deformed parallel

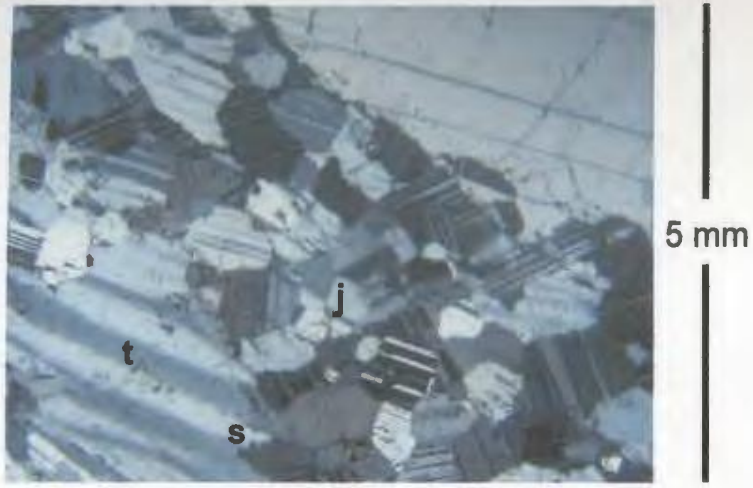

Figure 5.19: Thin section (XPL) of TLi anorthosite that contains large to small plagioclase crystals. Large crystals show deformation twins (t) and serrated grain margins (s). Small crystals show triple junctions (j) and equilibrated geometry.

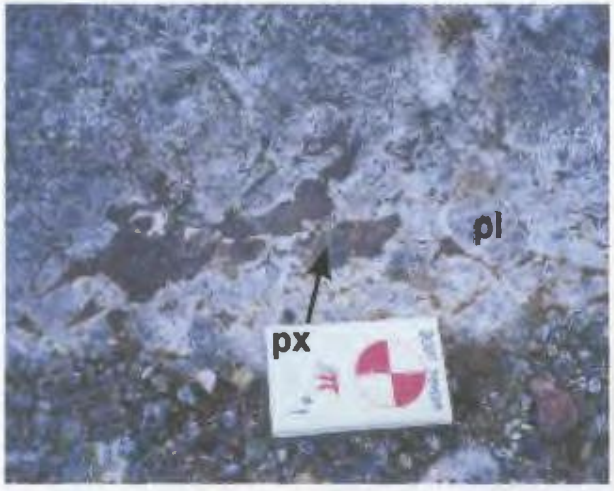

Figure 5.21: Large to very large plagioclase grains (pl) and poikilitic pyroxene crystals (px) in anorthositic rocks of TLi. Anorthositic rocks show a granular to poikilitic texture. Photo taken on hills to the north of Tessiuyarsuk Bay.

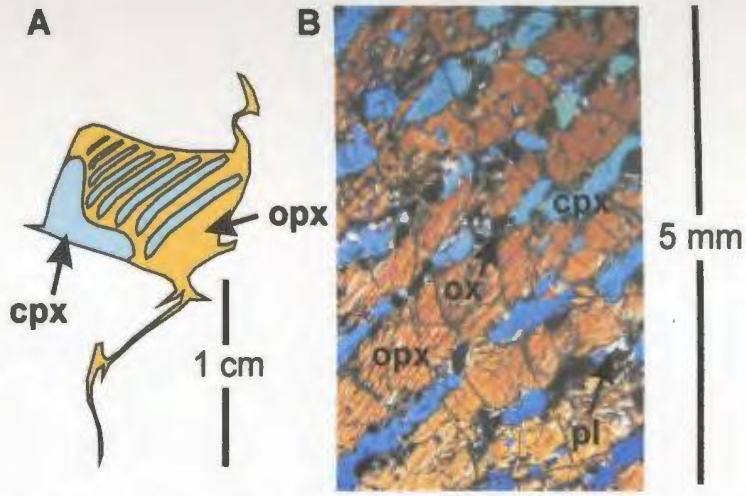

Figure 5.20: (A) Thin section sketch and (B) thin section photo (XPL) of the same poikilitic orthopyroxene crystal in TLi. Photo shows orthopyroxene host (opx) and exsolved clinopyroxene (cpx), plagioclase (pl) and Fe-Ti oxide (ox).

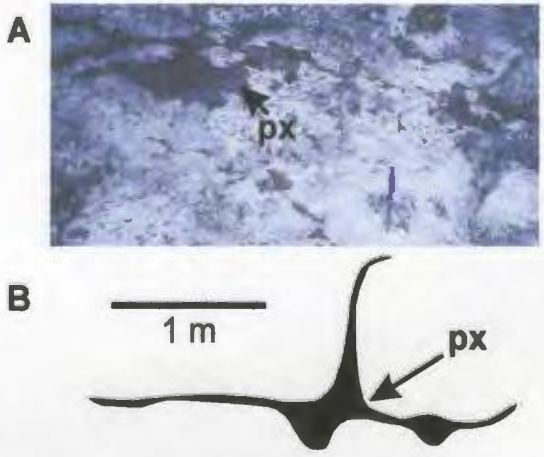

Figure 5.22: (A) Field photo and (B) field sketch of pyroxene pods (px) in TLi anorthosite. Sketch shows a pod that passes into pyroxene-rich veins. Photo and sketch taken on highlands to the northeast of Tasiyuyaksuk Brook.

to strike. These strongly deformed rocks are unique in that they occur within the Lister pluton inner zone, as opposed to the more common occurrence of strongly deformed rocks along intrusion margins.

Mineral compositions

Studies by Xue and Morse (1993, 1994) analyzed the mineral and whole rock chemistry for one sample of anorthosite from the Lister pluton (Lister massif in Xue and Morse, 1993; 1994) and grouped this anorthosite with the noritic anorthosite group (see Table 3.4). This study found that mineral compositions in anorthositic rocks of the Lister pluton inner zone range from An_{42-44} in plagioclase and averages En_{59} in orthopyroxene (Table 5.3). These compositions fall in the range shown by NB noritic anorthosite. Plagioclase and orthopyroxene crystals are homogeneous in composition. Orthopyroxene contains exsolved clinopyroxene (En_{40}) and <0.8 wt% Al_2O_3.

5.3.2 Lister pluton border zone (TLb)

Form and contacts

Geological mapping as part of this thesis outlined a unit of moderately dipping, layered, coarse-grained, leuconorite, leucogabbronorite and anorthosite that is here named the Lister pluton border zone (see Fig. 5.2). The base of this unit shows a gradational increase in the abundance of sub-horizontal, massive, anorthosite that marks the top of the Lister pluton inner zone. In the study area, the Lister pluton border zone is exposed east, south and west of the inner zone. In the east, the top of the border zone

shows a sharp and deformed contact with monzonitic rocks of the Kangilialuk sheet (see Fig. 5.11). In the south, the top of the border zone is truncated by anorthositic rocks that extend as sheets and veins from the base of the Bird sheet. In the west, the top of this unit cuts anorthositic and gabbronoritic rocks in the Tasiyuyaksuk sheet (see Fig. 5.6).

The eastern part of the Lister pluton border zone is 2.7 – 5.0 km thick, steeply (50° – 80°) east dipping and north-south striking (see Fig. 5.14). The southern border zone is 1.6 – 2.4 km thick, moderately (50° – 60°) south dipping and east-west striking (see Fig. 5.2). The western border zone is 1.3 – 4.0 km thick, moderately (~60°) west dipping and north-south striking. The thickness and structural transitions through the eastern, southern and western parts of the border zone are smooth. The orientation and thickness of the border zone defines an asymmetric, outward dipping envelope around the inner zone and suggests the form of a bell-jar pluton.

The contact with the Bird sheet comprises a zone of interleaved veins, sheets and slab-like xenoliths (Fig. 5.24) that is moderately dipping, broadly east-west striking and 1 – 2 km thick (see Figs 5.2, 5.40, 5.41). This zone strikes parallel to primary layering and foliation in both the Lister pluton border zone and the Bird sheet. As well, the anorthositic rocks of the Bird sheet are of uniform coarse-grain size right up to intrusive contacts with the Lister pluton border zone.

Petrography

The mineralogy and textures of anorthositic rocks in the border zone suggest that, like the inner zone, plagioclase is cumulus, pyroxene is intercumulus and Fe-Ti oxide is

Figure 5.23: Strongly deformed granitic dike in the Lister pluton inner zone. This dike is sub-vertically orientated and east-west striking. Photo taken southwest of Kaiktusuak point.

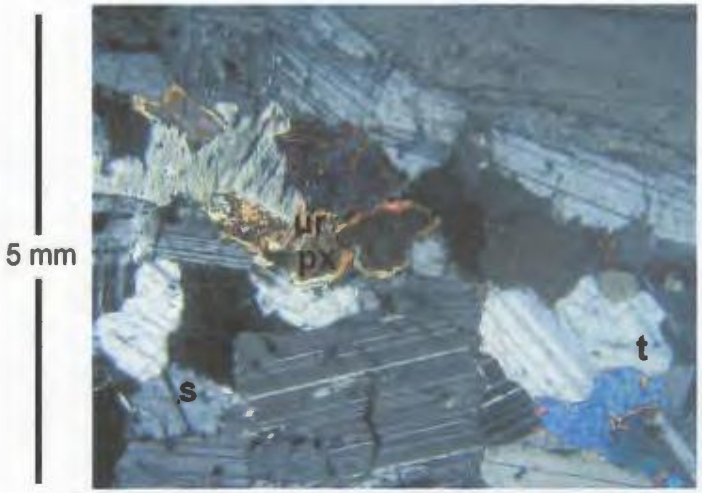

Figure 5.25: Thin section photo (XPL) of leucogabbronorite in TLb. Plagioclase shows deformation twins (t) and serrated margins (s). Pyroxene (px) is rimmed by uralite (ur).

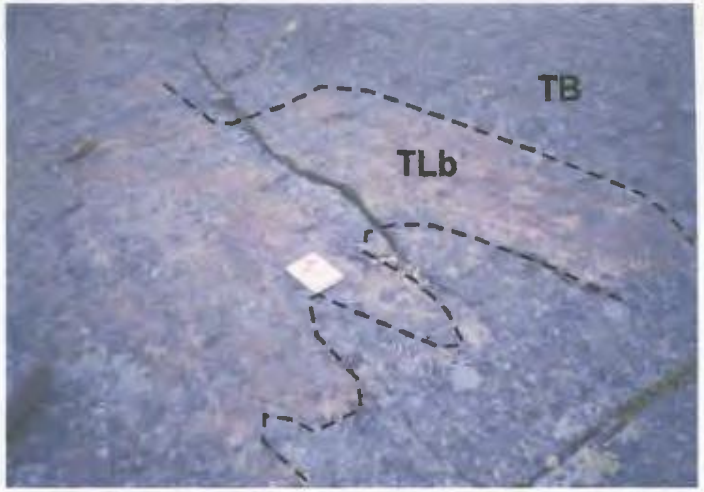

Figure 5.24: Xenolith of Lister pluton border zone anorthositic rocks (TLb) in Bird sheet anorthositic rocks (TB). TLb is layered and TB is massive. Dashed line outlines the xenolith. Photo taken west of Tessiuyarsuk Bay.

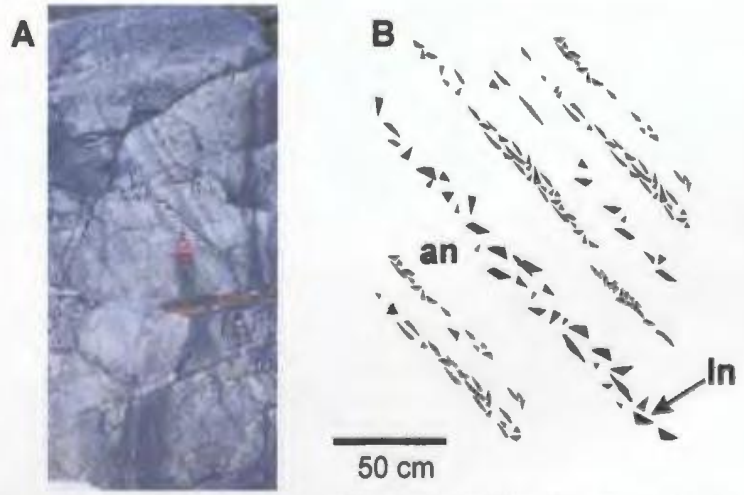

Figure 5.26: (A) Field photo and (B) field sketch of moderately east dipping primary layers in TLb. Sketch shows textural and modal contrast between granular-textured anorthosite (an) and poikilitic-textured leuconorite (ln) layers. Photo taken west of Kangilialuk Lake.

intercumulus. Similarly, cumulus plagioclase also shows abundant evidence for high-T deformation and recrystallization (Fig. 5.25).

In contrast, plagioclase crystals in the border zone are generally of smaller size (0.1 – 30 cm) relative to the inner zone. Orthopyroxene crystals also contain blebs and lamellae of exsolved clinopyroxene, and locally some crystals contain exsolved blebs and lamellae of plagioclase that suggest an original high-alumina composition. In some cases, orthopyroxene shows a tabular form that suggests it crystallized on the liquidus and elsewhere shows kinks and fractures that indicate it was deformed. Minor and accessory minerals consist of very small quartz and apatite grains.

Secondary minerals replaced up to 5% plagioclase and pyroxene crystals. Altered plagioclase contains sericite and saussurite that suggest hydrothermal alteration. Altered pyroxene contains uralite and amphibole that also suggest hydrothermal alteration. Some Fe-Ti oxide crystals show a partial corona of very small biotite laths.

Textures and structures

Anorthositic rocks are medium- to very coarse-grained and show an overall texture that ranges from poikilitic (~10 – 40% poikilitic crystals and aggregates) to granular (<10% poikilitic crystals and aggregates). Some poikilitic orthopyroxene crystals form sub-spherical oikocrysts that are 5 – 20 cm in diameter.

Anorthositic rocks are layered, foliated and/or mottled. Primary layering comprises rhythmic alternations of poikilitic and granular texture (Fig. 5.26). These layers are 0.1 – 10 m thick, 100's of m in lateral extent and moderately dipping to sub-

vertical. Foliated rocks contain lens-shaped, poikilitic, pyroxene crystals and crystal aggregates (Fig. 5.27) that comprise a flattened poikilitic texture. These lens-shaped forms are 1 – 5 cm in diameter, 0.05 – 0.5 cm thick and strike parallel to layering. Mottled rocks comprise interspersed patches of poikilitic and granular texture. These patches are sub-spherical in form and range from 0.1 – 10 m in diameter (Fig. 5.28).

Anorthositic rocks also contain planar aggregates of medium-sized to very large, poikilitic, pyroxene crystals (Fig. 5.29). These aggregates are 1 – 100 cm thick and 1 – 10's of m's long, and strike parallel to layering and foliation.

In the eastern-most ~700 m of the border zone, some layered rocks show granular texture (Fig. 5.30) and sigmoidal layers, and contain large plagioclase porphyroclasts with sigmoidal tails of small plagioclase grains (Fig. 5.31). These sigmoidal features suggest that primary layers were overprinted by dextral shear deformation. These deformed layers are 0.1 – 20 cm thick, steeply (70° – 80°) east dipping to sub-vertical and north-south striking. The orientation of these deformed rocks is parallel to compositional and gneissic layering in the Kangilialuk Lake country rock belt. As well, pyroxene-rich veins were emplaced parallel to layering in these deformed anorthositic rocks and show splay structures that indicate they were emplaced during dextral shearing (Fig. 5.32).

The eastern part of the Lister pluton border zone contains sub-vertically oriented and northwest-southeast striking dikes (see Map 1). These dikes consist predominantly of fine- to medium-grained monzonitic rocks. Ryan and James (2003) reported that a parallel set of pegmatoidal ferrodiorite dikes (the most easterly of the northwest-southeast

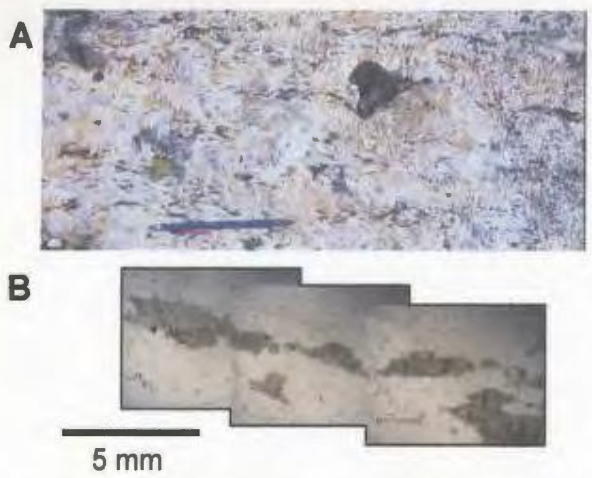

Figure 5.27: (A) Field photo and (B) thin section photo (XPL) of primary foliation in anorthosite of TLb. Pen lies parallel to foliation in field photo. Thin section photo shows a cross-section through a lens-shaped aggregate of pyroxene. Photo and sample taken west of Kangilialuk Lake.

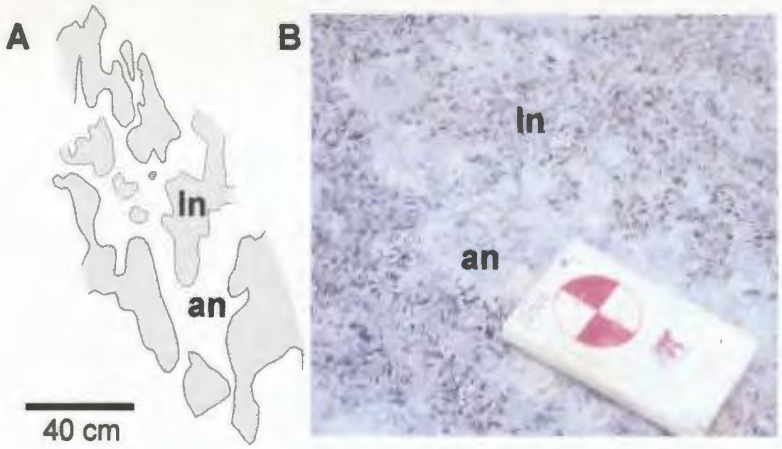

Figure 5.28: (A) Field sketch and (B) photo of mottled rocks in TLb. These rocks comprise interspersed patches of granular-textured anorthosite (an) and poikilitic-textured leuconorite (ln). Photo and sketch taken on hills above the northern shoreline of Nain Bay.

Figure 5.29: Aggregate of very large poikilitic pyroxene crystals in TLb leucogabbronorite. Photo taken southwest of Kangilialuk Lake.

Figure 5.30: Thin and strongly deformed primary layers of anorthositic rocks in the Lister pluton border zone. Photo taken southwest of Kangilialuk Lake.

dikes on Map 1) contain zircons that crystallized at ca. 1328 Ma. These relations indicate that, in the study area, the Lister pluton was emplaced and deformed prior to 1328 Ma.

Mineral compositions and whole rock chemistry

Mineral compositions in anorthositic rocks range from An_{41-47} in plagioclase and En_{57-62} in orthopyroxene (Table 5.3). These compositions fall in the range shown by NB noritic anorthosite. Plagioclase grains are homogeneous in composition. Orthopyroxene grains are also homogeneous in composition and contain <1.4 wt% Al_2O_3. The composition of clinopyroxene grains and exsolved lamellae ranges from En_{39-41}.

Table 5.3: Mineral compositions (*) and whole rock chemistry for TLb anorthositic rocks and comparative data for NB noritic and troctolitic anorthosite

Rock type	Sample	Pl*	Opx*	SiO_2	K_2O	Ca/Al	Sr/Ca*10	Mg/(Mg+Fe)	An/(An+Ab)
		An	En	wt%	wt%				CIPW
Lister pluton inner zone (TLi)									
px anor	00-24-7	43							
lgn	00-24-13	44	59						
Lister pluton border zone (TLb)									
ln	01-37-9	46	60						
lgn	02-5-7	42	60	55.27	0.70	0.95	0.14	0.33	0.51
lgn	01-12-15a	43	62						
lgn	02-22-7	44	58	54.54	0.79	0.97	0.13	0.22	0.50
lgn	02-24-23	41	57	52.98	0.66	1.15	0.13	0.28	0.47
lgn	02-15-14	47	60	54.65	0.74	0.92	0.14	0.35	0.49
ox an	02-11-15	45		47.41	0.56	1.17	0.14	0.03	0.51
defm an	02-8-6	43		54.63	0.71	0.96	0.15	0.14	0.50
Comparative data									
NB noritic		40 - 54	57 - 67	52 - 58	0.6 - 1.2	0.8 - 1.1	0.10 - 0.15	0.10 - 0.35	0.42 - 0.54
NB troctolitic		51 - 68	66 - 73	49 - 55	0.2 - 0.6	1.0 - 1.2	0.06 - 0.09	0.15 - 0.49	0.53 - 0.68

Whole rock chemistry of anorthositic rocks shows wt% SiO_2, wt% K_2O, Ca/Al, Sr/Ca and Mg/(Mg+Fe) that fall in the range shown by NB noritic anorthosite (Table 5.3,

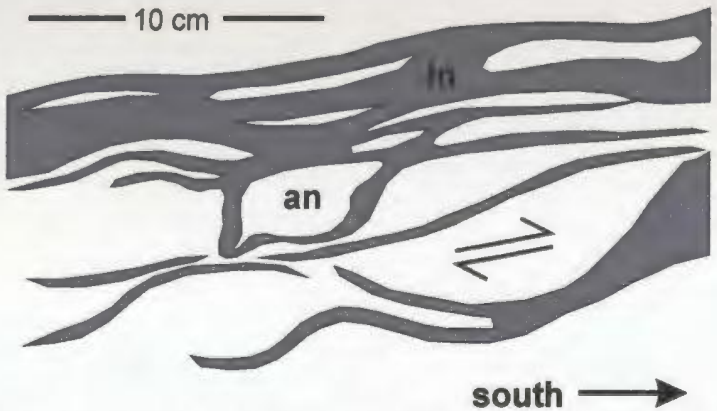

Figure 5.31:Field sketch of strongly deformed primary anorthosite (an) and leuconorite (ln) layers in the outer-most 50 m of the Lister pluton border zone. Layers show asymmetric forms that indicate they were overprinted by dextral shear deformation. Sketch made on the southern shoreline of Nain Bay.

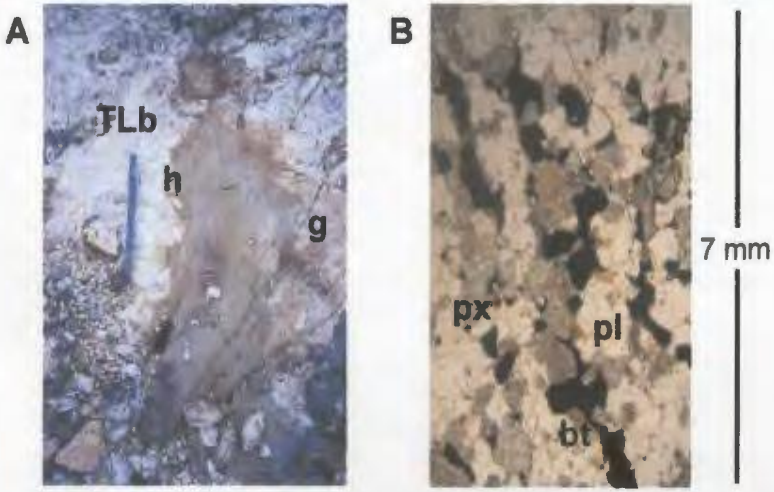

Figure 5.33: (A) Field photo and (B) thin section photo (PPL) of an oxide gabbronorite dike in anorthositic rocks of TLb. (A) Dike shows a sharp (h) to gradational (g) contact. (B) Rock contains small plagioclase grains (pl) pyroxene grains (px), sub-poikilitic oxide crystals (black in photo) and biotite laths (bt)

Figure 5.32: Pyroxene-rich vein in the Lister pluton border zone. Tip of the hammer points south. Splay structures (splay) indicate emplacement during dextral shearing. Photo taken north of Kangilialuk Lake.

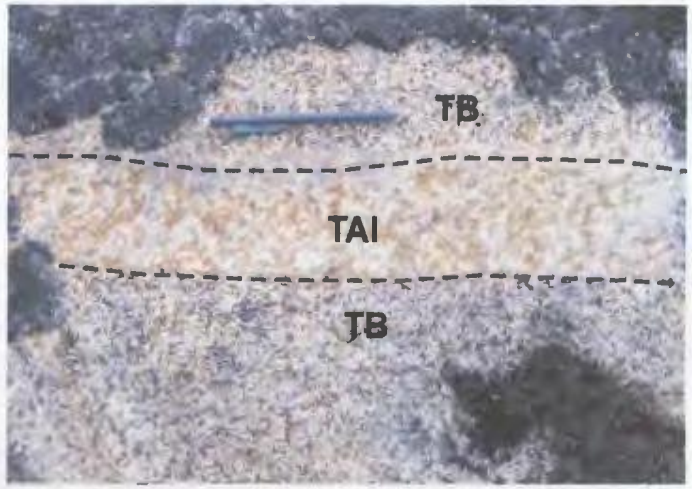

Figure 5.34: Leucogabbronorite of the Bird sheet (TB) cut by a gabbronorite dike that extends from the Anaktalik lower sheet (TAl). Dashed lines indicate intrusive contacts. Photo taken west of Tessiuyarsuk Bay.

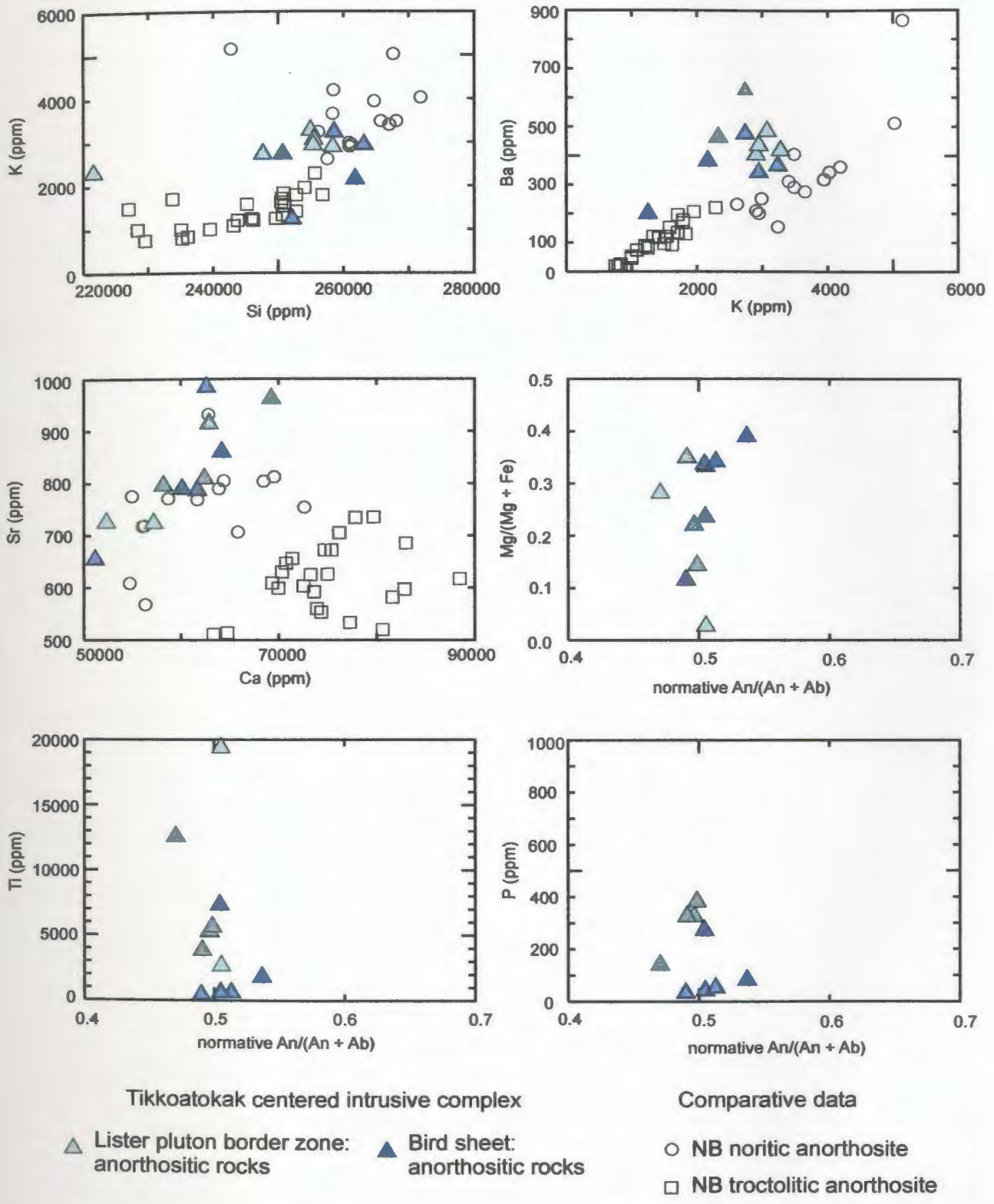

Figure 5.35: Whole rock chemistry for anorthositic rocks in the Lister pluton border zone and the Bird sheet, and comparative data for NB noritic and troctolitic anorthosite. The Lister pluton border zone is described in section 5.3.2 and the Bird sheet is described in section 5.4.

see Fig. 5.35). Whole rock Ba/K (0.16 – 0.26) is high in comparison to both NB noritic and troctolitic anorthosite (0.08 – 0.19). CIPW norms consist mostly of plagioclase and pyroxene, and show normative plagioclase compositions that fall in the range shown by NB noritic anorthosite.

The mineral compositions and whole rock chemistry of strongly deformed anorthositic rocks falls in the range shown by weakly deformed anorthositic rocks, although one sample (02-21-10) shows abundances of SiO_2 (56.40 wt%), Na_2O (5.85 wt%), K_2O (1.75 wt%), Rb (17 ppm) and Pb (8 ppm) that are high in comparison to weakly deformed anorthositic rocks.

Summary

Field relations, textures, mineral compositions, whole rock chemistry and compiled U-Pb geochronology indicate that the Lister pluton comprises part of the 'old anorthosite event' (after Yu and Morse, 1993) and the 'noritic anorthosite group' (after Xue and Morse, 1993; 1994). The outer-most part of the Lister pluton border zone contains strongly deformed rocks that were overprinted by Mesoproterozoic, dextral, sub-vertically oriented and north-south striking shear deformation.

Oxide gabbronorite sills

The Lister pluton border zone contains fine- to medium-grained oxide gabbronorite sills. These sills are most abundant in the eastern part of the border zone (see Fig. 5.10) and were intruded concordant to primary layering and foliation. Individual

sills are 0.1 – 10 m thick and 1 – 100 m long. Intrusive contacts are sharp or grade into anorthositic rocks that contain aggregates of small plagioclase, pyroxene and Fe-Ti oxide crystals (see Fig. 5.33). These aggregates are interstitial to larger cumulus plagioclase.

Oxide gabbronorite consists of small to medium-sized plagioclase and pyroxene grains, and small to medium-sized, sub-poikilitic, Fe-Ti oxide crystals (see Fig. 5.33). Some plagioclase and pyroxene crystals show tabular forms that suggest they crystallized on the liquidus. Accessory minerals consist of very small biotite laths, amphibole grains, apatite grains and zircon grains.

5.4 Bird sheet (TB)

Form and contacts

Geological mapping as part of this study found a unit of moderately dipping, layered, coarse-grained leucogabbronorite, leuconorite and anorthosite that is here named the Bird sheet (after Dead Bird Brook, Fig. 3.1). The bottom of this unit truncates anorthositic rocks in the Lister pluton border zone as described in section 5.3.2. The top of this unit is truncated by veins and sheets that extend from the base of the Anaktalik lower sheet (see Fig. 5.34).

The Bird sheet is 0.5 – 2.0 km thick, 17 km long, moderately (60° – 70°) south dipping and east-west striking (see Fig. 5.2). To the west, the sheet swings around into a moderately (60° – 70°) west dipping and north-south striking orientation. The contact with the Anaktalik lower sheet comprises a zone of veins, sheets and slab-like xenoliths

that is ~50 m thick. This zone strikes parallel to primary layering in the Bird sheet and the orientation of the Anaktalik lower sheet.

Petrography

The textures and mineralogy of anorthositic rocks in the Bird sheet are also similar to the anorthositic rocks of the Lister pluton (section 5.3). Hence, these similarities indicate that plagioclase is cumulus, pyroxene is intercumulus and Fe-Ti oxide is also intercumulus. In addition, cumulus plagioclase was likewise deformed and recrystallized at high-T. These similarities between all anorthositic rocks in the Tikkoatokak centered intrusive complex indicates that they all crystallized form plagioclase-rich magmas and that they were all partly deformed and recrystallized at high-T.

In general contrast to the anorthositic rocks of the Lister pluton, the anorthositic rocks in the Bird sheet contain plagioclase with minute rods of exsolved oxide and small inclusions of rounded pyroxene. Some plagioclase crystals show rims that were replaced by myrmekite (Fig. 5.36). Fe-Ti oxide crystals are small and show sub-poikilitic texture, suggesting that these oxides crystallized out of the intercumulus liquid. Minor and accessory minerals consist of small poikilitic inverted pigeonite crystals, very small quartz grains and very small apatite grains.

Textures and structures

The textures and structures of anorthosite, leucogabbronorite and leuconorite are also similar to equivalent rock types in the Lister pluton border zone. Primary layering and foliation are moderately (60° – 70°) south dipping and east-west striking in most of the sheet, and moderately (60° – 70°) west dipping and north-south striking in the western part. There is a smooth gradation in the orientation of layered and foliated rocks from south dipping to west dipping.

The Bird sheet contains a ~50 m wide belt of layered anorthositic rocks that show granular texture (Fig. 5.37) and sigmoidal strings of small pyroxene crystals. These strings suggest that the primary layers were overprinted by localized and sinistral shear deformation. Individual layers are 0.1 – 10 cm thick, moderately to steeply (45° – 60°) south dipping and east-west striking. The location of these strongly deformed rocks is shown on Fig. 5.40.

Mineral compositions and whole rock chemistry

Mineral compositions in anorthositic rocks range from An_{43-44} in plagioclase and averages En_{58} in orthopyroxene. These compositions fall in the range shown by NB noritic anorthosite (Table 5.4). Some plagioclase crystals show rims that are Ca-rich (up to $+An_{35}$) relative to the rest of the grain. Orthopyroxene contains <0.91 wt% Al_2O_3. The composition of clinopyroxene grains and exsolved lamellae ranges from En_{37-39}.

Whole rock chemistry of anorthositic rocks shows wt% SiO_2, Ca/Al, Sr/Ca and Mg/(Mg+Fe) that fall in the range shown by the Lister pluton and NB noritic anorthosite,

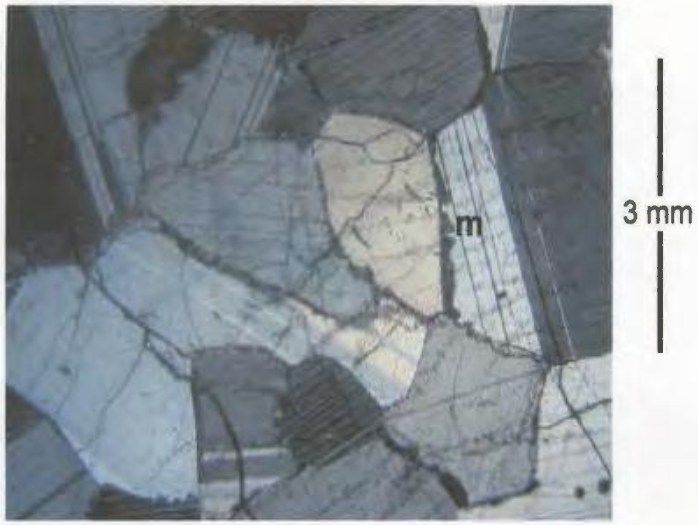

Figure 5.36: Thin section photo (XPL) of anorthosite in TB. Plagioclase crystals show equilibrated geometry and rims of calcic myrmekite (m).

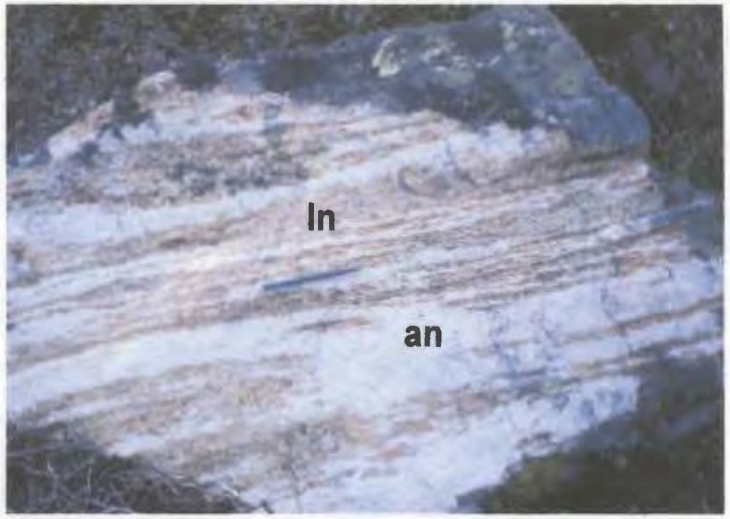

Figure 5.37: Strongly deformed primary layering in anorthositic rocks of the Bird sheet. Layers consist of fine-grained, granular-textured, anorthosite (an) and leuconorite (ln). Photo taken due west of Tessiuyarsuk Bay.

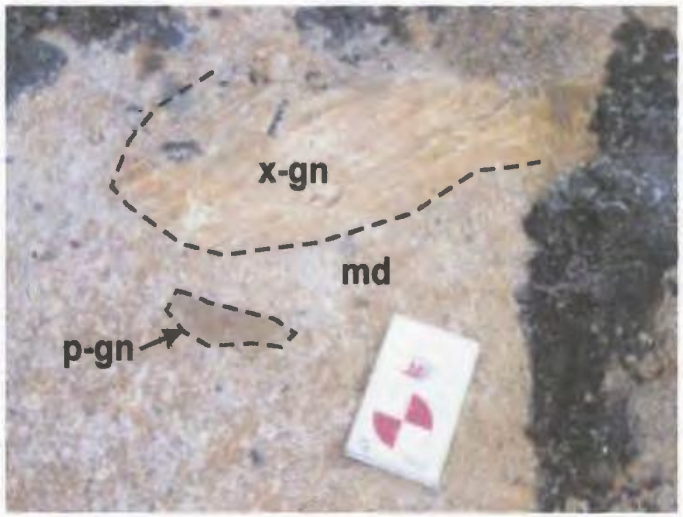

Figure 5.38: Xenoliths (x-gn) and pillows (p-gn) of gabbronorite in hybrid monzodiorite (md) that separates the Anaktalik lower and upper sheets. Xenoliths are layered and pillows are massive and fine-grained. Dashed lines outline xenoliths. Photo taken due west of Tessiuyarsuk Bay.

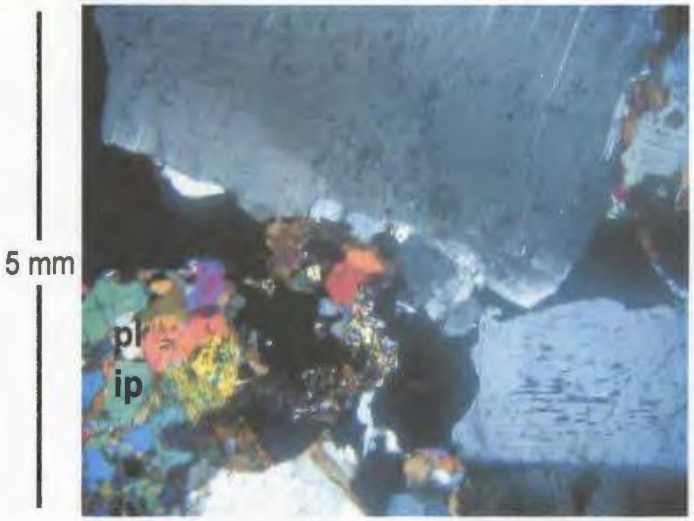

Figure 5.39: Thin section photo (XPL) of oxide gabbronorite in TA1. This rock contains large and tabular plagioclase crystals, and interstitial aggregates of small to medium-sized plagioclase (pl), inverted pigeonite (ip) and oxide (black in photo) grains.

whereas wt% K_2O falls below these ranges (see Fig 5.35). These lower overall abundances of K_2O likely reflect a decrease in the orthoclase component contained within cumulus plagioclase. Ba/K ratios (0.14 – 0.21) are high in comparison to NB noritic and troctolitic anorthosite (0.08 – 0.19). CIPW norms consist mostly of plagioclase and pyroxene, and show normative plagioclase compositions that fall in the range shown by NB noritic anorthosite. Mineral compositions and whole rock chemistry of strongly deformed anorthositic rocks fall in the range shown by weakly deformed anorthositic rocks, although the abundances of Sr (and Sr/Ca) are the highest found in anorthositic rocks of the Bird sheet.

Table 5.4: Mineral compositions (*) and whole rock chemistry of TB anorthositic rocks and comparative data for the Lister pluton (TL) and NB noritic and troctolitic anorthosite

Rock type	Sample	Pl*	Opx*	SiO_2	K_2O	Ca/Al	Sr/Ca x 10	Mg/(Mg+Fe)	An/(An+Ab)
		An	En	wt%	wt%				CIPW
Bird sheet (TB)									
lgn	02-24-19b	44	58	53.63	0.66	1.01	0.13	0.34	0.50
anor	01-15-5	43							
lgn	02-8-13			53.94	0.30	0.99	0.13	0.39	0.54
lgn	02-7-17ii			56.00	0.52	0.96	0.13	0.34	0.51
anor	02-7-17i			55.32	0.78	0.93	0.13	0.24	0.50
defm anor	02-8-19	44		56.30	0.71	0.91	0.16	0.12	0.49
Comparative data									
TL		41 - 47	57 - 62	53 - 55	0.7 - 0.8	0.9 - 1.2	0.13 - 0.15	0.14 - 0.35	0.47 - 0.51
NB noritic		40 - 54	57 - 67	52 - 58	0.6 - 1.2	0.8 - 1.1	0.10 - 0.15	0.10 - 0.35	0.42 - 0.54
NB troctolitic		51 - 68	66 - 73	49 - 55	0.2 - 0.6	1.0 - 1.2	0.06 - 0.09	0.15 - 0.49	0.53 - 0.68

Summary

Anorthositic rocks in the Bird sheet show: (a) a form that parallels the form of the Lister pluton border zone, (b) structures that parallel structures in the Lister pluton, and

(c) similar rock types to the Lister pluton. For these reasons, the Bird sheet is included with the Lister pluton in the Tikkoatokak centered intrusive complex.

5.5 Anaktalik sheet (TA)

A geological map by Wheeler (1969) shows a small body of adamellitic rock near the entrance of Anaktalik Brook into Anaktalik Bay. A geological map by Ryan (1990) shows that this body consists of country, granitic and Fe-rich gabbroic to dioritic rocks. Geological mapping as part of this study found that this body comprises a sheet of gabbronoritic rocks and a sheet of monzonitic rocks that are separated by a zone of mixed and mingled rocks.

Geological mapping as part of this study outlined the extent of these monzonitic and gabbronoritic rocks (Figs. 5.40, 5.41). The monzonitic rocks overlie the gabbronoritic rocks. The contact between these rocks comprises a zone of mixed and mingled rocks (see Fig. 5.38) that indicate the lower and upper sheets are of similar age. For these reasons, the gabbronoritic rocks are grouped into the Anaktalik lower sheet and the monzonitic rocks are grouped into the Anaktalik upper sheet.

5.5.1 Anaktalik lower sheet (TAl)

Form and contacts

Geological mapping as part of this study outlined a unit of moderately dipping, massive, coarse-grained, oxide gabbronorite and leucogabbronorite that is here named the Anaktalik lower sheet. The base of this unit truncates the top of the Bird sheet as

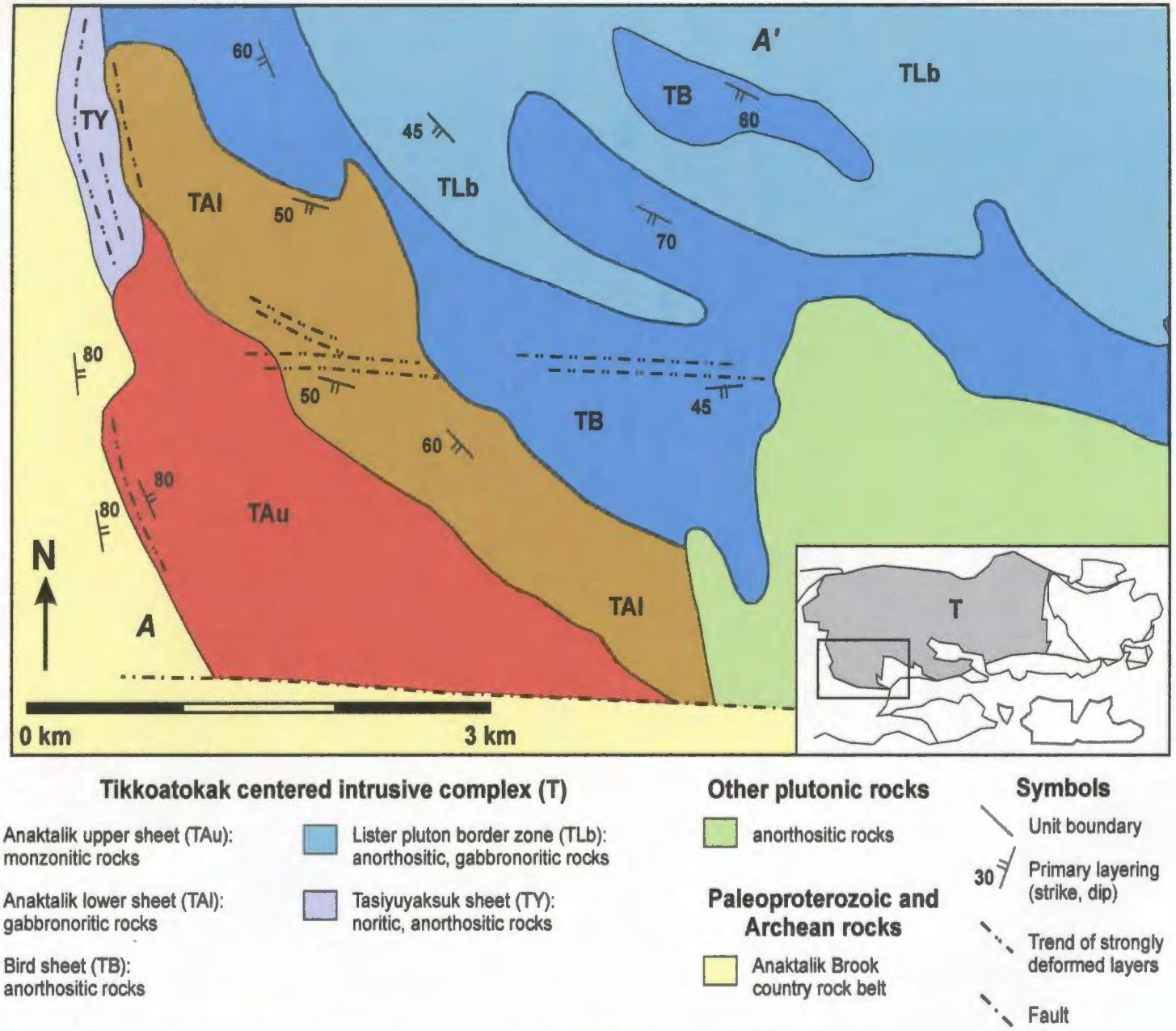

Figure 5.40: Solid geological map for the southwestern part of the Tikkoatokak centered intrusive complex. A and A' mark cross-section shown in Fig. 5.41.

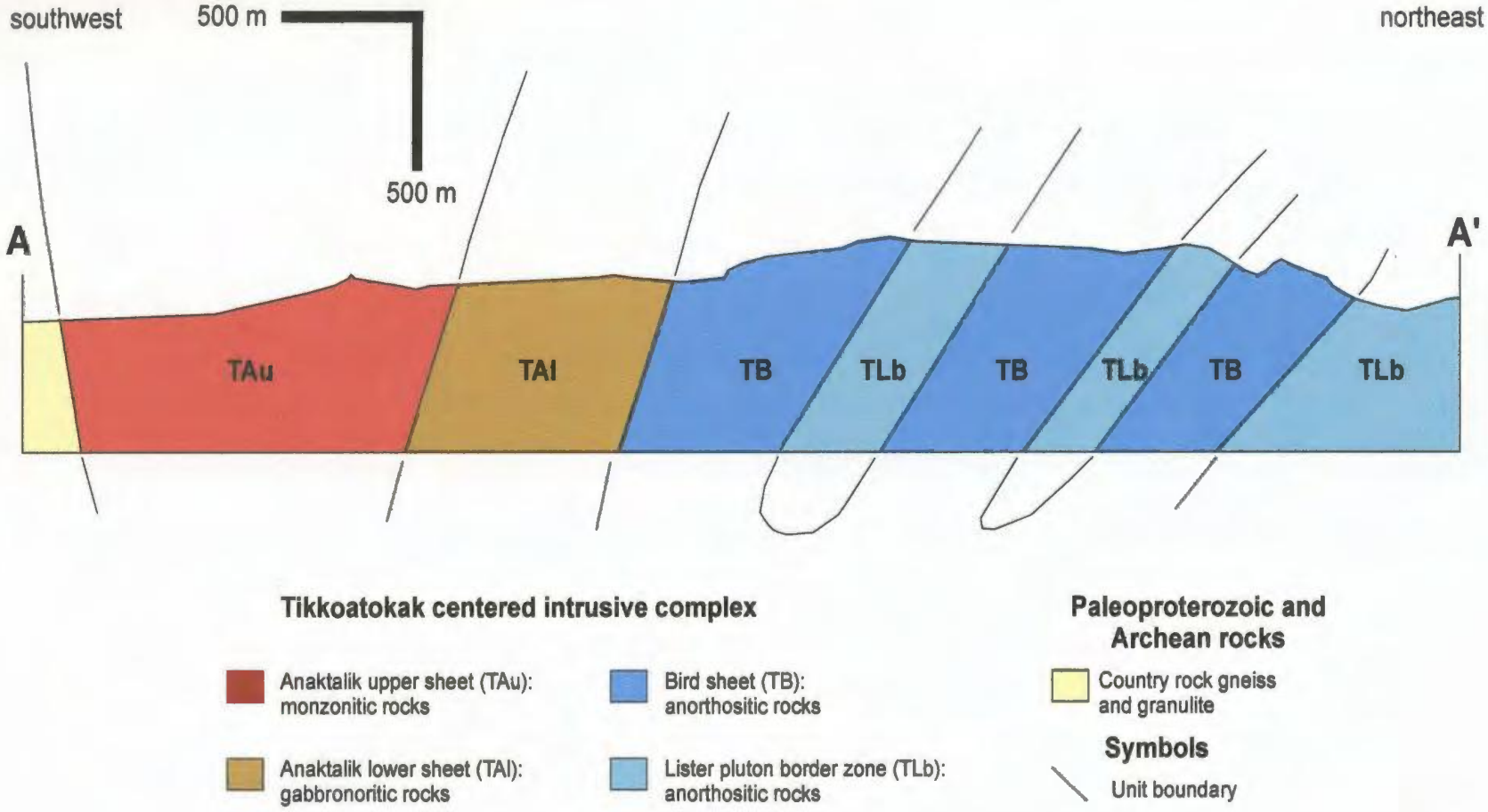

Figure 5.41: Southwest to northeast cross-section through the southwestern part of the Tikkoatokak centered intrusive complex. Localities A and A' are shown on Fig. 5.40.

described in section 5.3. The top of this unit comprises a ~200 m thick zone of xenoliths, pillows and hybridized rocks that marks the gradational contact with monzonitic rocks in the overlying Anaktalik upper sheet. Xenoliths and pillows consist of gabbronoritic rocks. The xenoliths are rounded to angular, medium-grained, and layered, whereas the pillows are lobate to rounded, fine-grained, and massive. The rocks that host these xenoliths and pillows consist of monzodiorite and monzogabbro (gabbroic rocks +/- xenocrysts of alkali feldspar). These rocks are intermediate in composition to gabbronoritic rocks in the lower sheet and monzonitic rocks in the upper sheet, thereby suggesting that they are hybrids.

The Anaktalik lower sheet is 0.5 – 0.9 km thick, 5.8 km long, moderately (50° – 60°) southwest dipping and northwest to southeast striking (Figs. 5.40, 5.41).

Petrography

Plagioclase and inverted pigeonite crystals are of similar medium to large size and show tabular to granular forms, suggesting that they crystallized together on the liquidus. Very large plagioclase laths suggest prolonged crystallization of plagioclase on the liquidus or xenocrysts that were derived from underlying anorthositic rocks. Some plagioclase crystals show interlobate to serrated margins that indicate they were partly deformed at high-T. Large plagioclase laths (Fig. 5.39) show an increase in blebs of exsolved K-feldspar towards grain margins. Fe-Ti oxide crystals are sub-poikilitic, suggesting that they crystallized out of the intercumulus liquid. Accessory minerals

consist of small quartz grains, small biotite laths, small hornblende grains, very small apatite grains and very small zircon grains.

Textures and structures

Gabbronorite is medium- to coarse-grained and shows an overall texture that ranges from granular to porphyritic. Leucogabbronorite is also medium- to coarse-grained and shows an overall texture that is poikilitic.

Gabbronorite and leucogabbronorite form massive rocks, and lesser abundances of rocks that are layered or mottled. Massive rocks comprise only granular, porphyritic or poikilitic texture. Primary layering comprises rhythmic alternations of granular- to porphyritic-textured gabbronorite and poikilitic-textured leucogabbronorite. Individual layers are ~10 – 100 cm thick, moderately southwest dipping and northwest to southeast striking. Mottled rocks comprise patches of poikilitic-textured leucogabbronorite that are interspersed in granular- to porphyritic-textured gabbronorite (Fig. 5.42). These leucogabbronorite patches are sub-spherical in form and range from 0.1 – 10 m in diameter.

The Anaktalik lower sheet contains two belts of compositionally layered, granular-textured, gabbronorite and pyroxene diorite (Fig. 5.43). One of these belts occurs within the interior of the sheet and is ~50 m wide. Individual layers in this belt are ~0.1 – 10 cm thick, moderately to steeply (45° – 60°) south dipping and east-west striking. In addition, the rocks in this belt contain sigmoidal strings of small pyroxene and Fe-Ti oxide crystals that indicate compositional layers were overprinted by sinistral shear

deformation. This belt is structurally continuous with the belt of strongly deformed rocks in the Bird sheet The second belt of compositionally layered rocks occurs in the western-most ~10 – 100 m of the Anaktalik sheet and lies adjacent to the Anaktalik Brook country rock belt. Individual layers in this belt are ~0.1 – 20 cm thick, sub-vertically oriented and north-south striking. The orientation of this layering is parallel to compositional and gneissic layering in the Anaktalik Brook country rock belt. Rock types contain large plagioclase porphyroclasts that were recrystallized into numerous very small grains. This orientation of layering and recrystallization of rock types suggests that these compositionally layered rocks were also overprinted by deformation.

Mineral compositions and whole rock chemistry

Mineral compositions in gabbronorite range from $An_{42–47}$ in plagioclase, $En_{45–60}$ for orthopyroxene component in inverted pigeonite and $En_{34–40}$ for the clinopyroxene component in inverted pigeonite. Plagioclase compositions fall in the range shown by anorthositic rocks in the Lister pluton and are Na-rich in comparison to Paleoproterozoic gabbroic granulite (Fig. 5.44, Table 5.5). Plagioclase shows either a slight reverse (up to $+An_5$) or normal (up to $-An_7$) zoning. Pyroxene compositions are Fe-rich in comparison to anorthositic rocks in the Lister pluton and Paleoproterozoic gabbroic granulite.

Whole rock chemistry of gabbronorite shows that wt% TiO_2, FeO_t and P_2O_5 are high in comparison to Paleoproterozoic gabbroic granulite (see Fig. 5.13). High abundances of these major elements are consistent with Fe-Ti oxide and apatite that were observed in thin section. Whole rock chemistry for one sample of strongly deformed

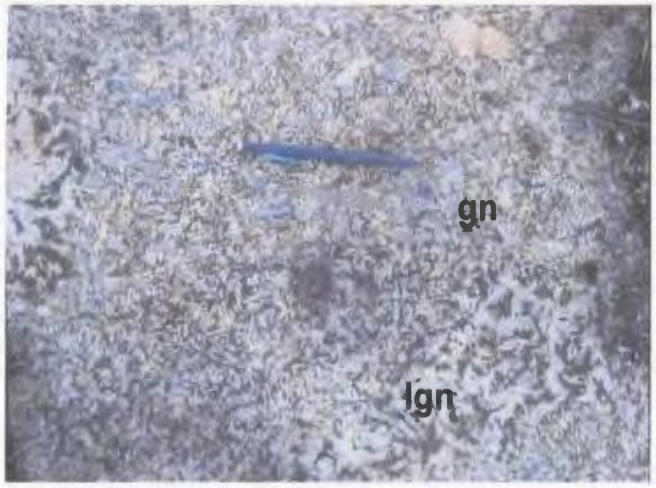

Figure 5.42: Mottled gabbronorite (gn) and leucogabbronorite (lgn) in TA1. Photo taken west of Tessiuyarsuk Bay.

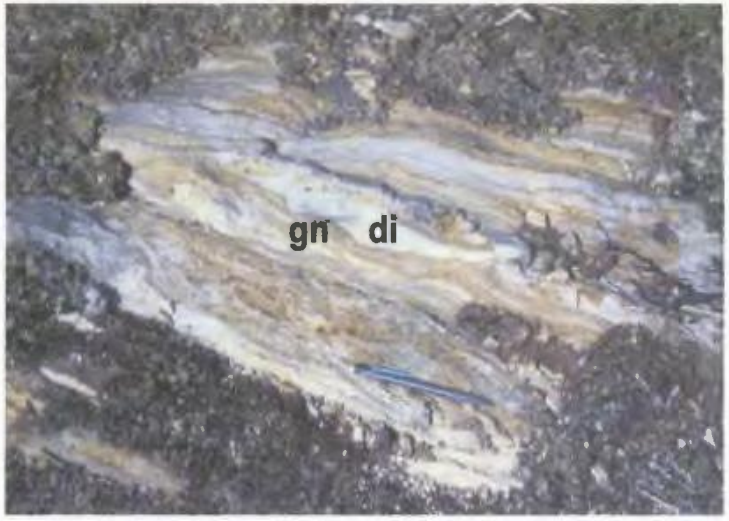

Figure 5.43: Strongly deformed compositional layers of gabbronorite (gn) and pyroxene diorite (di) in the Anaktalik lower sheet. Rock types are fine-grained and granular. Photo was taken north of Anaktalik Brook.

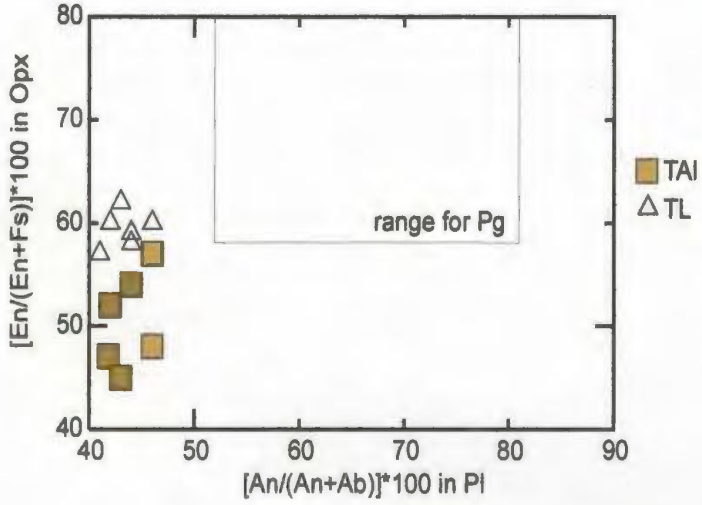

Figure 5.44: Comparison of orthopyroxene and plagioclase compositions in Anaktalik lower sheet gabbronorite (TA1) with those in anorthositic rocks of the Lister pluton (TL) and Paleoproterozoic gabbroic granulite (Pg).

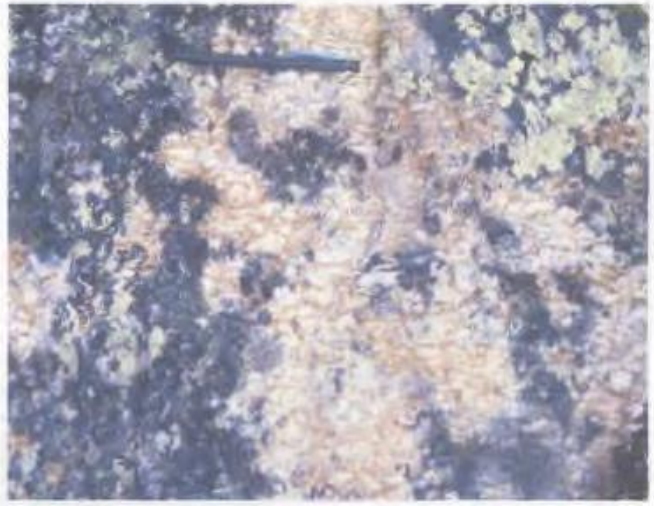

Figure 5.45: Strongly recrystallized plagioclase phenocrysts (white) in foliated monzodiorite of the Anaktalik upper sheet. Pen is aligned parallel to foliation and trends north-south. Photo taken south of Tasiyuyaksuk Brook.

gabbronorite shows relatively low wt% TiO_2 and P_2O_5, and high wt% MgO, that are consistent with a predominantly plagioclase-pyroxene mode in thin section. CIPW norms consist mostly of plagioclase, pyroxene +/- olivine, as well as 6 – 9% normative Fe-Ti oxide, 3 – 5% normative orthoclase and <1 – 5% normative apatite.

Table 5.5: Mineral compositions (*) and whole rock chemistry for TAl gabbronoritic and anorthositic rocks, and comparative data for anorthositic rocks of the Lister pluton (TL) and Paleoproterozoic gabbroic granulite (Pg)

Rock type	Sample	Pl*	Opx*	TiO_2	FeOt	MgO	P_2O_5
		An	En	wt%	wt%	wt%	wt%
Anaktalik lower sheet (TAl)							
gn	02-18-5	44	54				
gn	02-23-10	43	45	3.44	10.68	2.79	0.25
gn	02-15-23			3.36	18.81	2.95	1.53
gn	02-21-8	42	47	4.86	17.28	4.97	2.17
lgn	02-22-3	42	52				
lgn	02-24-15	46	56				
defm gn	02-17-20a	46	48	1.45	15.86	6.81	0.12
Comparative data							
TL		41 - 47	57 - 62				
Pg		51 - 81	58 - 85	0.4 - 0.8	11 - 13	7 - 31	<0.1

Summary

Gabbronoritic rocks in the Anaktalik lower sheet show: (a) a form that parallels the form of the Bird sheet and Lister pluton border zone, and (b) similar plagioclase composition to anorthositic rocks in the Lister pluton. In addition, the Bird and Anaktalik lower sheets were overprinted by a moderately south dipping, east-west striking, tectonic event that preceded emplacement of the Satosoak pluton. For these reasons, the Anaktalik lower sheet is included in the Tikkoatokak centered intrusive complex.

5.5.2 Anaktalik upper sheet (TAu)

Form and contacts

Geological mapping as part of this study outlined a unit of massive, coarse-grained, pyroxene-bearing monzodiorite, monzonite and quartz-monzonite that is here named the Anaktalik upper sheet. The bottom of this unit comprises a zone of mixed, mingled and hybridized rocks that mark the gradational contact with gabbronoritic rocks in the Anaktalik lower sheet (see Fig. 5.38). The top of this unit is marked by a sharp and concordant contact with Paleoproterozoic gabbroic granulite in the Anaktalik Brook country rock belt.

The Anaktalik upper sheet is 0.5 – 1.3 km thick and 3.8 km long. The sheet is moderately (50° – 60°) southwest dipping and northwest to southeast striking where it overlies the Anaktalik lower sheet, and is sub-vertically oriented at contacts with country rock (see Figs. 5.40, 5.41).

Petrography

Mesoperthite and plagioclase crystals are abundant, large in size and show granular to tabular forms. The tabular forms suggest that both of these minerals crystallized on the liquidus. Undulose extinction and interlobate grain margins indicate both feldspars were deformed and/or recrystallized at high-T. Orthopyroxene grains are small, fractured and contain blebs of exsolved clinopyroxene. Quartz grains are interstitial to feldspar and pyroxene grains. Accessory minerals consist of very small hornblende grains, biotite laths and zircon grains.

Textures and structures

Monzonitic rocks are medium- to coarse-grained and comprise an overall texture that is porphyritic. Massive rocks are abundant, show only porphyritic texture and contain cigar-shaped inclusions of fine-grained gabbronorite that are 1 – 2 cm thick and 5 – 10 cm long.

In the western-most ~10 – 100 m of the Anaktalik upper sheet, monzonitic rocks are compositionally layered and show strongly foliated porphyritic texture. Compositional layers comprise alternations of monzonitic and monzodioritic rocks. Individual layers are ~1 – 5 cm thick, sub-vertically oriented and north-south striking. The foliated rocks contain large phenocrysts of white weathering feldspars in a fine-grained groundmass of feldspar, quartz and pyroxene (Fig. 5.45). The phenocrysts are aligned and comprise a foliation that strikes parallel to compositional layering. In thin section, these feldspar phenocrysts comprise numerous small crystals of plagioclase, quartz and K-feldspar that indicate the phenocrysts were recrystallized. This orientation of layering, granular texture and recrystallized phenocrysts suggest that these compositionally layered and foliated rocks were overprinted by deformation.

Summary

Monzonitic rocks in the Anaktalik upper sheet are included in the Tikkoatokak centered intrusive complex because they were contemporaneous with gabbronoritic rocks in the Anaktalik lower sheet. The outer-most part of this sheet consists of strongly deformed rocks that are analogous to the 'marginal granulites' of the Nain batholith (see

Davies, 1973b; Brand, 1974; Berg and Briegel, 1981; Royse et al., 1999), although the monzonitic composition of these rocks is in contrast to the plagioclase-pyroxene modes that typify 'marginal granulites'.

5.6 Tectonic overprint

The margin of the Tikkoatokak centered intrusive complex contains rocks that: (a) are steeply dipping to sub-vertical, (b) are granular-textured, and (c) show various abundances of deformation structures. These plutonic rocks are here referred to as strongly deformed and comprise the structurally measurable tectonic overprint of the Tikkoatokak centered intrusive complex. This overprint occurs in belts that lie (a) adjacent to the Anaktalik Brook country rock belt (Fig. 5.2, 5.4), (b) adjacent to the Kangilialuk Lake country rock belt (Fig. 5.14), and (c) within the Bird and Anaktalik lower sheets (Fig. 5.40). This section summarizes the deformation in these three belts.

The strongly deformed plutonic rocks that lie adjacent to the Anaktalik Brook country rock belt (see Figs. 5.4, 5.40) were found throughout the Tasiyuyaksuk sheet, and in the western-most 10 – 100 m of the Anaktalik lower sheet and Anaktalik upper sheet (Fig. 5.46). All of these strongly deformed rocks, except for those in the northern part of the Tasiyuyaksuk sheet, are broadly sub-vertically oriented and north-south striking. The orientation of these rocks is parallel to compositional and gneissic layering in the Anaktalik Brook country rock belt. In addition, field relations show that the Lister pluton was emplaced after deformation of the Tasiyuyaksuk sheet and before deformation of the Anaktalik sheets. These findings suggest two episodes of deformation occurred in the

western margin of the Tikkoatokak centered intrusive complex, both of which produced strongly deformed plutonic rocks that are sub-vertically oriented and north-south striking.

The strongly deformed plutonic rocks that lie adjacent to the Kangilialuk Lake country rock belt (see Fig. 5.14) were found throughout the Kangilialuk sheet and in the eastern-most 700 m of the Lister pluton border zone (Fig. 5.46). The contact between these units was also strongly deformed. Deformed rocks in both of these units are steeply (70° – 80°) east dipping to sub-vertical and north-south striking. The orientation of these deformed rocks is parallel to compositional and gneissic layering in the Kangilialuk Lake country rock belt. This study found that the Kangilialuk sheet contains zircons that crystallized at 1341 +/- 4 Ma. In addition, strongly deformed rocks in the Lister pluton border zone were cut by monzonite dikes that crystallized at 1328 Ma and by the weakly deformed Mesoproterozoic Satosoak pluton (see chapter 7). These findings indicate that the eastern margin of the Tikkoatokak centered intrusive complex was deformed between ca. 1341 and 1328 Ma.

Strongly deformed plutonic rocks were also found in a ~50 m thick belt (see Fig. 5.40) that cuts across weakly deformed plutonic rocks in the Bird and the Anaktalik lower sheets (Fig. 5.46). Deformed rocks in both these sheets are moderately to steeply (45° – 60°) south dipping and east-west striking, thereby contrasting with the orientation of strongly deformed rocks adjacent to the Anaktalik Brook and Kangilialuk Lake country rock belts. The strongly deformed rocks in the Bird sheet were cut by the Mesoproterozoic Satosoak pluton (chapter 7), indicating that this tectonic overprint also developed in the Mesoproterozoic. These strongly deformed rocks are unique in that they

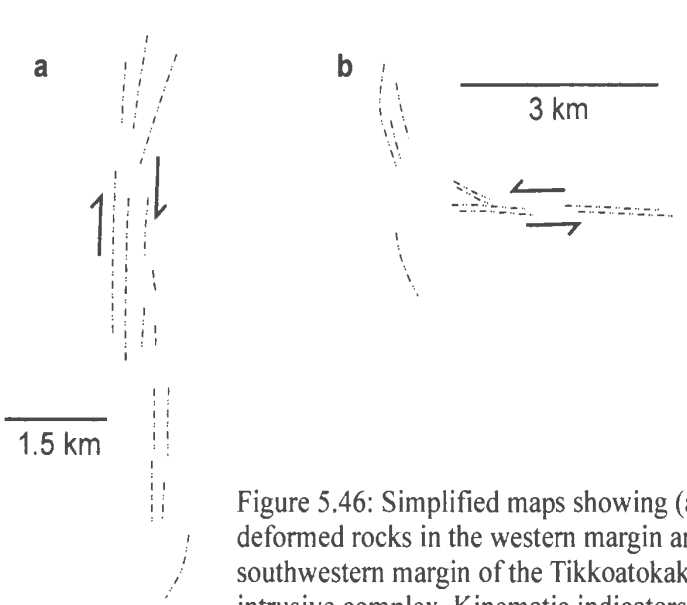

Figure 5.46: Simplified maps showing (a) strongly deformed rocks in the western margin and (b) southwestern margin of the Tikkoatokak centered intrusive complex. Kinematic indicators suggest dextral shearing in (a) and sinistral shearing in (b).

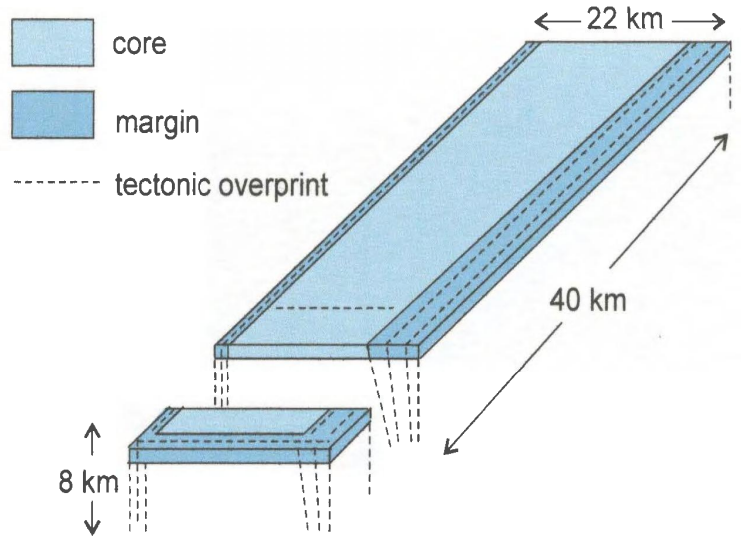

Figure 5.47: Schematic box model of the Tikkoatokak centered intrusive complex, showing the core, margin and tectonic overprint.

are: (a) east-west striking and (b) not restricted to contacts between plutonic rocks and country rocks.

5.7 Summary

This chapter described the form, structure, petrography, textures, structures, mineral composition, whole chemistry and/or geochronology of the Tasiyuyaksuk sheet, Kangilialuk sheet, Lister pluton, Bird sheet and Anaktalik sheet, and grouped all of these units into the Tikkoatokak centered intrusive complex. This section summarizes the overall structure of this centered intrusive complex in terms of a core, margin and tectonic overprint (Fig. 5.47).

The core of the Tikkoatokak centered intrusive complex is formed by the Lister pluton inner zone, which comprises a sub-horizontal and sheet-like form. Rocks in the core: (a) consist mostly of anorthosite, and (b) are massive to sub-horizontally layered. These anorthositic rocks were deformed and recrystallized at high-T. Mineral compositions and a previously published whole rock chemistry study (see Xue and Morse, 1993) indicate that the composition of anorthositic rocks fall in the range shown by NB noritic anorthosite.

The margin of the Tikkoatokak centered intrusive complex consists of the Tasiyuyaksuk sheet (TY), Kangilialuk sheet (TK), Lister pluton border zone (TLb), Bird sheet (TB) and the Anaktalik sheet (TA). The margin envelops the core and is outward dipping with respect to the core, thereby comprising the form of a bell-jar pluton. The units that are spatially associated show forms that are parallel to each other. Rocks in the

margin are: (a) anorthositic, gabbronoritic and monzonitic, (b) moderately dipping to sub-vertically oriented, (c) massive, mottled, layered and/or foliated, and (d) range from weakly to strongly deformed.

The strongly deformed rocks in the margin of the Tikkoatokak centered intrusive complex are: (a) sub-vertically oriented and north-south striking adjacent to the Anaktalik Brook country rock belt, (b) sub-vertically oriented and north-south striking adjacent to the Kangilialuk Lake country rock belt, and (c) moderately south dipping and east-west striking in the south part of the margin. North-south striking deformation occurred during dextral shear deformation and east-west striking deformation occurred during sinistral shear deformation. Most importantly, strong deformation of these rocks took place in the Mesoproterozoic during emplacement of the Nain batholith (1365 – 1270 Ma).

Chapter 6: Sophie centered intrusive complex (S)

The name Sophie centered intrusive complex is here proposed for spatially associated anorthositic, gabbronoritic and Fe-rich gabbroic rocks that lie in the vicinity of Mount Sophie. These rocks occur in the Unity pluton (SU), Airstrip sheet (SA), Pikaluyak sheet (SP) and Hosenbein pluton (SH) (Figs. 6.1, 6.2). The plutons are divided into inner zones and border zones. All of these units lie to the south of the Nain Hill country rock belt, east of the Kangilialuk Lake country rock belt and west of the Kauk Harbor country rock belt. This chapter describes the contact relations, form, petrography, textures, structures, mineral compositions and whole rock chemistry for each of these units. U-Pb isotope chemistry of zircons is presented for the Unity pluton and the Pikaluyak sheet. The order in which these units are described is from oldest to youngest based on field relations and U-Pb ages of zircons. A section entitled 'tectonic overprint' describes the strongly deformed plutonic rocks that occur in the margin of the Sophie centered intrusive complex.

Anorthositic rocks in the Hosenbein pluton form the bulk and the spatial center of the Sophie centered intrusive complex. The Unity pluton, Airstrip sheet and Pikaluyak sheet are included with the Hosenbein pluton in the Sophie centered intrusive complex for reasons given later in this chapter. This chapter also describes the tectonic overprint on the margin of the Sophie centered intrusive complex.

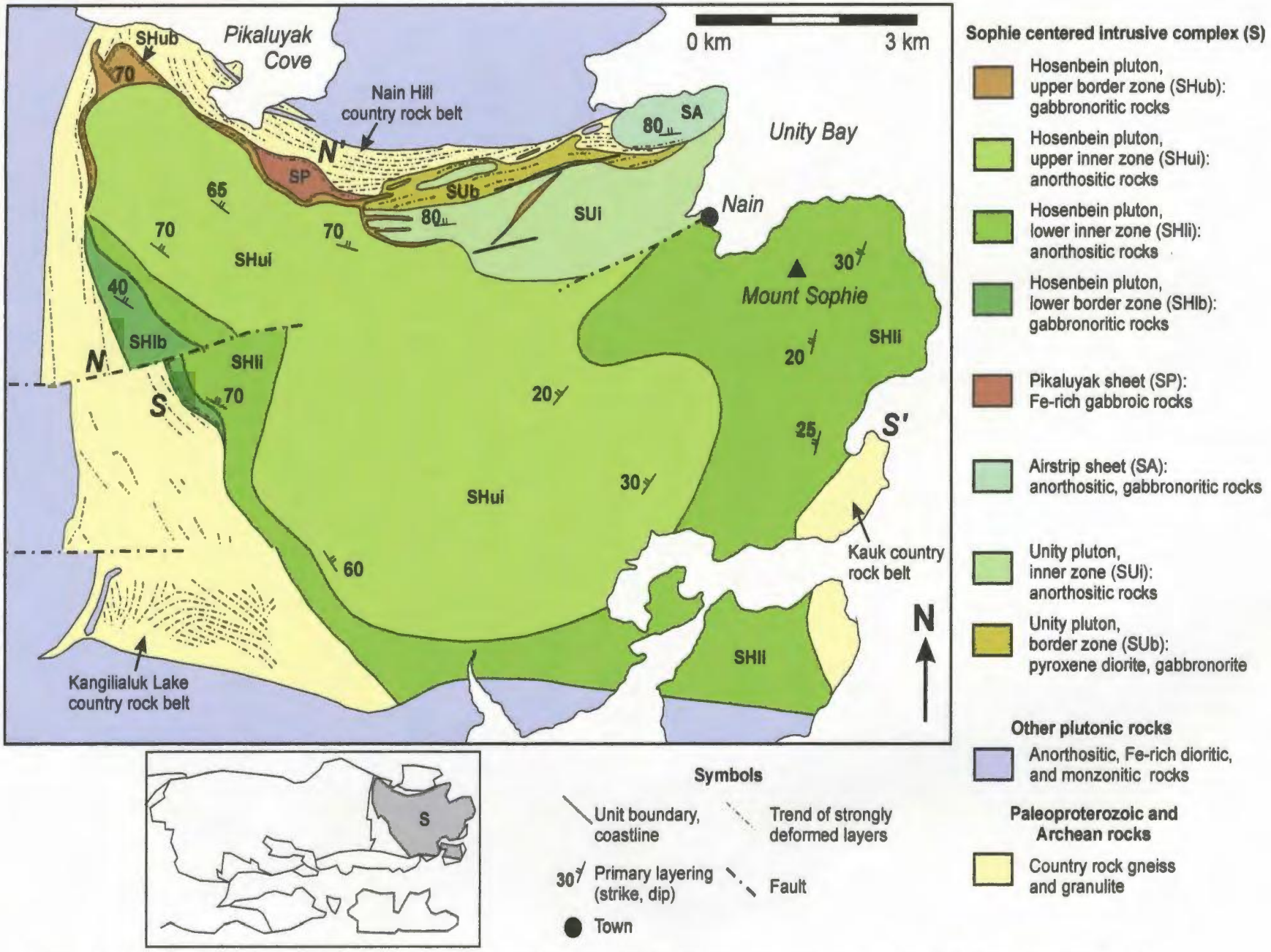

Figure 6.1: Solid geological map of the Sophie centered intrusive complex, Labrador. Cross-sections N-N' and S-S' are shown on Fig. 6.2.

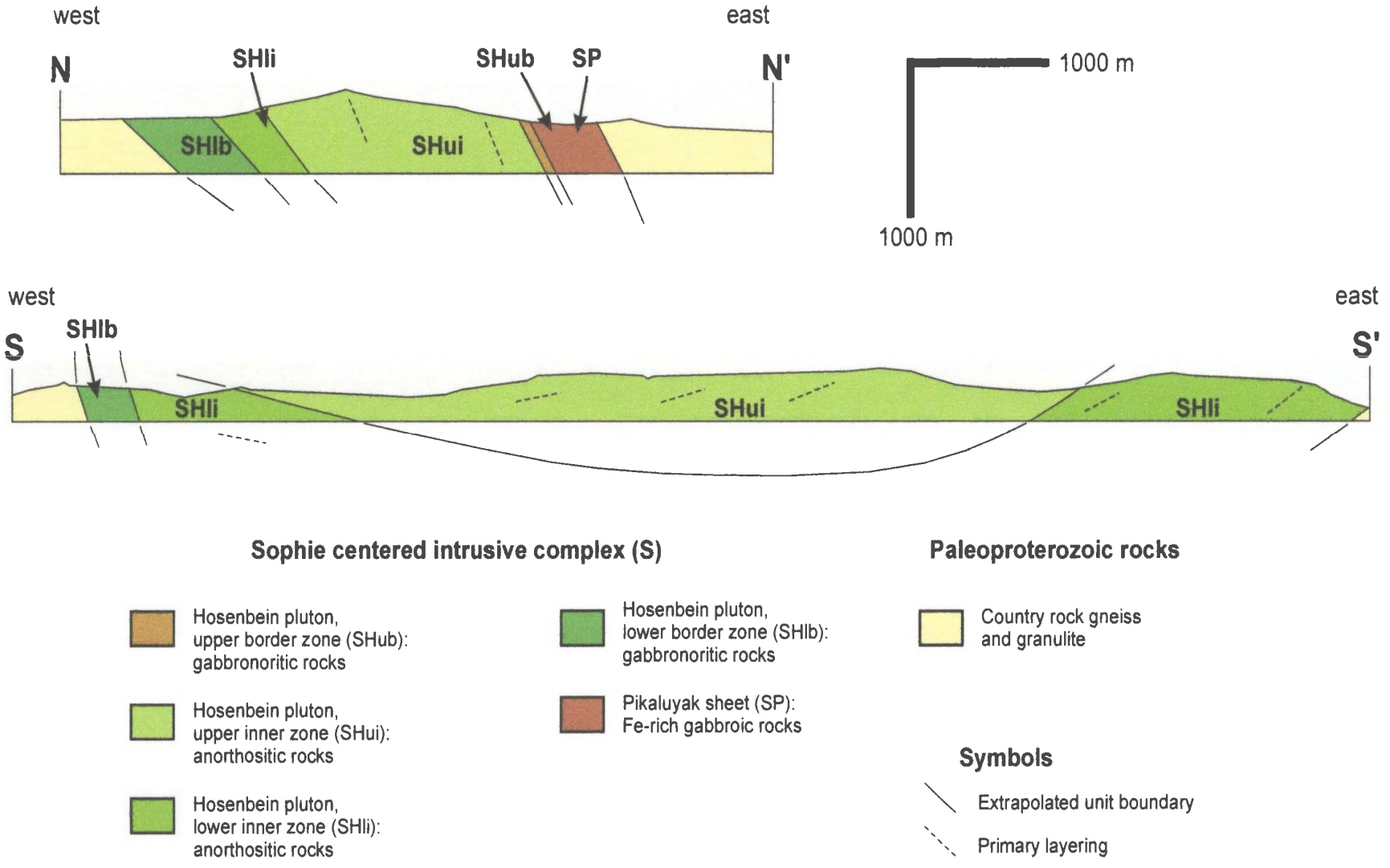

Figure 6.2: East-west cross-sections through the Sophie centered intrusive complex. These cross-sections are located on Figure 6.1.

6.1 Unity pluton (SU)

Geological maps by Ryan (2000a; 2001a) show four anorthositic intrusions in the vicinity of Mount Sophie, one of which he named the Unity Bay intrusion. Geological mapping as part of this study groups part of the Unity Bay intrusion of Ryan (2001a) into the Unity pluton. The Unity pluton is here divided into an inner zone of anorthositic rocks and a border zone of pyroxene diorite. The inner zone is similar to the locally recrystallized and strongly recrystallized anorthositic units described in the Unity Bay intrusion of Ryan (2000a; 2001a). The border zone was found during this study.

6.1.1 Unity pluton border zone (SUb)

A geological map by Wheeler (1969) shows that basement rocks underlie the north flank of Nain Hill. Studies by Rubins and de Waard (1971) and Rubins (1973) described these rocks as comprising layered norite, and/or olivine- and pyroxene-bearing granulite. Mapping by Ryan (2000a) showed that layered rocks and leuconorite of uncertain affinity underlie the north flank of Nain Hill, whereas a subsequent map (Ryan, 2001a) identifies these rocks as Archean layered mafic gneiss.

Mapping as part of this study found that the southernmost part of these layered rocks comprises a composite unit of steeply north dipping, compositionally layered, strongly deformed, pyroxene diorite, gabbronorite, anorthosite and leucogabbronorite. The mineralogy, mineral compositions and whole rock chemistry of all rock types were found to be more similar to Mesoproterozoic plutonic rocks than Paleoproterozoic gabbroic granulite (see below). Anorthosite and leucogabbronorite intruded pyroxene

diorite and gabbronorite, and grade into anorthositic rocks of the Unity pluton inner zone. As a result, pyroxene diorite and gabbronorite are here grouped into the Unity pluton border zone (Figs. 6.3, 6.4) and anorthositic rocks are grouped into the Unity pluton inner zone (see section 6.1.2).

Form and contacts

The part of the Unity pluton border zone described in this section consists of pyroxene diorite and gabbronorite. The southern boundary of the Unity pluton border zone shows an increased abundance of steeply dipping compositional layers of anorthosite and leucogabbronorite that mark the gradational contact with the Unity pluton inner zone (Fig. 6.5). The northern boundary shows a sharp and concordant contact with gabbroic granulite in the Nain Hill country rock belt. In addition, the Unity pluton border zone is truncated in the east by the Airstrip sheet and in the west by the Hosenbein pluton.

The Unity pluton border zone is 50 – 400 m thick, 4500 m long, steeply dipping (70°) to sub-vertical and east-west striking. The orientation of this unit is parallel and structurally continuous with the orientation of the Airstrip sheet, Pikaluyak sheet and Hosenbein pluton upper border zone (see Fig. 6.3).

Petrography

Pyroxene diorite and gabbronorite contains small to medium-sized plagioclase grains and ~10 – 50% small to medium-sized orthopyroxene and clinopyroxene grains

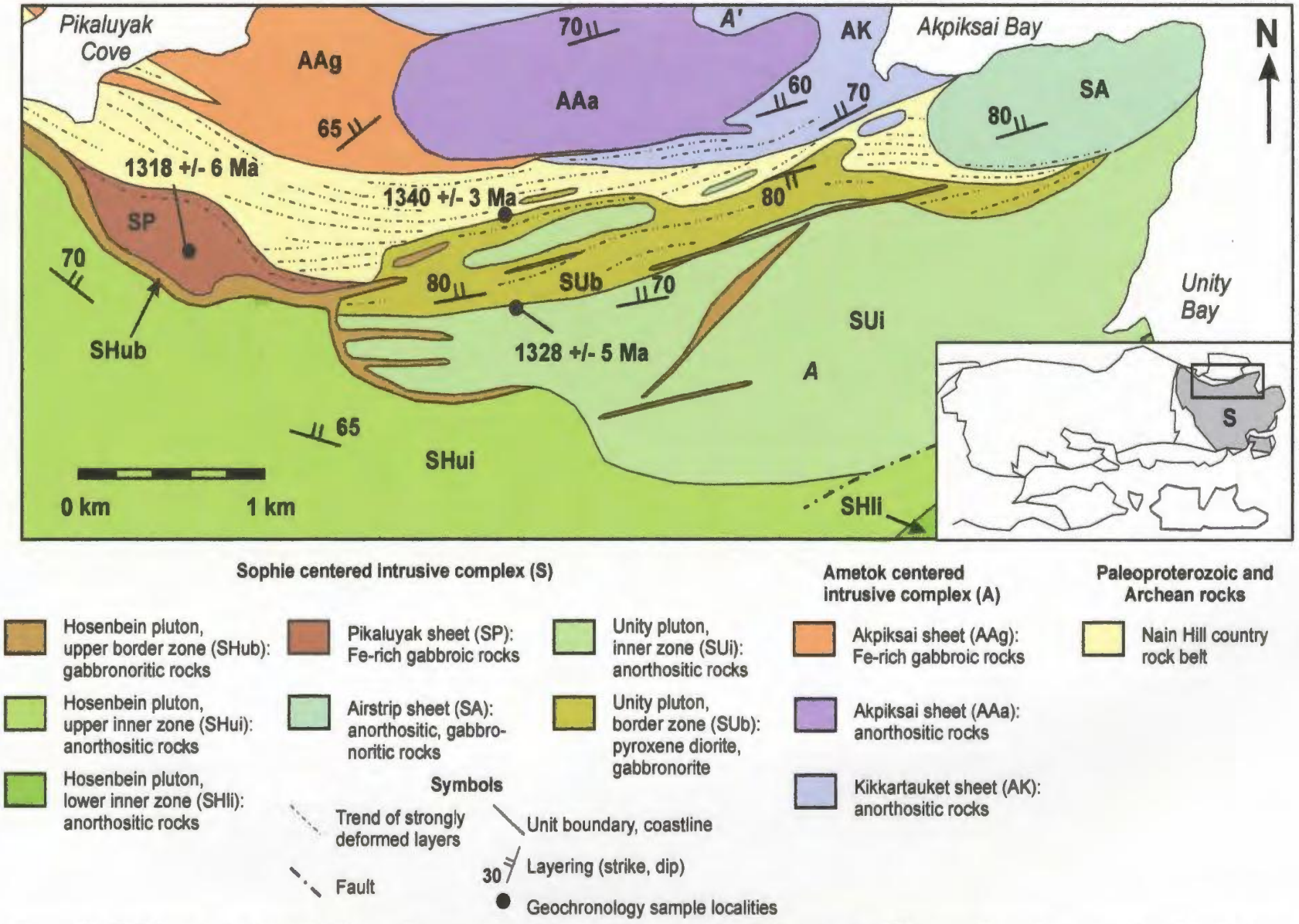

Figure 6.3: Solid geological map for the northeastern part of the Sophie centered intrusive complex. This map shows the sample localities for geochronological studies in this thesis. The Ametok centered intrusive complex is not described in this thesis. Cross-section A-A' is shown on Fig. 6.4.

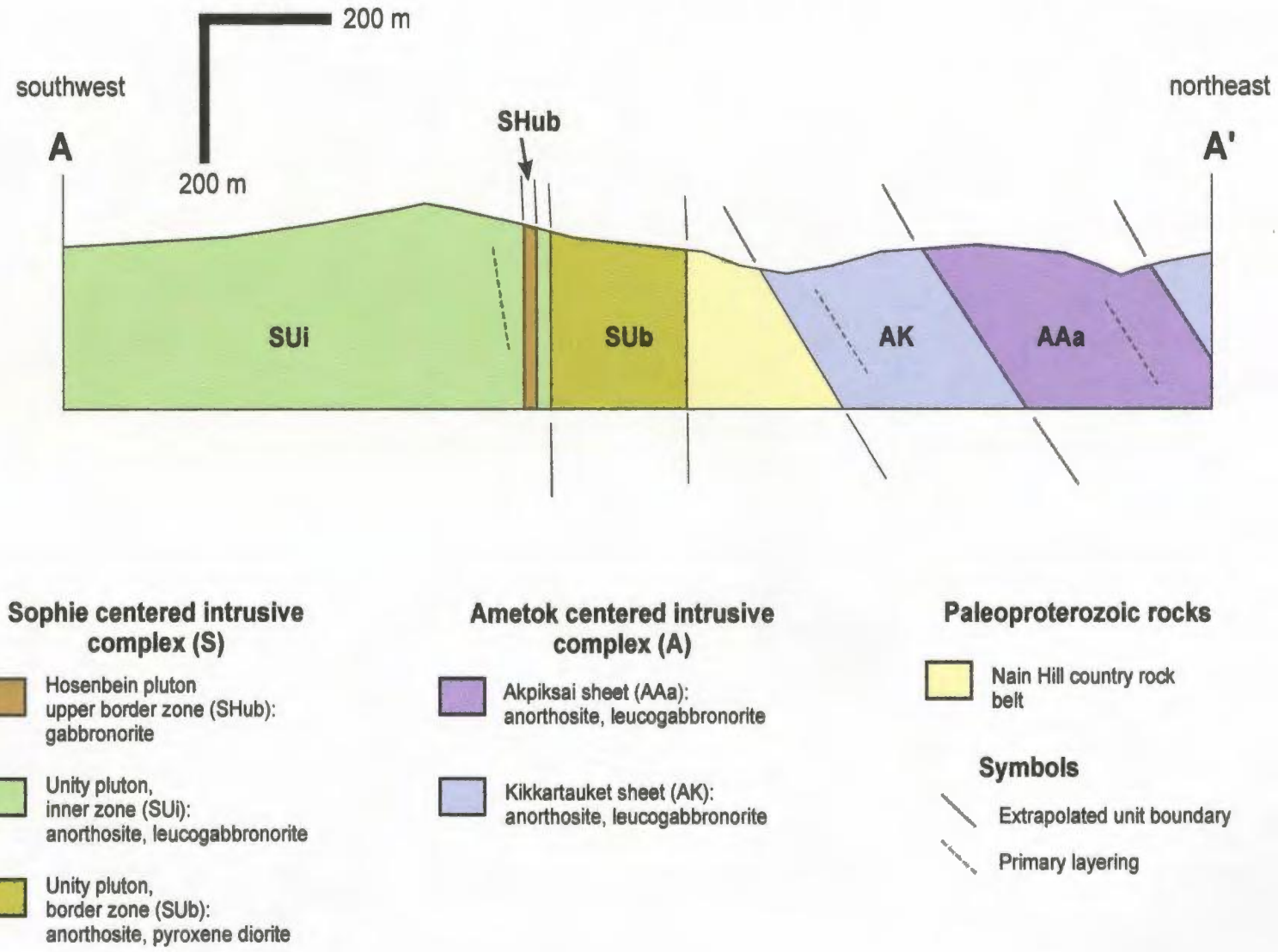

Figure 6.4: Southwest to northeast cross-section through the northeastern margin of the Sophie centered intrusive complex. The Ametok centered intrusive complex is not described in this thesis. This cross-section is located on Figure 6.3.

(Fig. 6.6). Plagioclase, orthopyroxene and clinopyroxene grains show interlobate grain margins, equilibrated geometries and triple junctions, indicating these grains were recrystallized at high-T. Minor and accessory minerals consist of very small quartz and Fe-Ti oxide grains. Most pyroxene crystals are rimmed or completely altered to uralite, suggesting significant hydrothermal alteration.

Textures and structures

Pyroxene diorite and gabbronorite are fine- to medium-grained and show an overall granular texture. These granular rocks show primary layering and are compositionally layered with younger anorthositic rocks of the Unity pluton inner zone. Primary layering comprises alternations of relatively pyroxene-rich (~30 – 50% pyroxene) and pyroxene-poor (~10 – 30% pyroxene) rocks. Individual layers are 1 – 10 cm thick, sub-vertically oriented and east-west striking. The granular texture and sub-vertical orientation of these rocks suggests they were deformed parallel to primary layering. In addition, the orientation of deformed primary layering is parallel to compositional layers of Unity pluton inner zone anorthositic rocks and layers in the Nain Hill country rock belt.

Mineral compositions and whole rock chemistry

Mineral compositions in pyroxene diorite and gabbronorite range from An_{35-45} in plagioclase and En_{52-55} in orthopyroxene. These plagioclase compositions are Na-rich in comparison to anorthositic rocks in the Hosenbein pluton and Paleoproterozoic gabbroic

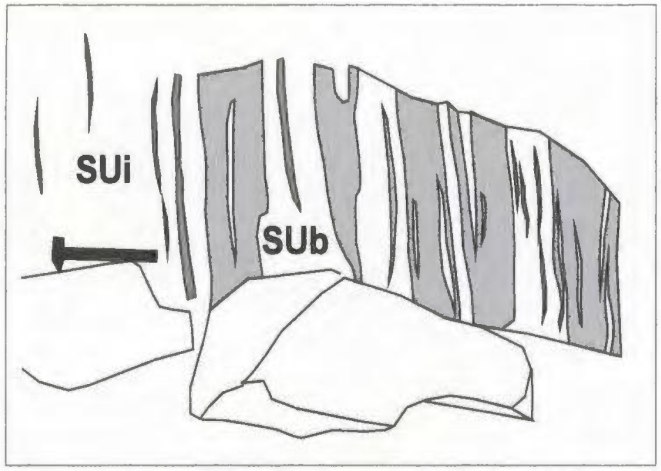

Figure 6.5: Sketch of the contact between the Unity pluton inner zone (SUi) and border zone (SUb). The contact is marked by an increase in pyroxene diorite layers (gray) and a decrease in anorthositic rocks (white). Sketch made on the north flank of Nain Hill.

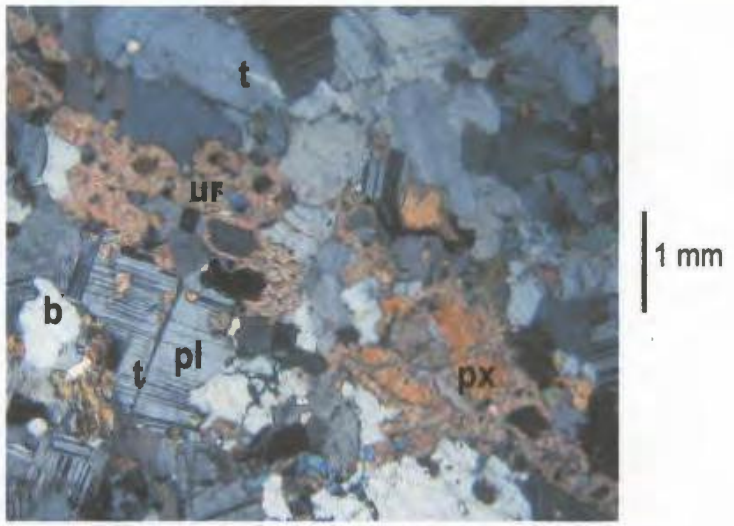

Figure 6.6: Thin section photo (XPL) of pyroxene diorite in SUb. Plagioclase (pl) shows deformation twins (t) and bulging grain margins (b). Pyroxene (px) is granular and shows thick rims of uralite (ur).

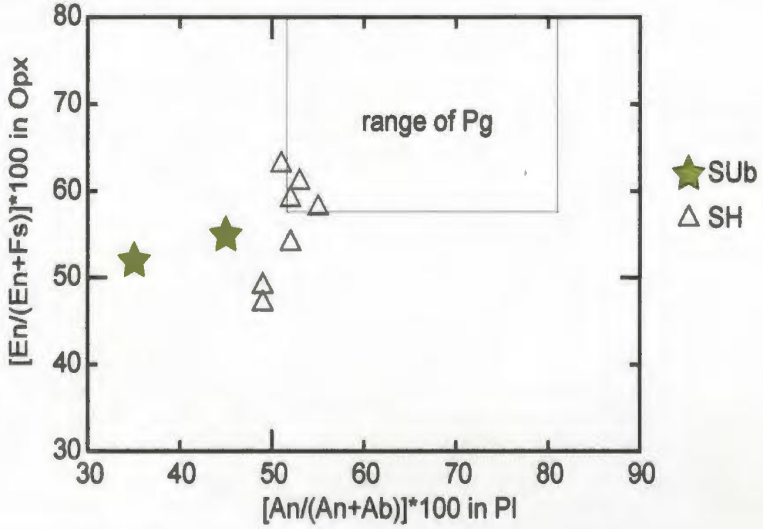

Figure 6.7: Comparison of orthopyroxene and plagioclase compositions in Unity border zone pyroxene diorite and gabbronorite (SUb) with Hosenbein pluton anorthositic rocks (SH) and Paleoproterozoic gabbroic granulite (Pg).

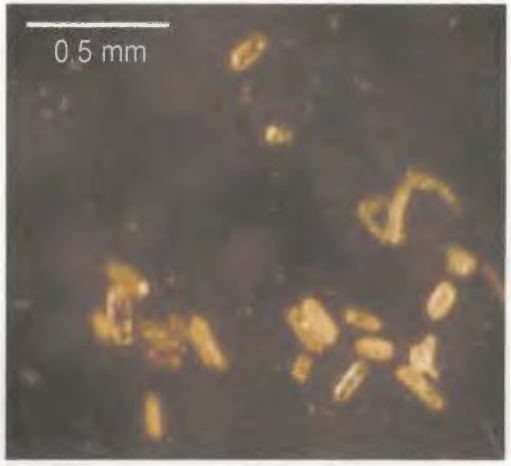

Figure 6.8: Binocular microscope photo of zircons from pyroxene diorite in SUb. These zircons show elongate forms and are generally devoid of inclusions.

granulite (Table 6.1, Fig. 6.7). In addition, these plagioclase compositions are Ca-rich in comparison to Paleoproterozoic enderbitic gneiss. Orthopyroxene compositions are similar to anorthositic rocks in the Hosenbein pluton and are Fe-rich in comparison to Paleoproterozoic gabbroic granulite. As well, orthopyroxene in pyroxene diorite and gabbronorite shows low wt% Al_2O_3 (<0.73 wt%) in comparison to gabbroic granulite (1.53 – 2.35 wt%). The composition of clinopyroxene in pyroxene diorite and gabbronorite averages En_{36}.

Table 6.1: Mineral compositions (*) and whole rock chemistry in SUb gabbronorite and pyroxene diorite, and comparative data for Hosenbein pluton anorthositic rocks (SH), Paleoproterozoic gabbroic granulite (Pg) and enderbitic gneiss (Pe).

Rock type	Sample	Pl*	Opx*	SiO_2	MgO	Na_2O	Cr	Ba	Sr
		An	En	wt%	wt%	wt%	ppm	ppm	ppm
Unity pluton border zone (SUb)									
defm gn	01-30-2b	45	55	52.27	5.16	3.3	111	562	676
defm gn	00-3-2a	43							
defm px di	01-30-12b	35	52						
defm px di	01-30-2a	38							
Comparative data									
SH		49 - 55	47 - 63	51 - 53	1.9 - 4.8	3.4 - 3.9	84 - 108	372 - 636	593 - 902
Pg		51 - 81	58 - 85	44 - 49	7 - 31	0.1 - 2.3	229 - 2008	0 - 243	31 - 385
Pe		29 - 33	60	63 - 64	2.5 - 3.0	3.5 - 3.9	80	452 - 659	430

Whole rock chemistry for gabbronorite shows broadly similar abundances of SiO_2, MgO, Na_2O, Cr, Ba and Sr in comparison to anorthositic rocks in the Hosenbein pluton, whereas abundances of SiO_2, Na_2O, Ba and Sr are high in comparison to Paleoproterozoic gabbroic granulite (see Fig. 6.9) and abundances of MgO and Cr are low (Table 6.1). In comparison to enderbitic gneiss, whole rock chemistry of gabbronorite shows high abundances of MgO, Cr and Sr, and low abundances of SiO_2, and Na_2O. These results suggest that the whole rock chemistry of gabbronorite in the

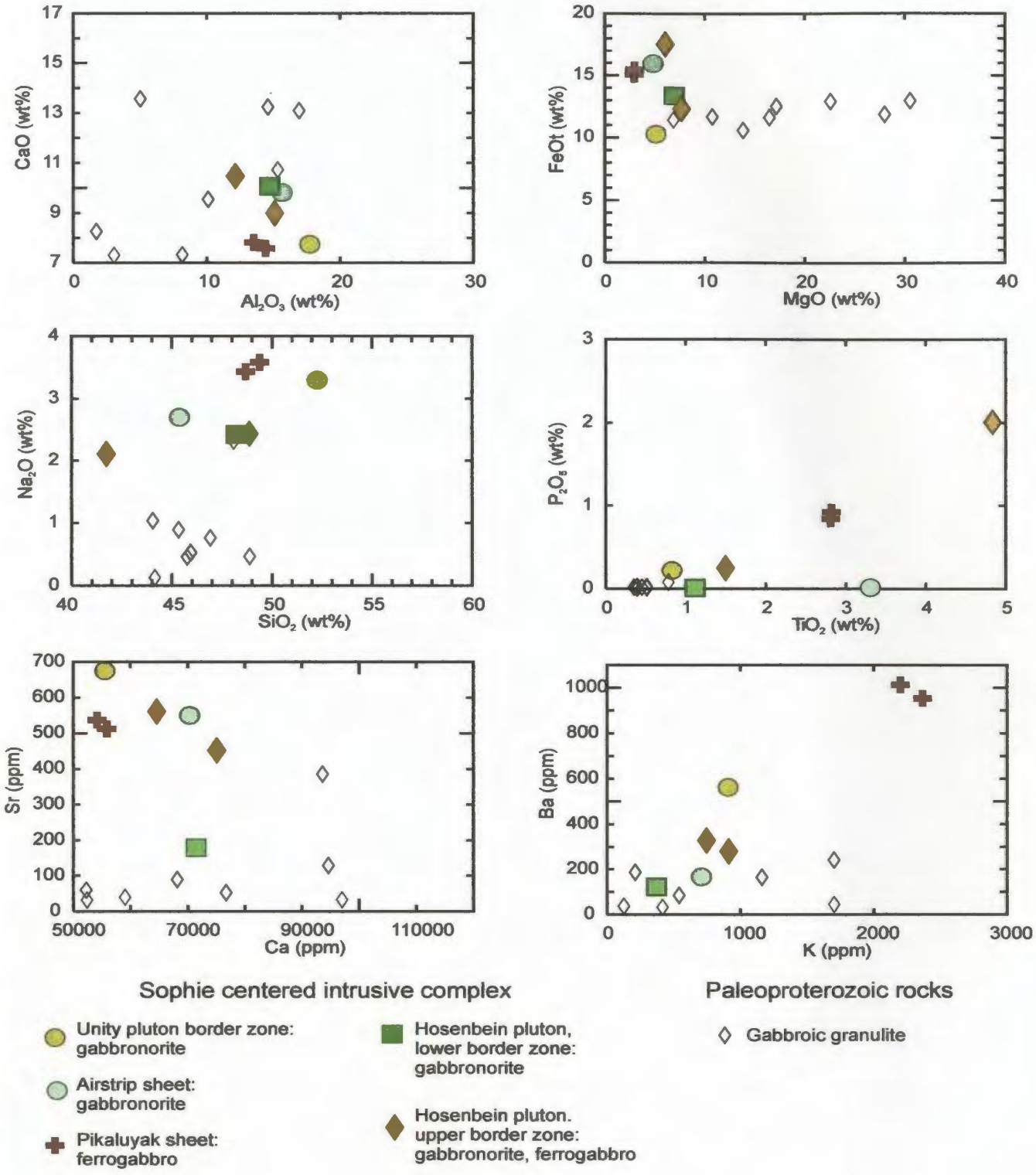

Figure 6.9: Whole rock chemistry for gabbronoritic and Fe-rich gabbroic rocks in the Sophie centered intrusive complex, and comparative data for Paleoproterozoic gabbroic granulite. Sections that describe these units are 6.1.1 for the Unity Bay border zone, 6.2 for the Airstrip sheet, 6.3 for the Pikaluyak sheet, 6.4.1 for the Hosenbein pluton lower border zone and 6.4.4 for the Hosenbein pluton upper border zone.

Unity pluton border zone is most similar to anorthositic rocks in the Hosenbein pluton. CIPW norms of gabbronorite consist mostly of plagioclase and pyroxene.

Geochronology of pyroxene diorite

U-Pb analysis of zircon was done on a sample taken from a layer of pyroxene diorite that lies near the contact with country rock. This sample was analyzed because mapping done for this study suggested it comprises a strongly deformed Mesoproterozoic rock in contrast to previous mapping that identified these rocks as country rock. The sample consists of pyroxene diorite that was recrystallized and was partly hydrothermally altered.

The sample contains accessory abundances of zircon. These zircons form small grains that are elongated and interstitial to plagioclase. The elongate form of the zircons suggests they are igneous in origin. Several zircons show prismatic tips (see Fig. 6.8) that suggest they are igneous in origin. Only one zircon grain was imaged with the electron microprobe. This grain shows concentric zoning or an older core (Fig. 6.10), although the latter is not indicated by the concordant U-Pb isotope ratios (Fig. 6.11).

Five zircon grains were analyzed for U and Pb isotope chemistry. All five of these zircons are yellow in color, elongated and lack visible inclusions. These zircons contain 12 – 22 ppm U and 2.7 – 5.0 ppm Pb (Table 6.2).

The $^{207}Pb/^{206}Pb$ ratios and ages for all analyzed zircons overlap in error and lie on or within 2% of concordia (see Fig. 6.11). The concordia age was calculated by

anchoring the lower intercept at 0 +/- 50 Ma. The upper intercept for these zircons lies at 1340.0 +/- 2.9 Ma.

Table 6.2: Description and chemistry of zircons separated from SUb pyroxene diorite

Grain	Zr 1	Zr 6	Zr 5	Zr 4	Zr 3
Color	yellow	yellow	yellow	yellow	yellow
Translucent	yes	yes	yes	yes	yes
Shape	elongate	elongate	elongate	elongate	elongate
Weight (ug)	10	12	40	6	3
Com. (Pb pg)	3.8	2	6.6	1.8	3.2
U (ppm)	17	18	12	22	16
Th/U	1.33	0.42	0.17	0.21	0.25
$^{206}Pb/^{204}Pb$	191	1490	1050	1107	250
Pb (ppm)	5.2	4.2	2.7	5	3.7
$^{206}Pb/^{238}U$	0.2257	0.2258	0.2307	0.2303	0.2318
% error	1.1	3	0.7	2.5	0.9
$^{207}Pb/^{235}U$	2.6965	2.6826	2.7349	2.7353	2.7631
% error	1.5	3	0.7	2.5	1
$^{207}Pb/^{206}Pb$	0.0866	0.0861	0.0859	0.0861	0.0864
% error	0.9	0.4	0.2	0.4	0.6
$^{206}Pb/^{238}U$ (Ma)	1312	1313	1338	1337	1344
$^{207}Pb/^{235}U$ (Ma)	1327	1324	1338	1338	1346
$^{207}Pb/^{206}Pb$ (Ma)	1353	1342	1338	1341	1348
+/- m.y.	16	7	4	8	12
Conc. (%)	98	98	100	100	100

Summary

The Unity pluton border zone shows: (a) a form that parallels the form of the Hosenbein pluton upper border zone (see Fig. 6.3), (b) consists of rock types that are most similar to anorthositic rocks in the Hosenbein pluton, and (c) contains igneous zircons that are Mesoproterozoic in age. In addition, the Unity pluton border zone shows a tectonic overprint (section 6.5) that is parallel to that in the Hosenbein pluton border zone. For these reasons, the Unity pluton border zone is included in the Sophie centered intrusive complex.

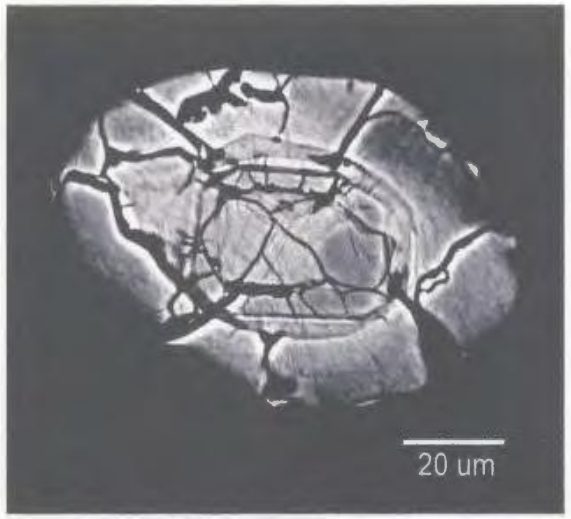

Figure 6.10: Electron backscatter image of a zircon from pyroxene diorite in SUb. The zircon shows concentric zoning or an inherited core, although the latter interpretation is not favored in light of predominantly concordant U-Pb isotope data (see Fig. 6.11).

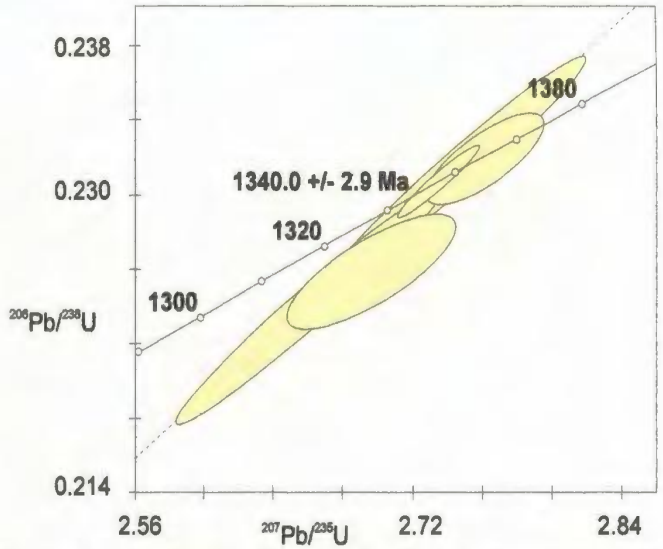

Figure 6.11: Concordia diagram for five zircon grains separated from SUb pyroxene diorite. Zircons define a concordia age of 1340 +/- 3 Ma when the lower intercept is anchored at 0 +/- 50 Ma. The mean square weighted deviate is 1.5.

Figure 6.12: Xenolith of Unity pluton inner zone anorthosite (SUi) in Hosenbein pluton upper inner zone leucogabbronorite (SHui). Dashed line shows outline of the xenolith. Photo taken south of Hosenbein Lake.

Figure 6.13: Thin section photo (XPL) of anorthosite in SUi. Plagioclase shows deformation twins (t), deformation bands (b) and serrated grain margins (s).

6.1.2 Unity pluton inner zone (SUi)

Form and contacts

Geological mapping as part of this study outlined a unit of massive, coarse-grained, anorthosite and leucogabbronorite that is here named the Unity pluton inner zone. The northern boundary of this unit shows an increased abundance of steeply dipping compositional layers of pyroxene diorite and gabbronorite that mark the gradational contact with the Unity pluton border zone (see Fig. 6.5). The southern and western boundaries of the Unity pluton inner zone are truncated by the Hosenbein pluton (Fig. 6.12), and the northeastern boundary of this unit is truncated by the Airstrip sheet.

The Unity pluton inner zone is exposed over 3.0 km in a northeast-southwest direction and 1.3 km in a northwest-southeast direction (see Fig. 6.3). A thickness is difficult to estimate in light of the lack of planar structures. Steeply (70°) north-dipping rocks in the Unity pluton inner zone occur near the contact with the border zone. Xenoliths of the Unity pluton inner zone are scattered over a 20 km^2 area in the Hosenbein pluton. Some of these xenoliths are rimmed by aggregates of medium-sized to large pyroxene grains. In addition, plutonic rocks of the Hosenbein pluton and Airstrip sheet are of uniform coarse grain size right up to contacts with xenoliths of the Unity pluton inner zone.

Petrography

Plagioclase crystals are abundant, of very large to large size (0.1 – 20 cm) and of granular to tabular form, suggesting that these crystals are cumulus. These crystals also

show deformation twins, deformation bands, serrated grain margins, equilibrated geometries and undulose extinction (Fig. 6.13) that indicate they were recrystallized and/or deformed at high-T. Pyroxene crystals are of relatively low abundance, small size and form aggregates that comprise relict and large poikilitic crystals (Fig. 6.14), suggesting that pyroxene crystallized out of the intercumulus liquid and was also recrystallized. Minor and accessory minerals consist of very small quartz and zircon grains.

Secondary minerals replaced 1 – 10% of the plagioclase and ~50 – 100% of the pyroxene. Altered plagioclase contains sericite, saussurite, quartz and/or calcite that are suggestive of hydrothermal alteration. Altered pyroxene contains uralite, Fe-Ti oxide, Mg-rich chlorite and amphibole that are also suggestive of hydrothermal alteration. In foliated rocks, the preferred orientation of amphibole laths is parallel to that of lens-shaped aggregates of pyroxene grains.

Textures and structures

Anorthositic rocks are medium- to very coarse-grained and show an overall texture that is granular. In some cases, anorthositic rocks contain medium-sized to large, relict, poikilitic pyroxene crystals. These rocks show an overall texture that is relict poikilitic.

Anorthositic rocks are generally massive, but some are mottled or foliated. Massive rocks comprise only granular texture. Mottled rocks comprise granular anorthosite with patches of relict poikilitic texture (Fig. 6.15). These patches are sub-

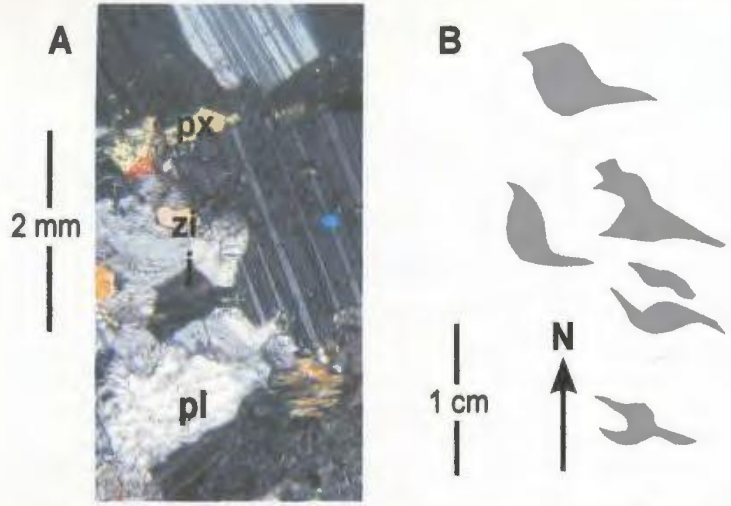

Figure 6.14: Thin section (A) photo (XPL) and (B) sketch of leucogabbronorite in SUi. (A) Plagioclase (pl) shows granular habits, triple junctions (j) and minor alteration to sericite. Pyroxene (px) shows (A) relict poikilitic texture and (B) forms clots that show asymmetric tails. The photo also shows accessory abundances of zircon (zi).

Figure 6.15: Mottled anorthositic rocks in SUi. Mottled rocks comprise patches of relict poikilitic-textured leucogabbronorite (lgn) in granular-textured anorthosite (an). Dashed line marks the outline of a leucogabbronorite patch. Photo taken on Nain Hill.

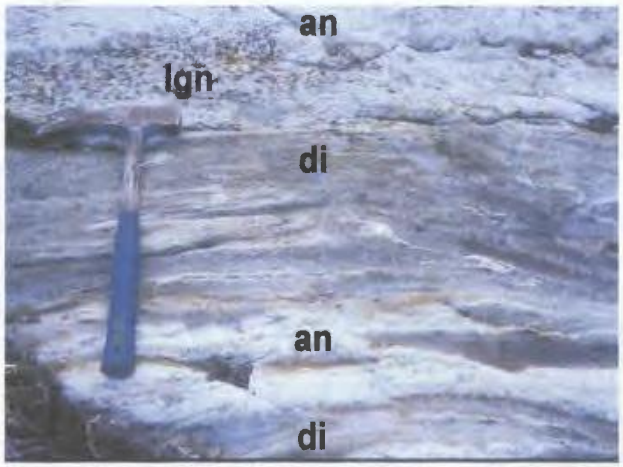

Figure 6.16: Strongly deformed and compositionally layered rocks in the northern-most part of SUi. Layers consist of granular-textured anorthosite (an), leucogabbronorite (lgn) and pyroxene diorite (di). Photo taken on north flank of Nain Hill.

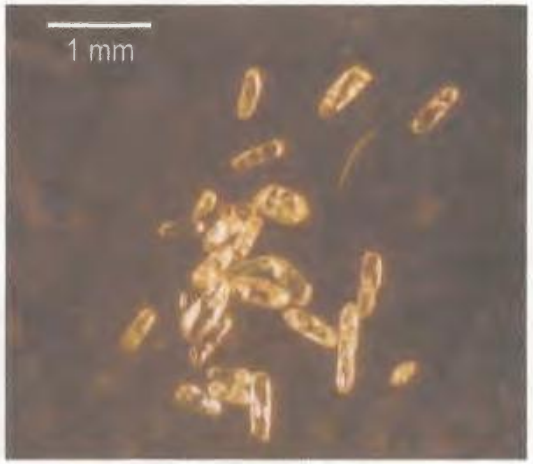

Figure 6.17: Binocular microscope photo of zircons from leucogabbronorite in SUi. These zircons are elongate and are generally devoid of inclusions.

spherical in form and range from 0.05 – 10 m in diameter. Foliated rocks contain medium-sized lens-shaped aggregates of very small pyroxene grains that comprise a relict, flattened, poikilitic texture. These lens-shaped aggregates are steeply (70°) dipping and east-west striking.

Anorthositic rocks also contain pods and planar aggregates that consist of medium-sized to very large poikilitic pyroxene crystals. Pods are sub-spherical in form and 10 – 150 cm in diameter. Aggregates are 1 – 10 cm thick and 0.3 – 10 m long, and strike parallel to foliated rocks.

Anorthositic rocks in the northern-most 100 m of the Unity pluton inner zone are compositionally layered with pyroxene diorite of the Unity pluton border zone (Fig. 6.16). These anorthositic rocks show only granular texture. Individual layers of anorthositic rocks are 1 – 50 cm thick, sub-vertically oriented and east-west striking. As well, these anorthositic rocks contain round pyroxene aggregates with sigmoidal tails of small granoblastic-textured pyroxene crystals (see Fig. 6.14). These tails suggest rotation of pyroxene aggregates during sinistral shear deformation, and suggest that compositionally layered rocks at the gradational contact between the Unity pluton border and inner zones were overprinted by sinistral shear deformation.

Mineral compositions and whole rock chemistry

Mineral compositions in anorthositic rocks range from An_{49-54} in plagioclase and average En_{51} in orthopyroxene. These mineral compositions fall in the range shown by the Hosenbein pluton (Table 6.3). One sample of deformed anorthosite shows plagioclase

compositions that average An_{45} and falls in the range shown by deformed gabbronorite in the Unity pluton border zone. Some plagioclase grains show rims that are Ca-rich ($+An_{1-22}$) relative to the rest of the grain. Orthopyroxene grains are homogeneous in composition and contain <0.2 wt% Al_2O_3. The compositions for the cores of relict clinopyroxene grains range from En_{35-41}.

Table 6.3: Mineral compositions (*) and whole rock chemistry of SUi anorthositic rocks and comparative data for the Hosenbein pluton anorthositic rocks (SH), NB noritic anorthosite and NB troctolitic anorthosite

Sample	Rock type	Pl*	Opx*	SiO_2	K_2O	Ca/Al	Sr/Ca x 10	Mg/(Mg+Fe)	An/(An+Ab)
		An	En	wt%	wt%				CIPW
Unity pluton inner zone (SUi)									
lgn	00-2-4	50		52.83	0.35	1.22	0.10	0.37	0.57
lgn	00-31-27	49	51						
an	01-30-29	49							
an	00-26-16i	53							
an	00-22-5	54							
defm an	00-25-5b	45							
Comparative data									
SH		49 - 55	47 - 63	51 - 53	0.3 - 0.4	1.11 - 1.26	0.09 - 0.12	0.21 - 0.37	0.56 - 0.59
NB noritic		40 - 54	57 - 67	52 - 58	0.6 - 1.2	0.8 - 1.1	0.10 - 0.15	0.10 - 0.35	0.42 - 0.54
NB troctolitic		51 - 68	66 - 73	49 - 55	0.2 - 0.6	1.0 - 1.2	0.06 - 0.09	0.15 - 0.49	0.53 - 0.68

The whole rock chemistry for one sample of leucogabbronorite shows wt% SiO_2, wt% K_2O, Ca/Al, Sr/Ca, Ba/K and Mg/(Mg+Fe) that falls within the range shown by the Hosenbein pluton (see Fig. 6.18). Ba/K (0.26) is high in comparison to both NB noritic and troctolitic anorthosite (0.08 – 0.19). CIPW norms consist mostly of plagioclase and pyroxene, and show normative plagioclase compositions that fall within the range shown by the Hosenbein pluton.

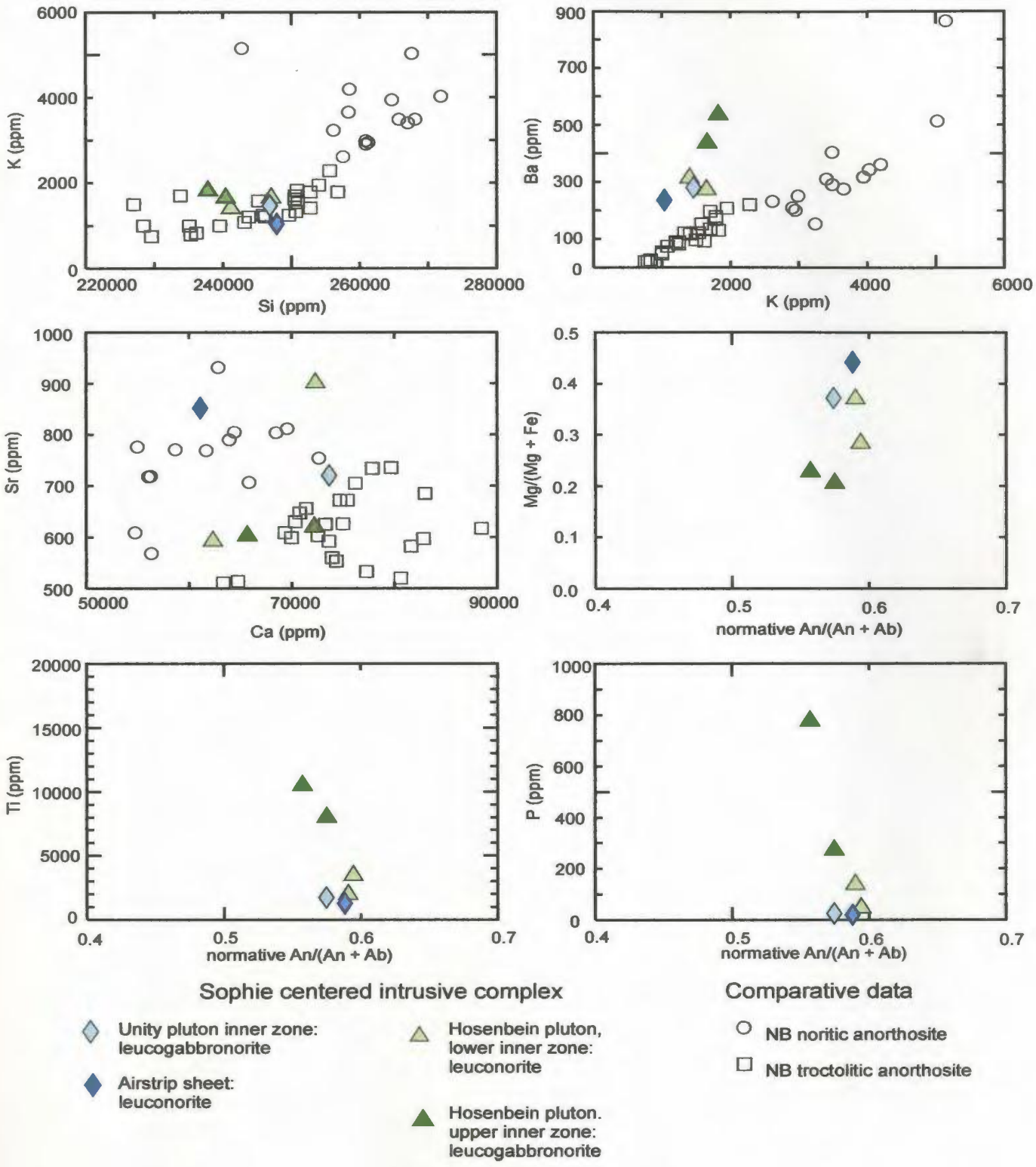

Figure 6.18: Whole rock chemistry for anorthositic rocks in the Sophie centered intrusive complex, and comparative data for NB noritic and troctolitic anorthosite. Sections that describe these units are 6.1.2 for the Unity pluton inner zone, 6.2 for the Airstrip sheet, 6.4.2 for the Hosenbein pluton lower inner zone and 6.4.3 for the Hosenbein pluton upper inner zone.

Geochronology of leucogabbronorite

U-Pb analysis of zircon was done on a sample taken from a layer of leucogabbronorite that lies at the gradational contact between the Unity pluton inner and border zones (see Fig. 6.3). In the field, these rocks were interpreted as strongly deformed Mesoproterozoic plutonic rocks. This sample was analyzed because the tectonic overprint on these rocks is steeply north dipping and east-west striking (Fig. 6.3), thereby comprising an overprint not widely recognized in the Nain batholith. The sample consists of leucogabbronorite that was deformed and partially altered.

Table 6.4: Descriptions and chemistry of zircons separated from SUi leucogabbronorite

Grain	Zr 3	Zr 6	Zr 7	Zr 8	Zr 9	Zr 11
Color	clear	clear	clear	yellow	yellow	yellow
Translucent	yes	yes	yes	yes	yes	yes
Shape	prismatic	prismatic	elongate	elongate	elongate	elongate
Weight (ug)	22	19	14	29	110	34
Com. (Pb pg)	15	5	5	3	4	9
U (ppm)	6	7	5	10	7	7
Th/U	1.77	1	1.14	1.4	1.24	1.11
$^{206}Pb/^{204}Pb$	143	369	215	1471	2590	382
Pb (ppm)	1.8	1.8	1.5	2.9	2	1.8
$^{206}Pb/^{238}U$	0.2377	0.203	0.2268	0.2261	0.2228	0.2222
% error	5.9	7.1	0.6	13.4	7.2	4.3
$^{207}Pb/^{235}U$	2.8216	2.3996	2.6875	2.6705	2.6183	2.6238
% error	6.6	7.1	1	13.4	7.2	4.3
$^{207}Pb/^{206}Pb$	0.086	0.0857	0.0859	0.0856	0.0852	0.0856
% error	3	0.5	0.8	0.7	0.4	0.5
$^{206}Pb/^{238}U$ (Ma)	1375	1192	1318	1314	1297	1294
$^{207}Pb/^{235}U$ (Ma)	1361	1242	1325	1320	1306	1307
$^{207}Pb/^{206}Pb$ (Ma)	1340	1332	1337	1330	1320	1330
+/- m.y.	57	9	15	14	8	10
Conc. (%)	102	91	99	99	99	98

Leucogabbronorite contains accessory abundances of zircon that form small, elongate and round, grains in thin section (see Fig. 6.14). Separated zircons are elongate

and some show prismatic tips (see Fig. 6.17) that suggest an igneous origin. Backscatter imaging shows that the zircons are mostly homogeneous in composition, although some show a patchy zoning (Fig. 6.19).

Six zircon crystals were analyzed for U and Pb isotope chemistry. Three of these zircons are yellow and elongate, two of these zircons are clear and prismatic, and one of these zircons is clear and elongate. All of these grains lack visible inclusions, and contain <11 ppm U and <3 ppm Pb. The lack of inclusions and low U content (<30 ppm) of these zircons is typical of anorthositic rocks in the Nain batholith (see Hamilton et al., 1994).

The yellow and elongate zircon crystals show $^{207}Pb/^{206}Pb$ ages of 1330 +/- 14, 1320 +/- 8 and 1330 +/- 10 Ma. These ages overlap, within error, with $^{207}Pb/^{206}Pb$ ages of 1340 +/- 57 Ma, 1332 +/- 9 Ma and 1337 +/- 15 Ma that were calculated for the clear zircons. If the yellow and clear zircons represent two populations then the concordia ages (anchored at 0 +/- 50 Ma) for these populations are 1326 +/- 6 Ma and 1334 +/- 9 Ma respectively. The clear zircons are generally prismatic and the concordia age for these zircons is older, suggesting that 1334 +/- 9 Ma is the crystallization age of the leucogabbronorite that hosts the zircons. The yellow zircons would therefore indicate post-emplacement re-setting or growth of zircon during high-T deformation. In the discussion chapter of this thesis (chapter 8) it is suggested that the strongly deformed rocks in the Unity pluton were developed in a shear zone that controlled the ascent and emplacement of magma. Hence, the yellow zircons may have been re-set or grown during an episode of magma emplacement and related tectonic movement in this shear zone. An

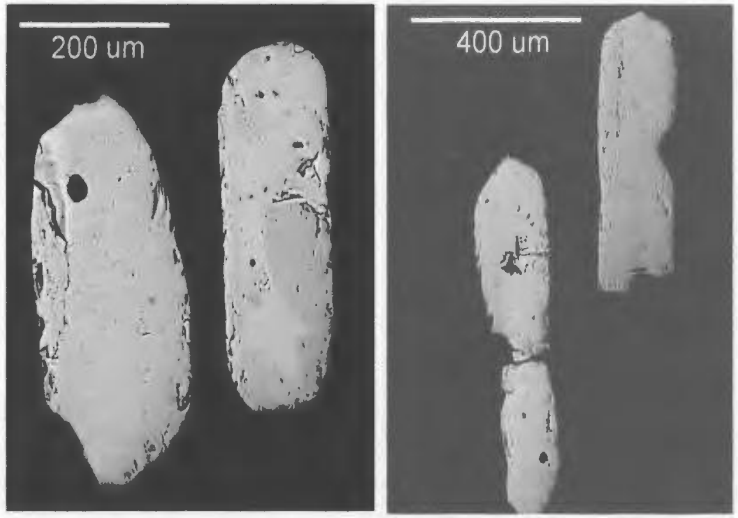

Figure 6.19: Electron backscatter images of zircons from leuco-gabbronorite in SUi. These zircons are homogeneous or show a patchy zoning, and contain small inclusions of apatite.

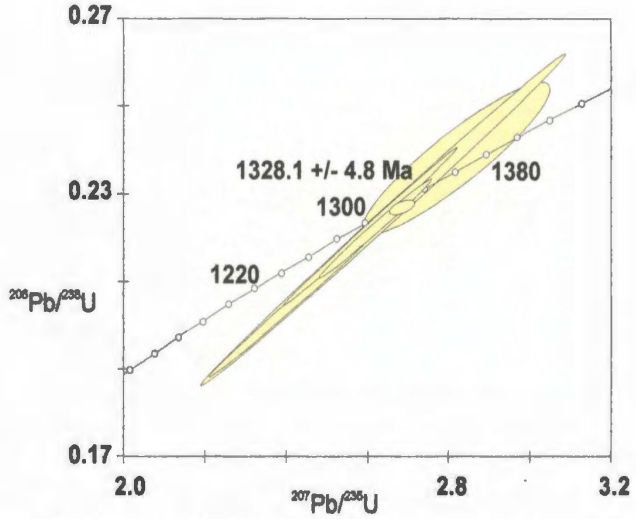

Figure 6.20: Concordia diagram for six zircons separated from leuco-gabbronorite in SUb. Zircons define a concordia age of 1328 +/- 5 Ma when the lower intercept is anchored at 0 +/- 50 Ma. The mean square weighted deviate is 1.20.

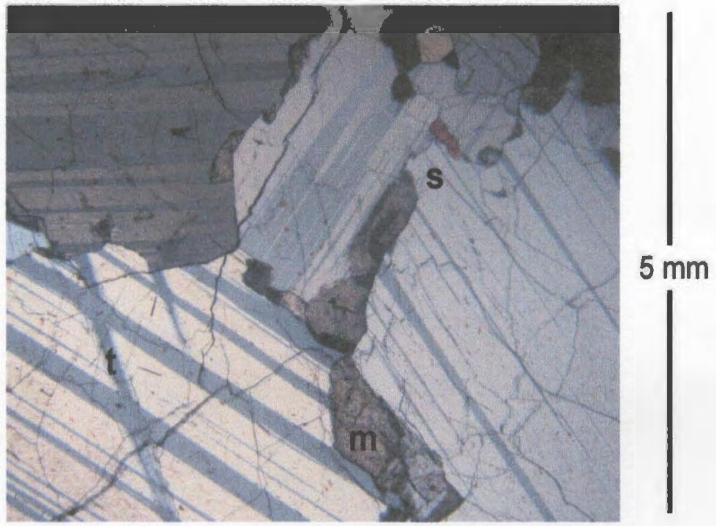

Figure 6.21: Thin section photo (XPL) of anorthosite in SA. Plagioclase shows deformation twins (t), serrated grain margins (s) and rims of calcic myrmekite (m).

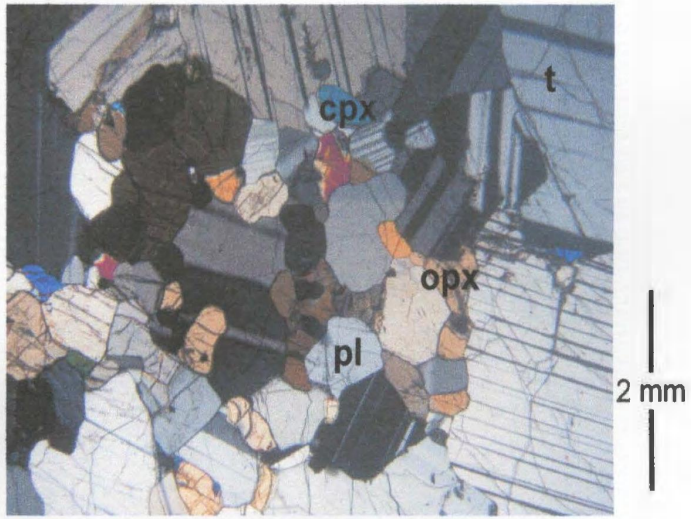

Figure 6.22: Thin section photo (XPL) of porphyritic gabbronorite in SA. Large plagioclase laths show deformation twins (t). The groundmass consists of small plagioclase (pl), orthopyroxene (opx), clinopyroxene (cpx) and oxide grains (black in photo).

example of a younger magma pulse emplaced into this shear zone is the Pikaluyak sheet (1318 +/- 7 Ma, see below).

However, since all six zircons show $^{207}Pb/^{206}Pb$ ages that overlap in error and lie on or within 9% of concordia, a concordia age was also calculated for all six zircons. This age was calculated by anchoring the lower intercept at +/- 50 Ma, and yields an upper intercept age of 1328.1 +/-4.8 Ma (Fig. 6.20).

Summary

The Unity pluton inner zone: (a) is spatially associated with the Hosenbein pluton, (b) shows similar mineral compositions and whole rock chemistry to anorthositic rocks in the Hosenbein pluton and (c) contains igneous zircons that are Mesoproterozoic in age. For these reasons, the Unity pluton inner zone is included in the Sophie centered intrusive complex.

6.2 Airstrip sheet (SA)

Ryan (2001a) grouped anorthositic rocks near the Nain airstrip into the "Unity Bay intrusion", although a 1:50 000 geological map by Ryan (2001b) noted that anorthositic rocks near the Nain airstrip are distinct from those of the "Unity Bay intrusion". Ryan (2001b) described these distinct anorthositic rocks as comprising massive to weakly layered, locally foliated and partially recrystallized anorthosite and leuconorite. The extent of these rocks was first mapped during this study.

Form and contacts

Geological mapping as part of this study outlined a unit of steeply dipping, layered, medium- to coarse-grained, anorthosite and leuconorite that is here named the Airstrip sheet (after the airstrip in Nain, Fig. 3.1). The southern-most part of the sheet consists of compositionally layered anorthositic rocks and gabbronorite. This gabbronorite is also included with the Airstrip sheet.

The southern boundary of the Airstrip sheet truncates the Unity pluton or is marked by a sharp, strongly deformed and concordant contact with Paleoproterozoic gabbroic granulite in the Nain Hill country rock belt. The northern boundary of this unit lies underneath Akpiksai Bay.

The Airstrip sheet is 1.5 km long, ~700 m thick, steeply dipping (70° – 80° N) and east-west striking (Fig. 6.3). The orientation of this unit is parallel to the Unity pluton border zone and the eastern-most part of the Hosenbein pluton border zone (see Fig. 6.2). Xenoliths of recrystallized and deformed rocks from the Unity pluton occur in the Airstrip sheet, indicating that the Unity pluton was recrystallized and deformed prior to emplacement of the Airstrip sheet.

Petrography

Anorthosite and leuconorite contain plagioclase crystals that are abundant, of large to very large size and of tabular to granular form, suggesting that plagioclase is cumulus. These crystals also show various abundances of deformation twins, bent twins, equilibrated geometries and serrated grain margins that indicate they were partly

recrystallized and/or deformed at high-T. Some crystals were overgrown by myrmekite (Fig. 6.21). Pyroxene crystals are low in abundance, of medium size and show poikilitic to sub-poikilitic texture, suggesting that pyroxene crystallized out of the intercumulus liquid. Some poikilitic pyroxene crystals consist of numerous very small pyroxene grains, indicating that large poikilitic crystals were recrystallized. Orthopyroxene crystals contain exsolved blebs of clinopyroxene and minute rods of Fe-Ti oxide. Laths of orthopyroxene are rarely seen and show tabular forms that suggest crystallization on the liquidus, as well as kinks and fractures that indicate it was recrystallized. Leuconorite also contains aggregates of small plagioclase, orthopyroxene +/- Fe-Ti oxide, biotite and amphibole grains that are interstitial to cumulus plagioclase. The predominantly plagioclase-orthopyroxene mineralogy is similar to the mineralogy of the Hosenbein pluton lower inner zone to the south.

Gabbronorite consists of small to medium-sized plagioclase and pyroxene grains, large plagioclase laths, medium-sized to large orthopyroxene laths and small Fe-Ti oxide grains (Fig. 6.22). Lath-like forms suggest that plagioclase and orthopyroxene crystals grew on the liquidus. In addition, plagioclase crystals show deformation twins, serrated grain margins and grain fractures that indicate they were recrystallized and/or deformed at high-T. Orthopyroxene crystals contain exsolved clinopyroxene. Small Fe-Ti oxide grains comprise ~5 – 10% of the mode.

Textures and structures

Anorthositic rocks are medium- to coarse-grained and show textures that range from poikilitic (10 – 35% poikilitic crystals) to granular (<10% poikilitic crystals). Gabbronorite is fine- to medium-grained and shows an overall texture that ranges from granular to porphyritic.

Anorthositic rocks are massive, mottled, layered and foliated. Massive rocks show granular or poikilitic texture, whereas mottled rocks comprise interspersed patches of granular and poikilitic texture. These patches are sub-spherical in form and range from 0.5 – 20 m in diameter. Primary layering comprises rhythmic alternations of poikilitic and granular texture. Individual layers are 10 – 200 cm thick and steeply dipping. Foliated rocks contain lens-shaped sub-poikilitic pyroxene crystals that are oriented parallel to primary layering. These foliated rocks are interpreted as a primary, flattened, poikilitic texture.

Anorthositic rocks also contain planar aggregates of medium-sized to large poikilitic pyroxene crystals. These aggregates are 1 – 5 cm thick and 10 – 100's of cm's long. Some aggregates strike parallel to layered and foliated rocks, whereas others are randomly striking.

The southernmost ~50 m of the sheet consists of compositionally layered anorthositic and gabbronoritic rocks that show only granular texture (Fig. 6.23). Individual layers are 1 – 30 cm thick, sub-vertically oriented and east-west striking. The granular texture and sub-vertical orientation of these compositionally layered rocks suggest that they were overprinted by deformation. In addition, the orientation of these

rocks is parallel to the orientation of strongly deformed rocks in the Unity pluton and the Nain Hill country rock belt.

Mineral compositions and whole rock chemistry

The whole rock chemistry for one sample of leuconorite shows Ba/K (0.32) that is similar to anorthositic rocks in the Hosenbein pluton (0.22 – 0.35), wt% K_2O and Ca/Al that are slightly low, and Sr/Ca and Mg/(Fe+Mg) that are slightly high (Table 6.5, see Fig. 6.18). Ba/K is high in comparison to NB noritic and troctolitic anorthosite (0.08 – 0.19). CIPW norms consist mostly of plagioclase and pyroxene, and show normative plagioclase compositions that fall in the range shown by the Hosenbein pluton.

Table 6.5: Whole rock chemistry of SA leuconorite and comparative data for anorthositic rocks in the Hosenbein pluton (SH), NB noritic anorthosite and NB troctolitic anorthosite

Rock type	Sample	SiO_2	K_2O	Ca/Al	Sr/Ca x 10	Mg/(Mg+Fe)	An/(An+Ab)
		wt%	wt%				CIPW
Airstrip sheet (SA)							
In	01-32-9a	53.04	0.25	1.09	0.14	0.44	0.59
Comparative data							
SH		49 - 55	0.3 - 0.4	1.11 - 1.26	0.09 - 0.12	0.21 - 0.37	0.56 - 0.59
NB noritic		52 - 58	0.6 - 1.2	0.8 - 1.1	0.10 - 0.15	0.10 - 0.35	0.42 - 0.54
NB troctolitic		49 - 55	0.2 - 0.6	1.0 - 1.2	0.06 - 0.09	0.15 - 0.49	0.53 - 0.68

Mineral compositions in one gabbronorite sample average An_{48} in plagioclase and En_{59} in orthopyroxene. These compositions are similar to anorthositic rocks in the Hosenbein pluton and are Na- and Fe-rich in comparison to Paleoproterozoic gabbroic granulite (Table 6.6, Fig. 6.24). Whole rock chemistry of this sample shows wt% TiO_2, wt% FeOt, wt% Na_2O and ppm Sr that are high in comparison to the range shown by

gabbroic granulite, whereas wt% MgO is low (see Fig. 6.9). The CIPW norm consists mostly of plagioclase, pyroxene and olivine, as well as 6% normative Fe-Ti oxide.

Table 6.6: Mineral compositions (*) and whole rock chemistry of SA gabbronorite and SP ferrogabbro, and comparative data for anorthositic rocks in the Hosenbein pluton (SH) and Paleoproterozoic gabbroic granulite (Pg)

Rock type	Sample	Pl*	Opx*	TiO_2	FeOt	MgO	P_2O_5
		An	En	wt%	wt%	wt%	wt%
Airstrip sheet (SA)							
defm gn	01-32-9b	48	59	3.30	15.94	4.80	0.02
Pikaluyak sheet (SP)							
Fe-g	00-29-12b	51	32				
Fe-g	01-31-8			2.82	15.44	2.98	0.92
Fe-g	00-29-8	49	31				
Fe-g	00-29-10	52	36				
defm Fe-g	00-29-12a			2.81	15.07	2.94	0.84
Comparative data							
SH		49 - 55	47 - 63	0.3 - 1.8	4.8 - 8.1	1.9 - 4.9	<0.4
Pg		51 - 81	58 - 85	0.4 - 0.8	11 - 13	7 - 31	<0.1

Summary

Anorthositic and gabbronoritic rocks in the Airstrip sheet: (a) are spatially associated with the Hosenbein pluton, (b) show a form that parallels the form of the Unity pluton border zone, (c) show structures that parallel structures in the Unity pluton, (d) show whole rock chemistry of a anorthositic rock that is broadly similar to anorthositic rocks in the Hosenbein pluton, (e) show mineral compositions in a gabbronoritic rock that fall in the range shown by anorthositic rocks of the Hosenbein pluton, and (f) show whole rock chemistry of a gabbronoritic rock that is distinct from Paleoproterozoic gabbroic granulite. For these reasons, the Airstrip sheet is included with the Hosenbein and Unity plutons in the Sophie centered intrusive complex.

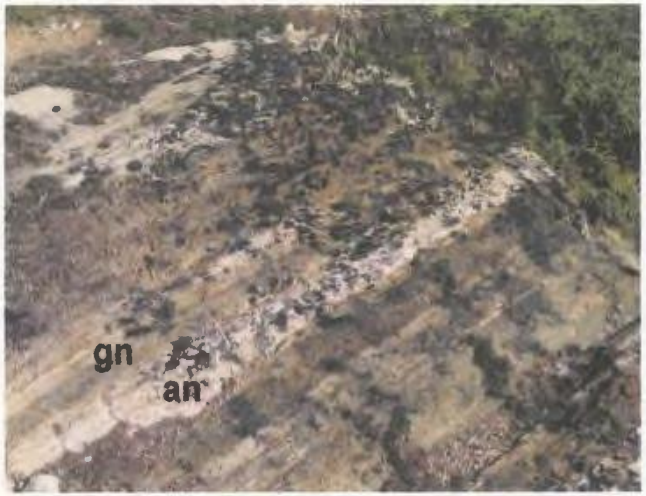

Figure 6.23: Strongly deformed and compositionally layered rocks in the lower-most ~50 m of the Airstrip sheet. Layered rocks comprise fine- to medium-grained granular anorthositic rocks (an) and gabbronorite (gn). Photo taken on the eastern flank of Nain Hill.

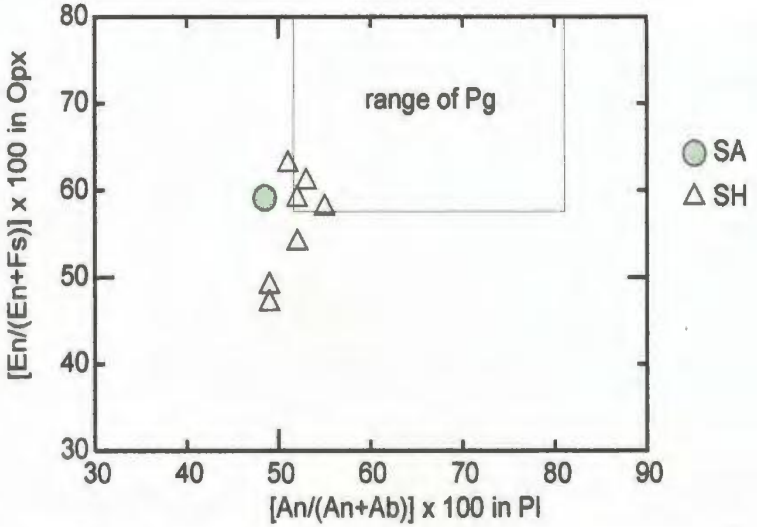

Figure 6.24: Comparison of orthopyroxene and plagioclase compositions in Airstrip gabbronorite (SA) with anorthositic rocks in the Hosenbein pluton (SH) and Paleoproterozoic gabbroic granulite (Pg).

Figure 6.25: Xenolith of Pikaluyak sheet ferrogabbro (SP) in Hosenbein upper inner zone leucogabbronorite (SHui). Dashed line marks the outline of the xenolith. Photo taken due south of Pikaluyak Cove.

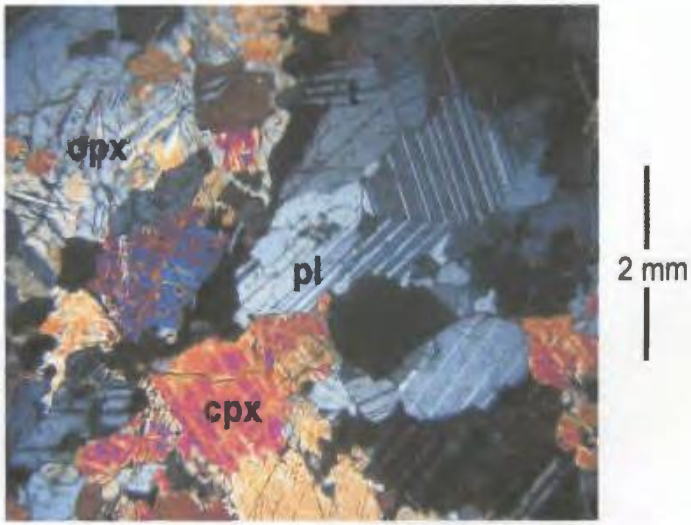

Figure 6.26: Thin section photo (XPL) of ferrogabbro in SP. Plagioclase (pl) shows granular forms and deformation twins (t). Inverted pigeonite consists of coarsely exsolved orthopyroxene (opx) and clinopyroxene (cpx). Fe-Ti oxide is sub-poikilitic (black in photo).

6.3 Pikaluyak sheet (SP)

Form and contacts

Geological mapping as part of this study found a unit of moderately dipping, massive to foliated, medium- to coarse-grained, ferrogabbro and leucogabbronorite that is here named the Pikaluyak sheet (after Pikaluyak Cove, Fig. 3.1). The bottom of this unit is truncated by the Hosenbein pluton (Fig. 6.25). The top of this unit comprises a sharp, strongly deformed and concordant contact with Paleoproterozoic gabbroic granulite in the Nain Hill country rock belt.

The Pikaluyak sheet is up to 400 m thick, 1500 m long, moderately (50° – 70°) northeast dipping and northwest-southeast striking (100° – 140°) (see Fig. 6.3). The orientation of this unit is parallel to the orientation of the underlying Hosenbein pluton.

Petrography

Ferrogabbro contains plagioclase and inverted pigeonite crystals that are medium-sized and granular in form. These grains show interlobate grain margins, serrated grain margins and equilibrated geometries (Fig. 6.26) that indicate they were recrystallized at high-T. Larger plagioclase crystals show deformation twins and deformation bands that also indicate they were deformed at high-T. Inverted pigeonite is coarsely exsolved. Fe-Ti oxide shows sub-poikilitic texture that suggests it crystallized out of the intercumulus liquid. Minor and accessory minerals consist of small to medium-sized Fe-rich olivine grains, very small apatite grains, small K-feldspar grains, very small zircon grains, very small biotite laths and small amphibole grains.

Textures and structures

Ferrogabbro is medium-grained and shows an overall texture that ranges from granular to poikilitic. Leucogabbronorite is medium- to coarse-grained and shows an overall texture that is poikilitic.

Ferrogabbro and leucogabbronorite form massive, mottled and foliated rocks. Massive rocks comprise only granular or poikilitic texture. Mottled rocks comprise interspersed patches of granular and poikilitic texture. These patches are sub-spherical in form and range from 0.1 – 10 m in diameter. Foliated rocks contain medium-sized, lens-shaped, sub-poikilitic, Fe-Ti oxide crystals (Fig. 6.27) that comprise a primary, flattened, poikilitic texture. These lens-shaped crystals strike parallel to the unit contacts as well as primary layering and foliation in the underlying Hosenbein pluton.

Leucogabbronorite also contains veins that consist of sub-poikilitic Fe-Ti oxide crystals, biotite laths and amphibole crystals (Fig. 6.27). These veins are 0.1 – 5 cm thick, 1 – 10's of cm's long and strike parallel to foliated rocks.

The upper-most ~50 m of the Pikaluyak sheet consists of compositionally layered anorthositic and Fe-rich gabbroic rocks (Fig. 6.28). Both rock types are granular-textured. Individual layers are 1 – 30 cm thick, steeply dipping (70°) to sub-vertically oriented and northwest to southeast striking. The orientation of these rocks is parallel to compositional and gneissic layering in the adjacent Nain Hill country rock belt. Very fine trains (<1 cm thick) of Fe-Ti oxides and pyroxene in Fe-rich gabbroic layers are sigmoidal and suggest sinistral shear deformation. These findings suggest that compositionally layered rocks in

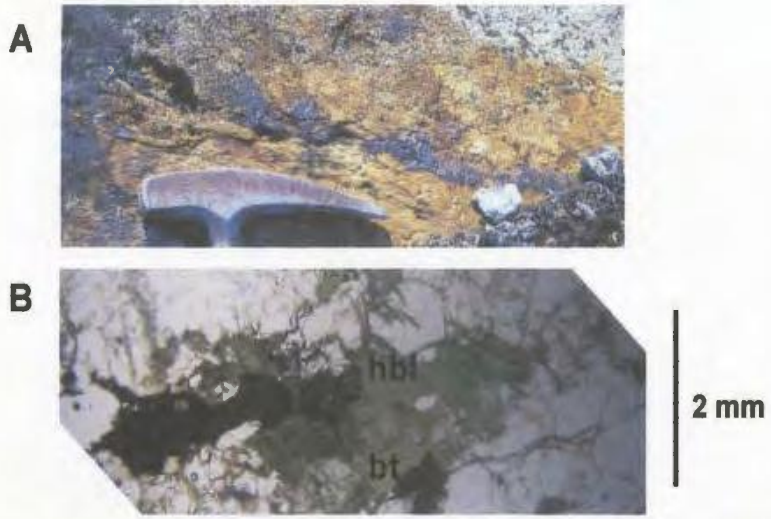

Figure 6.27: (A) Field photo of Fe-Ti oxide-rich vein and (B) thin section photo (PPL) of lens-shaped Fe-Ti-oxide-rich aggregate in foliated ferrogabbro of SP. The aggregate also contains biotite (bt) and hornblende (hbl). Field photo taken south of Pikaluyak Cove.

Figure 6.28: Strongly deformed and layered ferrogabbro in the uppermost ~50 m of the Pikaluyak sheet. Dashed lines shows the trend of these sub-vertically orientated layered rocks. Photo taken south of Pikaluyak Cove.

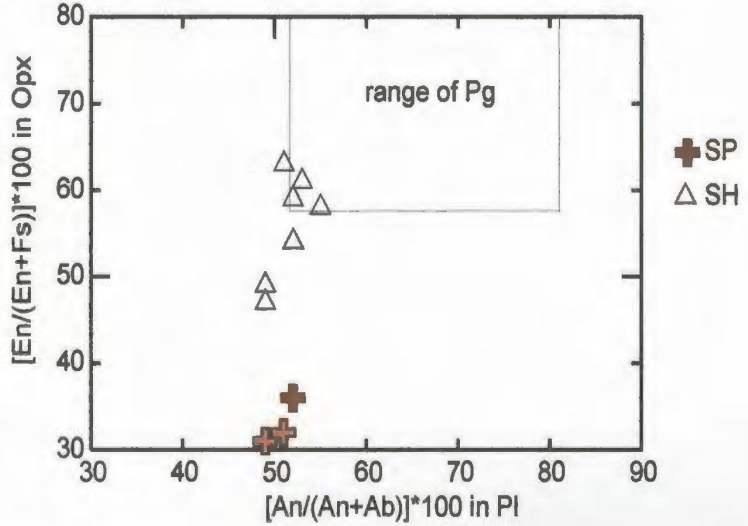

Figure 6.29: Comparison of orthopyroxene and plagioclase compositions in Pikaluyak ferrogabbro (SP) with anorthositic rocks in the Hosenbein pluton (SH) and Paleoproterozoic gabbroic granulite (Pg).

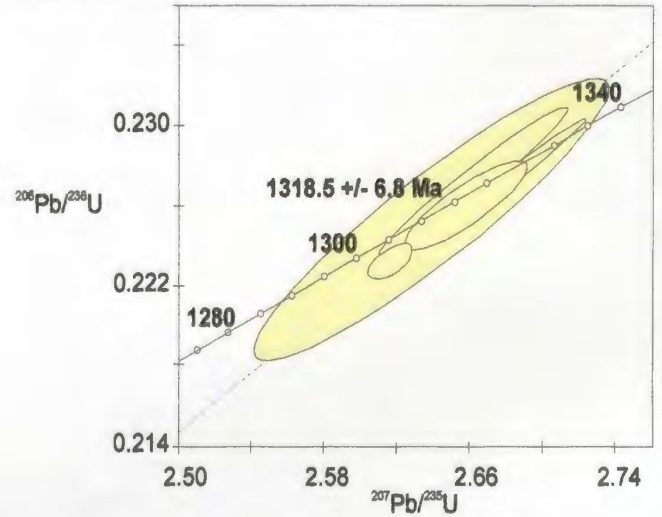

Figure 6.30: Concordia diagram for five zircon grains separated from ferrogabbro in the Pikaluyak sheet. These zircons define a concordia age of 1318 +/- 6.8 Ma when the lower intercept is anchored at 0 +/- 50 Ma. The mean square weighted deviate is 2.8.

the upper-most part of the Pikaluyak sheet were overprinted by sinistral shear deformation.

Mineral compositions and whole rock chemistry

Mineral compositions in ferrogabbro range from An_{49-52} in plagioclase, En_{31-36} for orthopyroxene component in inverted pigeonite and En_{24-28} for clinopyroxene component in inverted pigeonite (see Table 6.6). These plagioclase compositions are similar to anorthositic rocks in the Hosenbein pluton, and Na-rich in comparison to Paleoproterozoic gabbroic granulite. Pyroxene compositions are Fe-rich in comparison to both anorthositic rocks in the Hosenbein pluton and Paleoproterozoic gabbroic granulite (Fig. 6.29).

Whole rock chemistry of ferrogabbro shows wt% TiO_2, FeOt, Na_2O, K_2O and P_2O_5, as well as ppm Sr and Ba, that are high in comparison to Paleoproterozoic gabbroic granulite (see Fig. 6.9). High abundances of these elements are consistent with accessory abundances of ilmenite, alkali feldspar and apatite that were observed in thin section. CIPW norms consist mostly of plagioclase and pyroxene, as well as 5% Fe-Ti oxide, 3% orthoclase and 2% apatite. Pikaluyak ferrogabbro contains high abundances of wt% K_2O, ppm Ba and ppm Y in comparison to all other anorthositic and gabbronoritic rocks of the Sophie centered intrusive complex.

Geochronology

U-Pb analysis of zircon was done on a ferrogabbro sample collected from the central part of the Pikaluyak sheet (see Fig. 6.3). This sample was analyzed in order to determine the age of a weakly deformed unit in the study area. Zircon forms small grains and is skeletal, occurring as interstitial grains to plagioclase and pyroxene. These zircons are interpreted as igneous crystallization products.

Table 6.7: Descriptions and chemistry of zircons separated from SP ferrogabbro

Grain	Zr 1	Zr 2	Zr 3	Zr 4	Zr 5
Color	yellow	yellow	yellow	yellow	yellow
Translucent	yes	yes	yes	yes	yes
Shape	prismatic	prismatic	prismatic	prismatic	prismatic
Weight (ug)	8	20	86	16	26
Com. (Pb pg)	3	2	3	6	2
U (ppm)	10	13	16	23	10
Th/U	0.89	0.89	0.9	0.8	1
$^{206}Pb/^{204}Pb$	460	1487	7954	919	2259
Pb (ppm)	2.5	3.3	4.3	5.9	2.6
$^{206}Pb/^{238}U$	0.2266	0.2257	0.2231	0.2284	0.228
% error	1	3.2	0.4	1.3	1.7
$^{207}Pb/^{235}U$	2.659	2.639	2.615	2.686	2.663
% error	1.1	3.2	0.4	1.3	1.7
$^{207}Pb/^{206}Pb$	0.0851	0.0848	0.085	0.0853	0.0847
% error	0.6	1.3	0.5	0.2	0.4
$^{206}Pb/^{238}U$ (Ma)	1317	1312	1298	1326	1324
$^{207}Pb/^{235}U$ (Ma)	1317	1312	1305	1325	1318
$^{207}Pb/^{206}Pb$ (Ma)	1318	1311	1315	1323	1309
+/- m.y.	12	10	5	8	10
Conc. (%)	100	100	99	100	101

Five zircons were analyzed for U and Pb isotope chemistry. All of these zircons are yellow in color and prismatic in form, and contain 10 – 23 ppm U and 2.5 – 5.9 ppm Pb (Table 6.7).

The $^{207}Pb/^{206}Pb$ ratios of all five zircons overlap in error and lie on or within 1% of concordia. A concordia age was calculated by anchoring the lower intercept at 0 +/- 50 Ma, which yields an upper intercept age of 1318.5 +/- 6.8 Ma (Fig. 6.30). This upper intercept is interpreted as the crystallization age for this unit.

Summary

Fe-rich gabbroic rocks in the Pikaluyak sheet: (a) are spatially associated with the Hosenbein pluton, (b) show a form that parallels the form of the Hosenbein pluton upper border zone, (c) show structures that parallel structures in the Hosenbein pluton, (d) show plagioclase compositions that fall in the range shown by anorthositic rocks in the Hosenbein pluton, and (e) contain igneous zircons that are Mesoproterozoic in age. For these reasons, the Pikaluyak sheet is included with the Hosenbein pluton in the Sophie centered intrusive complex.

6.4 Hosenbein pluton (SH)

Ryan (2001a) noted four anorthositic intrusions in the vicinity of Mount Sophie and named one of these intrusions after Hosenbein Lake. Ryan (2000a) described this "Hosenbein Lake intrusion" as comprising a base of olivine gabbro that is gradational upward into locally layered and seriate-textured leuconorite. Ryan (2000a) also noted that the "Hosenbein Lake intrusion" cut the Unity pluton. Subsequent mapping by Ryan (2001a) found a fourth intrusion of anorthositic rocks that he named the "South Channel

Cairn intrusion". Ryan (2001a) described this intrusion as comprising massive to well-layered leucogabbro, leuconorite and anorthosite.

Geological mapping as part of this study groups parts of the "Hosenbein Lake" and "South Channel Cairn intrusions" into the Hosenbein pluton. This pluton extends for a maximum of 11.5 km in a northwest to southeast direction and 9.0 km in a northeast to southwest direction, and is here divided into a lower border zone, lower inner zone, upper inner zone and upper border zone.

6.4.1 Hosenbein pluton lower border zone (SHlb)

Form and contacts

Geological mapping as part of this study outlined a composite unit of moderately dipping, weakly to strongly deformed, gabbronorite, olivine gabbronorite and leucogabbronorite. This unit is here named the Hosenbein pluton lower border zone. The base of this unit shows a sharp, weakly to strongly deformed and concordant contact with Paleoproterozoic gabbroic granulite in the Kangilialuk Lake country rock belt. The top of this unit shows an increase in the abundance of more gently dipping anorthositic rocks that mark the gradational contact with the Hosenbein pluton lower inner zone.

The Hosenbein pluton lower border zone extends for 3.2 km in a northwest-southeast direction and 0.8 km in a northeast-southwest direction. This zone is moderately (30° – 50°) east dipping to sub-vertical, north-south striking and up to ~500 m thick (Figs. 6.1, 6.2). Primary layering and strongly deformed rocks in the lower border zone strike parallel to unit contacts and primary layering in the overlying lower

inner zone. Parts of the lower border zone show a gradation from weakly to strongly deformed, whereas strongly deformed rocks also occur as xenoliths in weakly deformed rocks of the lower border zone (Fig. 6.31). In addition, xenoliths of weakly deformed leucogabbronorite occur in weakly deformed gabbronorite. These relations indicate that the lower border zone is composite.

Petrography

Weakly deformed gabbronorite and olivine gabbronorite consist of small to medium-sized plagioclase grains and laths, orthopyroxene grains, laths, poikilitic and/or sub-poikilitic crystals, clinopyroxene grains and olivine grains (Fig. 6.32). Some grains show equilibrated geometries and triple junctions that suggest grain margins were equilibrated at high-T. Lath-like forms of plagioclase and orthopyroxene suggest that these minerals crystallized on the liquidus. Olivine grains occur as inclusions in poikilitic orthopyroxene crystals. In addition, poikilitic orthopyroxene crystals contain abundant blebs of exsolved clinopyroxene. Fe-Ti oxide occurs as small grains in accessory abundances.

Strongly deformed gabbronorite contains plagioclase, orthopyroxene and clinopyroxene grains that show local development of triple junctions (Fig. 6.33) and equilibrated geometries, indicating that most grain margins were equilibrated at high-T. Plagioclase grains show deformation twins that indicate they were deformed at high-T. Orthopyroxene grains show kinks and fractures that indicate they were also deformed.

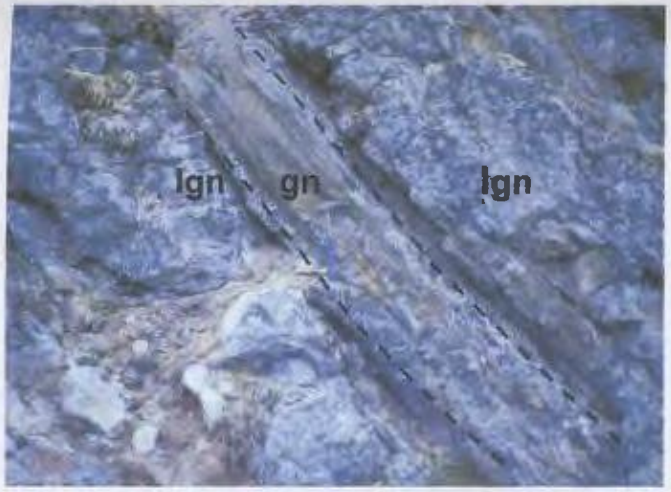

Figure 6.31: Xenolith of layered gabbronorite (gn) in massive leucogabbronorite (lgn) of SHlb. Dashed line marks the outline of the xenolith. Photo taken northeast of Kangilialuk Lake.

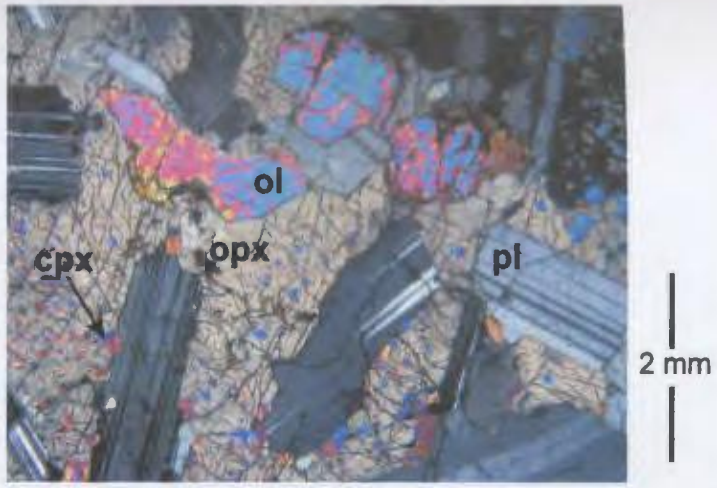

Figure 6.32: Thin section photo (XPL) of olivine gabbronorite in SHlb. Photo shows tabular plagioclase (pl), granular olivine (ol) and poikilitic orthopyroxene (opx). Orthopyroxene contains blebs of exsolved clinopyroxene (cpx).

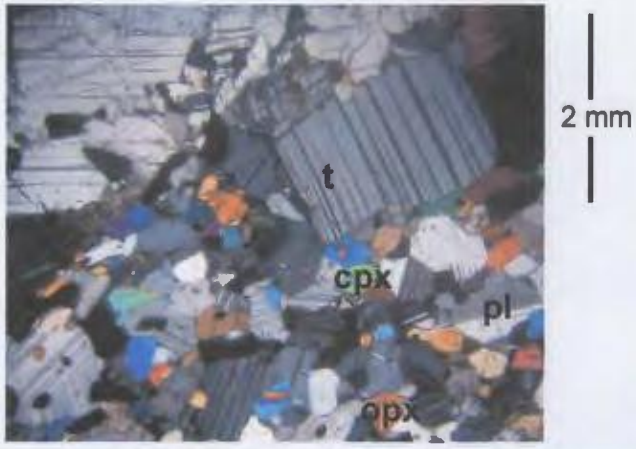

Figure 6.33: Thin section photo (XPL) of porphyritic gabbronorite in SHlb. Large plagioclase laths show deformation twins (t). The groundmass consists of small plagioclase (pl), orthopyroxene (opx), clinopyroxene (cpx) and oxide (black in photo) grains.

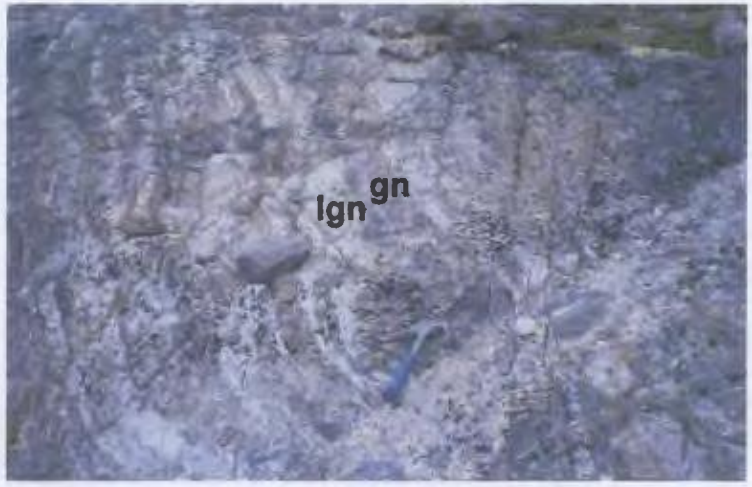

Figure 6.34: Strongly deformed and compositionally layered gabbronorite (gn) and leucogabbronorite (lgn) in SHlb. Layers are subvertically orientated and broadly north-south striking. Photo taken east of Kangilialuk Lake.

Textures and structures

Olivine gabbronorite and gabbronorite are fine- to medium-grained, and are weakly to strongly deformed. Weakly deformed rocks show an overall texture that ranges from granular to porphyritic, whereas strongly deformed rocks show an overall texture that is predominantly granular. Leucogabbronorite is medium-grained and shows an overall texture that is poikilitic in weakly deformed rocks and granular in strongly deformed rocks.

Weakly deformed olivine gabbronorite, gabbronorite and leucogabbronorite form massive, layered and foliated rocks. Massive rocks comprise only one rock type and texture. Primary layering comprises gradational alternations of all rock types and textures. Individual layers are 1 – 20 cm thick and are moderately (40°) dipping. Foliated rocks are either porphyritic-textured and contain plagioclase and pyroxene laths that are aligned parallel to the plane of primary layering, or poikilitic-textured and contain lens-shaped sub-poikilitic pyroxene crystals that are also aligned parallel to the plane of layering.

Parts of the lower border zone are 'strongly deformed'. The strongly deformed rocks comprise compositionally layered leucogabbronorite and gabbronorite that show only granular texture (Fig. 6.34). Individual layers are 0.5 – 10 cm thick, steeply dipping (70°) to sub-vertical and north-south to northwest-southeast striking. The orientation of these rocks is parallel to primary layering in the lower border zone, as well as compositional and gneissic layering in the adjacent Kangilialuk Lake country rock belt.

Mineral compositions and whole rock chemistry

Mineral compositions in olivine gabbronorite average An_{59} in plagioclase, Fo_{45} in olivine, En_{57} in orthopyroxene and En_{37} in exsolved clinopyroxene. These mineral compositions fall in the range shown by Paleoproterozoic gabbroic granulite, but the well-preserved igneous textures of these rocks (see Fig. 6.32) suggest that these rocks comprise part of the Hosenbein pluton.

Table 6.8: Mineral compositions (*) and whole rock chemistry for SHlb gabbronoritic rocks and comparative data for anorthositic rocks of the Hosenbein pluton (SH) and Paleoproterozoic gabbroic granulite (Pg)

Rock type	Sample	Pl*	Opx*	TiO_2	FeOt	MgO	P_2O_5
		An	En	wt%	wt%	wt%	wt%
Hosenbein pluton lower border zone (SHlb)							
ol gn	00-21-16	59	57				
defm gn	00-25-9d	52	59	1.11	13.27	7.02	0.01
Comparative data							
SH		49 - 55	47 - 63	0.3 - 1.8	4.8 - 8.1	1.9 - 4.9	<0.4
Pg		51 - 81	58 - 85	0.4 - 0.8	11 - 13	7 - 31	<0.1

The mineral compositions for one sample of strongly deformed gabbronorite average An_{52} in plagioclase, En_{59} in orthopyroxene and En_{40} in clinopyroxene (Table 6.8). These compositions fall in the range shown by anorthositic rocks of the Hosenbein pluton, and in the Na- and Fe-rich end of the range shown by Paleoproterozoic gabbroic granulite (Fig. 6.35). The whole rock chemistry for this sample shows TiO_2 and FeOt that are slightly high in comparison to Paleoproterozoic gabbroic granulite, and wt% MgO that is relatively low (see Fig. 6.9). This study also found Mesoproterozoic gabbronoritic rocks with relatively high abundances of TiO_2 and FeOt in the Anaktalik lower sheet

(section 5.4) and the Pikaluyak sheet (section 6.3). This strongly deformed sample of gabbronorite is therefore here included with the Hosenbein pluton lower border zone.

Summary

The gabbronoritic rocks in the Hosenbein pluton lower border zone: (a) are localized below the Hosenbein pluton lower inner zone, and (b) are gradational from weakly to strongly deformed. Weakly deformed rocks are included as part of the Sophie centered intrusive complex because they show well-preserved igneous textures. Strongly deformed rocks are included as part of the Sophie centered intrusive complex because they show: (a) mineral compositions that are similar to anorthositic rocks of the Hosenbein pluton, and (b) whole rock abundances of TiO_2 and FeOt that are high. High abundances of these oxides are typical of other Mesoproterozoic gabbronoritic rocks in the study area. The strongly deformed rocks are reminiscent of descriptions of 'marginal granulites' by other workers (see Davies, 1973b; Brand, 1974; Berg and Briegel, 1981; Royse et al., 1999).

6.4.2 Hosenbein pluton lower inner zone (SHil)

Form and contacts

Geological mapping as part of this study outlined a unit of massive to sub-horizontally layered leuconorite and anorthosite that is here named the Hosenbein pluton lower inner zone. This unit comprises the shape of a horseshoe (see Fig. 6.1). The top of the unit shows a gradational increase in the abundance of leucogabbronorite that marks

the base of the Hosenbein pluton upper inner zone. The western boundary of this unit shows a gradational increase in the abundance of moderately dipping gabbronoritic rocks that mark the top of the Hosenbein pluton lower border zone. The eastern boundary consists of gently west dipping anorthositic rocks that overlie gently east-dipping Paleoproterozoic gabbroic granulite, whereas the southern boundary is truncated by sills and dikes derived from the Satosoak pluton (Fig. 6.36).

The eastern to southern part of the Hosenbein pluton lower inner zone extends over 6.4 km in a north-south direction and 1.4 – 3.9 km in an east-west direction (see Fig. 6.1), and is up to 1700 m thick. This part of the lower inner zone is sub-horizontal to gently (20° – 30°) west dipping and north of northeast striking (010° – 025°). The western part of the lower inner zone extends over 7.3 km in a northwest-southeast direction and 0.3 – 1.2 km in a northeast-southwest direction, and is up to 1000 m thick. This part of the lower inner zone is moderately (50° – 65°) northeast dipping and east of southeast striking (100° – 120°). An east-west cross-section shows a bowl-shaped form (see Fig. 6.2).

Petrography

Plagioclase crystals are abundant, of large to very large size (0.5 – 20 cm) and of tabular to granular form, suggesting that these crystals are cumulus. These crystals show various abundances of deformation twins, bent twins, equilibrated geometries, hairline fractures and serrated grain margins (Fig 6.37) that indicate they were partly recrystallized and/or deformed at high-T. Orthopyroxene crystals are of relatively low

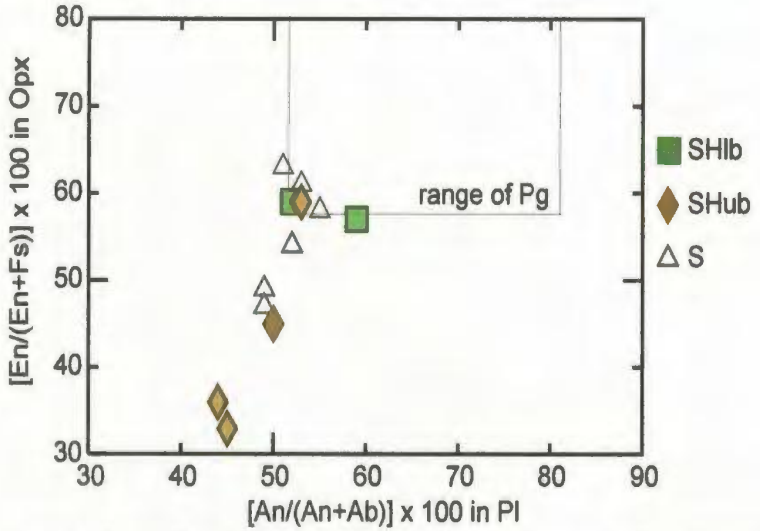

Figure 6.35: Comparison of orthopyroxene and plagioclase compositions in the Hosenbein pluton lower (SHlb) and upper (SHub) border zones, anorthositic rocks of the Hosenbein pluton and Paleoproterozoic gabbroic granulite (Pg).

Figure 6.36: Sill of Satosoak pluton border zone (KSb) gabbronorite that cuts Hosenbein pluton inner lower zone (SHli) leuconorite. Dashed line marks the intrusive contact. Photo taken west of Kauk Harbor.

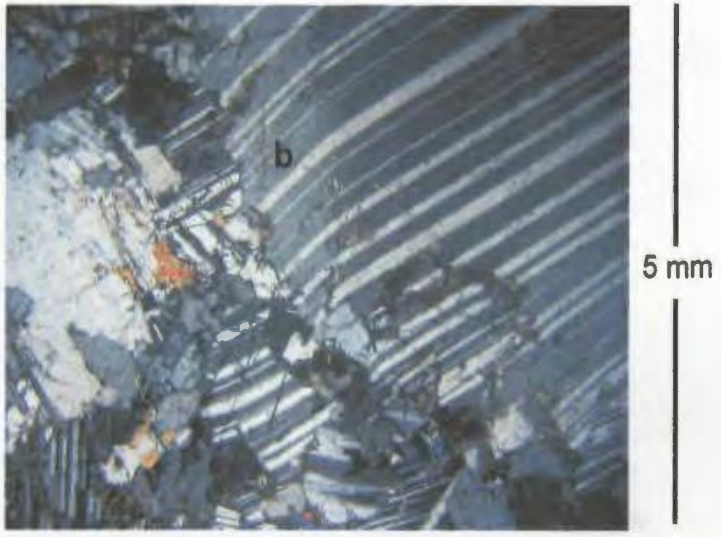

Figure 6.37: Thin section photo (XPL) of anorthosite in SHli. Plagioclase shows bent twins (b), undulose extinction and subgrain development.

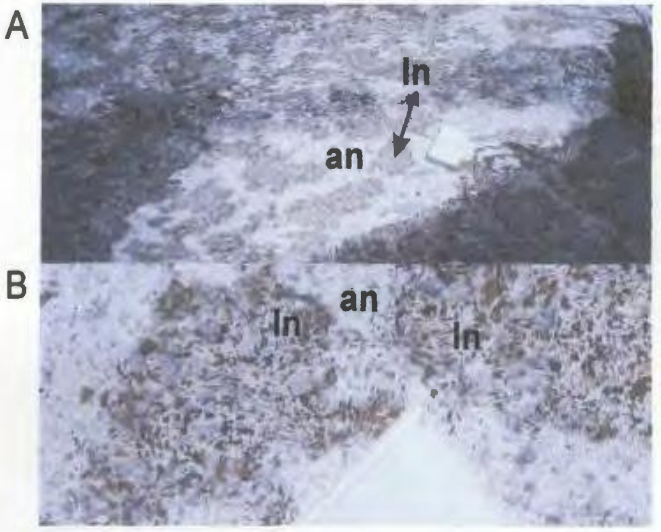

Figure 6.38: (A) Overview and (B) close-up photo of mottled rocks in SHli. Rock comprises patches of granular-textured anorthosite (an) and poikilitic-textured leuconorite (ln). Photo taken on west flank of Mount Sophie.

abundance, medium size and show poikilitic to sub-poikilitic texture, suggesting that orthopyroxene crystallized out of the intercumulus liquid. These intercumulus orthopyroxenes contain exsolved blebs and lamella of clinopyroxene, and minute rods of oxide. Exsolved plagioclase is rarely seen and suggests a high-alumina pyroxene. Leuconorite also contains aggregates of small plagioclase, orthopyroxene +/- Fe-Ti oxide, biotite and amphibole grains that are interstitial to cumulus plagioclase.

Textures and structures

Anorthositic rocks are medium- to very coarse-grained and show an overall texture that ranges from poikilitic (10 – 35% poikilitic crystals and aggregates) to granular (<10% poikilitic crystals and aggregates). Some poikilitic-textured rocks contain orthopyroxene crystals that form sub-spherical oikocrysts ranging from 2 – 10 cm in diameter.

Leuconorite and anorthosite form massive, mottled, layered and/or foliated rocks. Massive rocks show only granular or poikilitic texture. Mottled rocks comprise interspersed patches of poikilitic and granular texture. These patches are sub-spherical in form and range from 0.05 – 100 m in diameter (Fig. 6.38). Primary layering comprises rhythmic alternations of granular and poikilitic texture (Fig. 6.39). Individual layers are 10 – 200 cm thick, 30 to 100's of m in lateral extent and sub-horizontal to gently dipping. Foliated rocks contain medium-sized to large, lens-shaped, sub-poikilitic pyroxene crystals and aggregates of norite. These lens-shaped crystals and aggregates are 1 – 5 cm

in diameter, 0.01 – 0.5 cm thick and strike parallel, or oblique, to primary layering. Foliated rocks are here interpreted as a primary and flattened poikilitic texture.

Anorthositic rocks also contain planar aggregates of medium-sized to large poikilitic pyroxene crystals (Fig. 6.40). These aggregates are 1 – 10 cm thick, 1 – 10's of m's long, usually steeply dipping and randomly oriented. Some of these aggregates intersect at T-junctions and show sigmoidal foliation that suggests they were emplaced into late-magmatic shear zones.

Mineral compositions and whole rock chemistry

Mineral compositions of anorthositic rocks range from An_{51-56} in plagioclase and En_{58-63} in orthopyroxene. These plagioclase and orthopyroxene compositions, respectively, fall in the range shown by the more Ca-rich plagioclase and Mg-rich orthopyroxene compositions in NB noritic anorthosite (Table 6.9). Both plagioclase and pyroxene crystals are homogeneous in composition. Orthopyroxene crystals and exsolved clinopyroxene (En_{39-41}) are Mg-rich relative to pyroxenes in the Hosenbein pluton upper inner zone (see section 6.4.3). Orthopyroxene also contains <0.9 wt% Al_2O_3.

Whole rock chemistry of anorthositic rocks show wt% SiO_2, wt% K_2O and Ca/Al that fall in the range shown by NB troctolitic anorthosite, whereas Sr/Ca falls in the range shown by NB noritic anorthosite (see Table 6.9, Fig. 6.18). Ba/K (0.22 – 0.29) is high in comparison to both NB noritic and troctolitic anorthosite (0.09 – 0.18). CIPW norms consist mostly of plagioclase and pyroxene, and show normative plagioclase compositions that fall in the range shown by NB troctolitic anorthosite.

Table 6.9: Mineral compositions (*) and selected whole rock chemistry data for SHli and SHui anorthositic rocks, and comparative data for NB noritic and troctolitic anorthosite

Rock type	Sample	Pl*	Opx*	SiO_2	K_2O	Ca/Al	Sr/Ca x 10	Mg/(Mg+Fe)	An/(An+Ab)
		An	En	wt%	wt%				CIPW
Hosenbein pluton lower inner zone (SHli)									
ln	01-24-14	51	63	51.61	0.34	1.15	0.12	0.28	0.59
ln	00-22-11	55	58	52.87	0.40	1.11	0.10	0.37	0.59
ln	00-1-10	52	59						
ln	00-7-19	53	61						
anor	01-20-15	56							
Hosenbein pluton upper inner zone (SHui)									
lgn	01-31-2	49	47	51.45	0.40	1.19	0.09	0.21	0.58
lgn	01-33-31			50.89	0.44	1.26	0.09	0.23	0.56
lgn	00-3-6	49	47						
lgn	01-34-4	52	54						
anor	00-2-13	52							
lgn	00-20-6b	52							
anor	00-22-2	53							
Comparative data									
NB noritic		40 - 54	57 - 67	52 - 58	0.6 - 1.2	0.8 - 1.1	0.10 - 0.15	0.10 - 0.35	0.42 - 0.54
NB troctolitic		51 - 68	66 - 73	49 - 55	0.2 - 0.6	1.0 - 1.2	0.06 - 0.09	0.15 - 0.49	0.53 - 0.68

6.4.3 Hosenbein pluton upper inner zone (SHui)

Form and contacts

Geological mapping as part of this study outlined a unit of sub-horizontal to moderately dipping, massive to layered, leucogabbronorite and anorthosite. This unit is here named the Hosenbein pluton upper inner zone. The bottom of this unit shows a gradational increase in the abundance of leuconorite that marks the top of the Hosenbein pluton lower inner zone. In the northwest, the top of this unit shows a gradational increase in the abundance of gabbronoritic rocks that mark the bottom of the Hosenbein pluton upper border zone. In the northeast, the top of this unit truncates the Unity pluton.

The Hosenbein upper inner zone extends over 9.1 km in a northwest-southeast direction and 1.9 – 5.5 km in a northeast-southwest direction (see Fig. 6.1). The central

Figure 6.39: Primary layering in SHli. Layers consist of granular-textured anorthosite (an) and poikilitic-textured leuconorite (ln). Photo taken along north shore of Kauk Harbor.

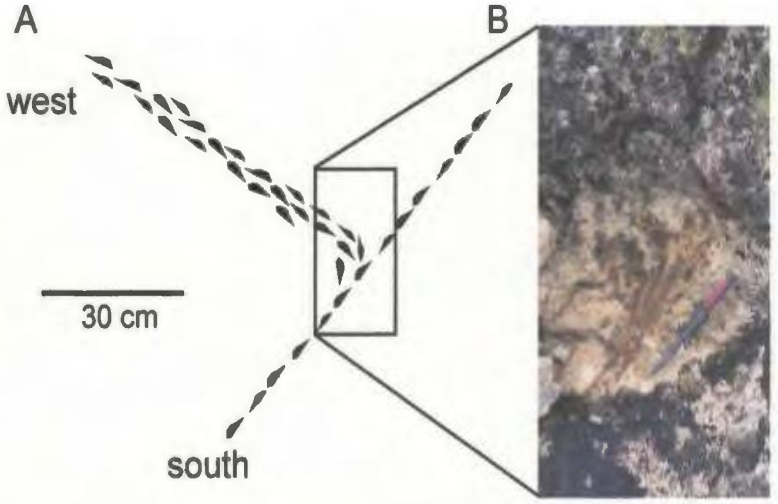

Figure 6.40: (A) Simplified field sketch and (B) photo of the same planar pyroxene aggregate in SHli anorthositic rocks. Sketch and photo show asymmetric foliation that indicates north-south dextral shearing. Photo and sketch taken south of Mount Sophie.

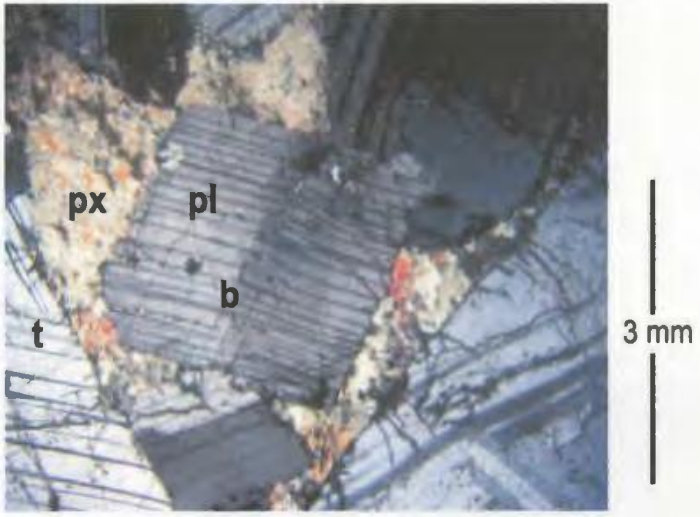

Figure 6.41: Thin section photo (XPL) of leucogabbronorite in SHui. Plagioclase (pl) shows deformation twins (t), bent twins (b) and undulose extinction. Pyroxene (px) shows relict poikilitic texture and is mostly altered to uralite.

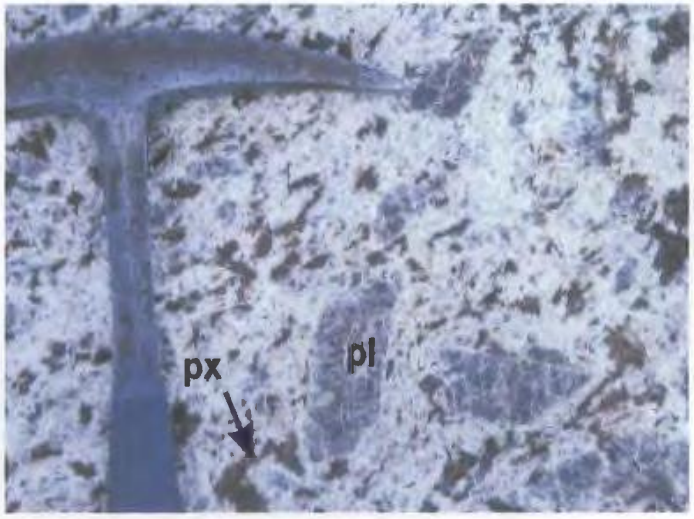

Figure 6.42: Poikilitic-textured leucogabbronorite in SHui, showing very large plagioclase crystals (pl) and medium-sized to large poikilitic pyroxene crystals (px). Photo taken near Hosenbein Lake.

part of the upper inner zone is up to 700 m thick, sub-horizontal to gently (20°) west dipping and northeast striking (045°). The northwestern lobe of the upper inner zone is up to 1500 m thick, moderately (50° – 65°) northeast dipping and east of southeast striking (100° – 120°) (see Fig. 6.2). The upper inner zone contains abundant xenoliths of the Unity pluton inner zone that are sub-spherical to slab-like in form and range from 0.1 – 100 m in size (see Fig. 6.12). Rocks of the Hosenbein pluton upper inner zone are of uniform coarse grain-size right up to the contacts with these xenoliths. The upper inner zone also contains dikes and patches of oxide gabbronorite.

Petrography

The petrography of plagioclase and orthopyroxene crystals is similar to the Hosenbein pluton lower inner zone. In addition, the upper inner zone contains clinopyroxene that is medium-sized and granular to sub-poikilitic form. The upper inner zone also contains Fe-Ti oxide crystals that show sub-poikilitic texture and are abundant (up to 10% mode) relative to the lower inner zone. Accessory minerals consist of very small apatite grains. The relatively high abundances of intercumulus clinopyroxene, Fe-Ti oxide and apatite suggest that the intercumulus mineralogy of the upper inner zone is evolved in comparison to the lower inner zone.

Secondary minerals have replaced up to 5% of the plagioclase and 10 – 100% of the pyroxene. Minerals that replaced plagioclase consist of sericite, saussurite, muscovite, calcite and quartz, whereas those that replaced pyroxene consist of uralite, green amphibole and/or chlorite (Fig. 6.41). The high abundances of secondary minerals in the

upper inner zone contrast with a lack of these minerals in the lower inner zone, and indicate that the upper inner zone is both evolved and hydrothermally altered.

Textures and structures

Anorthositic rocks are medium- to very coarse-grained and show an overall texture that ranges from poikilitic (10 – 35% poikilitic crystals and aggregates, Fig. 6.42) to granular (<10% poikilitic crystals and aggregates). These rocks are massive, mottled, layered and/or foliated. The textural characteristics of these structures are similar to those in the Hosenbein pluton lower inner zone and are therefore descriptions of these structures are here not repeated. In addition, primary layers in the western and northern part of the inner zone are moderately (50° – 65°) dipping (Fig 6.43).

Mineral compositions and whole rock chemistry

Mineral compositions of anorthositic rocks range from An_{49-53} in plagioclase and En_{47-54} in orthopyroxene. These compositions fall in the range shown by NB noritic anorthosite (see Table 6.9). The rims of some plagioclase grains are Ca-rich ($+An_{2-7}$) relative to the rest of the grain. Cores of relict orthopyroxene crystals are Fe-rich relative to the lower inner zone and contain <1.1 wt% Al_2O_3. Cores of relict clinopyroxene (En_{32-39}) crystals are also Fe-rich relative to the lower inner zone, suggesting that pyroxene compositions are evolved in the upper inner zone as compared to the lower inner zone.

The whole rock chemistry of anorthositic rocks show wt% SiO_2, wt% K_2O and Sr/Ca that fall in the range shown by NB troctolitic anorthosite (see Table 6.9, Fig. 6.18).

Ca/Al is high in comparison to both NB troctolitic and noritic anorthosite, and reflects modal abundances of clinopyroxene in these samples. Ba/K (0.32 – 0.35) is high in comparison to NB troctolitic and noritic anorthosite (0.08 – 0.19), whereas Mg/(Mg+Fe) is low in comparison to the Hosenbein pluton lower inner zone. These upper inner zone anorthositic rocks also show higher abundances of TiO_2, P_2O_5, Sc, Ba, Zr and Y in comparison to lower inner zone anorthositic rocks, suggesting that the upper inner zone is evolved in comparison to the lower inner zone. CIPW norms consist mostly of plagioclase and pyroxene, and show normative plagioclase compositions that fall in the range shown by NB troctolitic anorthosite.

Ferrogabbro patches and dikes

The upper inner zone contains patches and dikes of medium- to coarse-grained ferrogabbro. Patches are sub-spherical in form and range from 0.1 – 100 m in diameter, whereas dikes are 10 – 50 cm thick (Fig. 6.44) and strike parallel to primary layering in the host rock. Intrusive contacts are sharp or grade into leucogabbronorite that contains interstitial aggregates of small plagioclase, pyroxene and Fe-Ti oxide grains.

Ferrogabbro patches and dikes consist of small to medium-sized plagioclase and pyroxene grains and sub-poikilitic Fe-Ti oxide crystals. Poikilitic Fe-Ti oxide crystals occur when modal abundances exceed ~5%. Accessory minerals consist of very small apatite, biotite and amphibole grains.

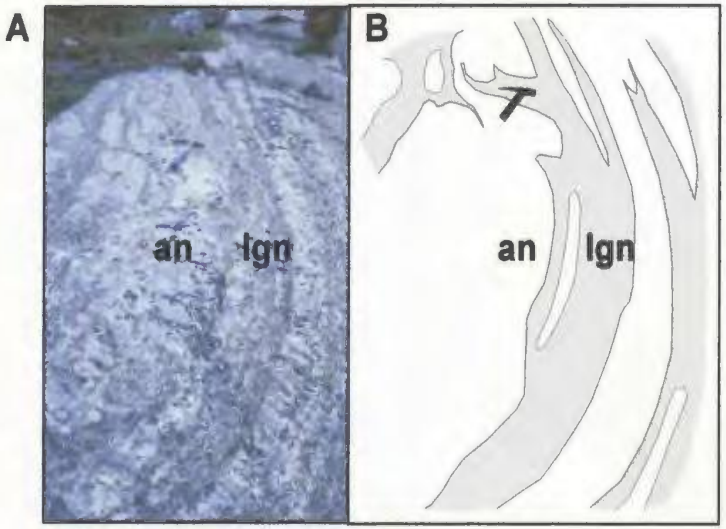

Figure 6.43: (A) Photo and (B) field sketch of the same primary layers in SHui. Sketch emphasizes the modal variations in anorthosite (an) and leucogabbronorite (lgn). Photo and sketch taken north of Hosenbein Lake.

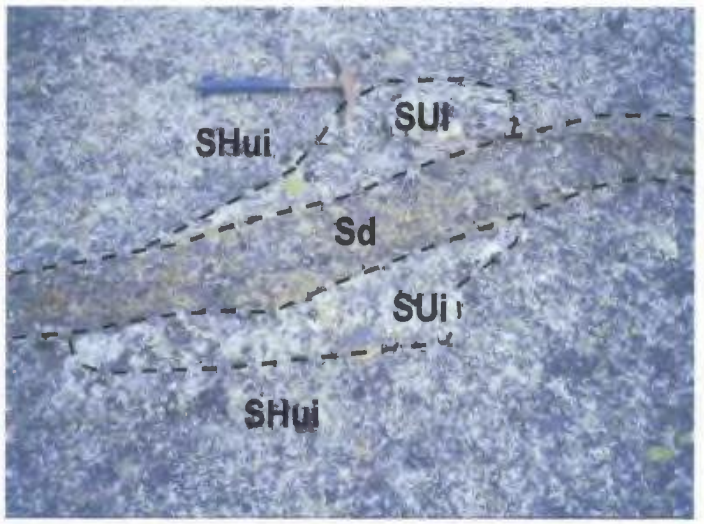

Figure 6.44: Ferrogabbro dike (Sd) in the Hosenbein pluton upper inner zone (SHui). Dike also cuts across a deformed anorthosite xenolith that was derived from the Unity pluton inner zone (SUi). Dashed lines outline the dike and xenolith. Photo taken north of Hosenbein Lake.

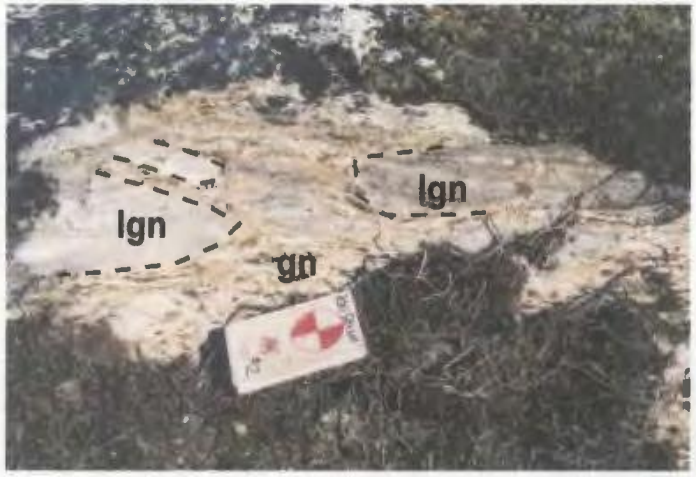

Figure 6.45: Xenoliths of strongly deformed leucogabbronorite (lgn) in strongly foliated gabbronorite (gn) of SHub. Dashed lines outline the xenoliths. Photo taken south of Pikaluyak Cove.

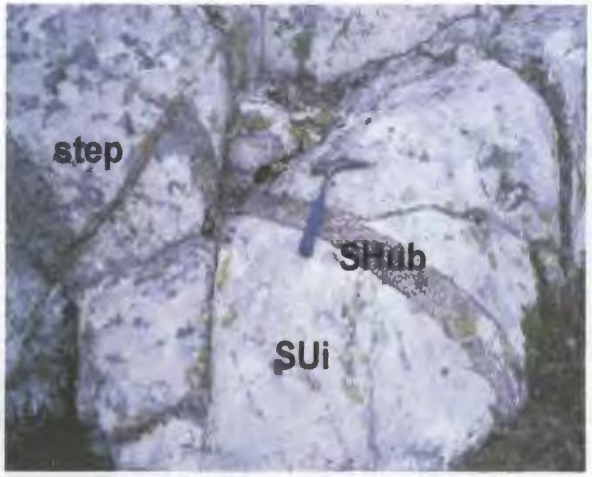

Figure 6.46: Gabbronorite dike that extends from the Hosenbein pluton upper border zone (SHub) into the Unity pluton inner zone (SUi). Dike shows straight contacts and step-like morphology (step). Photo taken on Nain Hill.

6.4.4 Hosenbein pluton upper border zone (SHub)

Form and contacts

Geological mapping as part of this study outlined a moderately dipping, strongly to weakly deformed, composite unit of gabbronorite, oxide gabbronorite and leucogabbronorite. This unit is here named the Hosenbein pluton upper border zone. The bottom of this unit shows a gradational increase in the abundance of anorthosite that marks the top of the Hosenbein pluton upper inner zone. The top of this unit shows a sharp and concordant contact with Paleoproterozoic gabbroic granulite in the Nain Hill and Kangilialuk Lake country rock belts.

The Hosenbein pluton upper border zone extends for 6.7 km in a north-south to northwest-southeast direction and for 0.1 – 0.6 km in an east-west to northeast-southwest direction. This zone is moderately (50° – 70°) north dipping to sub-vertical, arcuate striking and mostly ~100 m thick (see Figs. 6.1, 6.3). Parts of the upper border zone show a gradation from weakly deformed to strongly deformed rocks, whereas strongly deformed rocks also occur as xenoliths in weakly deformed rocks (Fig. 6.45). These relations indicate that the upper border zone is composite.

Gabbronorite dikes (0.1 – 50 m thick) extend from the Hosenbein upper border zone into foliated anorthositic rocks of the Unity pluton (see Fig. 6.2). These dikes strike parallel to compositional layering and foliation in the Unity pluton, and show straight walls, step-like morphology (Fig. 6.46) and bayonet apophyses that indicate they were emplaced during brittle fracturing. These relations indicate that the Unity pluton was

solidified and deformed prior to the emplacement of the Hosenbein pluton upper border zone.

Petrography

Weakly deformed gabbronorite contains small to medium-sized grains of plagioclase, orthopyroxene and clinopyroxene, and large laths of plagioclase and orthopyroxene. The petrography of weakly deformed oxide gabbronorite is similar to gabbronorite, but oxide gabbronorite also contains medium-sized grains of inverted pigeonite and small sub-poikilitic crystals of Fe-Ti oxide (Fig. 6.47). Both rock types show plagioclase and pyroxene with interlobate grain margins that suggest recrystallization at high-T. Leucogabbronorite consists of medium-sized to large plagioclase grains and laths, and medium-sized sub-poikilitic pyroxene crystals. Accessory minerals consist of very small apatite and zircon grains that are especially abundant in oxide gabbronorite. Overall, these weakly deformed rocks contain plagioclase +/- orthopyroxene as cumulus phases and pyroxene, Fe-Ti oxide, apatite and zircon as intercumulus phases.

Strongly deformed gabbronorite and oxide gabbronorite consist of small to medium-sized plagioclase, pyroxene +/- Fe-Ti oxide grains. In both rock types, grain margins are equilibrated, serrated and/or interlobate (Fig. 6.48). These margins indicate that these grains were recrystallized at high-T. In addition, plagioclase grains show deformation twins and undulose extinction that indicate it was deformed at high-T.

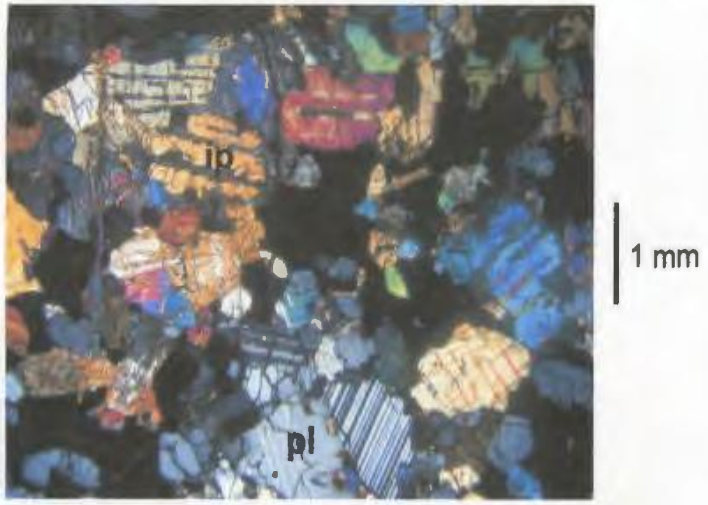

Figure 6.47: Thin section photo (XPL) of weakly deformed, oxide gabbronorite in SHub. Plagioclase (pl) and coarsely exsolved inverted pigeonite (ip) show bulging grain margins. Fe-Ti oxide is sub-poikilitic (black in photo).

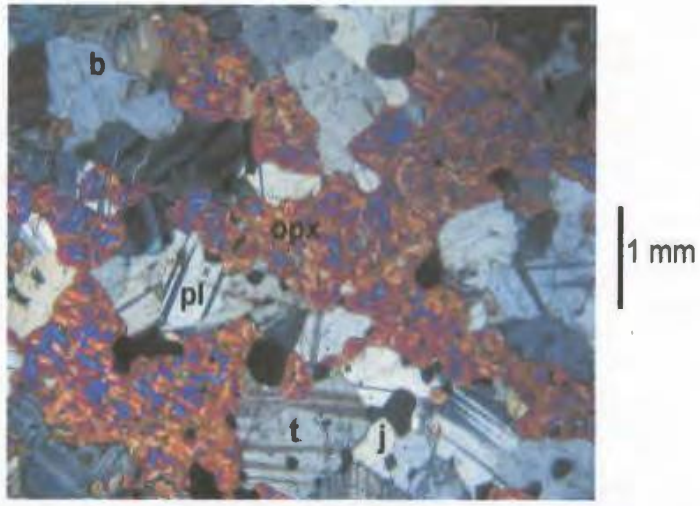

Figure 6.48: Thin section photo (XPL) of strongly deformed gabbronorite in SHub. Plagioclase (pl) shows deformation twins (t), triple junctions (j) and bulging grain margins (b). Orthopyroxene (opx) preserves relict poikilitic texture.

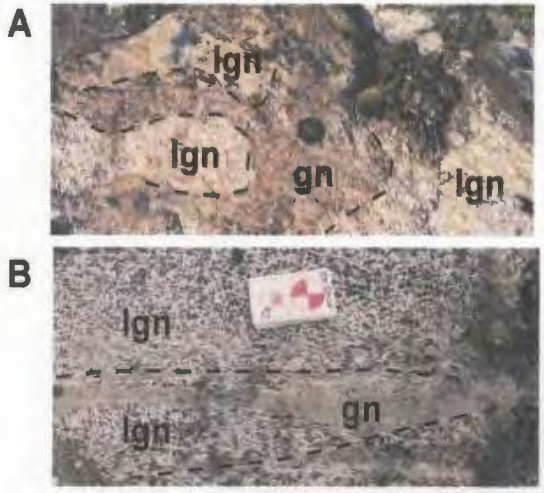

Figure 6.49: (A) Mottled and (B) layered rocks in SHub. (A) Mottled rocks comprise patches of poikilitic-textured leucogabbronorite (lgn) in granular textured oxide gabbronorite (gn). (B) Layered rocks comprise schlieren of gabbronorite in foliated leucogabbronorite. Dashed lines outline the patches and trends of schlieren. Photos taken south of Pikaluyak Cove.

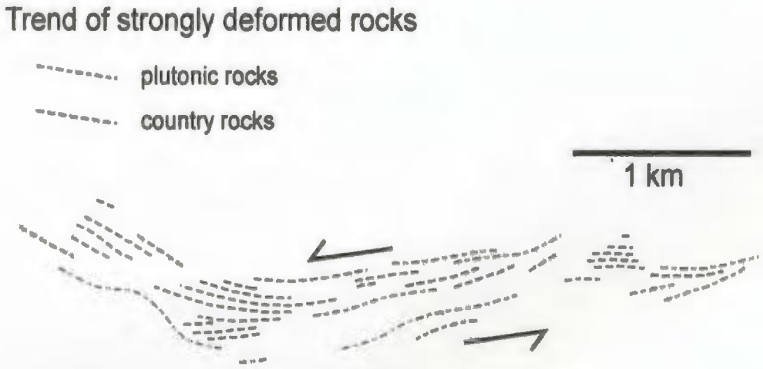

Figure 6.50: Simplified map showing strongly deformed plutonic rocks and country rocks along the northern margin of the Sophie centered intrusive complex. The trend of these layers suggests sinistral shear deformation.

Textures and structures

Gabbronorite and oxide gabbronorite is fine- to medium-grained and shows an overall texture that ranges from granular to porphyritic or poikilitic. Leucogabbronorite is medium- to coarse-grained and shows an overall poikilitic texture.

Weakly deformed gabbronorite, oxide gabbronorite and leucogabbronorite form massive, mottled, layered and foliated rocks. Massive rocks consist only of one rock type and texture. Mottled rocks comprise patches of poikilitic-textured leucogabbronorite in granular- to porphyritic-textured gabbronorite or oxide gabbronorite (Fig. 6.49). These patches are sub-spherical in form and range from 10 – 200 cm in diameter. Primary layering comprises gradational alternations of all rock types and textures. Individual layers are moderately dipping, 1 – 30 cm thick and 2 – 100 m in length. Granular gabbronorite also occurs as schlieren in poikilitic-textured leucogabbronorite. These schlieren strike parallel to layered rocks and are 1 – 5 cm thick and 100 – 500 cm long. Foliated rocks are either porphyritic-textured and contain plagioclase and pyroxene laths that are aligned parallel to the plane of primary layering, or poikilitic-textured and contain lens-shaped poikilitic pyroxene crystals that are also aligned parallel to the plane of layering.

Parts of the upper border zone also contain compositionally layered gabbronorite, oxide gabbronorite and leucogabbronorite. All of the rock types in compositionally layered rocks show only granular texture. Individual layers are 1 – 10 cm thick and steeply (70°) dipping to sub-vertically oriented. These layers are northwest to southeast striking where they lie adjacent to the Nain Hill country rock belt, and north-south

striking where they lie adjacent to the Kangilialuk Lake country rock belt. In both cases, compositional layering within the upper border zone strikes parallel to primary layering, as well as compositional and gneissic layering in the adjacent country rock belts. The granular texture and orientation of these rocks suggests that they were overprinted by deformation. The stresses associated with this deformation were oriented within and perpendicular to the plane of primary layering and intrusive contacts.

Mineral compositions and whole rock chemistry

Mineral compositions of gabbronorite and leucogabbronorite range from An_{50-53} in plagioclase, En_{45-59} in orthopyroxene (Table 6.10) and average En_{34} in clinopyroxene. These compositions fall in the range shown by anorthositic rocks of the Hosenbein pluton and are Na-rich and Fe-rich in comparison to Paleoproterozoic gabbroic granulite. Whole rock chemistry for one sample of gabbronorite shows abundances of TiO_2, Na_2O, P_2O_5, Sr and Ba that are high in comparison to Paleoproterozoic gabbroic granulite (see Fig. 6.9).

Mineral compositions of oxide gabbronorite range from An_{44-48} in plagioclase, En_{33-36} for orthopyroxene component in inverted pigeonite and En_{28-29} for clinopyroxene component in inverted pigeonite (Table 6.10). These compositions are Na- and Fe-rich in comparison to anorthositic rocks in the Hosenbein pluton and Paleoproterozoic gabbroic granulite (see Fig. 6.35). Whole rock chemistry for one sample of oxide gabbronorite shows high abundances of TiO_2, FeOt and P_2O_5 in comparison to gabbroic granulite (see Fig. 6.9). High abundances of these elements is consistent with modal abundances of Fe-

Ti oxide and apatite observed in thin section. CIPW norms consist mostly of plagioclase, pyroxene and olivine.

Table 6.10: Mineral compositions (*) and whole rock chemistry for SHub gabbronoritic rocks, and comparative data for anorthositic rocks in the Hosenbein pluton (SH) and Paleoproterozoic gabbroic granulite (Pg).

Rock type	Sample	Pl*	Opx*	TiO_2	FeOt	MgO	P_2O_5
		An	En	wt%	wt%	wt%	wt%
Hosenbein pluton upper border zone (SHub)							
gn	01-28-5b	50	45	1.49	12.41	7.65	0.25
lgn	00-26-16ii	53	59				
ox gn	00-30-19	44	36				
ox gn	01-34-1			4.84	17.65	6.02	2.01
ox gn	00-3-2e	48					
defm ox gn	01-31-16	45	33				
Comparative data							
SH		49 - 55	47 - 63	0.3 - 1.8	4.8 - 8.1	1.9 - 4.9	<0.4
Pg		51 - 81	58 - 85	0.4 - 0.8	11 - 13	7 - 31	<0.1

Summary

The gabbronoritic rocks in the Hosenbein pluton upper border zone: (a) are localized above the Hosenbein pluton upper inner zone, (b) are gradational from weakly to strongly deformed, (c) contain gabbronoritic rocks that show similar mineral compositions to anorthositic rocks of the Hosenbein pluton, and (d) contain gabbronoritic rocks that contain Na-rich plagioclase, Fe-rich pyroxene and high abundances of TiO_2, FeOt, P_2O_5, Sr and/or Ba. In terms of (d), these compositional characteristics have been noted in other Mesoproterozoic gabbronoritic rocks of the study area (see TAl, SP, SA, SHlb) as well. For these reasons, both the weakly and strongly deformed rocks of the Hosenbein pluton upper border zone are included with the Sophie centered intrusive complex.

6.5 Tectonic overprint

The Sophie centered intrusive complex contains plutonic rocks that: (a) are steeply dipping to sub-vertically oriented, (b) are granular-textured, and (c) show various deformation structures. These plutonic rocks are here referred to as strongly deformed and comprise the structurally measurable tectonic overprint of the Sophie centered intrusive complex. This overprint occurs in belts that lie: (a) adjacent to the Nain Hill country rock belt, and (b) adjacent to the Kangilialuk Lake country rock belt.

The strongly deformed plutonic rocks that lie adjacent to the Nain Hill country rock belt (see Fig. 6.3) were found throughout the Unity pluton, lowermost ~50 m of the Airstrip sheet, uppermost ~50 m of the Pikaluyak sheet and uppermost ~50 m of the Hosenbein pluton upper inner zone. The strongly deformed rocks that lie adjacent to the eastern part of the Nain Hill country rock belt are steeply north dipping and east-west striking (Fig. 6.50), whereas rocks lying to the west are steeply northeast to east dipping and northwest-southeast to north-south striking (see Fig. 6.1). The rocks in the Unity pluton and the Pikaluyak sheet were overprinted by sinistral shear deformation. In addition, the strongly deformed rocks of the Unity pluton contain igneous zircons that are Mesoproterozoic in age and occur as xenoliths in the Airstrip sheet and the Hosenbein pluton. This indicates that: (a) sub-vertical and east-west striking, sinistral shear, deformation was Mesoproterozoic in age and (b) that this deformation was episodic. The orientation of these strongly deformed plutonic rocks is parallel to compositional layering in the Nain Hill country rock belt. The strongly deformed character of these rocks, occurrence at the margin of an anorthositic intrusion and plagioclase-pyroxene

mineralogy suggest similarity to the marginal granulites described by previous workers (see Davies, 1973b; Brand, 1974; Berg and Briegel, 1981; Royse et al., 1999).

The strongly deformed plutonic rocks that occur adjacent to the Kangilialuk Lake country rock belt (see Fig. 6.1) were found in the Hosenbein pluton lower and upper border zones (Fig. 6.51). These strongly deformed rocks are steeply east dipping to sub-vertically oriented and broadly north-south striking. In addition, the orientation of these rocks is parallel to compositional layering in the Kangilialuk Lake country rock belt. The strongly deformed character of these rocks, occurrence at the margin of an anorthositic intrusion and plagioclase-pyroxene mineralogy suggest similarity to the marginal granulites described by previous workers (see Davies, 1973b; Brand, 1974; Berg and Briegel, 1981; Royse et al., 1999).

Strongly deformed plutonic rocks were also found north of the Nain Hill country rock belt (see Fig. 6.3). These strongly plutonic rocks occur in the southeastern part of the Ametok centered intrusive complex. This centered intrusive complex is separated from the Sophie centered intrusive complex by ~50 – 100 m of Paleoproterozoic gabbroic granulite. The southern-most part of the Ametok centered intrusive complex consists of anorthositic rocks that show: (a) steeply dipping layers, and (b) only granular texture. These layers range from <1 – 20 cm thick (Fig. 6.51) and are interpreted as strongly deformed. The orientation of these strongly deformed rocks is parallel to: (a) strongly deformed rocks in the northern part of the Sophie centered intrusive complex, and (b) Paleoproterozoic gabbroic granulite in the Nain Hill country rock belt. These strongly deformed rocks were developed over a ~1 km thickness (see Fig. 6.3). These rocks are

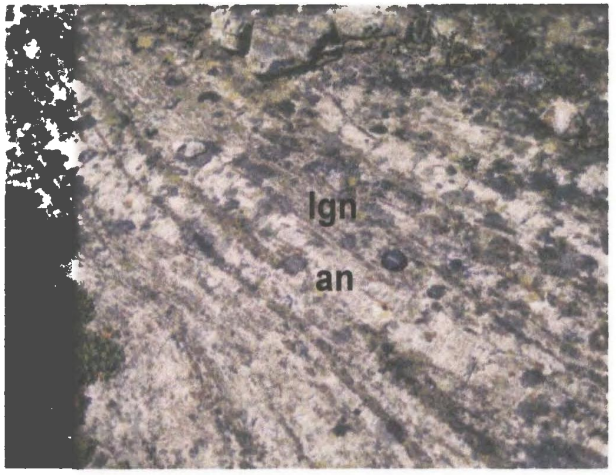

Figure 6.51: Strongly deformed, layered, granular-textured anorthositic rocks in the southern-most part of the Ametok centered intrusive complex. Layered rocks consist of anorthosite (an) and leucogabbronorite (lgn). Photo taken at the northern base of Nain Hill.

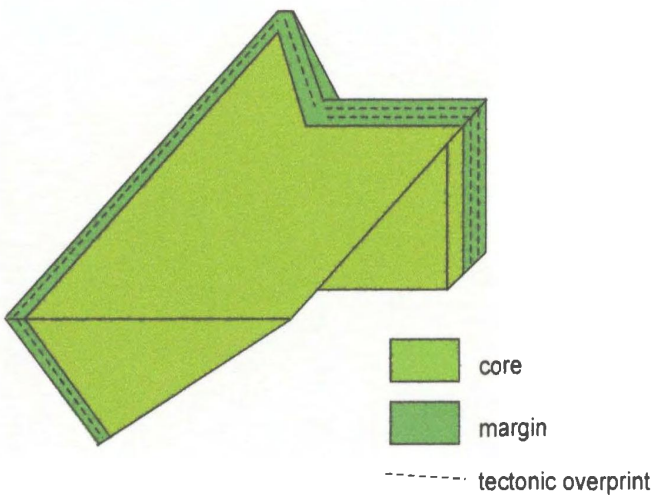

Figure 6.52: Schematic block model for the Sophie centered intrusive complex showing the core, margin and tectonic overprint.

mentioned here to illustrate that sub-vertically oriented and east-west striking deformation occurs in other centered intrusive complexes as well.

6.6 Summary

This chapter has described the form, structure, petrography, textures, structures, mineral compositions, whole chemistry and/or geochronology of the Unity pluton, Airstrip sheet, Pikaluyak sheet and Hosenbein pluton, and grouped all of these units into the Sophie centered intrusive complex. This section summarizes the overall structure of this centered intrusive complex in terms of a core, margin and tectonic overprint (Fig. 6.52).

The core of the Sophie centered intrusive complex consists of the Unity pluton inner zone and the Hosenbein pluton inner zones (lower, upper). Rocks in the core are; (a) anorthositic, and (b) massive, mottled, layered and/or foliated. The anorthositic rocks in the Unity pluton inner zone were recrystallized and deformed prior to emplacement of the Hosenbein pluton. The Hosenbein pluton inner zone was also partly recrystallized and deformed at high-T. Mineral compositions are similar to NB noritic anorthosite. Whole rock chemistry is mostly similar to NB troctolitic anorthosite and shows high Ba/K. CIPW norms consist mostly of plagioclase and pyroxene. The Unity pluton inner zone also contains igneous zircons that crystallized at 1328 +/- 5 Ma.

The margin of the Sophie centered intrusive complex consists of the Unity pluton border zone, Airstrip sheet, Pikaluyak sheet and the Hosenbein pluton border zones (lower, upper). Rocks in the margin are; (a) anorthositic, gabbronoritic and Fe-rich

gabbroic, (b) moderately dipping to sub-vertical, (c) massive, layered and/or foliated, and (d) weakly to strongly deformed. Mineral compositions in gabbronoritic and anorthositic rocks are similar to that of anorthositic rocks in the Hosenbein pluton inner zones, whereas oxide gabbronorite and Fe-rich gabbroic rocks contain more Na-rich plagioclase and Fe-rich pyroxene. Whole rock chemistry of gabbronoritic rocks shows high TiO_2, FeOt, Na_2O, P_2O_5, Sr/Ca and/or Ba/K in comparison to Paleoproterozoic gabbroic granulite. In addition, the Unity pluton border zone and the Pikaluyak sheet contain igneous zircons that crystallized at 1341 +/- 4 and 1318 +/- 7 Ma respectively.

The margin of the Sophie centered intrusive complex contains rocks that were strongly deformed in the Mesoproterozoic. These strongly deformed rocks are: (a) sub-vertically oriented and east-west striking where they lie adjacent to the eastern part of the Nain Hill country rock belt, (b) steeply northeast to east dipping and northwest-southeast to north-south striking where they lie adjacent to the western part of the Nain Hill country rock belt and (c) sub-vertically oriented and north-south striking where they lie adjacent to the Kangilialuk Lake country rock belt. The kinematic indicators suggest that east-west striking rocks were deformed in a sinistral shear zone.

Chapter 7: Kikkertavak centered intrusive complex (K)

The Kikkertavak centered intrusive complex is the name proposed for ~900 km^2 of spatially associated anorthositic, gabbronoritic and troctolitic rocks in the central part of the Nain batholith (Fig. 7.1). The northwestern part of this intrusive complex is exposed in the study area and consists of the Akuliakatak pluton (KA), Satosoak pluton (KS) and Tabor pluton (KT) (Figs. 7.2, 7.3). This chapter describes the contact relations, form, petrography, textures, structures, mineral compositions and whole rock chemistry for each of these plutons. Ferrodiorite dikes that occur in the Akuliakatak and Satosoak plutons are also described. The order in which these plutons are described is oldest to youngest based on field relations. A section entitled 'tectonic overprint' summarizes the strongly deformed plutonic rocks that occur in the margin of the Kikkertavak centered intrusive complex.

Anorthositic rocks in the Satosoak pluton form the bulk and the spatial center for the northwestern part of the Kikkertavak centered intrusive complex. The Akuliakatak and Tabor plutons are included with the Satosoak pluton in the Kikkertavak centered intrusive complex for reasons given in this chapter. This chapter also describes the tectonic overprint on the margin of the Kikkertavak centered intrusive complex.

7.1 Regional extent of the Kikkertavak centered intrusive complex

The geological maps of Wheeler (1969) and Ryan (1990) show that anorthositic rocks are continuous to the east and south of the study area (see Fig 7.1). The eastern and western boundaries of these anorthositic rocks are clearly defined by intrusive contacts

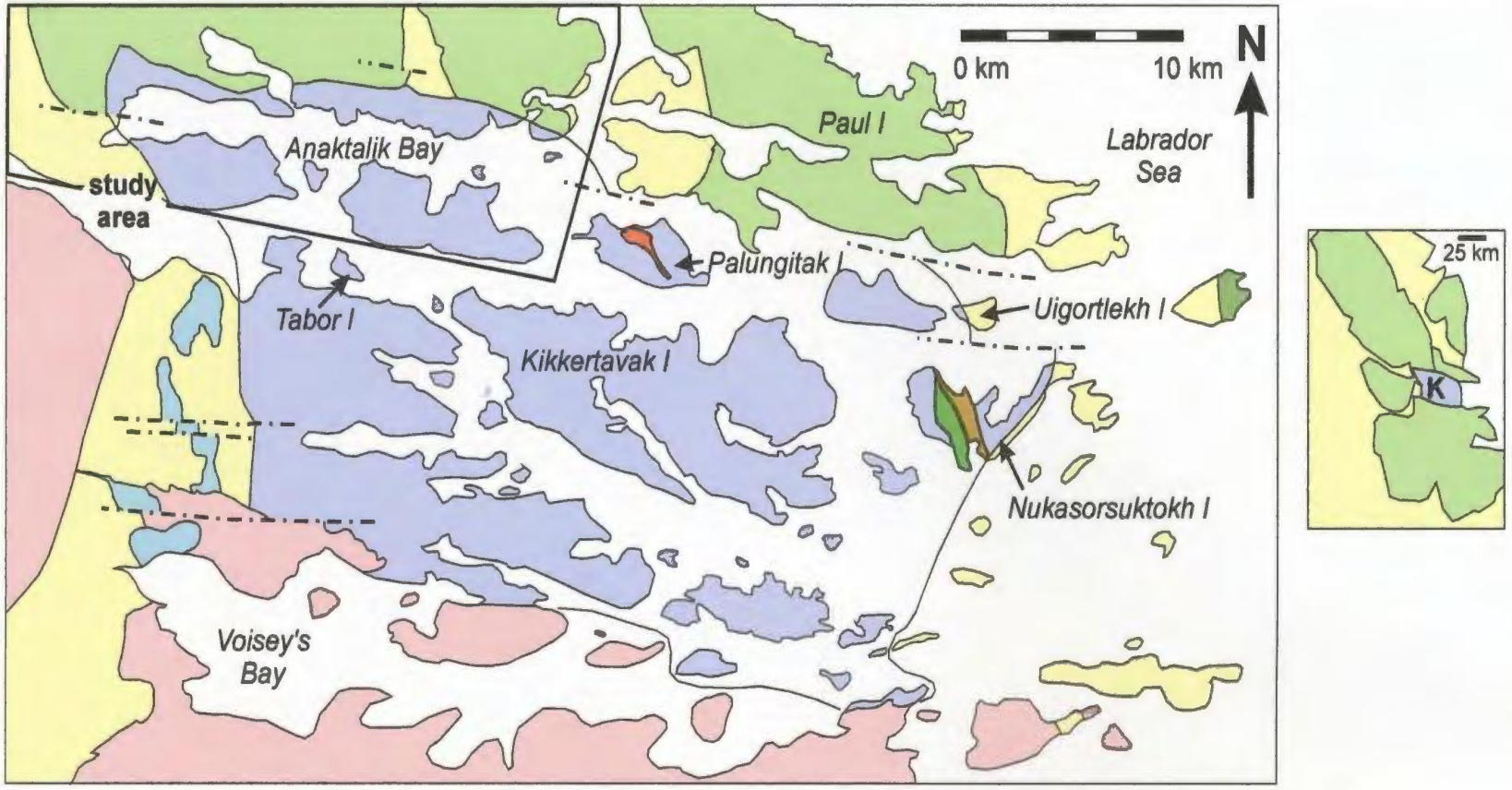

Figure 7.1: Solid geological map of the Kikkertavak centered intrusive complex. The part of this intrusive complex that lies west of Palungitak Island and north of Tabor Island was examined in this study. Geology outside of the study area was compiled from maps by Ryan (1990) and in Berg et al. (1994). Inset locates the Kikkertavak centered intrusive complex in the Nain batholith.

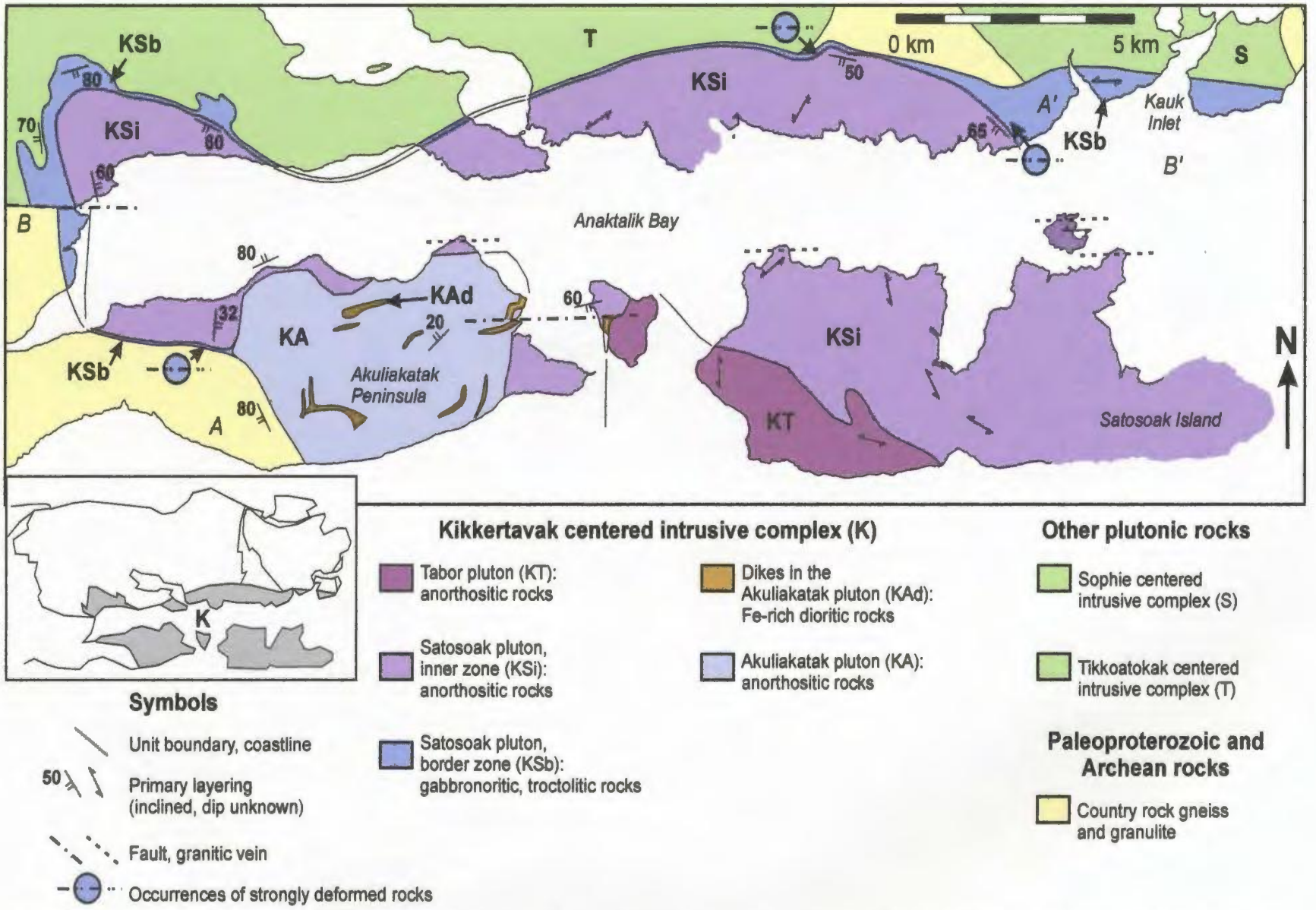

Figure 7.2: Solid geological map for the northwestern part of the Kikkertavak centered intrusive complex. Cross-sections A-A' and B-B' mark the are shown in Figure 7.3.

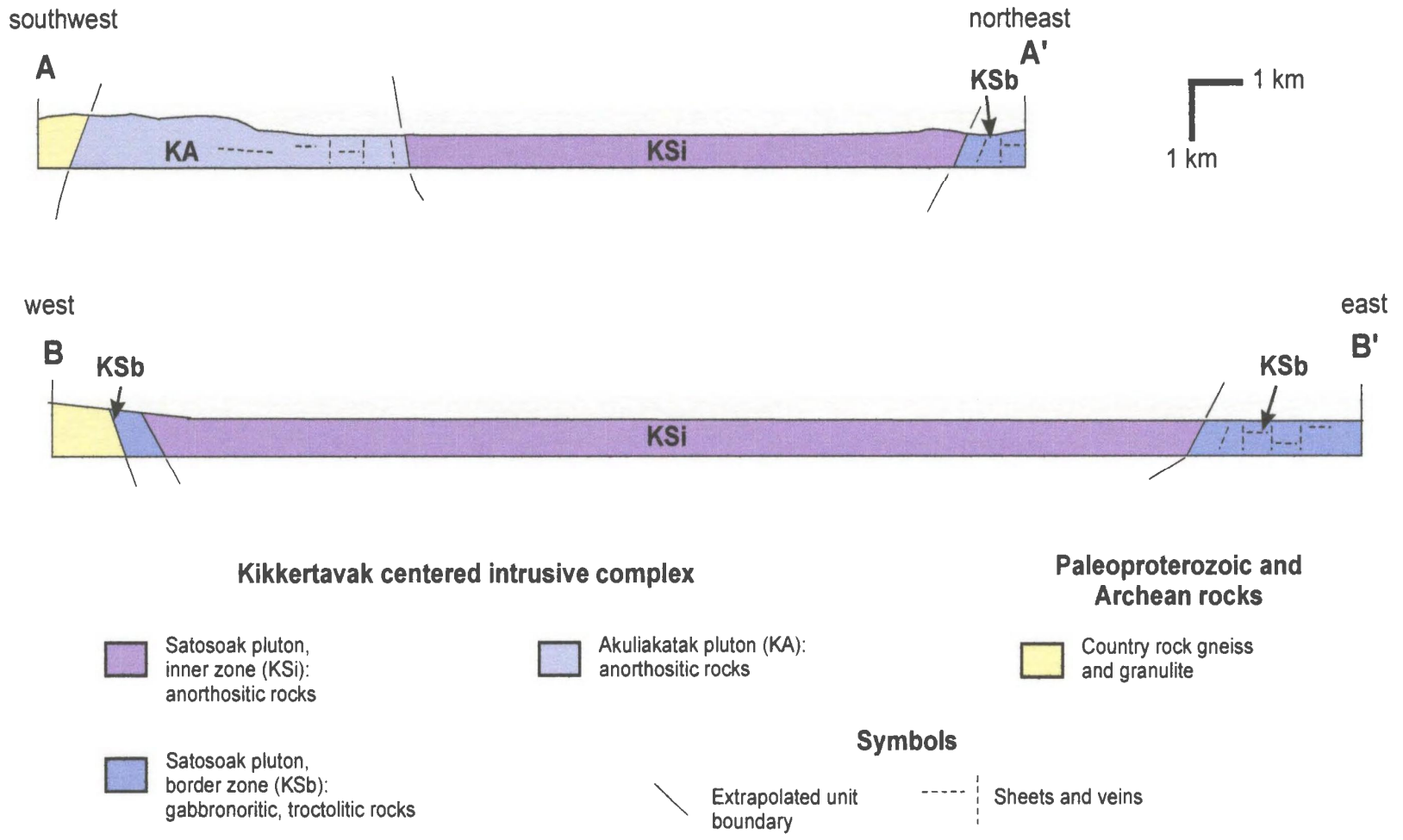

Figure 7.3: Northeast to southwest and east to west cross-sections through the northwestern part of the Kikkertavak centered intrusive complex. Cross-sections are located on Figure 7.2.

with country rock, whereas the southern boundary is truncated by granitic rocks (see Emslie in Berg et al., 1994). The northwestern boundary of these anorthositic rocks is examined in this chapter, and was extrapolated east to define the northern boundary of the Kikkertavak centered intrusive complex. Additional criteria for this extrapolation are described below and are largely based on geological mapping by Don Wright who participated in the same project as myself.

Tabor Island and Kikkertavak Island lie due south of the study area (see Fig. 7.1). A study by Hamilton et al. (1994) found that anorthositic rocks on both islands contain igneous zircons that crystallized at 1311 +/- 2 Ma. Mapping by Wright (pers. com., 2002) found that anorthositic rocks on Tabor Island and Kikkertavak Island are broadly 'dark-facies' and has suggested grouping these anorthositic rocks into a single composite intrusion that also includes anorthositic rocks on Palungitak Island, Uigortlekh Island and Nukasorsuktokh Island (see Fig. 7.1). To the north, the southern shoreline of Paul Island contains pale-facies anorthositic rocks (Emslie in Berg et al., 1994). As well, Paul Island is partly underlain by anorthositic rocks that contain igneous zircons that crystallized at 1319 +/- 1 Ma (in Hamilton et al., 1994). These studies suggest that an east-west trending boundary drawn between Paul Island to the north and Palungitak Island to the south (see Fig. 7.1) separates: (a) all dark-facies anorthositic rocks from composite dark- and pale-facies anorthositic rocks, and (b) anorthositic rocks with a crystallization age of 1311 +/- 2 Ma from anorthositic rocks with a crystallization age of 1319 +/- 2 Ma.

7.2 Akuliakatak pluton (KA)

The geological maps of Wheeler (1969) and Ryan (1990) show that the Akuliakatak peninsula consists of anorthosite. This anorthosite was not previously mapped in detail or sub-divided.

Form and contacts

This study found a unit of massive anorthosite, leuconorite and leucogabbronorite that is here named the Akuliakatak pluton (after the Akuliakatak Peninsula, see Fig. 7.4). The northern and eastern boundaries of this pluton are truncated by sheets and dikes that extend from the Satosoak pluton (Fig. 7.5). The western boundary abuts country rocks, but is poorly exposed, whereas the southern boundary is not exposed in the study area.

In the study area, the Akuliakatak pluton is exposed over 5 km in an east-west direction, 3 km in a north-south direction and is a minimum of 400 m thick. Xenoliths of the Akuliakatak pluton are scattered over an additional ~5 km^2 within the inner zone of the Satosoak pluton. Anorthositic rocks of the Satosoak pluton are of uniform coarse-grain size right up to intrusive contacts with the Akuliakatak pluton.

Petrography

Plagioclase crystals are abundant, of large to very large size (1 – 20 cm) and of tabular to granular form, suggesting that they are cumulus. These crystals also show deformation twins, undulose extinction, hairline fractures and interlobate grain margins (Fig. 7.6) that indicate they were recrystallized and/or deformed at high-T.

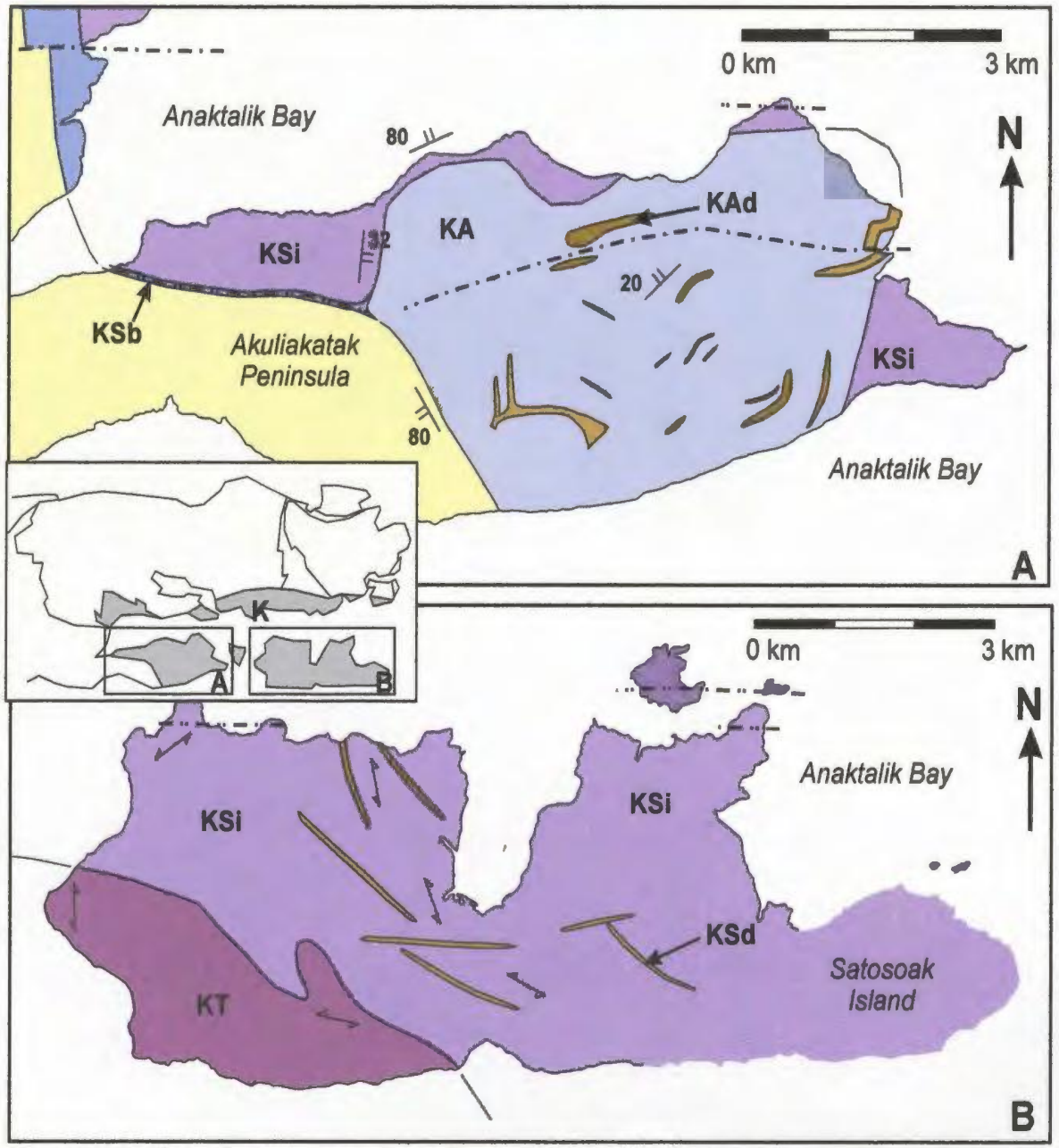

Kikkertavak centered intrusive complex (K)

- Tabor pluton (KT): anorthositic rocks
- Dikes in Satosoak pluton (KSd): Fe-rich dioritic rocks
- Satosoak pluton, inner zone (KSi): anorthositic rocks
- Satosoak pluton, border zone (KSb): gabbronoritic rocks
- Dikes in Akuliakatak pluton (KAd): Fe-rich dioritic rocks
- Akuliakatak pluton (KA): anorthositic rocks

Paleoproterozoic and Archean rocks

- Country rock gneiss and granulite

Symbols

- Unit boundary, coastline
- 50 Layering (inclined, dip unknown)
- Trend of strongly deformed layers and granitic veins
- Fault

Figure 7.4: Solid geological map for the northwestern part of the Kikkertavak centered intrusive complex on (A) the Akuliakatak Peninsula and (B) Satosoak Island.

Orthopyroxene crystals are of relatively low abundance, of small to medium size and show sub-poikilitic to poikilitic texture, suggesting that they crystallized out of the intercumulus liquid. Most orthopyroxene is retrogressed to green amphibole. Small pyroxene grains form large, relict, poikilitic crystals (Fig. 7.7) that indicate some of the intercumulus orthopyroxene was also recrystallized. Clinopyroxene also forms grains that comprise relict cores surrounded by amphibole.

Secondary minerals replaced 1 – 5% plagioclase and 10 – 100% pyroxene. Altered plagioclase contains sericite, epidote and quartz that suggest hydrothermal alteration. Altered pyroxene contains chlorite, uralite and amphibole that also suggest hydrothermal alteration.

Textures and structures

Anorthositic rocks are coarse- to very coarse-grained and show an overall texture that ranges from granular (<10% poikilitic crystals) to poikilitic (10 – 20% poikilitic crystals). Anorthositic rocks that occur adjacent to ferrodiorite dikes contain aggregates of small plagioclase, pyroxene and Fe-Ti oxide grains that are interstitial to cumulus plagioclase.

Anorthositic rocks are massive, mottled or layered. Massive rocks comprise only granular or poikilitic texture. Mottled rocks comprise interspersed patches of poikilitic and granular texture. These patches are sub-spherical in form and range from 0.1 – 100 m in diameter. Primary layering comprises rhythmic alternations of granular and poikilitic texture. Individual layers are sub-horizontally oriented and are ~0.1 – 2 m thick.

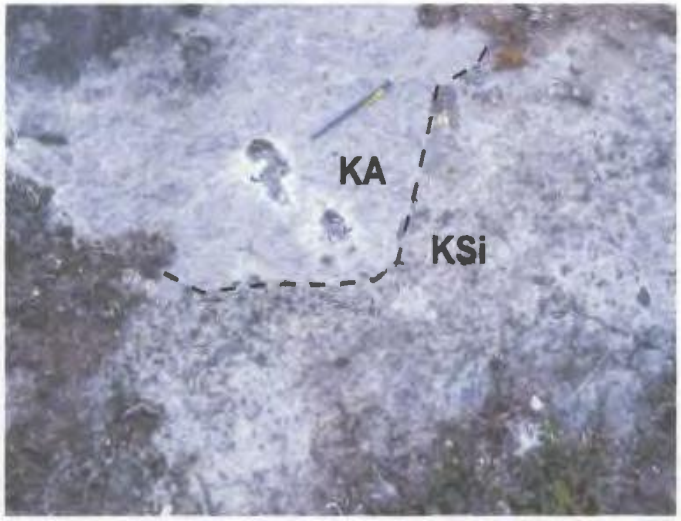

Figure 7.5: Xenolith of Akuliakatak pluton anorthosite (KA) in Satosoak pluton inner zone leuconorite (KSi). Dashed line outlines the xenolith. Photo taken on hills above Anaktalik Bay.

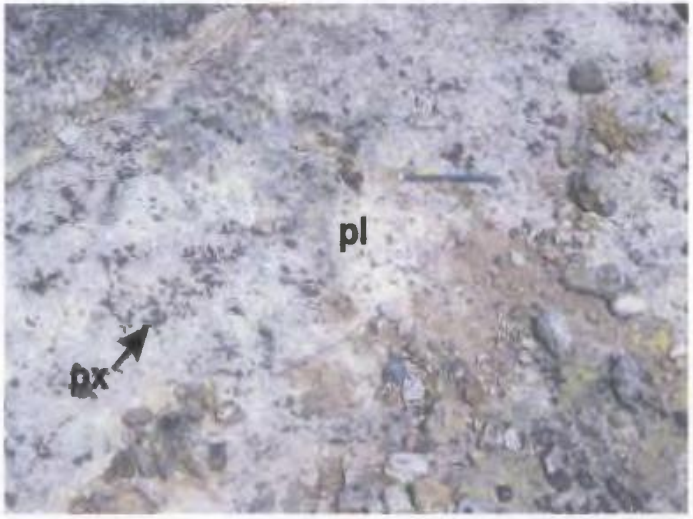

Figure 7.7: Poikilitic-textured leuconorite in KA. Poikilitic texture comprises plagioclase grains (pl) with interspersed oikocrysts of pyroxene (px). Photo taken on hills above Anaktalik Bay.

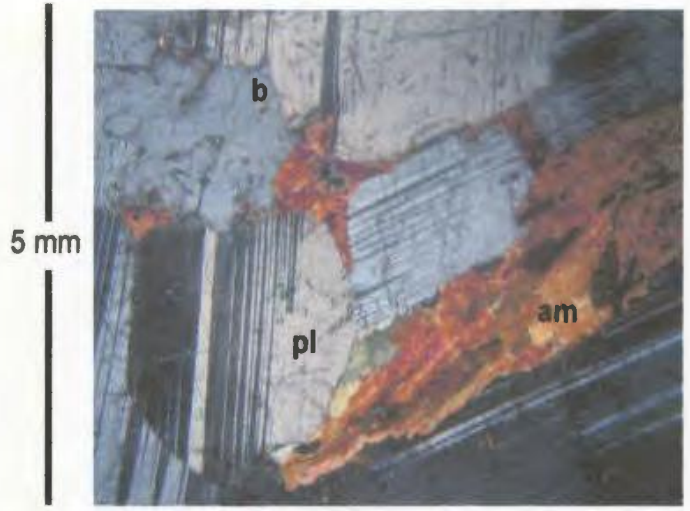

Figure 7.6: Thin section photo (XPL) of hydrothermally altered leuconorite in KA. Plagioclase (pl) shows interlobate grain margins (b) and pyroxene is altered to amphibole (am) and shows relict poikilitic texture.

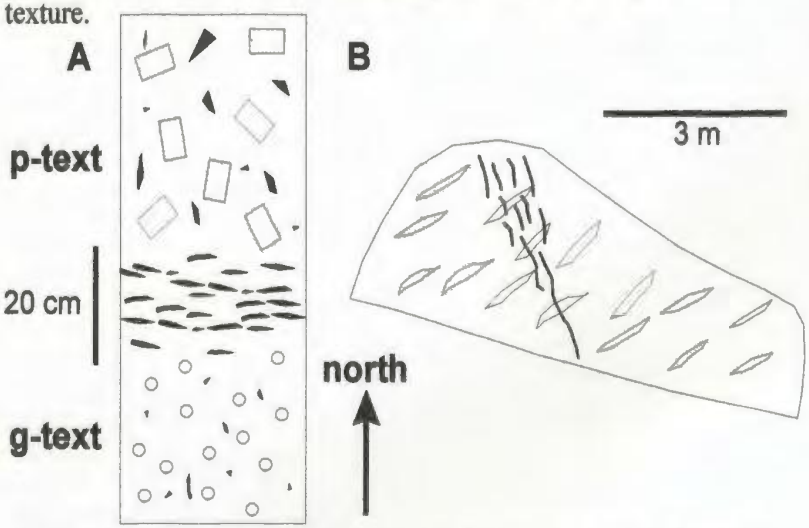

Figure 7.8: Field sketches showing: (A) ~20 cm of strongly foliated leuconorite that separates poikilitic-textured (p-text) and granular-textured (g-text) KA anorthositic rocks, and (B) strongly foliated leuconorite veins that cut across layered KA anorthositic rocks. Sketches made on the Akuliakatak Peninsula.

Anorthositic rocks also contain pods that consist of large to very large poikilitic pyroxene crystals. These pods are sub-spherical in form and range from 10 – 100 cm in diameter.

Foliated rocks occur in zones that are ~10 – 200 cm thick, separate large (100 – 500 m) patches of poikilitic-textured rocks from granular-textured rock or cut across layered rocks (Fig. 7.8). These zones are steeply dipping (70°) to sub-vertical and randomly striking, and are interpreted as shear zones.

Mineral compositions and whole rock chemistry

Mineral compositions in one sample of anorthosite average An_{45} in plagioclase. This plagioclase composition is Na-rich in comparison to anorthositic rocks in the Satosoak pluton and falls in the range shown by NB noritic anorthosite (Table 7.1). Relict cores of clinopyroxene grains show an average composition of En_{36}.

Table 7.1: Mineral compositions (*) and whole rock chemistry for KA anorthositic rocks and comparative data for Satosoak pluton anorthositic rocks (KS), NB noritic anorthosite and NB troctolitic anorthosite

Rock type	Sample	Pl*	SiO_2	K_2O	Ca/Al	Sr/Ca x 10	Mg/(Mg+Fe)	An/(An+Ab)
		An	wt%	wt%				CIPW
Akuliakatak pluton (KA)								
In	02-30-3a	45	53.68	0.43	1.00	0.13	0.27	0.52
In	02-36-10		50.40	0.25	1.07	0.09	0.41	0.62
Comparative data								
KS		48 - 64	49 - 54	0.2 - 0.4	1.0 - 1.2	0.07 - 0.12	0.26 - 0.41	0.56 - 0.65
NB noritic		40 - 54	52 - 58	0.6 - 1.2	0.8 - 1.1	0.10 - 0.15	0.10 - 0.35	0.42 - 0.54
NB troctolitic		51 - 68	49 - 55	0.2 - 0.6	1.0 - 1.2	0.06 - 0.09	0.15 - 0.49	0.53 - 0.68

Whole rock chemistry of leuconorite shows wt% SiO_2, wt% K_2O, Ca/Al, Ba/K and Mg/(Mg+Fe) that falls in the range shown by anorthositic rocks in the Satosoak

pluton (Fig. 7.9, Table 7.1). Ba/K (0.21 – 0.24) is high in comparison to both NB noritic and troctolitic anorthosite (0.09 – 0.18). Sr/Ca is high in comparison to, or falls in the range shown by, anorthositic rocks in the Satosoak pluton. CIPW norms consist mostly of plagioclase, pyroxene +/- olivine. Normative plagioclase compositions are low in comparison to, or fall in the range shown by, anorthositic rocks in the Satosoak pluton.

Summary

Anorthositic rocks in the Akuliakatak pluton are: (a) spatially associated with anorthositic rocks in the Satosoak pluton, and (b) show whole rock chemistry that falls in the range shown by the Satosoak pluton. For these reasons, the Akuliakatak pluton is included with the Satosoak pluton in the Kikkertavak centered intrusive complex.

Ferrodiorite dikes

The Akuliakatak pluton contains ferrodiorite dikes and sills (see Fig. 7.4) that were also cut by the Satosoak pluton (Fig. 7.10), indicating that ferrodiorite dikes were intruded into the Akuliakatak pluton prior to emplacement of the Satosoak pluton. Ferrodiorite dikes range from 'thick' (50 – 100 m wide) to 'narrow' (10 – 50 m wide), and are sub-vertically to sub-horizontally oriented. Thick dikes are moderately dipping (45° E) to sub-vertical and broadly east-west or north-south striking. Narrow dikes are moderately dipping (45° E) to sub-vertical and broadly northeast-southwest to northwest-southeast striking. Intrusive contacts with the anorthositic rocks of the Akuliakatak pluton are sharp or grade into anorthositic rocks with interstitial aggregates of ferrodiorite.

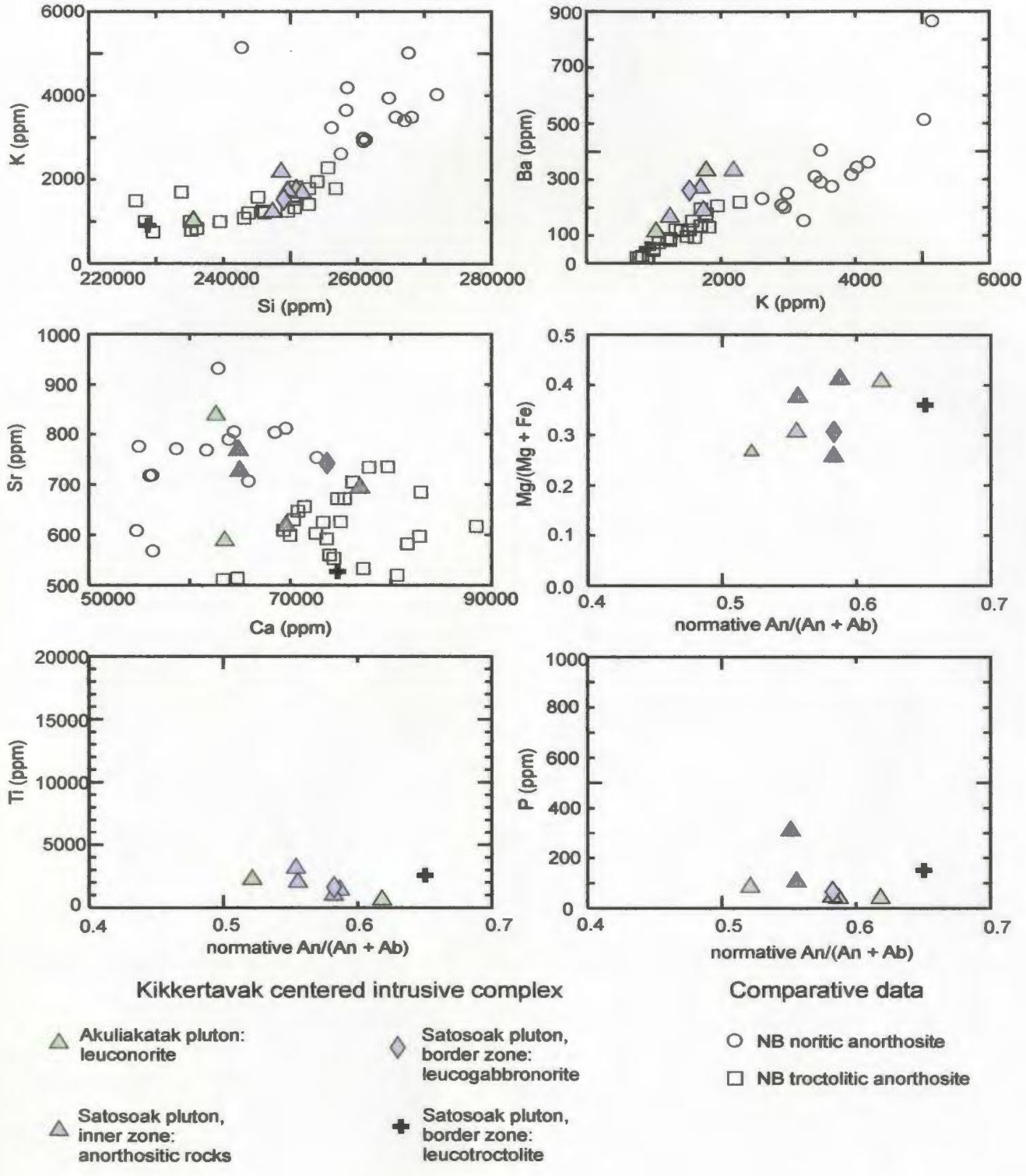

Figure 7.9: Whole rock chemistry for anorthositic rocks in the Kikkertavak centered intrusive complex, and comparative data for NB noritic and troctolitic anorthosite. Section 7.1 describes the Akuliakatak pluton, 7.2.1 describes the Satosoak pluton inner zone and 7.2.2 describes the Satosoak pluton border zone.

Ferrodiorite contains small to medium-sized plagioclase and inverted pigeonite grains that show interlobate grain margins (Fig. 7.11), indicating they were recrystallized and/or deformed at high-T. Small Fe-Ti oxide crystals show sub-poikilitic texture that suggests they crystallized out of the intercumulus liquid. Accessory minerals consist of small to very small antiperthite, quartz, Fe-rich olivine, biotite, amphibole, apatite and zircon grains.

Table 7.2: Mineral compositions (*) and whole rock chemistry of KA ferrodiorite dikes and comparative data for KA anorthositic host rocks

Rock type	Sample	Pl*	Opx*	TiO_2	FeOt	K_2O	P_2O_5	V	Rb	Zr
		An	En	wt%	wt%	wt%	wt%	ppm	ppm	ppm
Dikes in the Akuliakatak pluton (KA)										
Fe-di	02-30-1	30	29	3.91	16.83	1.06	1.26	95	4	150
Fe-di	02-28-2a	34		3.55	16.84	0.39	1.32	206	<1	5
Fe-di	02-28-12			2.57	17.47	1.35	0.83	20	<1	1525
Comparative data										
KA		45		0.1 - 0.4	3.4 - 6.7	0.2 - 0.4	<0.1	5 - 34	<1	<9

Mineral compositions in ferrodiorite range from An_{30-34} in plagioclase, average En_{29} for orthopyroxene component in inverted pigeonite, and range from En_{25-33} for clinopyroxene component in inverted pigeonite. These plagioclase compositions are Na-rich in comparison to host anorthositic rocks of the Akuliakatak pluton (Table 7.2), suggesting that they are evolved relative to the anorthositic rocks. Whole rock chemistry of ferrodiorite shows high wt% TiO_2, FeOt, K_2O and P_2O_5, and high ppm V, Rb and/or Zr, in comparison to anorthositic host rocks. The high abundances of these elements are consistent with Fe-Ti oxide, alkali feldspar, apatite and zircon observed in thin section. CIPW norms consist mostly of plagioclase, pyroxene +/- olivine, as well as 5 – 8%

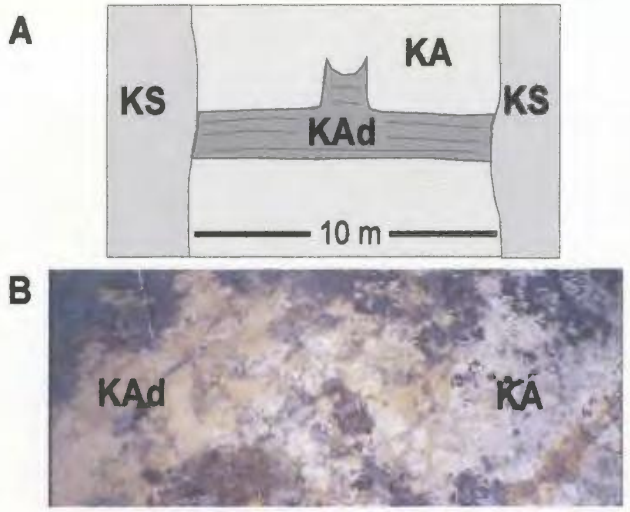

Figure 7.10: (A) Field sketch of a ferrodiorite sill (KAd) in anorthositic rocks of the Akuliakatak pluton (KA), both of which were cut by the Satosoak pluton (KS). (B) Contact between a ferrodiorite dike and KA anorthositic rocks. Photo and sketch taken on the Akuliakatak Peninsula.

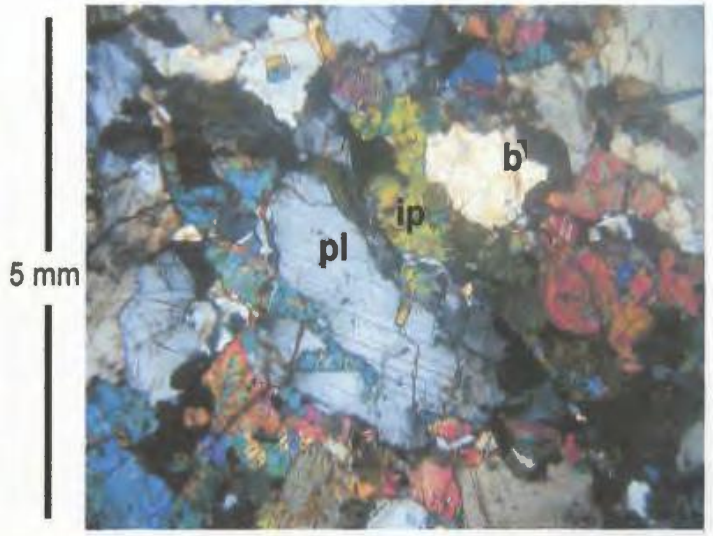

Figure 7.11: Thin section photo (XPL) of ferrodiorite within a dike that cuts KA. Ferrodiorite contains plagioclase (pl) and inverted pigeonite (ip) with bulging grain margins (b), and Fe-Ti oxides (black in photo).

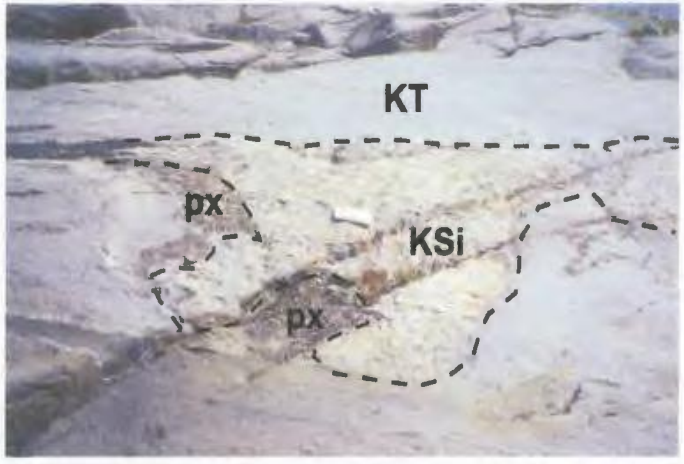

Figure 7.12: Xenolith of Satosoak pluton inner zone anorthosite (KSi) in Tabor pluton leuconorite (KT) . Dashed line shows outline of the xenolith. An aggregate of large pyroxene grains (px) occurs on the margin of the xenolith. Photo taken on western shoreline of Satosoak Island.

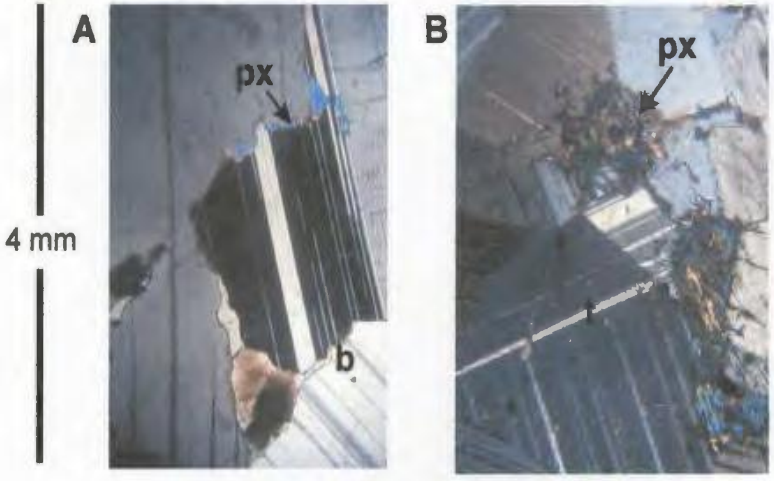

Figure 7.13: Thin section photos (XPL) of anorthosite in KSi with (A) primary pyroxene (px) and (B) altered pyroxene (px). Plagioclase in (A) shows tabular forms and interlobate grain margins (b), whereas plagioclase in (B) shows equilibrated geometry and deformation twins (t).

normative orthoclase, 5 – 7% normative Fe-Ti oxide and normative 2 – 4% apatite. Two samples contain >2118 ppm S that suggest accessory abundances of sulfides.

7.3 Satosoak pluton (KS)

A geological map by Wheeler (1969) shows that dark-facies anorthositic rocks are exposed along the northern shoreline of Anaktalik Bay, and that anorthositic rocks underlie all of Satosoak Island. Maps by Rubins (1973) and Ryan (2000a; 2001a) also show dark-facies anorthosite along the northern shoreline of Anaktalik Bay. Mapping by Ryan (2000a, 2001a) grouped these dark-facies rocks (leucotroctolite, olivine leuconorite, troctolite in Ryan, 2001a) into the Tessiuyarsuk intrusion.

Geological mapping as part of this study provides the first detailed mapping of Satosoak Island, which is underlain mostly by anorthositic rocks that are here grouped into the Satosoak pluton (after Satosoak Island, see Fig. 3.1). Mapping as part of this study also incorporated the Tessiuyarsuk intrusion of Ryan (2001a) into the Satosoak pluton. The Satosoak pluton is here divided into an inner zone and a border zone (see Fig. 7.2).

7.3.1 Satosoak pluton inner zone (KSi)

Form and contacts

Geological mapping as part of this study outlined a unit of massive, coarse-grained, anorthosite, leuconorite and olivine leuconorite that is here named the Satosoak pluton inner zone. The north, and part of the south, boundary of this unit shows a

gradational increase in the abundance of troctolite and gabbronorite that marks the inner boundary of the Satosoak pluton border zone. The south boundary is also truncated by veins and sheets that extend from the Tabor pluton (Fig. 7.12), or truncates the Akuliakatak pluton (see Fig. 7.5). The southeastern most part of the pluton is not exposed in the study area.

The Satosoak pluton inner zone is 20 km long in an east-west direction, 2 – 10 km wide in a north-south direction (see Fig. 7.2) and a minimum of 300 m thick. The overall form of this pluton is a rectangle that is elongated in an east-west direction. Sheets and dikes of the Satosoak pluton inner zone were intruded into the Akuliakatak pluton and are oriented at ~025°/30° E and ~075°/80° N. The northern and southern boundaries of the Satosoak pluton inner zone are steeply inward dipping, thereby comprising a bowl-shaped cross-section for the inner zone (see Fig. 7.3). The boundary formed with the Tabor pluton comprises a 1 – 2 km wide zone that trends at ~120°. This zone comprises sheets of the Tabor pluton and xenoliths of the Satosoak pluton inner zone. These xenoliths are sub-spherical to slab-like in form and are up to 50 m in size. In addition, these xenoliths are rimmed by aggregates of medium-sized to large pyroxene grains (see Fig. 7.12). Anorthositic rocks of the Tabor pluton are of uniform medium- to coarse-grain size right up to contacts with Satosoak pluton xenoliths.

Petrography

Plagioclase crystals are of high abundance, large to very large size and tabular to granular form, suggesting that these crystals are cumulus. Tabular plagioclase shows

interlobate grain margins (Fig. 7.13) that indicate it was recrystallized at high-T, and granular plagioclase shows equilibrated geometry and deformation twins that indicate it was also recrystallized and/or deformed at high-T. The recrystallized and deformed grains are most abundant in anorthosite and less abundant in leuconorite. Minute rods of Fe-Ti oxide are abundant in all plagioclase crystals. Orthopyroxene crystals are of relatively low abundance and show poikilitic to sub-poikilitic texture (Figs. 7.13, 7.14), suggesting that orthopyroxene crystallized out of the intercumulus liquid. These orthopyroxene crystals also contain blebs of exsolved clinopyroxene and plates of Fe-Ti oxide. Olivine forms medium-sized to large granules that are generally rimmed with orthopyroxene. Clinopyroxene crystals are small and occur in minor abundances on the rims of plagioclase and orthopyroxene crystals.

The anorthositic rocks also contain aggregates of small plagioclase, pyroxene +/- Fe-Ti oxide grains that are interstitial to cumulus plagioclase. These aggregates also contain very small biotite laths and amphibole grains, and relatively high abundances of secondary minerals. Anorthositic rocks that lie next to granitic veins contain aggregates of small to medium-sized quartz grains, feldspar grains, biotite laths and amphibole grains that are also interstitial to cumulus plagioclase (Fig. 7.15).

Secondary minerals are abundant (5 – 10% mode) in anorthositic rocks that occur adjacent to granitic veins. These secondary minerals consist of sericite and quartz that replaced plagioclase, and uralite that replaced pyroxene. In addition, these secondary minerals suggest that anorthositic rocks that lie adjacent to granitic veins were hydrothermally altered.

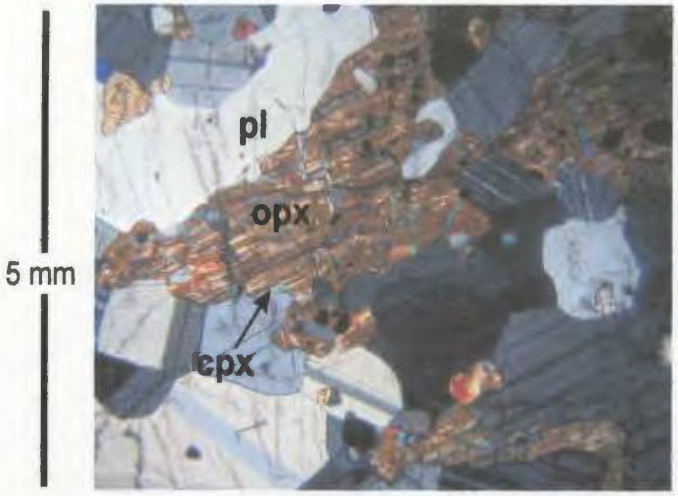

Figure 7.14: Thin section photo (XPL) of leuconorite in KSi. Leuconorite contains medium-sized plagioclase grains (pl) and medium-sized poikilitic orthopyroxene (opx). Orthopyroxene contains exsolved clinopyroxene (cpx).

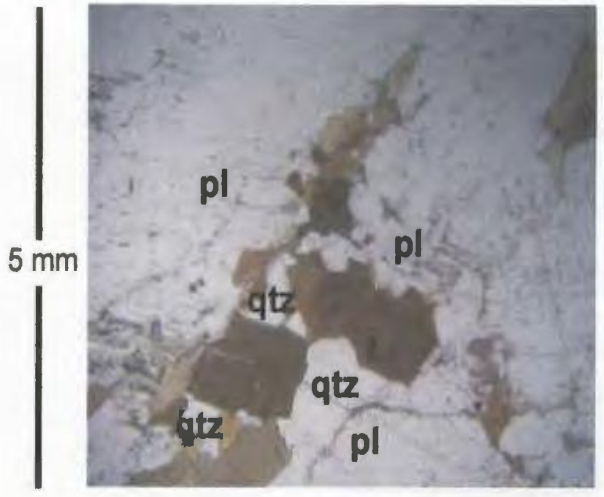

Figure 7.15: Thin section photo (PPL) of poikilitic biotite (brown in photo) and quartz (qtz) aggregate in KSi anorthosite. The sample was taken adjacent to a granitic vein. Plagioclase in KSi anorthosite is marked (pl).

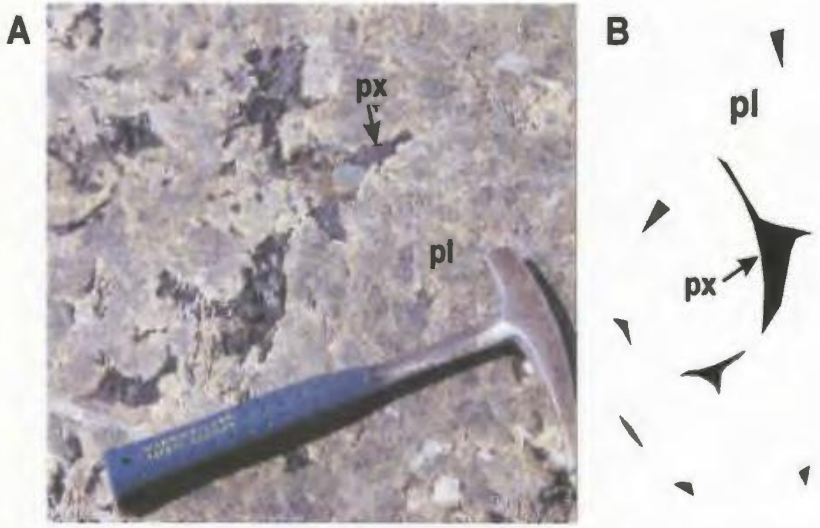

Figure 7.16: (A) Photo and (B) schematic field sketch of massive KSi anorthosite. Anorthosite contains large plagioclase grains (pl) and large poikilitic pyroxene crystals (px). Photo taken on north shoreline of Anaktalik Bay.

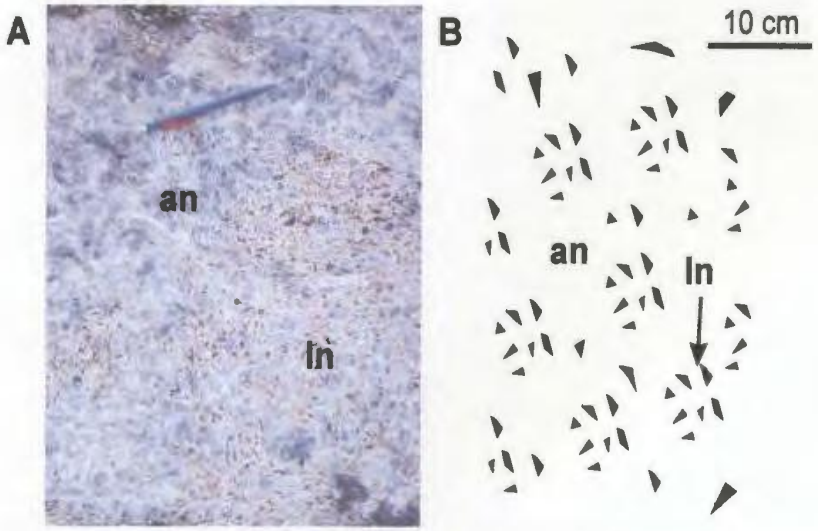

Figure 7.17: (A) Photo and (B) schematic field sketch of mottled rock in KSi. Mottled rock comprises patches of granular-textured anorthosite (an) and poikilitic-textured leuconorite (ln). Photo taken on north shoreline of Anaktalik Bay.

Textures and structures

Leuconorite, anorthosite and olivine leuconorite are medium- to very coarse-grained and show an overall texture that ranges from poikilitic (10 – 35% poikilitic crystals and aggregates) to granular (5 – 10% poikilitic crystals and aggregates).

Anorthositic rocks are massive, mottled or layered. Massive rocks comprise only granular (Fig. 7.16) or poikilitic texture. Mottled rocks comprise patches of interspersed granular and poikilitic texture (Fig. 7.17). These patches are sub-spherical to planar in form and range from 0.1 – 50 m in size. Planar patches define a crude primary layering. This type of layering strikes parallel to unit contacts or is broadly north-south trending in the eastern part of the inner zone (see Fig. 7.2). Anorthositic rocks also contain planar aggregates of large to very large poikilitic pyroxene crystals (Fig. 7.18). These planar aggregates are 1 – 5 cm thick and 30 – 200 cm long, and are predominantly sub-vertical and north-south or east-west striking.

Mineral compositions and whole rock chemistry

Mineral compositions in anorthositic rocks range from An_{50-52} in plagioclase and average En_{64} in orthopyroxene (Table 7.3). These compositions fall in the Ca-rich plagioclase and Mg-rich pyroxene end of the range shown by NB noritic anorthosite. Orthopyroxene contains <1.9 wt% Al_2O_3. The composition of clinopyroxene averages En_{37}, and the compositions of all minerals are homogeneous. The plagioclase composition in one sample of anorthosite that lies adjacent to a granitic vein (02-25-10b) averages An_{47}, and shows rims that are Na-rich (An_{16}) relative to the core.

Whole rock chemistry of anorthositic rocks shows wt% K_2O that falls in the range shown by NB troctolitic anorthosite, whereas wt% SiO_2, Ca/Al, Sr/Ca and Mg/(Mg+Fe) fall in the range shown by both NB noritic and troctolitic anorthosite (Table 7.3, see Fig. 7.9). Ba/K (0.17 – 0.22) is high in comparison to both NB noritic and troctolitic anorthosite (0.09 – 0.18). CIPW norms consist mostly of plagioclase and pyroxene, and show normative plagioclase compositions that fall in the range shown by NB troctolitic anorthosite.

Table 7.3: Mineral compositions (*) and whole rock chemistry for KSi anorthositic rocks, and comparative data for NB noritic and troctolitic anorthosite

Sample	Rock type	Pl*	Opx*	SiO_2	K_2O	Ca/Al	Sr/Ca x 10	Mg/(Mg+Fe)	An/(An+Ab)
		An	En	wt%	wt%				CIPW
Satosoak pluton inner zone (KSi)									
02-30-3b	In	50	64	53.86	0.41	1.04	0.12	0.38	0.56
01-13-21b	In	52		52.92	0.30	1.10	0.09	0.41	0.59
01-13-21a	anor	52		53.39	0.42	1.07	0.09	0.26	0.58
02-25-10a	anor			53.19	0.53	1.07	0.11	0.27	
Comparative data									
NB noritic		40 - 54	57 - 67	52 - 58	0.6 - 1.2	0.8 - 1.1	0.10 - 0.15	0.10 - 0.35	0.42 - 0.54
NB troctolitic		51 - 68	66 - 73	49 - 55	0.2 - 0.6	1.0 - 1.2	0.06 - 0.09	0.15 - 0.49	0.53 - 0.68

Whole rock chemistry of anorthosite with poikilitic aggregates of granitic rock (02-25-10b) shows relatively high abundances of SiO_2 (55.93 wt%), Na_2O (4.57 wt%), K_2O (0.61 wt%), Ba (591 ppm) and Zr (56 ppm) in comparison to 'average' anorthositic rocks (anorthosite and leuconorite in Table 7.3) of the Satosoak pluton. High abundances of these elements reflect the modal abundances of quartz that were observed in thin section, as well as the Na-rich plagioclase compositions obtained with the microprobe. Likewise, CIPW norms indicate minor abundances of quartz (5%) and orthoclase (4%).

Ferrodiorite dikes

The inner zone of the Satosoak pluton was intruded by ferrodiorite dikes (see Fig. 7.4). These ferrodiorite dikes show an arcuate strike that ranges from steeply (70°) east dipping and north-south (165°) striking in the west, to steeply north dipping and east-west (120°) striking in the east. Individual dikes are 1 – 30 m thick. Intrusive contacts with anorthositic rocks of the Satosoak pluton inner zone are sharp or grade into anorthositic rocks with interstitial aggregates of ferrodiorite. In addition, ferrodiorite dikes in the Satosoak pluton inner zone contain large plagioclase laths and lens-shaped aggregates of large plagioclase grains (Fig. 7.19).

Table 7.4: Whole rock chemistry for a KSi ferrodiorite dike and an inclusion of leucogabbronorite in this dike, and comparative data for KSi anorthositic rocks

Rock type	Sample	TiO_2	FeOt	K_2O	P_2O_5	V	Ba	Zr
		wt%	wt%	wt%	wt%	ppm	ppm	ppm
Fe-rich dioritic dike in KSi								
Fe-di	02-31-8ii	3.62	16.55	0.41	1.13	181	1228	974
lgn lens	02-31-8i	0.53	5.33	0.35	0.14	38	362	129
Comparative data								
KSi		0.2 - 0.6	1.1 - 4.6	0.3 - 0.5	<0.1	11 - 61	267 - 433	9 - 34

Ferrodiorite shows similar petrography to ferrodiorite that forms dikes in the Akuliakatak pluton. Whole rock chemistry for one sample of ferrodiorite shows high wt% TiO_2, wt% FeOt, wt% P_2O_5, ppm V and ppm Zr in comparison to host anorthositic rocks (Table 7.4).

Lens-shaped aggregates of leucogabbronorite in ferrodiorite dikes consist of medium-sized to large plagioclase grains and medium-sized poikilitic pyroxene crystals (see Fig. 7.19). These lenses show an overall poikilitic texture, and are 1 – 5 cm thick, 5 –

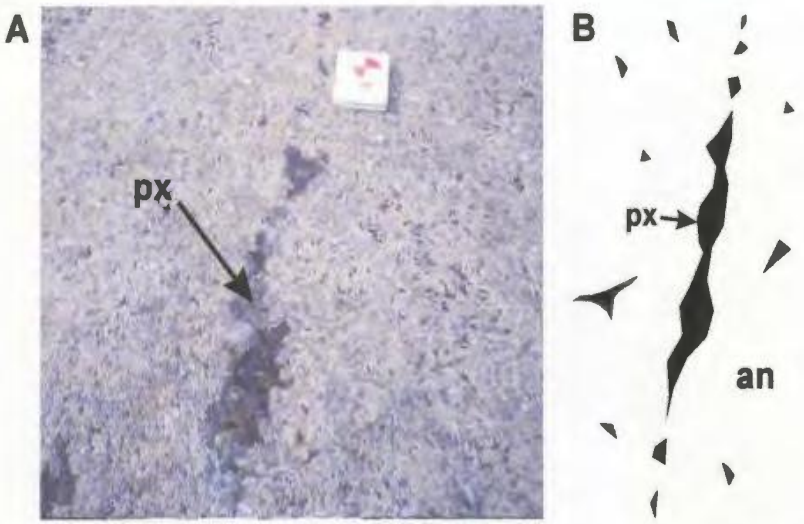

Figure 7.18: (A) Photo and (B) field sketch of a planar aggregate of large poikilitic pyroxene crystals (px) in KSi anorthosite (an). Photo taken on northern shoreline of Satosoak Island.

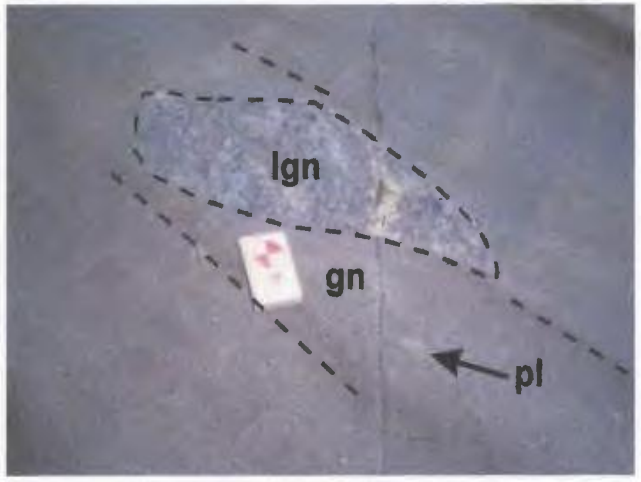

Figure 7.20: Xenolith of leucogabbronorite (lgn) in gabbronorite (gn) of KSb. Gabbronorite shows a diffuse primary layering and scattered phenocrysts of plagioclase (pl). Dashed line outlines the xenolith and indicates the trend of layering. Photo taken along the northwestern shoreline of Anaktalik Bay.

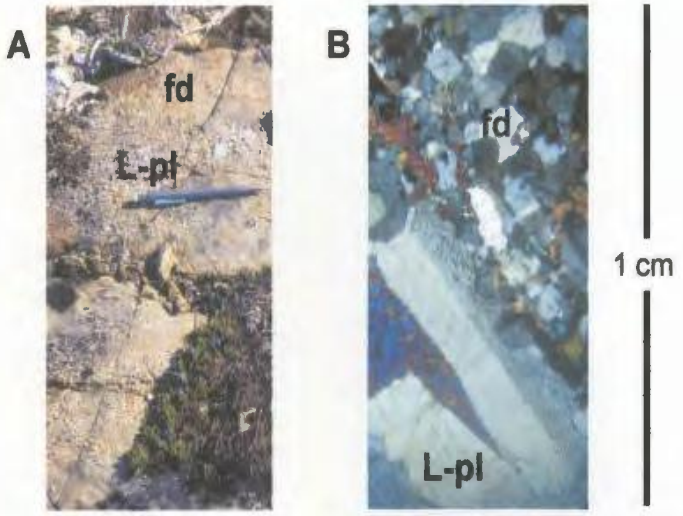

Figure 7.19: (A) Field and (B) thin section (XPL) photos of a ferrodiorite dike in anorthositic rocks of KSi. Both photos show relatively fine-grained ferrodiorite (fd) with large plagioclase crystals (L-pl). Field photo taken on Satosoak Island.

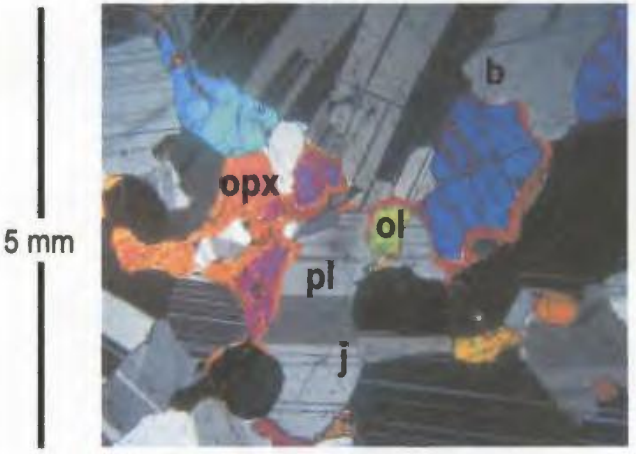

Figure 7.21: Thin section photo (XPL) of leucotroctolite in KSb. Leucotroctolite consists of tabular plagioclase (pl), granular olivine (ol) and poikilitic-textured orthopyroxene crystals (opx). Plagioclase shows triple junctions (t) and bulging grain margins (b).

20 cm long and strike parallel to the intrusive contacts of the dike. Whole rock chemistry of a leucogabbronorite lens shows wt% FeOt, wt% P_2O_5 and ppm Zr that are slightly higher in comparison to anorthositic host rocks of the Satosoak pluton inner zone (Table 7.4).

7.3.2 Satosoak pluton border zone (KSb)

Form and contacts

Geological mapping as part of this study found a moderately dipping, strongly deformed to weakly deformed, composite unit of gabbronorite, oxide gabbronorite, melagabbronorite, leucogabbronorite, anorthosite, troctolite and leucotroctolite. This unit is here named the Satosoak pluton border zone (see Fig. 7.2). The outer boundary of this unit cuts sharply and discordantly across Paleoproterozoic gabbroic granulite, and anorthositic rocks in the Tikkoatokak centered intrusive complex and the Sophie centered intrusive complex. The inner boundary of this unit shows a gradational increase in the abundance of massive leuconorite, anorthosite and olivine leuconorite that mark the base of the Satosoak pluton inner zone.

The Satosoak pluton border zone envelops the Satosoak pluton inner zone to the north, west and south. The northern part of the border zone is 50 – 600 m thick, 20 km long, moderately (50° – 60°) south dipping and east of northeast to east of southeast striking (070° – 120°) (see Figs. 7.2, 7.3). The western part of the border zone is 200 m thick, 5000 m long, moderately (60° – 70°) west dipping to sub-vertical and north-south

striking. The southern side of the border zone is 50 – 100 m thick, 3000 m long, sub-vertical and east-west striking.

The contacts with Paleoproterozoic gabbroic granulite comprise weakly to strongly deformed anorthosite, leucogabbronorite and gabbronorite. These weakly to strongly deformed rocks also occur as xenoliths in weakly deformed rocks (Fig. 7.20), indicating that the border zone is composite. The contact with the Tikkoatokak centered intrusive complex is fine-grained and has the appearance of a chilled margin. The contact with the Sophie centered intrusive complex comprises a stockwork of sills and dikes that were emplaced within massive anorthositic rocks of the Sophie centered intrusive complex (see Fig. 6.36).

Petrography

Troctolite and leucotroctolite are weakly deformed. These rocks contain plagioclase crystals that are of small to medium size and of tabular to granular form, suggesting that these crystals grew on the liquidus. Some plagioclase grains show triple junctions, interlobate grain margins and equilibrated geometries (Fig. 7.21) that indicate the grain margins were equilibrated at high-T. Olivine crystals are granular in form and are rimmed by orthopyroxene, suggesting peritectic reaction of olivine crystals to orthopyroxene. Orthopyroxene and clinopyroxene crystals show sub-poikilitic texture, suggesting that they crystallized out of the intercumulus liquid. Fe-Ti oxide crystals are of small size and occur in accessory abundance.

Gabbronorite, oxide gabbronorite and melagabbronorite range from weakly to strongly deformed. These rocks contain plagioclase, orthopyroxene and clinopyroxene, all of which are of small to medium size and granular form (Fig. 7.22). Strongly deformed rocks contain mostly grains, whereas weakly deformed rocks also contain medium-sized to large plagioclase and/or orthopyroxene laths. The grains in strongly deformed rocks show interlobate grain margins, serrated grain margins, triple junctions and/or equilibrated geometry that indicate they were recrystallized at high-T (Fig. 7.23). Laths in weakly deformed rocks are generally fractured and kinked. Oxide gabbronorite also contains small grains of Fe-Ti oxide that comprise up to 10% of the mode. Accessory minerals consist of very small apatite grains, biotite laths and/or amphibole grains.

Leucogabbronorite also ranges from weakly to strongly deformed. These rocks contain plagioclase crystals that are of high abundance and large size, suggesting that they are cumulus. Plagioclase also shows granular forms with equilibrated geometries, triple junctions (Fig. 7.24) and serrated margins that indicate they were recrystallized at high-T. Plagioclase also contains abundant and very small inclusions of pyroxene. One sample of leucogabbronorite is cut by a penetrative fracture cleavage that suggests it was deformed at lower temperatures as well. Orthopyroxene and clinopyroxene crystals are of low abundance, of small to medium size and show poikilitic to sub-poikilitic texture, suggesting that they crystallized out of the intercumulus liquid.

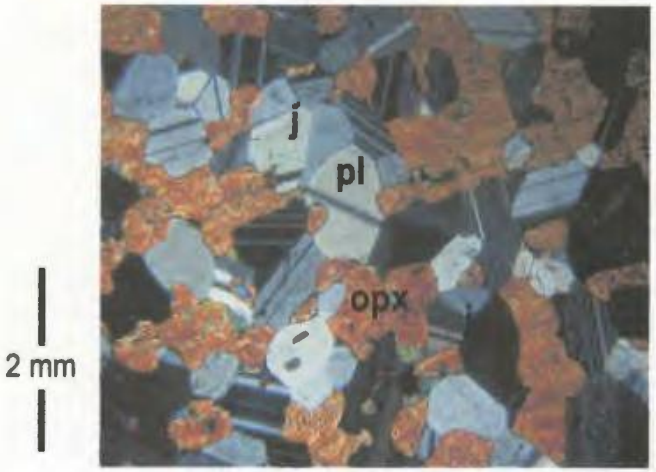

Figure 7.22: Thin section photo (XPL) of deformed norite in KSb. Norite consists of small plagioclase (pl) and orthopyroxene (opx) grains. Grains show triple junctions (j) and equilibrated geometry.

Figure 7.23: Thin section photo (XPL) of weakly deformed gabbronorite in KSb. Gabbronorite consists of medium-sized and fractured orthopyroxene laths (L-opx), and small to medium-sized plagioclase (pl), orthopyroxene (opx) and clinopyroxene (cpx) grains.

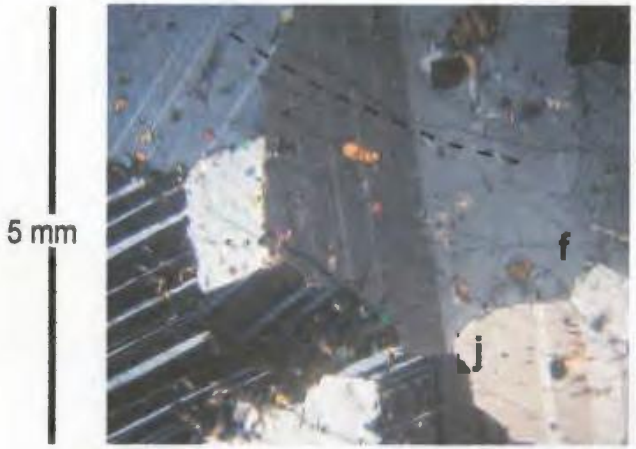

Figure 7.24: Thin section photo (XPL) of leucogabbronorite in KSb. Plagioclase crystals show triple junctions (j), fracture cleavage (f), equilibrated geometry and very small inclusions of pyroxene. Dashed line indicates the trend of the fracture cleavage.

Figure 7.25: Strongly deformed gabbronorite (gn) and leucogabbronorite (lgn) in KSb. Layering is steeply south dipping and east-west striking. Photo taken along the northern shoreline of Anaktalik Bay.

Textures and structures

Troctolite, leucotroctolite, gabbronorite and melagabbronorite are fine- to medium-grained and show an overall texture that ranges from granular to porphyritic. Leucogabbronorite is medium- to coarse-grained and shows an overall poikilitic texture.

All rock types in the border zone are massive or layered. Massive rocks are most abundant and comprise only one rock type and texture. Primary layering comprises rhythmic alternations of: (a) leucotroctolite and troctolite, and (b) gabbronorite, melagabbronorite and leucogabbronorite (see Fig. 7.20). Individual layers are 1 – 20 cm thick, 1 – 50 m in length and moderately dipping.

The border zone contains compositionally layered gabbronoritic and anorthositic rocks that show only granular texture (Fig. 7.25). These compositional layers are ~0.5 – 5 cm thick, sub-vertically oriented and east-west striking. Some compositional layers of gabbronorite show a sigmoidal pattern (Fig. 7.26) that suggests they were overprinted by sinistral shear deformation. The granular texture, steep orientation and sigmoidal layers in these rocks suggest that they were overprinted by shear deformation. The stresses associated with this deformation were oriented within and perpendicular to the planes of primary layering and unit contacts.

Mineral compositions and whole rock chemistry

Mineral compositions of troctolite and leucotroctolite range from An_{54-64} in plagioclase and En_{41-44} in clinopyroxene, and average Fo_{56} in olivine and En_{67} in orthopyroxene. These compositions fall within the range shown by Paleoproterozoic

gabbroic granulite (Fig. 7.27, Table 7.5). Some rims of plagioclase crystals are Ca-rich (+An_{21}) relative to the rest of the grain. Whole rock chemistry of leucotroctolite shows wt% SiO_2, wt% K_2O, Ca/Al, Sr/Ca and Mg/(Mg+Fe) that fall in the range shown by NB troctolitic anorthosite (see Fig. 7.9). CIPW norms of leucotroctolite consist mostly of plagioclase, pyroxene and olivine.

Table 7.5: Mineral compositions (*) and whole rock chemistry for KSb troctolitic and gabbronoritic rocks, and comparative data for anorthositic rocks in the Satosoak pluton inner zone (KSi) and Paleoproterozoic gabbroic granulite (Pg)

Rock type	Sample	Pl*	Opx*	TiO_2	FeOt	MgO	K_2O	P_2O_5
		An	En	wt%	wt%	wt%	wt%	wt%
Satosoak pluton border zone (KSb)								
tr	00-5-13b	54						
ltr	02-24-19a	64	67**	0.43	6.17	4.50	0.22	0.07
gn	00-5-12	45	56	0.45	9.52	6.89	0.48	0.02
gn	01-23-13a	56	71	0.45	11.94	14.09	0.10	0.01
gn	02-10-12	45	51	3.71	13.67	4.47	0.56	0.98
mgn	01-18-20		64					
defm gn	02-25-18	49	65	0.09	13.77	7.42	0.14	0.04
Comparative data								
KS		50 - 52	64	0.2 - 0.6	1.1 - 4.6	0.5 - 3.2	0.3 - 0.5	<0.1
Pg		51 - 81	58 - 85	0.4 - 0.8	11 - 13	7 - 31	0.1 - 0.4	<0.1

Mineral compositions of gabbronorite and melagabbronorite range from An_{45-56} in plagioclase, En_{51-71} in orthopyroxene and En_{37-44} in clinopyroxene. These compositions overlap with the range shown by anorthositic rocks in the Satosoak pluton and also fall in the range shown by Paleoproterozoic gabbroic granulite (see Fig. 7.27). Likewise, whole rock chemistry of gabbronorite and melagabbronorite also fall in the range shown by Paleoproterozoic gabbroic granulite (see Fig. 7.30). Whole rock chemistry for one sample of weakly deformed oxide gabbronorite shows high wt% TiO_2,

K_2O and P_2O_5 in comparison to the range shown by Paleoproterozoic gabbroic granulite. CIPW norms consist mostly of plagioclase, pyroxene and olivine.

Mineral compositions of leucogabbronorite range from An_{48-51} in plagioclase, En_{59-65} in orthopyroxene and En_{38-42} in clinopyroxene. These compositions overlap with the range shown by anorthositic rocks in the Satosoak pluton inner zone (Table 7.6). Whole rock chemistry for one sample of leucogabbronorite shows wt% SiO_2, wt% K_2O, Ca/Al, Sr/Ca, Mg/(Fe+Mg) and Ba/K that fall in the range shown by anorthositic rocks in the Satosoak pluton inner zone (see Fig. 7.9). Ba/K (0.24) is high in comparison to both NB troctolitic and noritic anorthosite (0.09 – 0.18). CIPW norms consist mostly of plagioclase and pyroxene, and show normative plagioclase compositions that fall in the range shown by NB troctolitic anorthosite.

Table 7.6: Mineral compositions (*) and whole rock chemistry for KSb anorthositic rocks, and comparative data for KSi anorthositic rocks, NB noritic anorthosite and NB troctolitic anorthosite

Sample	Rock type	Pl*	Opx*	SiO_2	K_2O	Ca/Al	Sr/Ca x 10	Mg/(Mg+Fe)	An/(An+Ab)
		An	En	wt%	wt%				CIPW
Satosoak pluton border zone (KSb)									
01-23-6	lgn	51	59	53.27	0.37	1.08	0.10	0.31	0.58
01-23-13b	defm lgn	48	65						
01-23-12	defm lgn	50							
Comparative data									
KSi		50 - 52	64	53 - 54	0.3 - 0.5	1.0 - 1.1	0.09 - 0.12	0.27 - 0.41	0.56 - 0.58
NB noritic		40 - 54	57 - 67	52 - 58	0.6 - 1.2	0.8 - 1.1	0.10 - 0.15	0.10 - 0.35	0.42 - 0.54
NB troctolitic		51 - 68	66 - 73	49 - 55	0.2 - 0.6	1.0 - 1.2	0.06 - 0.09	0.15 - 0.49	0.53 - 0.68

Summary

The Satosoak pluton border zone is localized around the Satosoak pluton inner zone. The border zone is composite and consists of troctolitic, gabbronoritic and anorthositic rocks. Troctolitic rocks are included in the Kikkertavak centered intrusive

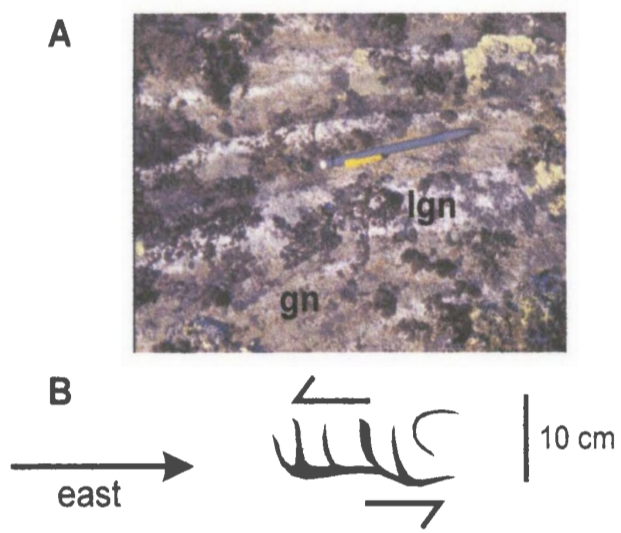

Figure 7.26: (A) Strongly deformed and layered gabbronorite (gn) and leucogabbronorite (lgn) in KSb. (B) Field sketch shows layers with asymmetric patterns that indicate sinistral shear deformation. Photo and sketch made on the Akuliakatak Peninsula.

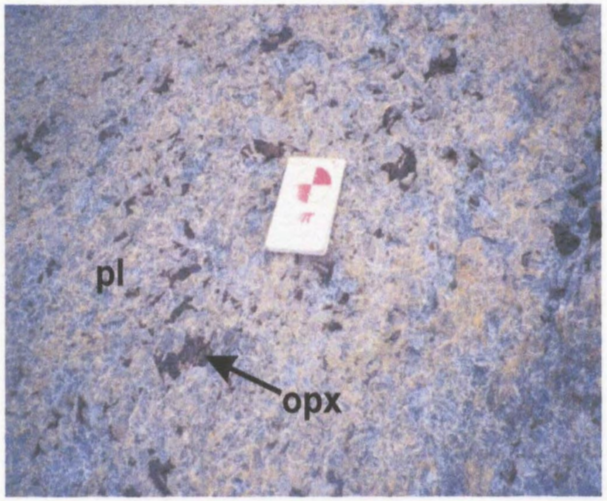

Figure 7.28: Massive granular-textured anorthosite in KT. Anorthosite contains very large plagioclase grains (pl) and poikilitic orthopyroxene crystals (opx). Photo taken on southwestern corner of Satosoak Island.

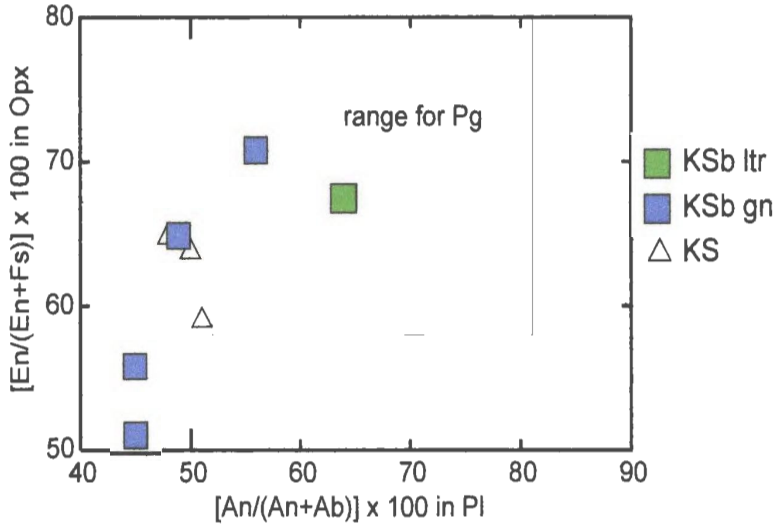

Figure 7.27: Comparison of orthopyroxene and plagioclase compositions for Satosoak pluton border zone (KSb) leucotroctolite (ltr) and gabbronorite (gn), Satosoak pluton anorthositic rocks (KS) and Paleoproterozoic gabbroic granulite (Pg).

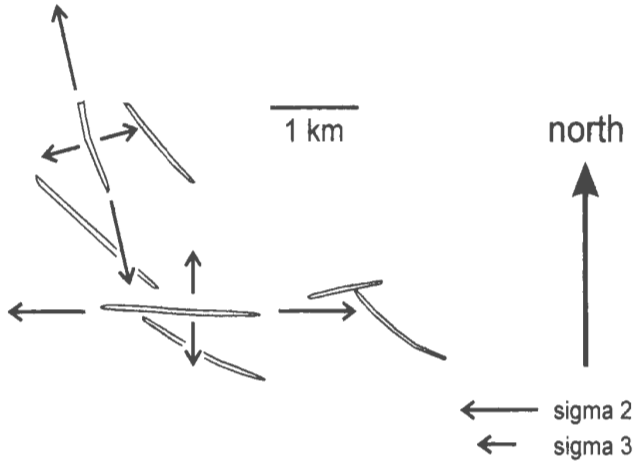

Figure 7.29: Orientation of Fe-rich dioritic dikes in the Satosoak pluton inner zone. The orientation of these dikes suggests that localized east-west and north-south directed stress acted on the Satosoak pluton during dike emplacement.

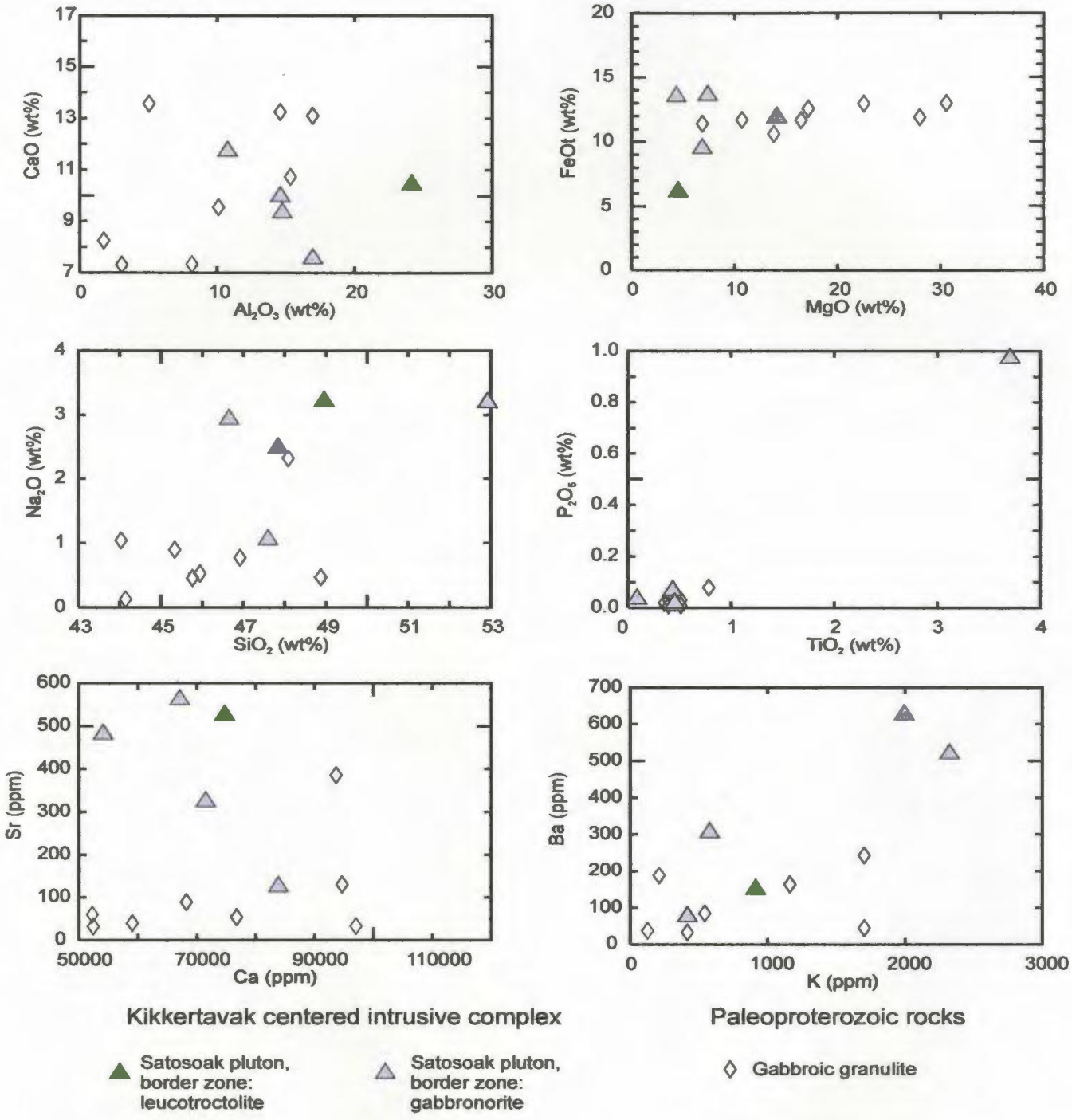

Figure 7.30: Whole rock chemistry for leucotroctolite and gabbronoritic rocks in the Satosoak pluton border zone, and comparative data for Paleoproterozoic gabbroic granulite.

complex because they: (a) cut across Mesoproterozoic rocks, (b) host xenoliths of gabbronoritic rocks, and (c) are only weakly deformed. Gabbronoritic rocks are included in Kikkertavak centered intrusive complex because: (a) they cut across Mesoproterozoic plutonic rocks, (b) they range from weakly to strongly deformed, and (c) show mineral compositions that overlaps with the range shown by anorthositic rocks in the Satosoak pluton inner zone. Anorthositic rocks are in the Kikkertavak centered intrusive complex because: (a) they are layered with gabbronoritic rocks, and (b) they show similar mineral and whole rock chemistry to anorthositic rocks in the Satosoak pluton inner zone.

7.4 Tabor pluton (KT)

Geological maps by Wheeler (1969) and Ryan (1990) show that anorthositic rocks underlie Satosoak Island and Tabor Island. Tabor Island lies outside of the study area but was visited by the author during a day trip in 2002. A study by Yu and Morse (1993) found that anorthositic rocks on Tabor Island comprised part of the Main anorthosite event (ca. 1240 Ma by $^{40}Ar/^{39}Ar$ dating of plagioclase). A U-Pb dating study by Hamilton et al. (1994) found that zircons in anorthositic rocks on Tabor Island crystallized at 1311 +/- 2 Ma.

Form and contacts

Geological mapping as part of this study found a unit of massive anorthosite and leuconorite at the southwest end of Satosoak Island (see Fig. 7.4). An boat excursion south of the study area found that these anorthositic rocks correlate with those in the

Tabor Island quarry. The anorthositic rocks on the southwestern tip of Satosoak Island are therefore here grouped into the Tabor pluton (after Tabor Island, see Fig. 7.1). The northern boundary of this unit truncates the Satosoak pluton inner zone. This boundary was described in section 7.3.2. No other boundaries of this unit are exposed in the study area.

In the study area, the Tabor pluton underlies the southwestern 10 km^2 of Satosoak Island (see Fig. 7.4) and is exposed up to ~5 km to the south (D. Wright, pers. com., 2002).

Textures and structures

Anorthosite and leuconorite consist of large to very large plagioclase laths and grains, and various abundances (5 – 35%) of large poikilitic orthopyroxene crystals and small poikilitic Fe-Ti oxide crystals. These grains, laths and crystals comprise an overall texture that ranges from granular (5 – 10% poikilitic crystals) to poikilitic (10 – 35% poikilitic crystals).

Anorthositic rocks are massive or mottled. Massive rocks comprise only granular or poikilitic texture (Fig. 7.28). Mottled rocks comprise patches of interspersed granular and poikilitic texture. These patches are sub-spherical in form and range from 0.5 – 100 m in diameter. Anorthositic rocks also contain planar aggregates of large poikilitic orthopyroxene crystals. These planar aggregates are 1 – 5 cm thick, 0.1 – 5 m long, sub-vertical and randomly striking.

Summary

The anorthositic rocks of the Tabor Island pluton are spatially associated with anorthositic rocks in the Satosoak pluton. For these reasons, the Tabor pluton is included with the Satosoak pluton in the Kikkertavak centered intrusive complex.

7.5 Tectonic overprint

The margin of the Kikkertavak centered intrusive complex contains plutonic rocks that: (a) are moderately dipping to sub-vertical, layered, (b) are granular-textured, and (c) show sigmoidal layers. These rocks are here referred to as strongly deformed. In addition, the Kikkertavak centered intrusive complex was cut by an arcuate trending swarm of Fe-rich dioritic dikes and east-west striking granitic veins. These strongly deformed rocks, dikes and veins preserve the structurally measurable tectonic overprint of the Kikkertavak centered intrusive complex.

The strongly deformed plutonic rocks occur in the Satosoak pluton border zone. These strongly deformed rocks are mostly moderately dipping to sub-vertical and east-west striking, and are cut by weakly deformed rocks. In addition, strongly deformed rocks show sigmoidal layers that suggest primary layering was overprinted by sinistral shear deformation. These findings suggest that a sub-vertically oriented and east-west striking Mesoproterozoic shear zone helped to deform parts of the border zone.

Anorthositic rocks of the Satosoak pluton inner zone were cut by an arcuate striking swarm of Fe-rich dioritic dikes. These dikes are exposed on Satosoak Island (see Fig. 7.4). The gradational contacts of these dikes suggest that their emplacement was

broadly contemporaneous with the crystallization of anorthositic rocks. The orientation of these dikes suggests that the anorthositic rocks were strained by sub-horizontally oriented east-west and north-south directed stresses (Fig. 7.29).

The Satosoak pluton inner zone was cut by granitic patches, networks (Fig. 7.31) and veins. All of these occurrences of granitic rocks are bound by anorthositic rocks with aggregates of quartz and biotite grains (see Fig. 7.15), suggesting that these granitic rocks were emplaced in the late stages of crystallization of the host anorthositic rocks. The veins are sub-vertically oriented and east-west striking, and exhibit splay and en echelon structures that indicate they were emplaced during sinistral shear deformation. Like the ferrodiorite dikes, the orientation of these veins indicates that the Satosoak pluton inner zone was strained by sub-horizontally oriented, east-west and north-south directed stresses. The predominantly east-west orientation of these veins suggests that the magnitude of east-west directed stress was than north-south directed stress.

7.6 Summary

This chapter described the form, contacts, petrography, textures, structures, mineral compositions and/or whole chemistry of the Akuliakatak and Satosoak plutons, and the contacts, structure and texture of the Tabor pluton. All of these plutons were grouped into the Kikkertavak centered intrusive complex. This section describes the overall structure of the Kikkertavak centered intrusive complex in terms of a core, margin and tectonic overprint (Fig. 7.32).

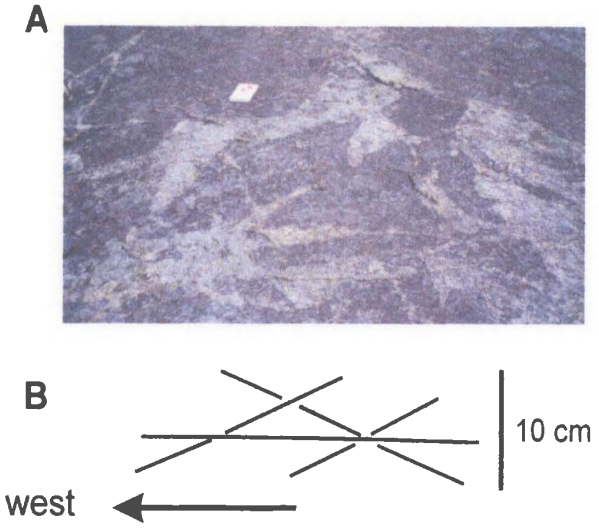

Figure 7.31: Granitic veins in anorthositic rocks of KSi showing (A) net-veined occurrence and (B) vein-like occurrence. The orientation of veins suggests they were emplaced under east-west and north-south directed stress. Photo and sketch made on the north shoreline of Satosoak Island.

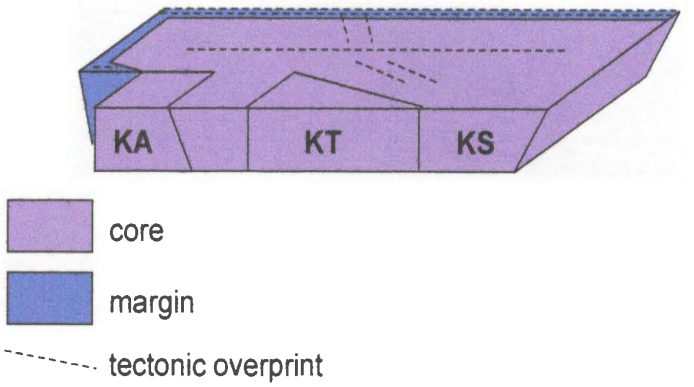

Figure 7.32: Box-model for the NW part of the Kikkertavak centered intrusive complex showing core, margin and tectonic overprint, as well as the Akuliakatak pluton (KA), Satosoak pluton (KS) and the Tabor pluton (KT).

The core of the Kikkertavak centered intrusive complex consists of the Akuliakatak pluton, Satosoak pluton inner zone and the Tabor pluton. Rocks in the core are: (a) anorthositic, and (b) massive and/or mottled, and were partly recrystallized and/or deformed at high-T. Mineral compositions are similar to NB noritic anorthosite, whole rock chemistry is similar to NB troctolitic and noritic anorthosite, and CIPW norms for anorthositic rocks consist mostly of plagioclase, pyroxene +/- olivine. The core also contains ferrodiorite dikes that contain high abundances of Ti, Fe, P, Zr, V +/- K and Rb in comparison to anorthositic host rocks.

The margin of the Kikkertavak centered intrusive complex consists of the Satosoak pluton border zone. Rocks in the margin are: (a) anorthositic, gabbronoritic or troctolitic, (b) moderately dipping to sub-vertical, and (c) layered, foliated and/or strongly deformed. Anorthositic rocks were recrystallized and/or deformed at high-T and show similar mineral compositions, whole rock chemistry and CIPW norms to anorthositic rocks in the core. Gabbronoritic rocks were recrystallized and/or strongly deformed at high-T, and contain Na-rich plagioclase and Fe-rich pyroxene in comparison to Paleoproterozoic gabbroic granulite. Troctolitic rocks show well-preserved igneous textures.

The margin of the Kikkertavak centered intrusive complex contains strongly deformed rocks that are sub-vertically oriented and east-west striking. The core of the Kikkertavak centered intrusive complex contains Fe-rich dioritic dikes and granitic veins that were emplaced under sub-horizontally oriented, east-west directed and north-south directed stress.

Chapter 8: Discussion

Geological mapping in the study area divided the rock types into: (a) country rock, and (b) centered intrusive complexes. Country rock was divided into four units; Archean granitoid and amphibolite gneiss, Archean or Paleoproterozoic gabbroic granulite, Archean or Paleoproterozoic metasedimentary gneiss and Paleoproterozoic enderbitic gneiss. The intrusive complexes are further divided into a core and a margin. The cores consist of anorthositic rocks. The margins consist of anorthositic and gabbronoritic rocks +/- monzonitic, Fe-rich gabbroic and troctolitic rocks. For the most part, rocks grouped into units of country rock, core and margin were distinguished in the field and/or by petrographic study. In some cases, however, strongly deformed gabbronoritic rocks in the margins of intrusive complexes were found to abut strongly deformed gabbroic granulite in the country rock. The previous chapters described several occurrences of these strongly deformed gabbronoritic rocks and presented field relations, contact relations, petrographic descriptions, textural and structural descriptions, mineral composition data, whole rock chemistry data and/or U-Pb isotope data that suggests these rocks comprise parts of a centered intrusive complex.

This discussion chapter is divided into six parts. The first part suggests that all zircon ages obtained in this study indicate the igneous age of crystallization, and that the development of tectonic overprints in the margins of centered intrusive complexes shows a broad overlap (1365-1270 Ma) with the time frame of igneous crystallization. The origin of this deformation is discussed in part two, and the implications with respect to the transport and emplacement of magma is discussed in part three. The fourth part of this

chapter investigates the origin of textures and structures in anorthositic rocks. The fifth part of this chapter compares new and previously published mineral compositional, whole rock chemical and geochronological data in order to describe the compositional evolution of anorthositic magmas in the study area and in the Nain batholith as a whole.

8.1 Comments on zircons and tectonic overprints

This section presents some comments on the zircon ages obtained as part of this study and on the tectonic overprints observed in the margins of centered intrusive complexes. It is suggested that the zircons indicate the igneous age of crystallization, and that the deformation occurred in the same time frame as igneous crystallization.

8.1.1 Comments on zircons

The ages of the zircons analyzed in this study are all Mesoproterozoic, suggesting that they are igneous in age. A summary is presented that suggests the forms and concordia plots also indicate an igneous origin for the zircons. On the other hand, the backscattered electron images of these zircons show that they are unzoned or that they exhibit a patchy zoning. Such zoning, or lack of zoning, is in contrast to the concentric zoning that is typically ascribed to igneous zircon crystals (see Corfu et al., 2003), and possible origins for the zircon crystals are discussed.

The U-Pb isotopic composition of four separate zircon populations was described in chapters 5 (Kangilialuk) and 6 (Unity inner and border zones, Pikaluyak sheet). Each population contains zircons that: (a) are elongate in form, (b) show prismatic tips, and (c)

lies on or within 2% of concordia. The elongate forms and/or prismatic tips indicate a euhedral zircon structure, which suggests final growth in a melt or fluid (Hanchar and Miller, 1993; Corfu et al., 2003). The concordant ages suggest that the zircons retained all of their Pb and that there is no inherited component. These data thereby strongly suggests that the zircons analyzed in this study grew only in a melt or fluid.

Patchy zoning, or a lack of zoning, in zircon crystals has been linked to late-magmatic recrystallization and hydrothermal alteration in deep-seated settings, and to straining of zircon crystals during magma emplacement (Corfu et al., 2003). It has also been suggested that zircons with patchy and/or no zoning are metamict (Hanchar and Miller, 1993). Since three out of the four zircon populations in this study were collected from strongly deformed intrusive rocks, an origin for the patchy and lack of zoning by recrystallization, hydrothermal alteration and/or straining is plausible. On the other hand, the U-Pb isotopic compositions lie on, or within, 2% of concordia, thereby suggesting that these zircons are not metamict. Instead, these concordant isotopic compositions suggest that no Pb was removed or added to the zircon. Hence, it is suggested that although the zircons in the study area may have been recrystallized, hydrothermally altered and/or strained, the U-Pb ages obtained from them indicate an igneous age of crystallization.

8.1.2 Comments on the tectonic overprint

The margins of centered intrusive complexes contain anorthositic, gabbronoritic, monzonitic and/or Fe-rich gabbroic rocks. The previous three chapters summarized

several reasons why each unit was included in a centered intrusive complex. Several of these units contain rock types that are strongly deformed (see Figs. 5.8, 5.9, 5.30, 5.31, 5.37, 5.43, 6.5, 6.16, 6.28, 6.34, 6.45, 7.25, 7.26) and share similarities with the descriptions of 'marginal granulites' provided by previous workers (see Davies, 1973b; Brand, 1974; Berg and Briegel, 1981; Royse et al., 1999). The findings from this study suggest that these 'marginal granulites' comprise the outer-most parts of Mesoproterozoic centered intrusive complexes in the Nain batholith.

Strongly deformed rocks in the: (a) Tasiyuyaksuk sheet were cut by weakly deformed rocks in the Lister pluton border zone (Fig. 5.6), (b) Lister pluton border zone were cut by weakly deformed rocks in the Satosoak pluton (Fig. 5.14), (c) Bird sheet were cut by weakly deformed rocks in the Satosoak pluton (Fig. 5.40), (d) Unity pluton were cut by weakly deformed rocks in the Airstrip sheet and the Hosenbein pluton (Fig. 6.3), (e) Hosenbein pluton lower border zone occur as xenoliths in weakly deformed rocks of the lower border zone, (f) Hosenbein pluton upper border zone occur as xenoliths in weakly deformed rocks of the upper border zone (Fig. 6.45), and (g) Satosoak pluton border zone occur as xenoliths in weakly deformed rocks of the border zone. These findings indicate that strongly deformed rocks were developed in the Mesoproterozoic, which is consistent with previously published field-based inferences of Mesoproterozoic deformation (see Woodward, 1972; Morse and Wheeler, 1973; Berg, 1975; Berg and Briegel, 1981; Morse, 1981c; Cadman et al., 1993; Royse and Park, 2000).

Strongly deformed rocks in the margins of centered intrusive complexes are gradational into weakly deformed rocks. The strongly deformed rocks show thinner layers and steeper dips in comparison to weakly deformed rocks. Weakly deformed rocks show poikilitic, porphyritic and/or granular texture, whereas strongly deformed rocks show mostly granular texture. Weakly and strongly deformed rocks are therefore linked by: (a) a thinning and steepening of layering and foliation, and (b) an increase in granular texture. There are no discrete fractures or faults that separate strongly deformed plutonic rocks from weakly deformed plutonic rocks. Marshak and Mitra (1988, p. 226) suggested that a lack of such discrete fractures and faults suggests a continuous and smooth variation of shear strain magnitude across the shear zone, and that the deformation was ductile. Therefore, the strongly deformed plutonic rocks in the study area were likely developed in ductile shear zones. The aforementioned field relations indicate that these ductile shear zones were Mesoproterozoic in age.

8.2 Tectono-magmatic setting

It has been shown that the margins of centered intrusive complexes contain strongly deformed rocks, and that these deformed rocks were formed in high-T, Mesoproterozoic, shear zones. This section summarizes the structure and extent of these shear zones, and uses new and previously published U-Pb geochronology to place some time constraints on their activity.

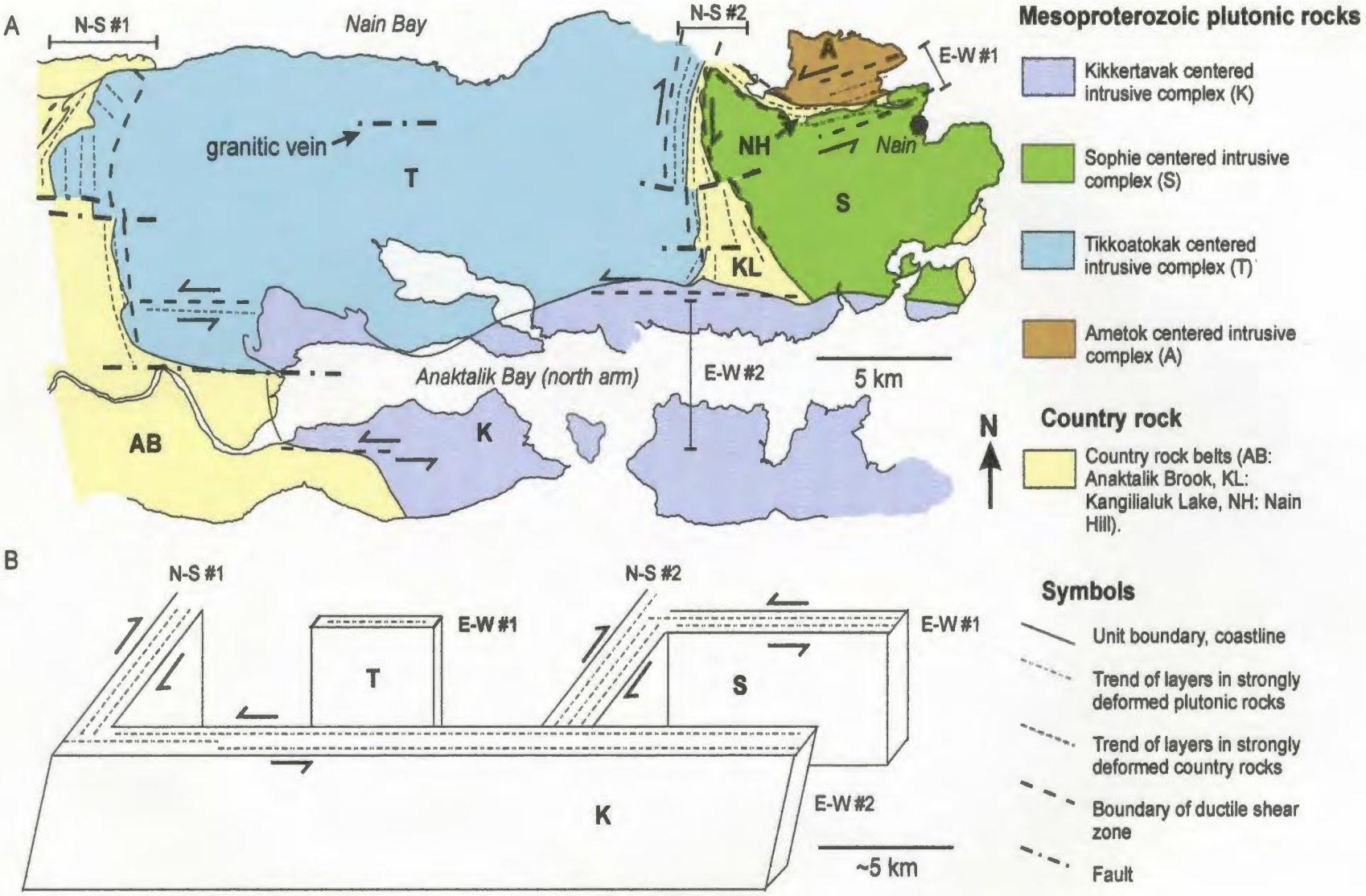

Figure 8.1: (A) Simplified geological map and (B) box-model of the study area showing the location of the four shear zones (N-S #1,2, E-W #1, 2) and centered intrusive complexes. Box-model is drawn at approximately the same scale as the map.

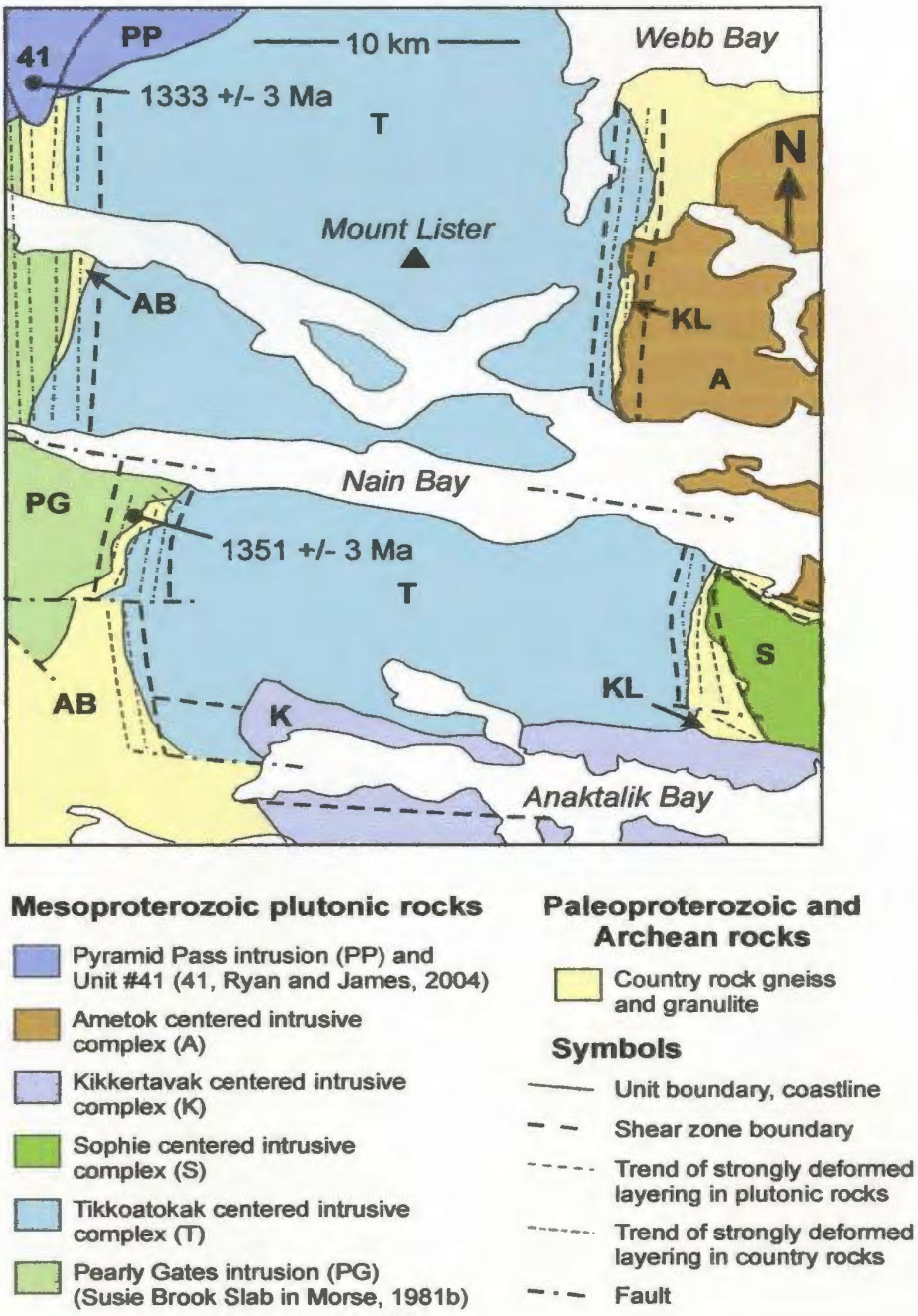

Figure 8.2: Simplified regional map showing the western part of the study area (south of Nain Bay) and compiled mapping north of the study area (from Wheeler, 1969; Ryan, 1990; Ryan and James, 2003; Gaskill, 2005). Map shows that the Anaktalik Brook (AB) and Kangilialuk Lake (KL) country rock belts are structurally continuous north of the study area, and are also spatially associated with north-south trending strongly deformed Mesoproterozoic plutonic rocks.

8.2.1 Ductile shear zones in the study area

Planar fabrics in the strongly deformed rocks in the study area are predominantly: (a) sub-vertical and north-south striking, or (b) moderately dipping to sub-vertical and east-west striking. The north-south striking rocks form belts in the: (a) western margin of the Tikkoatokak centered intrusive complex (Figs. 5.4, 5.40), and (b) eastern margin of the Tikkoatokak centered intrusive complex (Fig. 5.14). These belts are here referred to as north-south shear zone #1 and #2 (Fig. 8.1), respectively. The east-west striking rocks form belts in the: (a) northern margin of the Sophie centered intrusive complex (Fig. 6.3), and (b) southern margin of the Tikkoatokak centered intrusive complex (Fig. 5.40). These belts are here referred to as east-west shear zone #1 and #2 (see Fig. 8.1), respectively. The following parts of this section describe the chronology of these shear zones and the structural relations between shear zones and adjacent country rock belts. The regional extent of these shear zones (Fig. 8.2), based on extrapolation from work done in the study area, is also summarized.

8.2.1.i North-south shear zone #1

North-south shear zone #1 occurs in the western margin of the Tikkoatokak centered intrusive complex and consists of strongly deformed rocks in the Tasiyuyaksuk sheet, Anaktalik lower sheet and the Anaktalik upper sheet. The Tasiyuyaksuk sheet was cut by weakly deformed rocks of the Lister pluton border zone and was therefore deformed in north-south shear zone #1 prior to emplacement of the Lister pluton (Fig. 8.3). The Anaktalik lower and upper sheets are younger than the Lister pluton border

zone, indicating that the Anaktalik sheets were deformed in north-south shear zone #1 after emplacement of the Lister pluton. These findings indicate that north-south shear zone #1 was: (a) periodically activated, and (b) was active before and after emplacement of the Lister pluton.

North-south shear zone #1 lies adjacent to and strikes parallel to the Paleoproterozoic and/or Archean rocks of the Anaktalik Brook country rock belt (Figs. 5.4, 5.40). The rock types and structure of this country rock belt suggest that it is a Paleoproterozoic structure, thereby indicating that north-south shear zone #1: (a) lies adjacent to a Paleoproterozoic structure, and (b) was deformed parallel to a Paleoproterozoic structure. A study by Royse and Park (2000) found a similar relation between deformed plutonic rocks of the Nain batholith and Paleoproterozoic structures, and suggested that Mesoproterozoic shear zones were developed on re-activated Paleoproterozoic structures. Similarly, north-south shear zone #1 may have been developed on a re-activated Paleoproterozoic structure.

The Anaktalik Brook country rock belt was also intruded by the Hare Hill monzonite (1351 +/- 3 Ma in Ryan and James, 2003) that lies ~500 m west of the Tasiyuyaksuk sheet (Fig. 5.4). Strongly deformed layers in the Hare Hill monzonite strike parallel to strongly deformed rocks in the Tasiyuyaksuk sheet and to layering in the Anaktalik Brook country rock belt (Myers, pers. com., 2000). These relations suggest that the Hare Hill monzonite was also deformed in north-south shear zone #1, and that this shear zone was active after 1351 Ma.

Geological maps by Wheeler (1969), Ryan (1990) and Ryan and James (2003) show that the rocks that are here grouped into the Anaktalik Brook country rock belt are lithologically and structurally continuous north of the study area (see Fig. 8.2). This northward continuation of country rock is bound by the Pearly Gates intrusion (Susie Brook Slab in Morse, 1981b) to the west. Mapping by Morse (1981b) described layered anorthositic rocks in the Pearly Gates intrusion as deformed, steeply (70°) east dipping and north-south striking. Morse (1981b) suggested that these deformed rocks were developed during syn-plutonic, north-south, extension. The orientation of these deformed rocks described by Morse (1981b) is parallel to strongly deformed rocks in north-south shear zone #1, suggesting that this shear zone is continuous north of the study area.

The northern extent of north-south shear zone #1 is cut by a composite intrusion of monzonite and ferrodiorite (unit 19 in Ryan and James, 2003; unit 41 in Ryan and James, 2004). Ryan and James (2003, p. 153) suggested that this intrusion was emplaced into strongly deformed anorthosite and that "even though this unit has a planar fabric...the fabric seems to be a magmatic alignment...rather than a penetrative foliation and lineation". As well, Ryan and James (2003, p. 153) suggested that these fabrics are "less intense than those exhibited by...Hare Hill". U-Pb isotopes show that zircons in this monzonite intrusion crystallized at 1333 +/- 3 Ma (in Ryan and James, 2004; see Fig. 8.2). These relations indicate that some of the strongly deformed rocks that comprise part of north-south shear zone #1 were overprinted by deformation between 1351 +/- 3 Ma and 1333 +/- 3 Ma.

8.2.1.ii North-south shear zone #2

North-south shear zone #2 occurs in the eastern margin of the Tikkoatokak centered intrusive complex (see Figs. 8.1, 8.2) and consists of strongly deformed rocks in the Kangilialuk sheet and the Lister pluton border zone. The Kangilialuk sheet contains igneous zircons that crystallized at 1341 +/- 4 Ma. The Lister pluton border zone shows sigmoidal structures in anorthositic rocks and splay structures in pyroxene-rich veins that indicate the border zone was overprinted by dextral shear deformation. The contact between the Kangilialuk sheet and the Lister pluton border zone is tectonic and indicates these two units were deformed together. These findings indicate dextral shear deformation in north-south shear zone #2 after 1341 +/- 4 Ma (Fig. 8.4).

North-south shear zone #2 lies adjacent and strikes parallel to Paleoproterozoic and/or Archean rocks in the Kangilialuk Lake country rock belt. The rock types and structure of this country rock belt suggest that it is a Paleoproterozoic structure. These findings indicate that north-south shear zone #2: (a) lies adjacent to a Paleoproterozoic structure, and (b) was deformed parallel to a Paleoproterozoic structure, suggesting that north-south shear zone #2 was developed on a re-activated Paleoproterozoic structure.

The strongly deformed rocks in the Lister pluton border zone were cut by broadly sub-vertical and northwest-southeast striking dikes (see Map 1). Ryan and James (2003) found that some of these dikes crystallized ca. 1328 Ma, indicating that dextral shear deformation in north-south shear zone #2 occurred between 1341 +/- 4 and ca. 1328 Ma (see Fig. 8.4).

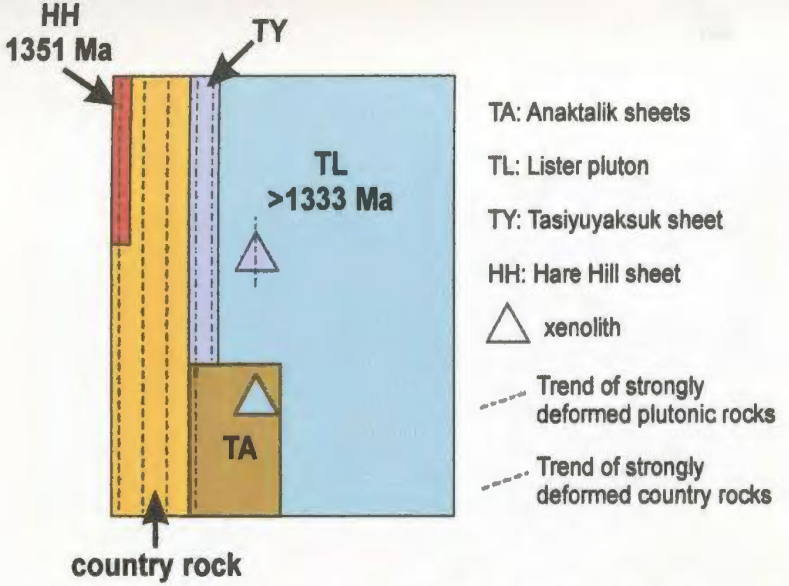

Figure 8.3: Schematic sketch showing the field and age relations of units in north-south shear zone #1. This shear zone was active during and/or after 1351 Ma.

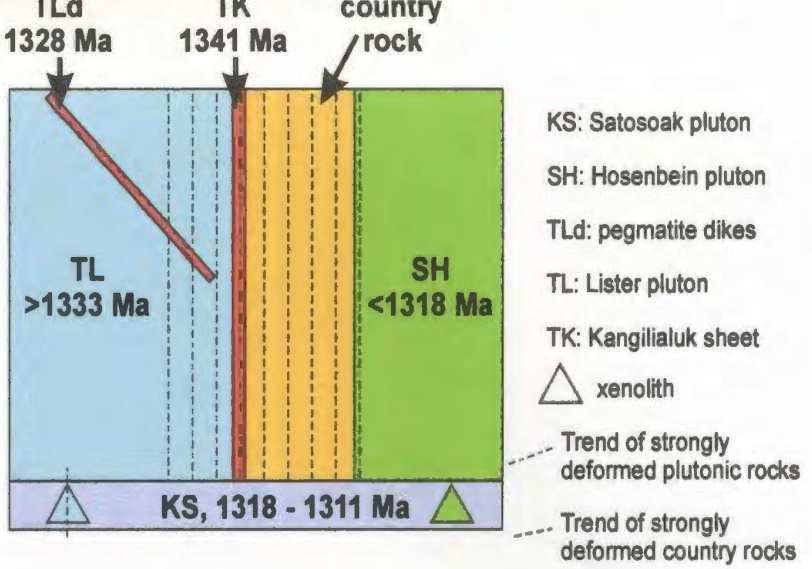

Figure 8.4: Schematic sketch showing the field and age relations of units in north-south shear zone #2. This shear zone was active between 1341 and 1328 Ma, and between 1318 and 1311 Ma.

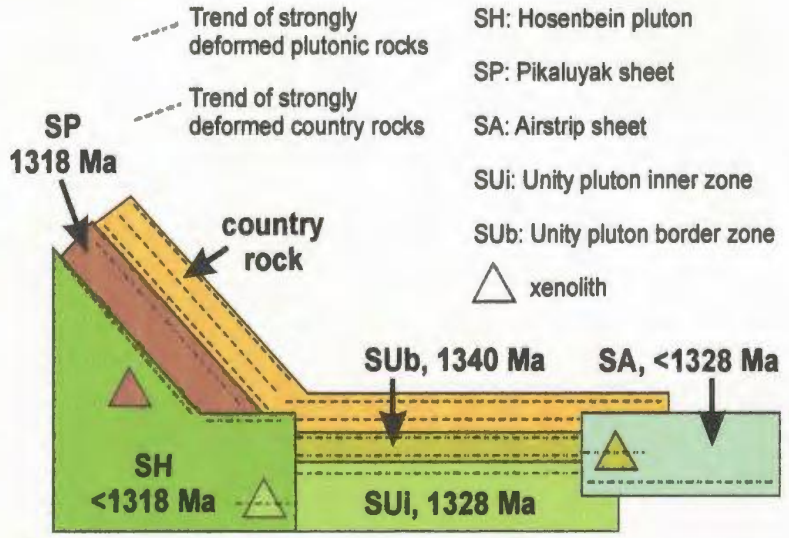

Figure 8.5: Schematic sketch showing the field and age relations of units in east-west shear zone #1. This shear zone was active between 1340 and 1318 Ma, and after emplacement of SA and SH.

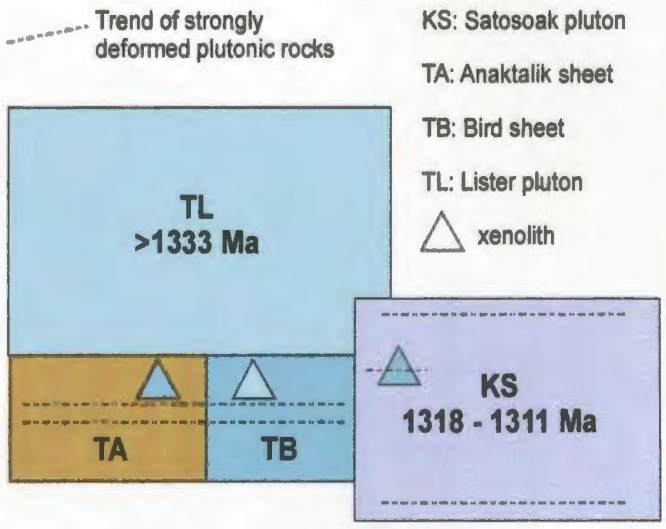

Figure 8.6: Schematic sketch showing the field and age relations of units in east-west shear zone #2. This shear zone was active before and after emplacement of the Satosoak pluton (1318 - 1311 Ma).

The Hosenbein pluton lower border zone (<1318 +/- 7 Ma) contains strongly deformed rocks that are moderately east dipping to sub-vertical and broadly north-south striking. These strongly deformed rocks lie ~200 – 600 m east of, and strike parallel to, strongly deformed plutonic rocks in the Kangilialuk sheet, plutonic rocks in the Lister pluton border zone and country rocks in the Kangilialuk Lake country rock belt. Therefore, the orientation of strongly deformed rocks in the Hosenbein pluton lower border zone suggests that they may comprise part of north-south shear zone #2 (see Figs. 8.1, 8.4). These strongly deformed rocks were developed after ca. 1318 Ma, thereby suggesting episodic displacement on north-south shear zone #2 between: (1^{st}) 1341 and 1328 Ma, and (2^{nd}) after 1318 Ma.

Geological maps by Wheeler (1969) and Ryan (2000a; 2001a) show that the country rock that is here grouped into the Kangilialuk Lake country rock belt is lithologically and structurally continuous north of the study area (see Fig. 8.2). This northward continuation of country rock is bound by the Tikkoatokak centered intrusive complex in the west. Studies by Ryan (2000, 2001a) and Royse and Park (2000) found that the eastern margin of the Tikkoatokak centered intrusive complex (Lister pluton, Kangilialuk sheet) contains strongly deformed rocks that are broadly sub-vertical and north-south striking. Royse and Park (2000) suggested that these strongly deformed rocks were formed in a dextral ductile shear zone. These strongly deformed rocks are structurally continuous with those in north-south shear zone #2, and show displacement that was also parallel to that in north-south shear zone #2. These findings suggest that north-south shear zone #2 is continuous for over 30 km due north of the study area.

8.2.1.iii East-west shear zone #1

East-west shear zone #1 occurs in the northern margin of the Sophie centered intrusive complex (see Figs. 8.1, 8.5) and consists of strongly deformed rocks in the Unity pluton, Airstrip sheet, Pikaluyak sheet and the Hosenbein pluton upper border zone. Igneous zircons crystallized at 1340 +/- 3 Ma in the Unity pluton border zone, 1328 +/- 5 Ma in the Unity pluton inner zone and 1318 +/- 7 Ma in the Pikaluyak sheet. The Airstrip sheet contains strongly deformed xenoliths of the Unity pluton. The Hosenbein pluton also contains strongly deformed xenoliths of the Unity pluton and weakly deformed xenoliths of the Pikaluyak sheet. In addition, the Hosenbein pluton was cut by the Satosoak pluton (minimum age of 1311 +/- 2 Ma). These relations indicate that the plutonic rocks in east-west shear zone #1 were: (a) periodically deformed, and (b) deformed between 1340 +/- 3 and 1311 +/- 2 Ma (Fig. 8.5).

East-west shear zone #1 lies adjacent to Paleoproterozoic and/or Archean rocks of the Nain Hill country rock belt. Compositional layers within the eastern part of this country rock belt are steeply north dipping and east-west striking. Further west, layers in this country rock belt rotate into a moderately east dipping and north-south striking orientation. The eastern part of this belt is therefore parallel to Paleoproterozoic structures whereas the western part is strongly discordant to Paleoproterozoic structures. Rubins (1973) suggested that the structure of the Nain Hill country rock belt comprises: (a) two zones or layers of country rock that were separated by intrusion of anorthositic rocks, or (b) two zones that are the limbs of a fold with its hinge to the north. An alternative explanation for the structure of this country rock belt is that Paleoproterozoic

structures in the west were rotated into Mesoproterozoic east-west shear zone #1. The form of the Nain Hill country rock belt suggests that this Paleoproterozoic structure was rotated into a sinistral shear zone, which is consistent with sigmoidal structures observed in strongly deformed plutonic rocks.

The Lister pluton inner zone was cut by sub-vertical, east-west striking, pink to red colored, granitic rocks that were emplaced and deformed in shear zones (Figs. 8.1, 5.23). These granitic veins are structurally continuous with a ~15 km westward extrapolation of east-west shear zone #1. Morse (1981c) found east-west striking granitic veins that cut the Lister pluton to the north of the study area, and grouped these granitic veins into a 'pink shearing event'. Morse (1981c) suggested that this pink shearing event occurred between emplacement of the Lister (old anorthosite event in Morse, 1981c) and Kiglapait intrusions (1306 +/- 2 Ma in Miller et al., 1997). A similar interpretation is favored for granitic veins in the study area, and suggests that east-west shear zone #1 is structurally continuous west of the Nain Hill country rock belt.

8.2.1.iv East-west shear zone #2

East-west shear zone #2 occurs in the southern margin of the Tikkoatokak centered intrusive complex (see Fig. 8.1) and consists of strongly deformed rocks in the Bird sheet and Anaktalik lower sheet. These sheets were emplaced after the Lister pluton, whereas the Bird sheet was emplaced and deformed prior to emplacement of the Satosoak pluton (between 1318 +/- 7 and 1311 +/- 2 Ma). These relations indicate that east-west

shear zone #2 produced strongly deformed rocks: (a) after emplacement of the Bird sheet (>1311 +/- 2 Ma), and (b) prior to 1318 +/- 7 or 1311 +/- 2 Ma (Fig. 8.6).

Geological mapping as part of this study found that the northern arm of Anaktalik Bay is mostly underlain by the Satosoak pluton. The border zone of this pluton contains strongly deformed rocks that are moderately south dipping to sub-vertical and east-west striking. In addition, the inner zone of this pluton contains Fe-rich dioritic dikes and granitic veins that were emplaced under sub-horizontally oriented east-west and north-south directed stresses. These strongly deformed rocks, dikes and veins are structurally continuous with an eastward extrapolation of east-west shear zone #2 (see Fig. 8.1). For this reason, it is suggested that east-west shear zone #2 was periodically activated during: (1^{st}) deformation in the southern margin of the Tikkoatokak centered intrusive complex and (2^{nd}) deformation of, as well as dike and vein emplacement in, the Satosoak pluton.

8.2.2 Regional correlations and tectono-magmatic setting

Findings from this study and previously published field descriptions and U-Pb ages suggest that north-south ductile shear zone #1 was active between 1351 and 1333 Ma, and north-south ductile shear zone #2 was active: (1^{st}) between 1341 and 1328 Ma, and (2^{nd}) after 1318 Ma. A study by Cadman et al. (1999) found tholeiitic dikes that were emplaced, deformed and strongly rotated into north-south shear zones at 1328 +/- 2 and 1316 +/- 2 Ma. These findings indicate that a sub-vertical and north-south striking episode of shear deformation overprinted plutonic rocks of the Nain batholith between 1351 and 1316 Ma. This episode of north-south oriented deformation is also consistent

with field studies by Berg and Briegel (1981) and Morse (1981c) that suggested deformed plutonic rocks in the Nain batholith developed during north-south extension. As well, these findings are consistent with a study by Royse and Park (2000) that suggested parts of the Nain batholith were deformed on re-activated Paleoproterozoic structures.

Findings from this study indicate that east-west ductile shear zone #1 was periodically active between 1341 and 1311 Ma and that east-west shear zone #2 was active after emplacement of the Lister pluton and before 1311 Ma. A study by Evans-Lamswood et al. (2000) on the Voisey's Bay intrusion (1333 +/- 1 Ma, Amelin et al., 1999), which lies ~15 km south of the study area, suggested that two chambers of this intrusion were connected by a conduit that was structurally controlled by a moderately south dipping to sub-vertical and east-west striking structure. Several studies (Wiebe, 1985b; Cadman et al., 1999) have described basaltic dikes that were emplaced into upper crustal and/or brittle east-west fractures shortly after the Nain batholith was emplaced. A Rb-Sr dating study by Carlson et al. (1993) found that these east-west striking dikes were emplaced at 1276 +/- 23 Ma. These new and previously published findings indicate that moderately south dipping to sub-vertical, east-west striking, structures were periodically active between 1341 and 1276 Ma. These east-west structures: (a) produced deformed rocks in the margins of centered intrusive complexes, and (b) controlled the ascent and emplacement of magma.

Berg (1977a) suggested that the Nain batholith was emplaced into a crustal-scale graben, whereas Yu and Morse (1993) suggested that the Nain batholith was emplaced

into an aborted rift zone. The paleo-isobars presented by Berg (1977a) indicate that this graben is broadly northwest-southeast striking (Fig. 8.7). In addition, Morse (1981c) and Berg and Briegel (1981) suggested that the Nain batholith was emplaced during north-south extension of the crust. These studies suggest that emplacement of the Nain batholith was contemporaneous with graben development and extension.

Hill (1982) mapped peralkaline volcanic rocks in the southeastern part of the Nain batholith and suggested that the Nain batholith was uplifted shortly after emplacement. Subsequent U-Pb dating of these peralkaline rocks (1289 Ma in Miller et al., 1997) supports the interpretation of Hill (1982). Wiebe (1985b) found that basaltic dikes in the Nain batholith crystallized at upper crustal levels and thereby also suggested that the Nain batholith was uplifted shortly after emplacement. Subsequent dating of these basaltic dikes (1276 +/- 26 Ma, Carlson et al., 1993) supports the interpretation of Wiebe (1985b). These studies suggest that emplacement of the Nain batholith was followed soon afterwards by crustal uplift.

The continental crust of present day Labrador comprised part of Laurentia in the Proterozoic (see Rivers, 1997; Rivers and Corrigan, 2000). Studies by Rivers (1997) and Rivers and Corrigan (2000) suggested that the southeastern margin of Laurentia comprised an active continental margin at 1500 – 1230 Ma (in Rivers and Corrigan, 2000). Rivers (1997) and Rivers and Corrigan (2000) suggested that Proterozoic anorthositic-granitic batholiths might comprise back-arc magmatic products that were related to this margin. The span of U-Pb ages obtained for the Nain batholith (1365 – 1270 Ma) overlaps with activity associated with this continental-magmatic arc (1500 –

1230 Ma), suggesting that the Nain batholith may also have been emplaced into this back-arc. In addition, the crustal uplift that immediately followed emplacement of the Nain batholith may have been the result of back-arc compression, which affects back-arc basins up to ~1600 km inboard from active continental margins (see Ziegler et al., 1998).

Several workers (Wheeler, 1972b; Buchan et al., 2001; Upton et al., 2003) have suggested that Labrador was linked to Greenland in the Mesoproterozoic. Upton (1973) and Wiebe (1985b) found that the east-west and north-south striking basaltic dikes that cut the Nain batholith (1273 +/- 26 Ma, in Carlson et al., 1993) are of similar composition to those in the Gardar Province of southwestern Greenland. The basaltic dikes in the Gardar Province contain xenoliths of anorthosite that were likely derived from anorthositic intrusions that are related to those presently exposed in Labrador (Upton et al., 2003). The oldest of these basaltic dikes are sub-vertical and east-west striking (Piper, 1995). In addition, Buchan et al. (2001) and Upton et al. (2003) describe an episode of lithospheric thinning and graben development in the Gardar Province at 1350 – 1140 Ma. This episode of thinning overlaps with emplacement of the Nain batholith between 1365 – 1270 Ma. The findings from this study and those of previous workers indicate that east-west shear zones in the Nain batholith were contemporaneous with lithospheric thinning and graben development in the Gardar Province.

To summarize, integration of new and previous studies on the Nain batholith with those elsewhere in Labrador and in western Greenland suggest that emplacement of the Nain batholith (1365 – 1270 Ma) was associated with: (a) north-south shear deformation (between 1351 and 1316 Ma), (b) east-west shear deformation (between 1341 and 1311

Ma), (c) back-arc extension (1500 – 1230 Ma), (d) lithospheric thinning and graben development (1350 – 1140 Ma), and (e) crustal uplift (1290 – 1276 Ma). Subsequent sections in this discussion suggest that crustal uplift also occurred during emplacement of the Nain batholith.

The crustal-scale graben that hosts the Nain batholith, as determined from the paleo-isobars of Berg (1977a), is oriented in a northwest-southeast direction. Assuming that the orientation of this graben was parallel to the maximum principal extensional stress, then the north-south and east-west oriented shear zones in the Nain batholith may represent resolved stress vectors that developed on: (a) crustal weaknesses (i.e. Paleoproterozoic structures), and (b) Mesoproterozoic structures that were broadly perpendicular to these weaknesses (Fig. 8.7). The next section of this discussion suggests that older intrusions in the Nain batholith were predominantly emplaced along crustal weaknesses (north-south shear zones), whereas younger intrusions were emplaced along Mesoproterozoic structures (east-west shear zones).

8.3 Emplacement of centered intrusive complexes

This section of the discussion described a model for the ascent and emplacement of anorthositic magmas that formed the centered intrusive complexes in the study area. Many workers (Buddington, 1969; Mitchell et al., 1996; Bhattacharya et al., 1998; Dempster et al., 1999) have concluded that anorthositic magmas were formed by the accumulation of plagioclase crystals into a fractionating basaltic magma at depth, and that these magmas were transported and emplaced with high abundances of plagioclase

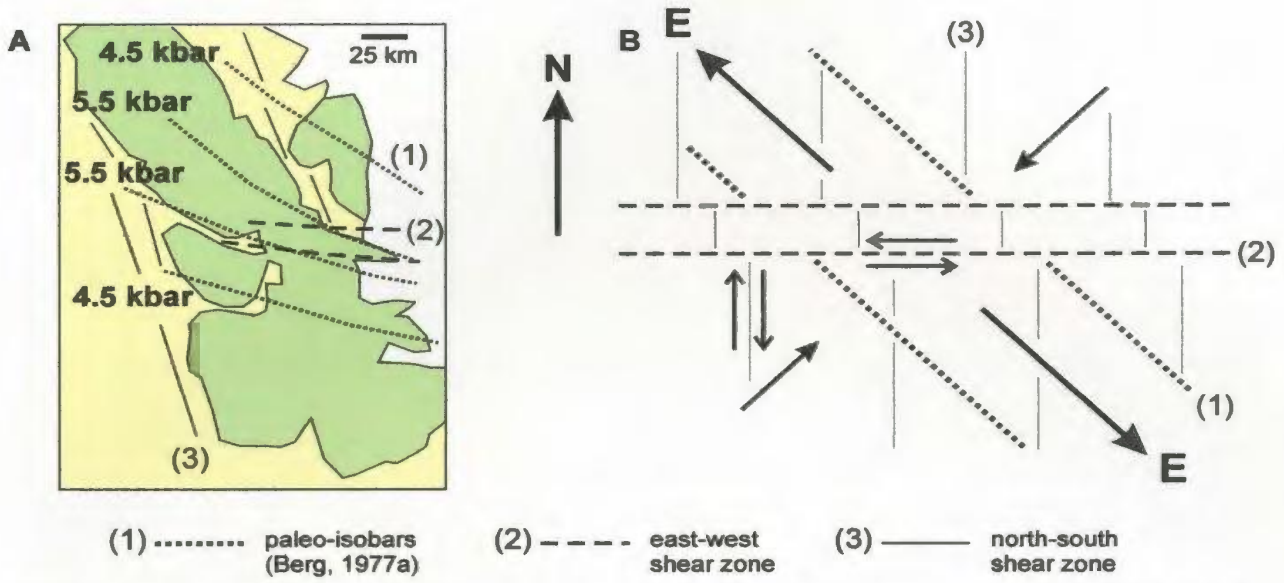

Figure 8.7: Plan view of (A) the Nain batholith and (B) a simplifed tectono-magmatic setting of the Nain batholith. Both plan views show: (1) the paleo-isobars of Berg (1977a), (2) Mesoproterozoic east-west shear zones, and (3) Mesoproterozoic north-south shear zones and structures. Plan view (B) suggests that, in the time period between 1365 and 1270 Ma, east-west sinistral and north-south dextral shear zones may have been generated by northwest to southeast directed extension (E) that trends parallel to the paleoisobars of Berg (1977).

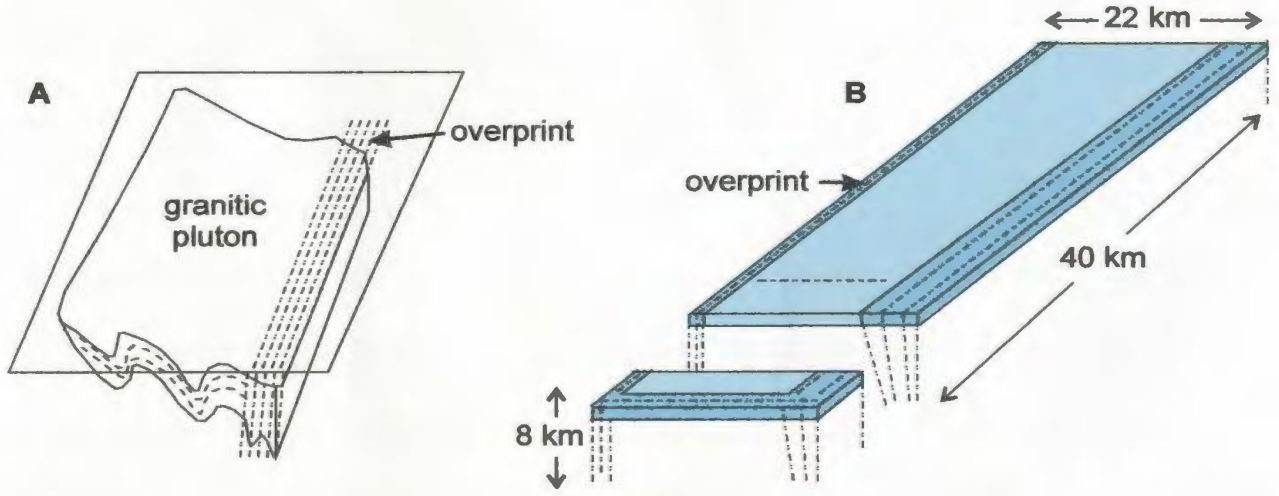

Figure 8.8: Comparison of models for (A) a granitic pluton from Brazil and (B) the Tikkoatokak centered intrusive complex. Both intrusive bodies show a tectonic overprint (dashed lines) in the margin. For the granitic pluton, Neves et al. (2003) suggested that this overprint developed by sub-solidus transcurrent movement along the same sub-vertical structure that fed the intrusion (after Neves et al., 2003).

crystals. Magmas with high contents of solids show high viscosity, which has probably led many workers (see Woussen et al., 1981; Duchesne, 1984; Scoates, 1990; Wiebe, 1990a; 1992, p. 228; Mitchell et al., 1995; 1996; Bhattacharya et al., 1998; Barnichon et al., 1999; Dempster et al., 1999; Mukherjee et al., 1999) to suggest that the ascent and emplacement of anorthositic magmas occurred in diapirs. This section presents some alternatives to diapiric ascent by comparing the structure of centered intrusive complexes in this study area to previously published studies on the structure of granitic intrusions. It is suggested below that granitic magmas are suitable analogues for anorthositic magmas. In addition, this section describes how the chronological evolution of intrusion forms in the study area shows that the emplacement of the Nain batholith was contemporaneous with crustal uplift.

8.3.1 Granitic magmas as analogues for anorthositic magmas

Viscosity and density are two important physical characteristic of magma. Magmas with relatively low viscosity exhibit liquid-state behavior, and likely underwent processes such as fracture-controlled transport and magmatic convection. Magmas with relatively high viscosity and low density are more suitable candidates for diapiric ascent, and probably convected at relatively slow rates (or not at all) in comparison to lower viscosity magmas. This section compares the viscosity and density of granitic and basaltic magmas, and suggests that granitic magmas, as opposed to basaltic magmas, are the most suitable analogues for anorthositic magmas.

End-member examples of low and high viscosity magmas are basaltic and granitic magmas. The viscosity of basaltic magmas typically ranges from 10^1 to 10^4 Pa*s at temperatures of ~1200-1000 °C. In contrast, the viscosity of a rhyolitic magma with ~1 wt% H_2O ranges from 10^6 to 10^7 Pa*s between 1200-1000 °C. Magmas with a viscosity of $<10^4$ Pa*s correspond to magmas with <25% crystals (see Fig. 1.1), whereas those with viscosity between 10^6 to 10^7 Pa*s correspond to magmas that contain between 40 and 50% crystals. The magmas parental to Proterozoic anorthositic rocks are estimated to have contained between 20 and 70% crystals (see Chapter 1). An intermediate abundance of ~40-50% plagioclase crystals corresponds to a viscosity that is most like a granitic (or rhyolitic) magma.

Density estimates for anorthosite magmas range from 2.6 – 2.75 g/cm^3, which is analogous to the density range of intermediate plagioclase (2.55 – 2.65 g/cm^3) and granitic rocks (2.6 – 2.8 g/cm^3) (Barnichon et al., 1999; Royse and Park, 2000). Mafic magmas are much denser, showing ranges of 2.7 – 3.1 g/cm^3 for basaltic rocks and 2.95 – 3.0 g/cm^3 for ferrodiorite (Royse and Park, 2000; Leitch, 2003). The density range for anorthositic rocks is therefore similar to that of granitic rocks.

The viscosity and density of the magmas that produced anorthositic rocks are therefore more like those of granitic (or rhyolitic) magmas then basaltic magmas. Hence, transport, emplacement and crystallization analogues for the anorthositic magmas are probably best gleaned from those developed for the granitic and rhyolitic magmas.

8.3.2 Tectonic controls on ascent

The margins of all centered intrusive complexes in the study area contain strongly deformed rocks that were developed in Mesoproterozoic ductile shear zones. Gleizes et al. (1998) suggested that the same tectonic movements that controlled the ascent and emplacement of granitic magma produced 'corridors' of high-T solid-state shear deformation in granitic plutons. Neves et al. (2003) suggested that groups of high-T tectonic structures in plutons represent the trace of the vertical conduits that fed the pluton. Applying a similar interpretation to this study suggests that the strongly deformed rocks in the margins of centered intrusive complexes were produced by the same tectonic structures that controlled the ascent and emplacement of magma. These tectonic structures are sub-vertically oriented, north-south or east-west striking, shear zones.

The north-south shear zones that bound centered intrusive complexes in the study were likely developed on re-activated Paleoproterozoic structures. These Paleoproterozoic structures developed during the collision of the North Atlantic and Rae cratons (see Mengel and Rivers, 1989; 1997; Rivers et al., 1996). A seismic and gravity study by Funck et al. (2000) showed that structures in the North Atlantic and Rae cratons are preserved down to the Moho, thereby suggesting that the Paleoproterozoic collisional zone extends down to the Moho. The Paleoproterozoic structures that bound centered intrusive complexes in the study area are therefore crustal scale-structures that could have acted as conduits for the transport of magma from the source area to the emplacement level. This interpretation is consistent with numerous studies (Brown et al., 1995; Cambray et al., 1995; Ferre et al., 1997; Gleizes et al., 1998; Duchesne et al., 1999) that

have suggested links between the emplacement of magma and transcurrent movement on crustal scale shear zones. In addition, plutonic rocks of the Nain batholith were emplaced during an episode of lithospheric backarc extension that would have promoted: (1^{st}) melting in the vicinity of shear zones at depth, and (2^{nd}) "sucking" of magmas into shear zones (see Ferre et al., 1997). Similarly, Hutton and Reavy (1992, p. 960) suggested that "individual transcurrent shear zones may not only control the ascent paths, sitting and emplacement mechanics of plutons, but they may also cause the genesis of the (plutons) themselves".

The margin of the Mesoproterozoic Tikkoatokak centered intrusive complex is bound by Mesoproterozoic north-south shear zones #1 and #2 (see Fig. 8.1), and contains Mesoproterozoic east-west shear zone #2. The margin of the Mesoproterozoic Sophie centered intrusive complex is bound by Mesoproterozoic east-west shear zone #1 and Mesoproterozoic north-south shear zone #2. The planar deformation fabrics in the Kikkertavak intrusive complex are structurally continuous with those in Mesoproterozoic east-west shear zone #2. Vauchez and Neves (1997) suggested that a spatial association (restriction in Vauchez and Neves, 1997) between plutonic rocks and contemporaneous shear zones is suggestive of shear-zone associated melt transport and emplacement (Fig. 8.8). Similarly, the spatial and temporal association between centered intrusive complexes and shear zones suggests shear-zone associated melt transport and emplacement.

The Tasiyuyaksuk sheet is broadly sub-vertically oriented and north-south striking, and lies parallel to the trend of north-south shear zone #1. The Kangilialuk sheet,

eastern Lister pluton border zone and Hosenbein pluton lower border zone are also broadly sub-vertically oriented and north-south striking, and lie parallel to the trend of north-south shear zone #2. The Unity pluton border zone, Pikaluyak sheet, Airstrip sheet and Hosenbein pluton upper border zone are broadly sub-vertically oriented and east-west striking, and lie parallel to the trend of east-west shear zone #1. The Bird sheet, Anaktalik lower sheet, Anaktalik upper sheet and Satosoak pluton are moderately south dipping and east-west striking, and lie parallel to east-west shear zone #2. It is suggested, following a study by Vauchez and Neves (1997), that a space-time association and alignment of plutonic units and shear zones is suggestive of shear-zone associated melt transport and emplacement.

The southwestern corner of the Tikkoatokak centered intrusive complex and the northwestern corner of the Kikkertavak centered intrusive complex lie at the intersection of north-south shear zone #1 and east-west shear zone #2 (see Fig. 8.1). In the Tikkoatokak centered intrusive complex, the Anaktalik sheet is deformed in both north-south shear zone #1 and east-west shear zone #2. This suggests that both these shear zones were active after the Anaktalik sheet was emplaced and may have been active at the same time. The southeastern corner of the Tikkoatokak centered intrusive complex lies at the intersection of north-south shear zone #2 and east-west shear zone #2. The northwestern corner of the Hosenbein pluton (Sophie centered intrusive complex) lies at the intersection of north-south shear zone #2 and east-west shear zone #1. The Hosenbein pluton contains rocks that were deformed in both of these shear zones, suggesting they may have been active at the same time. There are several studies (Rahaman et al., 1984;

Moreau et al., 1994; Dehls et al., 1998; Smoot, 1999) that suggest that intersecting sets of sub-vertical crustal-scale fractures (and/or shear zones) may control the ascent and emplacement of magma.

Xenoliths of strongly deformed plutonic rocks occur in weakly deformed plutonic rocks of the Lister pluton border zone, Bird sheet, Anaktalik sheet, Airstrip sheet, Hosenbein pluton border zones and the Satosoak pluton border zone. These rocks were deformed prior to emplacement of younger magmas, and indicate a tectono-magmatic setting that featured intermittent deformation and magma emplacement. The xenoliths comprise an earlier magma pulse that ascended along a shear zone. If parts of this earlier pulse were retained in the shear zone they would likely have been deformed after the shear zone closed. It is inferred that these deformed rocks were entrained as xenoliths when the shear zone re-opened in order to allow a younger pulse of magma to pass through. Similarly, a study by Vauchez and Neves (1997) suggested that shear-zone associated melt transport and emplacement may be indicated by xenoliths of deformed plutonic rocks that occur in weakly deformed plutonic host rocks.

Centered intrusive complexes in the study area: (a) are bound by ductile shear zones that strike parallel to regional structures, (b) are elongate parallel to ductile shear zones, (c) are structurally controlled at the intersections of ductile shear zones, and (d) contain xenoliths of strongly deformed plutonic rocks. These features are all characteristic of shear zone assisted melt transport and emplacement, and suggest that the anorthositic, gabbronoritic, monzonitic and Fe-rich gabbroic magmas that formed the

centered intrusive complexes were transported along sub-vertically oriented, north-south and east-west striking, shear zones.

8.3.3 Emplacement of magma

The emplacement of magma features a change from sub-vertically oriented flow to sub-horizontally oriented flow. In general, possible factors that help to determine emplacement include: (a) magmas that attain a level of neutral, or negative, buoyancy with respect to the host rocks, (b) intersection of a self-propagating dike with a highly ductile zone (shale, limestone), water-saturated zone, structurally isotropic zone or a freely slipping fracture, and (c) the Cook-Gordon mechanism (see Clemens and Mawer, 1992). The Cook-Gordon mechanism suggests that a fracture-parallel tensile stress, which is always associated with a self-propagating dike, will act to 'open' horizontal discontinuities (bedding planes, unit contacts) prior to the arrival of a self-propagating dike (see Clemens and Mawer, 1992). In the Nain batholith, the Kiglapait intrusion was emplaced at a contact between Archean gneiss and Paleoproterozoic cover rocks (Morse, 1969), suggesting that a sub-horizontal structure in the crust may have played some role in the emplacement of this intrusion. In the study area, however, only the country rock that occurs along the walls of centered intrusive complexes is preserved. Sub-horizontal discontinuities, if present, are therefore no longer preserved. The structures of these complexes, however, allow inferences to be made about the emplacement mechanisms and the rheology of the crust at the time of emplacement.

The Tikkoatokak centered intrusive complex consists of a sub-horizontal core that is enveloped by an outward dipping margin. The core extends for 40 km in a north-south direction, 20 km in an east-west direction and is a minimum of 1 km thick (Fig. 8.9). The margin is outward dipping with respect to the core and thereby defines an elongate bell-jar form for the Tikkoatokak centered intrusive complex (Fig. 8.10). Shear zones that assisted in the transport and emplacement of magma ('feeder zones') are located along the eastern, western and southern margins. Downward extrapolation of these feeder zones indicates that they do not coalesce into a single feeder zone at depth and thereby indicate at least two, and possibly three (east-west shear zone #2), separate feeder zones. A study by Ameglio et al. (1997) found that large flat-floored plutons have several feeder zones that indicate emplacement into ductile crust during extensional tectonics. A similar interpretation is favored for the Tikkoatokak centered intrusive complex. In addition, Petford et al. (2000) suggested that mid-crustal bell-jar plutons are emplaced by floor depression. Emplacement of the Tikkoatokak centered intrusive complex by floor depression is consistent with the composite structure and bell-jar form. Sub-vertical movement of crust during floor depression was most likely accommodated on the same sub-vertical fractures that fed the intrusion (see Dehls et al., 1998). For the Tikkoatokak centered intrusive complex, the younger magmas enveloped the older magmas as shown in Fig. 8.10. On the other hand, U-Pb isotope studies by Tettelaar (2005) show that older monzonitic and Fe-rich dioritic rocks (ca. 1365-1355 Ma) envelop younger anorthositic rocks (ca. 1345-1340 Ma) of the Pearly Gates pluton. Either way, the form of the

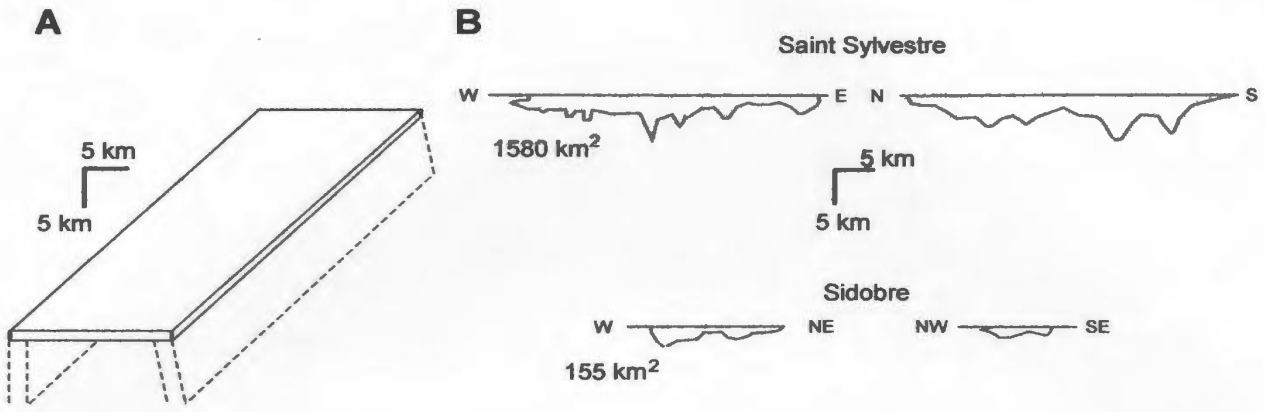

Figure 8.9: Comparison of (A) the exposed part of the Tikkoatokak centered intrusive complex with (B) gravity surveys through two granite batholiths in France and Spain (from Ameglio et al., 1997). The batholiths shown are relatively thin, extend largely in every horizontal direction and show several root (or feeder) zones. Ameglio et al. (1997) interpret these forms as indicating emplacement into ductile crust during extensional tectonics.

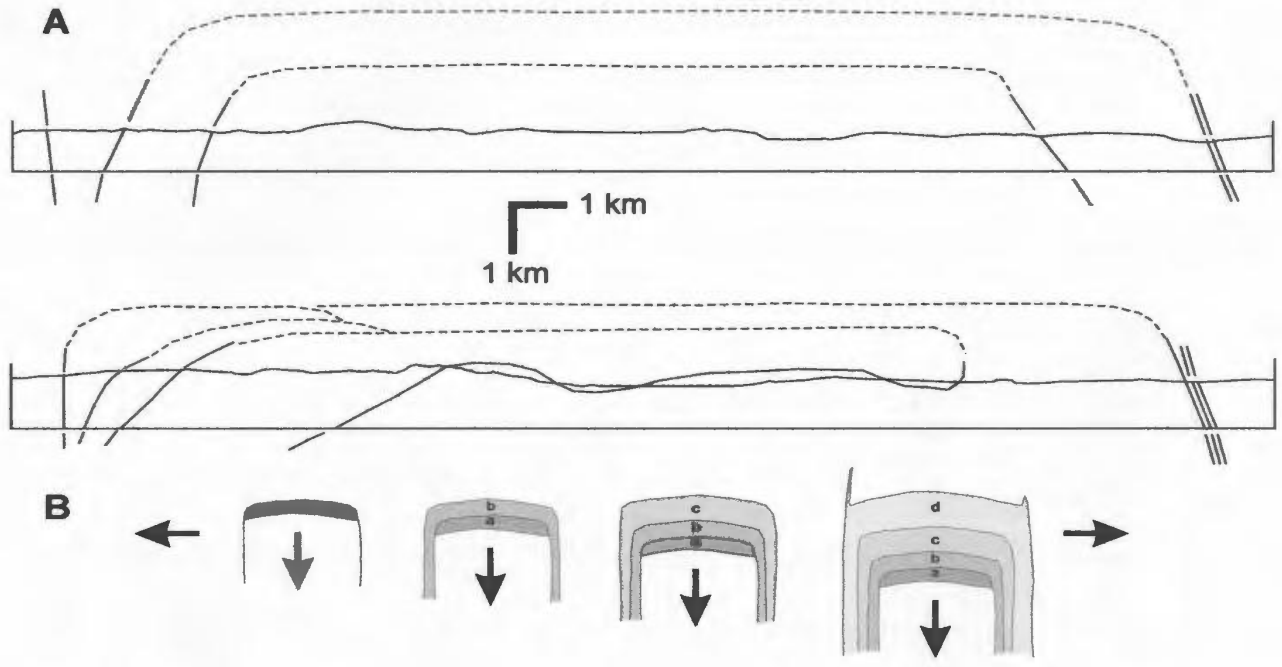

Figure 8.10: Comparison of (A) a cross-sections through the Tikkoatokak centered intrusive complex (see Fig. 5.3) and (B) a time-elapsed cross-section through a pluton emplaced by floor depression with cauldron subsidence. Figure (B) shows pluton growth by the successive emplacement of sheets (a)-(d) during sub-horizontal crustal extension and floor depression (adapted from Myers, 1975).

Tikkoatokak centered intrusive complex may therefore be linked to emplacement into ductile crust during: (a) extension and (b) floor depression.

The Satosoak pluton is the most completely exposed pluton in the northwestern part of the Kikkertavak centered intrusive complex. The Satosoak pluton is 20 km long, 2 – 10 km wide and a minimum of 300 m thick. The pluton is bowl-shaped in cross-section (Fig. 8.11). Shear zones that assisted in the transport and emplacement of magma ('feeder zones') occur in the Satosoak pluton border zone. Downward extrapolation of these feeder zones indicates that they may coalesce at depth. Ameglio et al. (1997) found that wedge-shaped plutons that are elongated in one direction and contain few root (feeder) zones were likely emplaced into dilating volumes of brittle crust during transcurrent tectonics.

The Sophie centered intrusive complex contains the Unity and Hosenbein plutons. The Unity pluton shows a strongly deformed northern margin (Figs. 6.3, 6.16). Although much of the Unity pluton is no longer exposed, it is suggested that this pluton was also emplaced into ductile crust because: (a) it was one of the earlier intrusions (1340 +/- 3, 1328 +/- 5 Ma), like the Tikkoatokak centered intrusive complex, emplaced into the Nain batholith (1365 – 1270 Ma), (b) it was emplaced near the Tikkoatokak centered intrusive complex, and (c) it has a margin that was strongly deformed in a ductile shear zone. The Hosenbein pluton (maximum age of 1318 Ma, minimum age of 1311 Ma) was emplaced ~10 – 20 m.y. after the Unity pluton and Tikkoatokak centered intrusive complex, and within ~10 m.y. of the Satosoak pluton. The Hosenbein pluton is sub-equant in plan view (Fig. 6.1) and bowl-shaped in cross-section (see Fig. 8.11). The bowl-shaped cross-

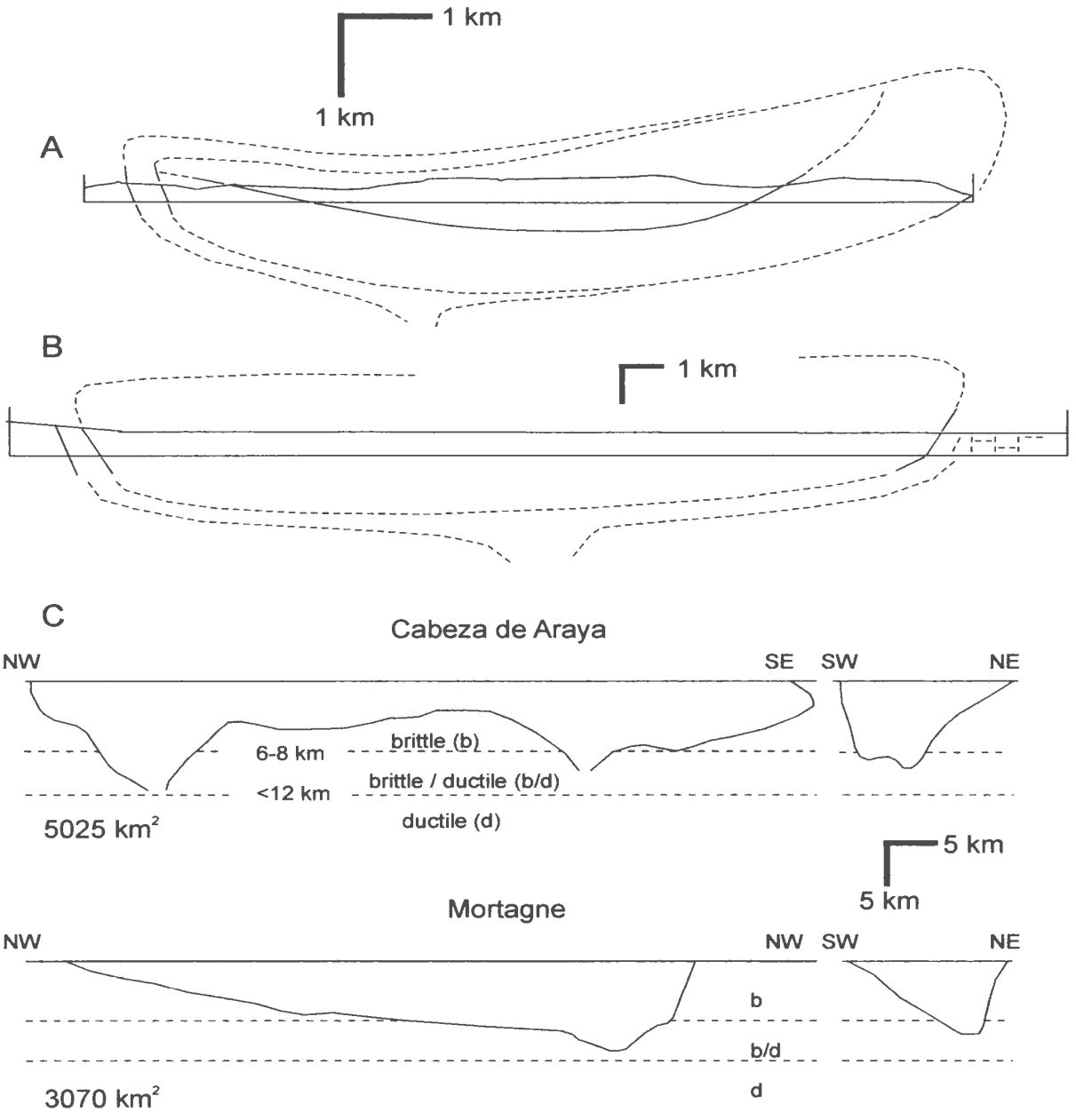

Figure 8.11: Comparison of cross-sections through the (A) Sophie (from Fig 6.2) and (B) Kikkertavak (from Fig 7.3) centered intrusive complexes with (C) gravity surveys through two granite batholiths in France and Spain (from Ameglio et al., 1997). The batholiths shown in (C) are relatively thick, extend largely in one horizontal direction and show few root (or feeder zones). Ameglio et al. (1997) interpreted these forms as indicating emplacement into dilating brittle crust during transcurrent tectonics.

section implies that feeder zones coalesce at depth. The bowl-shaped form and single feeder zone are similar to the Satosoak pluton, and suggest that the Hosenbein pluton was emplaced during transcurrent tectonics into dilating brittle crust. On the other hand, the sub-equant form is distinct from the east-west elongated form shown by the Satosoak pluton. It is suggested that the form of the Hosenbein pluton reflects a change from predominantly north-south to east-west structural control on the emplacement of magma.

8.3.4 What about diapiric ascent?

There are numerous studies (see Woussen et al., 1981; Duchesne, 1984; Scoates, 1990; Wiebe, 1990a; 1992, p. 228; Mitchell et al., 1995; 1996; Bhattacharya et al., 1998; Barnichon et al., 1999; Dempster et al., 1999; Mukherjee et al., 1999) that suggested the ascent and emplacement of anorthositic magmas occurs in diapirs. Ryan (in Berg et al., 1994) suggested that the Lister pluton may have been emplaced as a diapir. This section summarizes evidence that suggests the emplacement of the Lister pluton as a diapir was unlikely.

The total exposed area of the Lister pluton, based on previously published mapping by Ryan (1990; 2000a; 2001a), is 640 km^2, whereas the minimum thickness is 1 km. The minimum volume of anorthositic rocks in the Lister pluton is therefore:

$$V_{min} = (640\ km^2 \times 1\ km) = 640\ km^3$$

If this exposure comprises the form of one diapir, following Fig. 1.3, then the minimum diameter of a spherical diapir during ascent would be:

$$V_{min} = 4/3\pi r_{min}^3$$

$$r_{min} = ((3 \times V_{sphere})/(4*\pi))^{1/3}$$

$$r_{min} = 5.35 \text{ km}$$

$$\text{diameter}_{min} = 10.7 \text{ km}$$

Likewise, if the vertical thickness of the Lister pluton is similar to that of the Nain batholith (~8 – 10 km in Funck et al., 2000), then the maximum diameter of the 'Lister diapir' would have been 23 km. These results imply that if the Lister pluton was emplaced as one diapir, then the diameter of this diapir would have spanned between one quarter to one half of the underlying crust (Fig. 8.12). The 'space problem' generated by the ascent of one large diapir, as indicated by the structure, would have been significantly greater then that of an intrusion constructed from several (fracture-controlled?) magma pulses.

As shown in Fig. 8.12, the Lister pluton is too large to have ascended as a single diapir. On the other hand, it may be suggested that the Lister pluton was emplaced in pulses of smaller diapirs. It is important to note that when this line of reasoning is followed, the original reason for suggesting diapiric ascent for the Lister pluton (i.e. form) is no longer valid. As well, this pulsating diapiric ascent is often described as occurring in a zone of thermally weakened transtension (Paterson and Miller, 1998b), and therefore shares structural similarities to fracture-controlled ascent. Since the point of much of the discussion is to emphasize the underlying structural controls on the magmas during emplacement, a model of pulsating diapirism through a zone of crustal weakness also serves to strengthen arguments for underlying structural control.

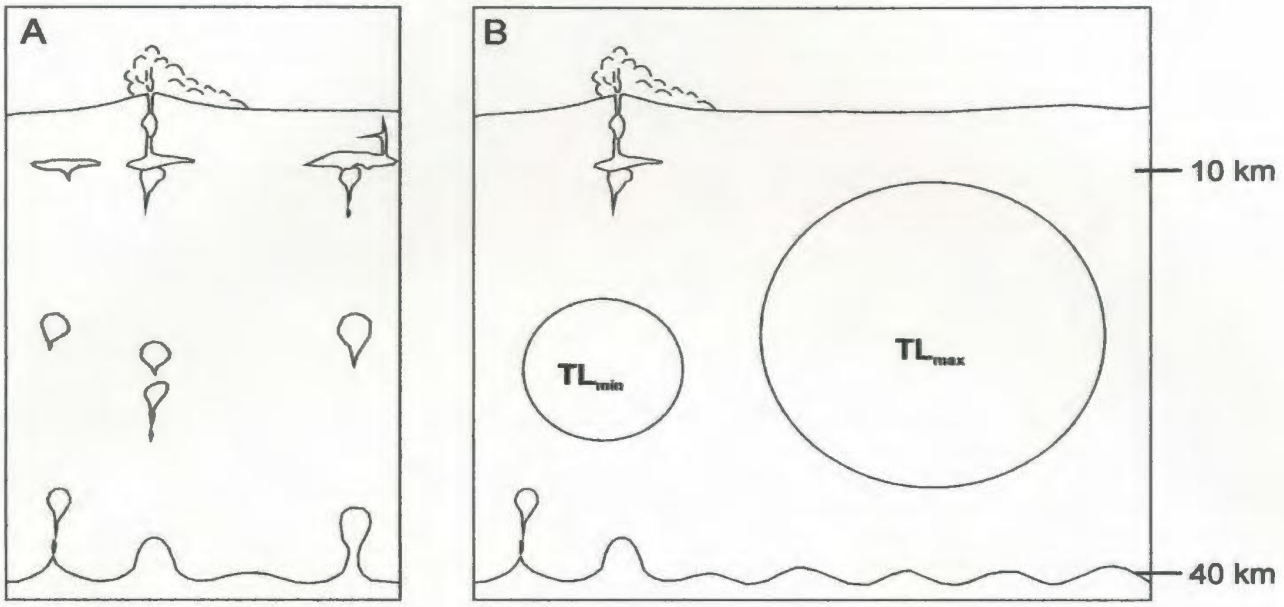

Figure 8.12: Schematic representations of (A) diapiric ascent and (B) schematic diapirs that represent the minimum and maximum diameters of the 'Lister diapir' (TL, see text) (diapiric ascent figure modified from Best and Christianson, 2001, p. 224).

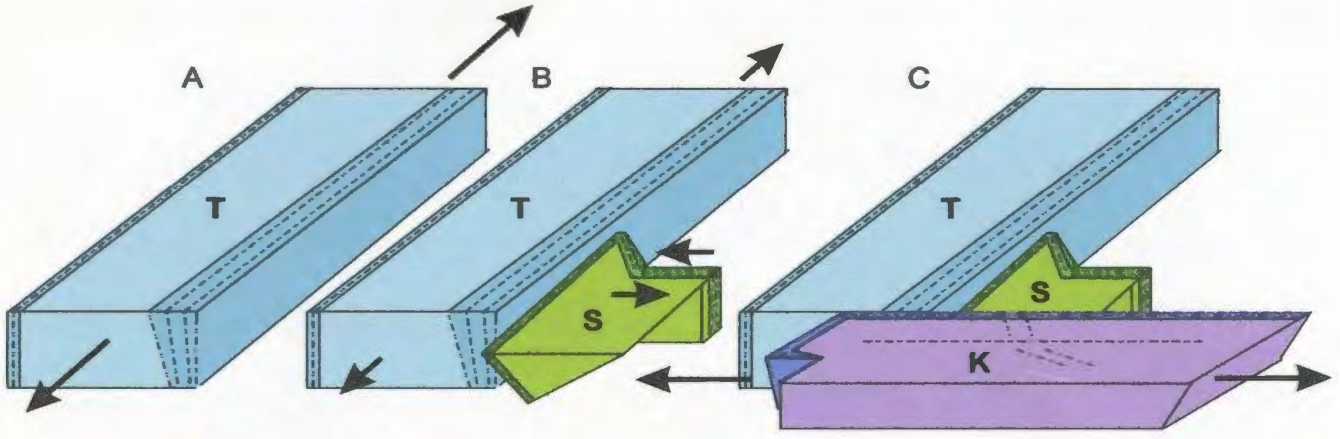

Figure 8.13: Emplacement and tectonic chronology of centered intrusive complexes in the study area showing (A) emplacement of the Tikkoatokak centered intrusive complex (T) that was controlled by north-south structures, (B), emplacement of the Sophie centered intrusive complex (S) that was controlled by north-south and east-west structures and (C) emplacement of the Kikkertavak centered intrusive complex (K) that was controlled by east-west structures. Legend for each centered complex is presented at the ends of chapters 5, 6 and 7.

A study by Funck et al. (2000) used wide-angle seismic and gravity imaging to study the structure of the Nain batholith and the underlying crust. The east-west cross-section line presented by Funck et al. (2000) lies along the southern boundary of the study area. The Funck et al. (2000) study shows that the Nain batholith extends to a depth of 8 to 11 km, and that the structures of the Torngat orogen exist below the Nain batholith and extends down to the Moho. The preservation of these structures below the Nain batholith suggests fracture-controlled ascent of magmas, since diapiric ascent would have likely have obliterated these structures (see Brown and Tryggvason, 2001).

8.3.5 Emplacement and intrusive form chronology

The Tikkoatokak centered intrusive complex comprises a rectangular form that is elongated in a north-south direction (Fig. 8.13). This centered intrusive complex was mostly emplaced >1333 +/- 2 Ma and was fed along north-south shear zones. Morse (1981c) suggested the Lister pluton was deformed during syn-plutonic north-south extension. Other intrusions that were emplaced at broadly similar times and deformed in a north-south orientation include the Hare Hill monzonite (1351 +/- 3 Ma). These findings indicate that magmas were emplaced and deformed along north-south shear zones during the early stages (1350 – 1330 Ma) of magma emplacement into the Nain batholith.

The northwestern part of the Kikkertavak centered intrusive complex comprises a rectangular form that is elongate in an east-west direction (see Fig. 8.13). This part of the Kikkertavak centered intrusive complex was emplaced after 1318 +/- 7 Ma, into brittle

crust along east-west shear zones. In addition, the northwestern part of the Kikkertavak centered intrusive complex post-dates magma emplacement and deformation in north-south shear zone #2.

The structure and chronology of centered intrusive complexes indicate that they were emplaced into (1st) *ductile* crust and along north-south shear zones before 1333 +/- 2 Ma and into (2nd) *brittle* crust and along east-west shear zones after 1318 +/- 7 Ma. These findings suggest that the crustal host rocks underwent a rheological change from ductile to brittle at some time between 1333 +/-2 and 1318 +/- 7 Ma. This rheological change may be related to uplift of the crust during emplacement of the Nain batholith. These findings contrast with previous work (Hill, 1982; Wiebe, 1985b) that suggested that Nain batholith was uplifted after emplacement. Another possibility is that the crust underwent isobaric cooling between ca. 1333 and 1318 Ma. Cooling of the crust, however, is inconsistent with the periodic emplacement of magmas into the Nain batholith at this time (see also Yoshinobu et al., 1998; Annen and Sparks, 2002). These findings suggest a change in the rheology of the crust and orientation of shear zones that transported between emplacement of the Tikkoatokak and Kikkertavak centered intrusive complexes.

8.4 Origin of textures and structures in anorthositic rocks

Rocks that crystallized from anorthositic magmas comprise the bulk of centered intrusive complexes in the study area. The forms and structures of these intrusions suggest that the anorthositic magmas were transported and emplaced along shear zones, thereby suggesting the rheology of anorthositic magma was liquid-state during ascent and

emplacement. This section of the discussion interprets the textures and structures of anorthositic rocks that were produced during the crystallization of anorthositic magmas, and suggests that textures and structures developed in a magma that exhibited mostly solid-state rheology.

8.4.1 Textures of anorthositic rocks

Proterozoic anorthositic rocks crystallized from anorthositic magmas that likely contained between 20 – 70% plagioclase crystals (see Buddington, 1969; Wiebe, 1990a; Longhi et al., 1993). In the study area, the crystallization of these anorthositic magmas produced anorthositic rocks with mostly massive texture. Several workers (see Wiebe, 1992; Pitcher, 1997) have suggested that massive texture indicates the stagnant crystallization of magma, thereby implying a limited role for processes like magmatic convection and crystal settling. A study by Philpotts and Carroll (1996) suggested that stagnant crystallization of magma is promoted by the formation of rigid crystal frameworks (Fig. 1.2). These workers suggested that such frameworks are formed when the magma contains >33% crystals, whereas studies by Marsh (1981) and Vigneresse et al. (1996) suggest that a crystal content of ~55% is required to form these frameworks. Comparing the estimated range of % crystal abundance in anorthositic magmas (20 – 70%) with that required to form crystal frameworks (33 – 55%) suggests that the crystallization of anorthositic magmas involved: (a) the formation of crystal frameworks upon emplacement, or (b) the formation of crystal frameworks after a relatively short interval of crystallization. The formation of these frameworks and resultant stagnant

crystallization is further suggested by the predominantly massive texture shown by anorthositic rocks in the study area.

Massive anorthositic rocks in the study area contain high abundances of cumulus plagioclase and show predominantly: (a) granular texture, or (b) poikilitic texture (Figs. 5.21, 5.28, 5.36, 6.15, 6.38, 6.39, 6.42, 6.43, 7.16, 7.17). These granular and poikilitic textures comprise: (a) impinging cumulus plagioclase grains and laths, and (b) interspersed poikilitic crystals and/or granular aggregates of plagioclase, pyroxene, Fe-Ti oxide and/or accessory minerals. These textures suggest that cumulus plagioclase crystals formed a continuous crystal framework within which the poikilitic crystals and aggregates were crystallized. This suggestion is consistent with several studies (Marsh, 1981; Irvine, 1982, p. 131; Brown, 1994; Philpotts and Carroll, 1996; Philpotts et al., 1996; Vigneresse et al., 1996; Hunter, 1996) that have suggested self-supporting frameworks of cumulus crystals are formed during crystallization. As well, the presence of these frameworks during crystallization is consistent with the Irvine (1982, p. 131) definition of a cumulate as "an igneous rock characterized by a cumulus framework of touching mineral grains".

Hunter (1996) suggested that granular texture indicates a cumulate that is fully or highly densified, whereas poikilitic texture indicates a cumulate that is partly densified and cemented. Densification refers to "all processes (that) increase the volume fraction of the cumulus phases" (Hunter, 1996, p. 92) and occurs by growth densification and compaction densification. Cementation refers to "the nucleation and growth of new, usually poikilitic or sub-poikilitic phases within the pores spaces" (Hunter, 1996, p. 92).

The interpretations of Hunter (1996) suggest that anorthositic rocks with granular texture were formed by the compaction and/or overgrowth of cumulus plagioclase, whereas anorthositic rocks with poikilitic texture were formed by the cementation of cumulus plagioclase by poikilitic pyroxene, Fe-Ti oxides and/or aggregates of interstitial liquid. In the previous paragraph it was suggested that cumulus plagioclase formed crystal frameworks during crystallization. Hence, the granular and poikilitic textures of anorthositic rocks in the study area suggest that crystallization involved compaction and/or overgrowth, and cementation, of these cumulus plagioclase frameworks.

Plagioclase crystals in anorthositic rocks of all centered intrusive complexes show grain margins that are: (a) serrated, and/or (b) interlobate (Figs. 5.19, 5.25, 6.13, 6.21, 6.37, 6.41, 7.6, 7.13). Several workers (see Lafrance et al., 1996; Rosenberg and Stuenitz, 2003) have suggested that these features form by subgrain rotation and associated grain boundary migration at 'high temperatures'. Lafrance et al. (1996) suggested that these high temperatures range from >600 – 800 °C. In addition, plagioclase crystals in anorthositic rocks of the study area show: (a) deformation twins, (b) deformation bands, and/or (c) undulose extinction (Figs. 5.19, 5.25, 6.13, 6.21, 6.37, 7.13). These features result from grain scale deformation during compaction followed by intragranular diffusion and climb of dislocations in the crystal lattice, and are also facilitated by high temperatures (see Lafrance et al., 1996). Considering that the Nain batholith has: (a) not been regionally deformed since emplacement (see Berg et al., 1994, p. 2), and (b) not been exposed to temperatures in excess of 150 – 250 °C since ~1230 Ma (see Yu and Morse, 1993), it is most likely that deformation and recrystallization of plagioclase

occurred in, or shortly after, the same time interval as emplacement of the Nain batholith (1365 – 1270 Ma). The deformation and recrystallization of cumulus plagioclase in the same time interval as magma emplacement is consistent with stress (including compaction) that accompanied crystallization.

Most anorthositic rocks in the study area show homogeneous plagioclase (Fig. 8.14) and pyroxene compositions. Several studies (Wager et al., 1960, Hunter, 1996) have suggested that cumulate rocks with: (a) granular (or adcumulate) texture, and (b) homogeneous mineral compositions were formed by 'open-system processes'. These open-system processes include: (a) the removal of interstitial liquid during cumulate compaction (see Hunter, 1996), and (b) adcumulus growth. Adcumulus growth requires that the interstitial melt in cumulus plagioclase frameworks underwent diffusive interchange with an overlying magma reservoir that: (a) was not found in the study area, and (b) is, by definition, absent from intrusions of anorthositic rocks. It is therefore more likely that the homogeneous mineral compositions of anorthositic rocks in the study area resulted from cumulate compaction and the removal of pyroxene-rich interstitial melts.

Anorthositic rocks in the Tikkoatokak and Sophie centered intrusive complexes show a relatively narrow range in normative plagioclase composition in comparison to whole rock Mg/(Mg + Fe) (Fig. 8.15), wt% TiO_2 and/or wt% P_2O_5 (see Figs. 5.35, 6.18, 7.9). These variations produce 'vertical fractionation trends' that contrast with the 'inclined fractionation trends' shown by layered mafic intrusions (Fig. 8.16). Petrographic study of anorthositic rocks in the study area indicates that the minerals hosting Mg, Fe, Ti and P (pyroxene, Fe-Ti oxide, apatite) are generally intercumulus in

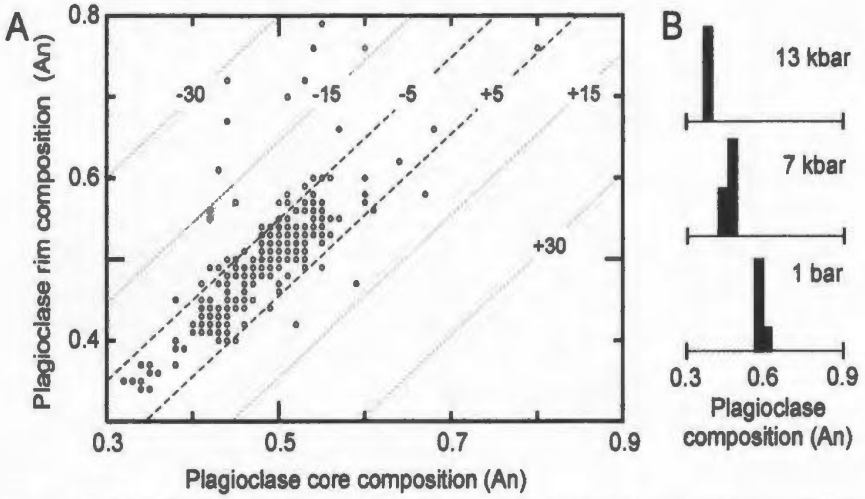

Figure 8.14: (A) Comparison of all plagioclase core and rim analyses obtained during this study (data in Appendix 1). The dashed lines indicate lines of constant reverse (negative) and normal (positive) zoning. (B) Experimental data on plagioclase compositions in tholeiitic liquids in near-liquidus experiments, showing an increase of Ab in plagioclase at higher pressures (from Longhi et al., 1993).

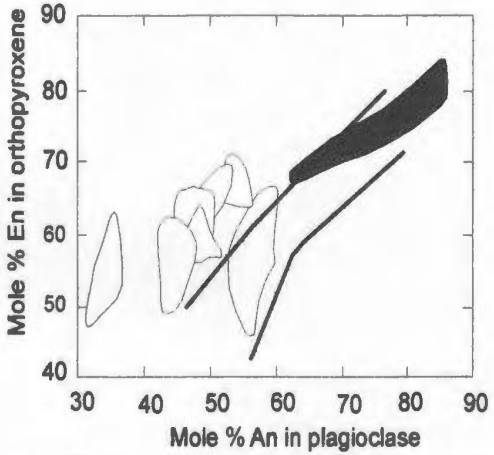

Figure 8.16: Comparisons of plagioclase and pyroxene compositions within Proterozoic anorthosite (white), and layered mafic intrusions (black, lines). Variations of anorthite and enstatite show 'vertical' trends in Proterozoic anorthosite and 'inclined' trends for layered mafic intrusions (modified from Ashwal, 1993, p. 131).

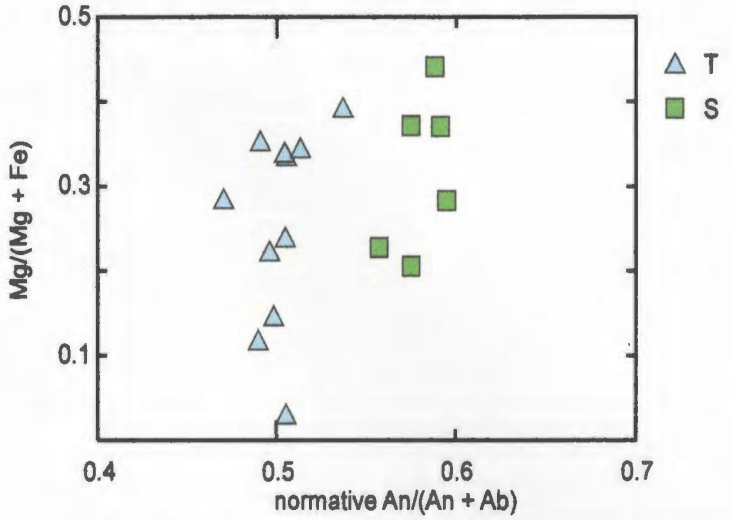

Figure 8.15: Whole rock comparison of Mg/(Fe+Mg) and normative plagioclase composition for anorthositic rocks in the Tikkoatokak (T) and Sophie (S) centered intrusive complexes. See text for additional discussion.

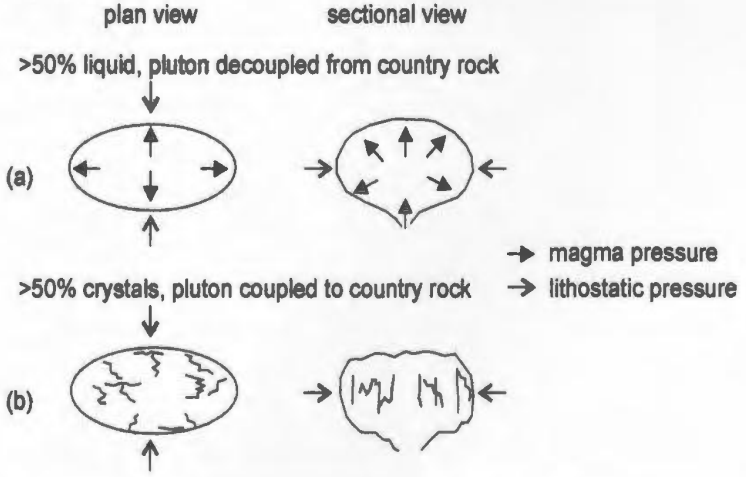

Figure 8.17: Stress acting on a pluton when (a) the magma pressure > lithostatic pressure and (b) lithostatic pressure >> magma pressure. The drop in magma pressure occurs when crystal frameworks were formed at ~50% crystals. Lines in (b) indicate joint-filled pegmatites and dikes (after Baros et al., 2001).

anorthositic rocks. Ashwal (1993, p. 132) suggested that vertical fractionation trends in anorthositic rocks resulted from the "equilibrium crystallization of trapped intercumulus liquid in a plagioclase crystal (framework)". A similar interpretation is favored to explain the whole rock chemistry variations observed in this study, thereby suggesting a rigid framework of cumulus plagioclase and a mobile interstitial liquid.

Whole rock chemistry for anorthositic rocks in the Hosenbein pluton inner zones shows relatively consistent normative plagioclase compositions, and higher Fe/(Fe + Mg), wt% TiO_2 and wt% P_2O_5 in the upper inner zone as compared to the lower inner zone (Fig. 6.18). These relations suggest that trapped intercumulus liquid migrated upwards through the plagioclase crystal framework in the Hosenbein pluton. This upward migration is inconsistent with the high density of intercumulus minerals (pyroxene, Fe-Ti oxide) with respect to the plagioclase that forms crystal frameworks (see Scoates, 2000). Upward migration is also inconsistent with gravity-induced compaction, since this process requires that cumulus minerals are of higher density in comparison to intercumulus minerals. A possible origin for this upward migration of intercumulus liquid is that compaction was induced by tectonic movement in the shear zones that bound the margins of centered intrusive complexes. Such a mechanism of compaction is described in as study by Barros et al. (2001). In this study, Barros et al. (2001) suggest that for the emplacement of the magma the magma pressure must exceed the lithostatic pressure (Fig. 8.17). During subsequent magma crystallization, the magma pressure continues to exceed the lithostatic pressure until a continuous framework of crystals is formed that couples the magma chamber to the country rock. Barros et al. (2001) suggest this occurs at ~50%

crystals. Further crystallization causes a decrease in the pore pressure and the related magma pressure, so that the lithostatic pressure begins to exceed the magma pressure. Once the lithostatic pressure exceeds the magma pressure, the magma chamber undergoes late-magmatic high-T deformation. Following this model, the following processes may have resulted in the upward migration of interstitial melt: (1^{st}) formation of a continuous cumulus plagioclase framework that couples the pluton to country rock, (2^{nd}) a drop in magmatic pressure coupled with shear deformation along the margins of the pluton, and (3^{rd}) deformation of cumulus plagioclase frameworks and upward squeezing of interstitial liquid. Downward transport, which is facilitated by higher densities, and lateral transport, which may also be facilitated by lithostatic pressure, are additional possibilities for the transport directions of interstitial liquid.

Oxide gabbronorite, ferrogabbro and/or ferrodiorite occur as dikes in the Lister pluton border zone, Akuliakatak pluton and the Satosoak pluton inner zone (Figs. 5.33, 6.44, 7.10, 7.11, 7.19). Intrusive contacts are sharp or grade into anorthositic rocks with poikilitic aggregates of dike-like composition. Petrography, mineral compositions and whole rock chemistry indicates that these dikes contain higher abundances of Na-rich plagioclase, Fe-Ti oxide (Ti, Fe, V), Fe-rich pyroxene (Fe), alkali feldspar (K, Ba), apatite (P) and zircon (Zr) (Tables 7.2, 7.4). Previous studies (see Mitchell et al., 1996; Bhatthacharya et al., 1998) have suggested that some ferrodiorite dikes in anorthositic intrusions were formed by the segregation of interstitial melts during the compaction of anorthositic magmas. The dikes described by Mitchell et al. (1996) contain high abundances of Fe, T, P incompatible elements and rare earth elements. Likewise,

ferrodiorite dikes in the study area contain high abundances of Fe, T, P, K, Ba and Zr and also occur in anorthositic rocks. These findings suggest that ferrodiorite dikes in anorthositic rocks of the study area were: (a) residual to the crystallization of anorthositic magmas, and (b) segregated and aggregated during compaction of cumulus plagioclase frameworks.

On a regional scale, anorthositic rocks in the Lister pluton (Tikkoatokak centered intrusive complex) are the most recrystallized and/or deformed. This recrystallization and deformation is evident in the microstructures of all anorthositic rocks observed in thin section (Figs. 5.19, 5.25) and the relatively wide and strongly deformed eastern margin of the intrusion (Fig. 5.14). In addition, it is the authors' impression that the Lister pluton contains the highest abundance of massive anorthosite sensu stricto (>90% plagioclase). In contrast, the anorthositic rocks in the Hosenbein (Sophie centered intrusive complex) and Satosoak (Kikkertavak centered intrusive complex) plutons were found to comprise sub-equal abundances of anorthosite, leucogabbronorite and leuconorite. As well, some of the anorthositic rocks in the Hosenbein and Satosoak plutons show no indicators of high-T deformation and/or recrystallization. These findings suggest that: (a) recrystallized and deformed anorthositic rocks contain low abundances of intercumulus pyroxene and Fe-Ti oxide, and (b) less recrystallized and deformed anorthositic rocks contain higher abundances of intercumulus pyroxene and Fe-Ti oxide. Lafrance et al. (1996) suggested that an inverse relation between the abundance of intercumulus pyroxene and recrystallized plagioclase resulted from the removal of pyroxene-rich interstitial liquid during the compaction of cumulus plagioclase. A similar interpretation

applied to anorthositic rocks in the study area suggests that anorthositic rocks in the Lister pluton were more compacted and cleansed of interstitial liquid in comparison to the Hosenbein and Satosoak plutons.

In summary, the textures, microstructures, mineral compositions and/or whole rock chemistry of anorthositic rocks in the study area indicate: (a) densification and cementation of cumulus plagioclase frameworks, (b) high-T recrystallization and deformation, (c) re-distribution and/or equilibrium crystallization of interstitial melt in a plagioclase crystal framework, and (d) segregation and aggregation of interstitial melt into ferrodiorite dikes. All of these characteristics are consistent with the formation of cumulus plagioclase frameworks and the compaction of these frameworks during the crystallization of anorthositic magmas. It is suggested that this compaction is related to the formation of a continuous crystal framework in anorthositic intrusions during crystallization, which promotes a decrease in the magmatic pressure and a related increase in the susceptibility of the pluton to tectonic deformation. The shear zones that bound the margins of centered intrusive complexes in the study area may have enhanced this tectonic deformation.

8.4.2 Hypothetical indicators of late-magmatic deformation and/or compaction

This section summarizes additional field and mineral composition characteristics noted in anorthositic rocks during this study, and suggests possible origins for their formation. In all cases, these features may also be linked to processes of late-magmatic deformation and/or compaction.

All anorthositic rocks in the study area contain planar aggregates and/or pods of large poikilitic pyroxene crystals (Fig. 5.22, 5.29, 5.32, 6.40, 7.18). In some cases, these aggregates are associated with high-T shear zones (Fig. 6.40) that suggest these aggregates were formed: (a) by late-magmatic remobilization of pyroxene-rich interstitial melts, and (b) during late-magmatic deformation of plagioclase crystal frameworks. Therefore, it is likely that these aggregates formed during late-magmatic fracturing of cumulus plagioclase frameworks and the migration and crystallization of pyroxene-rich interstitial liquids into these fractures. This fracturing may have occurred during: (a) late-magmatic deformation of plagioclase frameworks by tectonic activity along intrusion margins, and/or (b) passive fracturing and fracture-infilling as a result of magmatic cooling and contraction.

Aggregates of pyroxene also occur on the margins of anorthosite xenoliths (Fig. 7.12) that are hosted by anorthositic rocks. Such pyroxene-rich aggregates are common on the margins of anorthositic xenoliths in Proterozoic anorthositic rocks around the world (see Ashwal, 1993, p. 112: "in many cases, (xenolith)-matrix contacts are characterized by concentrations of mafic minerals"). A study by Paterson and Miller (1998a) suggested that pegmatitic growths on xenolith margins formed by the rotation of xenoliths during late-magmatic deformation and the crystallization of pegmatites in strain shadows. Similarly, rotation of anorthositic xenoliths during late-magmatic deformation may have resulted in compaction, segregation of pyroxene-rich interstitial melts and crystallization of these pyroxene-rich melts in strain shadows on the margins of xenoliths.

Locally, plagioclase crystals show rims of calcic plagioclase that are up to An_{30}-richer than the core (see Fig. 8.14). Morse and Nolan (1984) interpreted reverse rims in the Kiglapait intrusion as the result of crystallization that is open to plagioclase exchange between pore fluids and magma, yet closed to the augite component. The Kiglapait intrusion, however, crystallized from mostly liquid-state troctolitic magmas (see Morse, 1969) such that all cumulates were at one point in communication with large amounts of liquid. The magmas that formed the anorthositic rocks, on the other hand, likely contained significantly less (20-70%) liquid, thereby possibly limiting the exchange between pore fluids and liquid magma. A possible alternative explanation for these rims is that they are related to the process of cumulate compaction. Dick and Sinton (1979) and Hunter (1996) have suggested that cumulate compaction is associated with solution/reprecipitation of grains (diffusion creep). Solution of grains occurs at relatively high-pressure grain contacts (pressure dissolution), which would promote the dissolution of anorthite over albite (see Fig. 8.14B). This dissolved anorthite is then reprecipitated on the rims of plagioclase crystals as thin rims of reverse zoning and/or rims of calcic myrmekite.

Centered intrusive complexes in the study area contain weakly to strongly deformed anorthositic and gabbronoritic rocks, and weakly deformed Fe-rich gabbroic rocks. Microprobe work during this study shows that orthopyroxene in anorthositic and gabbronoritic rocks tend to higher abundances of wt% Al_2O_3 in comparison to Fe-rich gabbroic rocks (Fig. 8.18). Longhi et al., 1993 conducted experiments on tholeiitic liquids that show the incorporation of Al_2O_3 in orthopyroxene is predominantly related to

increases in pressure (Fig. 8.19). These results suggest that orthopyroxene in the weakly to strongly deformed anorthositic and gabbronoritic rocks crystallized at slightly higher pressure in comparison to weakly deformed Fe-rich gabbroic rocks. These higher pressures may be related to cumulate compaction and/or deformation at the level of emplacement, which is consistent with the weakly to strongly deformed occurrences of anorthositic and gabbronoritic rocks. These results suggest that some Al_2O_3-enrichment in pyroxene may be due to deformation at the emplacement level, although it is doubtful that this mechanism of enrichment can produce high-alumina megacrysts with up to 9 wt% Al_2O_3. Such enrichment requires tectonic overpressures of up to 5 kbar, and is unlikely given that tectonic overpressures in orogenies are insignificant with respect to lithostatic pressures.

8.4.3 Structures in anorthositic rocks

The previous section suggested that: (1^{st}) the crystallization of anorthositic magmas involved the formation of cumulus plagioclase frameworks and (2^{nd}) that these frameworks were compacted during crystallization. In addition, these frameworks would have promoted the stagnant crystallization of magma (see Philpotts et al., 1996). In light of these considerations, the structures of anorthositic rocks in the study area are here interpreted to have developed in stagnant magmas with crystal frameworks. The origin of structures is, like the textures, likely related to compaction and the redistribution of interstitial melt.

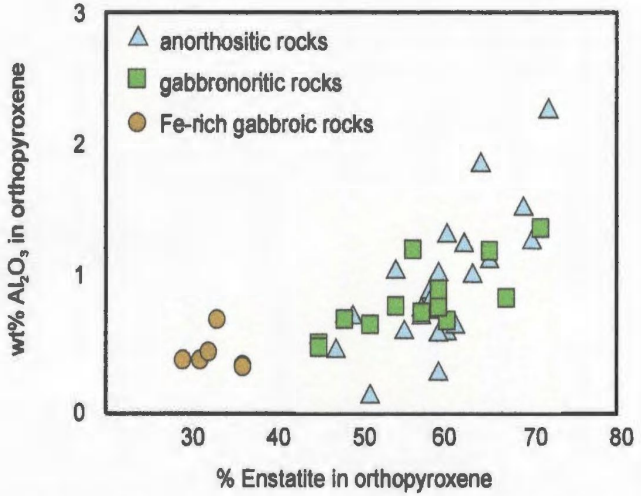

Figure 8.18: wt% Al_2O_3 in orthopyroxene vs. % enstatite in orthopyroxene for anorthositic, gabbronoritic and Fe-rich gabbroic rocks of the study area.

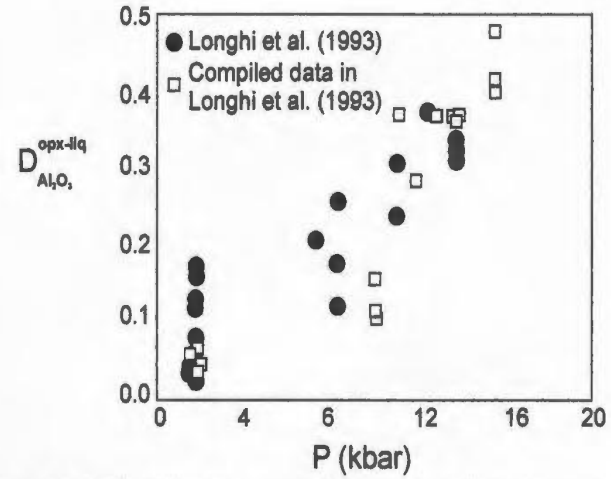

Figure 8.19: Results from experiments that show the variations of pressure (P) and molar partition coefficient (D) for Al_2O_3 in an orthopyroxene-liquid pair (simplified from Longhi et al., 1993). The results show a positive correlation between P and D.

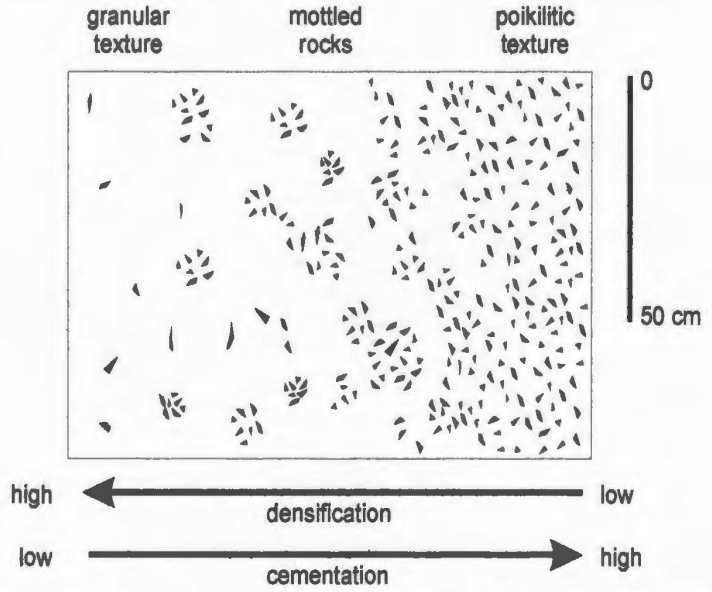

Figure 8.20: Textural representation of anorthositic rocks that range from highly cemented poikilitic texture, through mottled rocks, to highly densified granular texture.

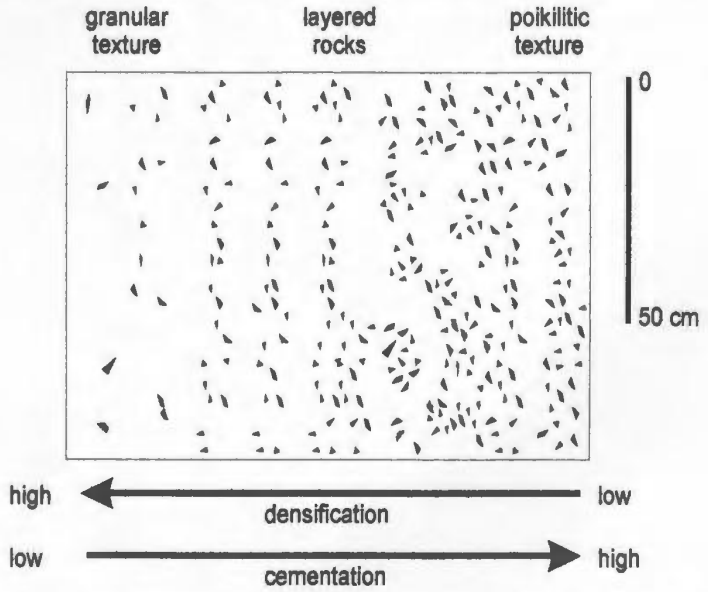

Figure 8.21: Textural representation of anorthositic rocks that range from highly cemented poikilitic texture, through layered rocks, to highly densified granular texture.

Mottled anorthositic rocks show granular and poikilitic texture that is interspersed in patches at 5 cm to 100's of m scales (Figs. 5.28, 5.42, 6.15, 6.38, 7.17). Granular texture formed by the densification of crystal frameworks, whereas poikilitic texture formed by the cementation of crystal frameworks (see Hunter, 1996). Since mottled anorthositic rocks contain both granular and poikilitic texture, they must have been produced by the partial densification and cementation of crystal frameworks (Fig. 8.20). The gradation shown in Fig. 8.20 implies that the transition from poikilitic, through mottled, to granular texture also incorporates a decrease in the abundance of poikilitic pyroxene. This decrease suggests the removal of pyroxene-rich interstitial liquid during densification and is consistent with the process of compaction. Mottled rocks are therefore interpreted as partially compacted cumulus plagioclase frameworks.

Layered anorthositic rocks show granular and poikilitic textures that are interspersed in planes (Figs. 5.26, 6.39, 6.43). An interspersed granular and poikilitic texture (Fig. 8.21) is also characteristic of mottled rocks (see Fig. 8.20) and it was suggested in the previous paragraph that this texture formed by the partial compaction of cumulus plagioclase frameworks. In the case of layered rocks, however, this process of partial compaction resulted in the distribution of poikilitic pyroxene into planes. In the study area, moderately to steeply dipping layered anorthositic are gradational into strongly deformed anorthositic and gabbronoritic rocks. These strongly deformed rocks were produced in ductile shear zones under non-isotropic stress. If these shear zones were active during crystallization, then the response of the crystal frameworks to non-isotropic stress would likely have been compaction in planes perpendicular to the axis of

maximum compressive stress. In addition, this compaction would have resulted in the aggregation of interstitial melt into planes that were normal to the principal compressive stress (see Naslund and McBirney, 1996). If sub-horizontal layers in the core of anorthositic intrusions formed by a similar mechanism than the maximum compressive stress in this part of the intrusion must have been vertical. This vertical stress suggests gravitational stress that may be related to roof collapse.

Foliated anorthositic rocks contain lens-shaped poikilitic crystals of pyroxene that were here interpreted as a flattened poikilitic texture (Fig. 5.27). Since poikilitic textures formed by the cementation of plagioclase crystal frameworks by pyroxene-rich interstitial melt, it is suggested that flattened poikilitic texture formed by the cementation of flattened crystal frameworks by pyroxene-rich interstitial melt. This suggests that some cumulus plagioclase frameworks were strained during cementation. This origin of foliated rocks in strained crystal frameworks is somewhat consistent with a study by McBirney and Hunter (1995, p. 77) that suggested some igneous foliations were produced "at a late stage, perhaps as a result of recrystallization under non-isotropic stress". Likewise, a study by Paterson and Miller (1998a) suggested that some magmatic fabrics are formed during coaxial straining of a crystal-rich magma near its solidus.

In summary, the structures of anorthositic rocks are here interpreted in terms of having formed in a magma with mostly solid-state rheology. Mottled and layered rocks were formed from cumulus plagioclase frameworks that were partially compacted under: (a) isotropic stress (mottled rocks), or (b) non-isotropic stress (layered rocks). Foliated rocks were formed by the deformation of these cumulus plagioclase frameworks under

non-isotropic stress. These findings suggest that structures in anorthositic rocks formed late in the crystallization history of the magma, and suggests that these structures may have potential as indicators of the directions of paleo-stress.

8.4.4 Comments on the rheology of anorthositic magma

The previous parts of this discussion have described how: (a) emplacement of anorthositic magmas occurred along shear zones, and (b) that textures and structures of anorthositic rocks developed by the compaction of crystal frameworks and the remobilization of interstitial melt. Finding (a) suggests that the ascent and emplacement of anorthositic magmas occurred as rheological liquids, whereas finding (b) suggests that textural and structural development of anorthositic magmas occurred in rheological solids. These findings are consistent with a parental magma that contained between 20 – 70% plagioclase crystals, since these crystals would have formed crystal frameworks shortly after emplacement (see Philpotts et al., 1996).

Proterozoic anorthositic magmas likely consisted of plagioclase crystals and fractionated basaltic liquid. Estimates for the % abundance of plagioclase crystals in these magmas ranges from 20 – 70%, whereby the % abundances of fractionated basaltic liquid ranges from 80 – 30%. If we assume that this fractionated basaltic liquid contained 66% plagioclase component and 35% Fe-Mg silicate and/or Fe-Ti oxide components, then the total plagioclase component of these anorthositic magmas ranges from:

$$\%Plag_{total} = 20\%\ Plag_{crystals} + 80\%(0.66Plag_{liquid})$$

$$\%\ Plag_{total} = 20\%\ Plag_{crystals} + 53\%Plag_{liquid}$$

$$\% \text{ Plag}_{\text{total}} = 73\%$$

and for 70% $\text{Plag}_{\text{crystals}}$

$$\% \text{ Plag}_{\text{total}} = 90\%$$

These calculations suggest that liquid-state anorthositic magmas likely contained between 73 – 90% crystal + liquid plagioclase component. In the Sophie and Kikkertavak centered intrusive complexes, this range in plagioclase abundances is fairly representative of the rock types observed in these intrusions. In the case of the Lister pluton inner zone, which contains mostly true anorthosite (90 – 100% plagioclase), relatively thorough compaction and removal of interstitial liquid must have occurred. This relatively thorough compaction is consistent with the high abundances of deformed and/or recrystallized cumulus plagioclase crystals in this pluton. The removed interstitial melts may have been relocated above, or below, the present erosional surface, or they may have been preserved in Fe-rich dioritic bodies like the Akpaume pluton (Fig. 5.1).

8.5 Compositional evolution of anorthositic rocks

This section compares the order of emplacement, mineral compositions and whole rock chemistry for the plutons that comprise the bulk of the Tikkoatokak, Sophie and Kikkertavak centered intrusive complexes. These plutons consist of, respectively, the Lister, Hosenbein and Satosoak plutons. On the basis of field relations, new zircon ages and previously published zircon ages, the order of emplacement for these anorthositic rocks is Lister first (minimum age of 1333 +/- 2 Ma), Sophie second (maximum age of 1318 +/- 7 Ma) and Satosoak third (cuts Sophie). This section suggests that, over time,

anorthositic magmas became: (a) depleted in Si, K and Ba, and (b) enriched in Ca and Mg/(Mg+Fe).

8.5.1 Compositional evolution in the study area

The composition of plagioclase crystals in anorthositic rocks ranges from An_{41-47} in the Lister pluton, An_{49-55} in the Hosenbein pluton and An_{48-64} in the Satosoak pluton (Table 8.1). These results suggest that plagioclase compositions in anorthositic rocks became more Ca-rich over time. Orthopyroxene compositions for these anorthositic plutons overlap in error (+/- En_2), although the most Mg-rich compositions do occur in the youngest anorthositic rocks (Satosoak pluton).

Table 8.1: Comparison of mineral compositions (*) and whole rock chemistry data for anorthositic rocks in the study area, and comparative data for NB noritic and troctolitic anorthosite

Intrusion	Pl*	Opx*	SiO2	K2O	Ca/Al	Sr/Ca x 10	Ba/K	Mg/(Mg+Fe)
	An	En	wt%	wt%				
Lister	41 - 47	57 - 62	53 - 55	0.7 - 0.8	0.92 - 1.15	0.13 - 0.15	0.16 - 0.26	0.14 - 0.35
Hosenbein	49 - 55	47 - 63	51 - 53	0.3 - 0.4	1.11 - 1.26	0.09 - 0.12	0.22 - 0.35	0.21 - 0.37
Satosoak	48 - 64	59 - 65	49 - 54	0.2 - 0.5	1.04 - 1.17	0.07 - 0.12	0.17 - 0.24	0.26 - 0.41
Comparative data								
NB noritic	40 - 54	57 - 67	52 - 58	0.6 - 1.2	0.8 - 1.1	0.10 - 0.15	0.08 - 0.19	0.10 - 0.35
NB troctolitic	51 - 68	66 - 73	49 - 55	0.2 - 0.6	1.0 - 1.2	0.06 - 0.09	0.12 - 0.17	0.15 - 0.49

The whole rock chemistry of anorthositic rocks shows high wt% SiO_2, wt% K_2O and Sr/Ca in the Lister pluton, high Ca/Al and Ba/K in the Hosenbein pluton and high Mg/(Mg+Fe) in the Satosoak pluton. The higher Sr/Ca ratios in the Lister pluton reflect overall lower abundances of Ca, since the abundances of Sr in anorthositic rocks of the Lister pluton (655 – 810 ppm) have a higher minimum value than those in Hosenbein (590 – 901 ppm) and Satosoak (526 – 768 ppm) plutons. The lower Ba/K ratios in

anorthositic rocks of the Lister pluton are the result of high wt% K_2O, since ppm Ba in the Lister pluton (655 – 810 ppm) is higher than that in the Hosenbein (372 – 636 ppm) and Satosoak (152 – 433 ppm) plutons. These results indicate that, over time, anorthositic magmas were depleted in the overall abundances of Si, K and Ba, and enriched in overall abundances of Ca and Mg/(Mg+Fe). The elements Si, Ba and K are: (a) more characteristic of crustal rocks as opposed to mantle rocks, and (b) concentrated in liquids that are residual to the crystallization of basaltic magmas. In case (b), magmas with high Si, Ba and K are evolved and magmas with high Ca and Mg/(Mg+Fe) are less evolved. Therefore, the compositional evolution of anorthositic rocks in the study area suggests the emplacement of: (a) magmas with a relatively large crustal component before magmas with a relatively small crustal component, and/or (b) more evolved magmas before less evolved magmas.

The generally accepted model for the petrogenesis of anorthositic magmas involves: (1^{st}) emplacement of basaltic magma at the base of the crust (underplating), (2^{nd}) fractional crystallization of this basaltic magma and concurrent assimilation of lower crustal components into this basaltic magma, and (3^{rd}) concentration of the plagioclase crystals in the basaltic magma, which forms the anorthositic magma. The 2^{nd} stage of this process results in more Fe-rich basaltic magmas via fractional crystallization and more crustal-like signatures through contamination. Hence, basaltic magmas that underwent a relatively long 2^{nd} stage should show relatively evolved basaltic compositions and relatively abundant crustal components. A relatively short 2^{nd} stage would show less evolved basaltic compositions and relatively low abundances of crustal

components. Hence, the diversity of anorthositic rocks in the study area may have been derived from different time lengths for fractional crystallization and assimilation (AFC) at depth. If this was the case, then the older anorthositic rocks underwent a relatively long stage of AFC processes and the younger anorthositic rocks underwent a relatively short stage. These different staging lengths suggest more rapid transit of magmas from the mantle-crust boundary to the emplacement level at later times in the history of the batholith, and suggest that thermal weakening of the crust may have played a role in determining the length of AFC processes and therefore the composition of magma.

The older anorthositic rocks in the study area contain plagioclase that is more Na-rich in comparison to the younger anorthositic rocks. Studies by Longhi et al. (1993) have shown that the partitioning of albite into plagioclase shows a positive correlation with pressure. Therefore on the basis of plagioclase composition alone, the older anorthositic rocks may have been generated at greater depth relative to the younger anorthositic rocks. This hypothesis may be further evaluated by examining the relationship between pressure and partition coefficient of Sr and plagioclase, and Ba and plagioclase, both of which are also enriched in the older anorthositic rocks.

Another possibility for the compositional differences is that partial melting of more crustal-type rocks generated the older anorthositic rocks, whereas partial melting of less crustal-type rocks generated the younger anorthositic rocks. The petrogenesis of anorthositic rocks from the melting of gabbroic sources in the lower crust has the subject of renewed study (Longhi et al., 1999; Duchesne et al., 1999; Bedard, 2000). These lower crustal sources were invoked in order to account for anorthositic rocks that show space-

time associations with: (a) gabbronoritic rocks, and (b) Fe-rich dioritic rocks. Troctolitic rocks, on the other hand, were more likely generated from partial melting of peridotitic sources. The oldest anorthositic rocks in the study area are associated only with Fe-rich gabbronoritic rocks, whereas the youngest anorthositic rocks are associated with gabbronoritic and troctolitic rocks. These associations suggest that the older anorthositic rocks may have ultimately been derived from gabbroic sources in the lower crust, whereas the younger anorthositic rocks were ultimately derived from gabbroic and peridotitic sources in the lower crust or the upper mantle.

8.5.2 Regional compositional evolution

This study compared the mineral compositions and whole rock chemistry of anorthositic rocks in the study area to previously published data that was grouped into NB noritic or NB troctolitic anorthosite. This section uses the results from these comparisons and previously published geochronology to propose sub-division of the Nain batholith into four intrusive episodes.

The bulk of anorthositic rocks in the Tikkoatokak centered intrusive complex show mineral compositions and whole rock chemistry that fall in the range shown by NB noritic anorthosite. The minimum age for the bulk of these anorthositic rocks is 1333 +/- 2 Ma, based on U-Pb dating of zircon by Hamilton et al. (1994) on the Apkaume intrusion north of the study area (Fig. 5.1). Mineral compositions and whole rock chemistry data for NB noritic anorthosite were compiled from studies by Xue and Morse (1993; 1994) on intrusions that they named the 'Bird Lake massif' and 'Susie Brook

Table 8.2: Mesoproterozoic plutonic rocks of the Nain batholith emplaced during episode 1 (1365 – 1330 Ma)

Intrusion	Rock type	Age (Ma)	Analysis	Reference
Tessiarsuyungoakh	monzonite	1364 +/- 3.5	U-Pb	Tettelaar, 2004
Tessiarsuyungoakh	ferrodiorite	1356 +/- 2	U-Pb	Tettelaar, 2004
Fraser Canyon	anorthosite	1356 +/- 2	U-Pb	Tettelaar, 2004
Hare Hill	monzonite	1351 +/- 3	U-Pb	in Ryan and James, 2003
Pearly Gates	anorthosite	1344 +/- 2	U-Pb	Tettelaar, 2004
Kangilialuk	monzonite	1341 +/- 4	U-Pb	this study
Unity	pyroxene diorite	1340 +/- 3	U-Pb	this study
Pants Lake south	troctolite	1337 +/- 2	U-Pb	Smith et al., 2001
Voisey's Bay	troctolite	1333 +/- 1	U-Pb	Amelin et al., 1999
Apkaume	ferrodiorite, hybrid	1333 +/- 2	U-Pb	Hamilton et al., 1994
Akpaume	leuconorite	1331 +/- 2	U-Pb	Hamilton et al., 1994
Unity	leucogabbronorite	1328 +/- 5	U-Pb	this study

Slab'. A geological map by Ryan and James (2003) grouped these intrusions into the interior and margin of the Pearly Gates intrusion. This intrusion consists of anorthositic rocks that are referred to as NB noritic anorthosite in this study and are of similar composition to the bulk of anorthositic rocks in the Tikkoatokak centered intrusive complex. U-Pb dating of zircon on the western margin of the Pearly Gates intrusion suggests that this intrusion crystallized at 1344 +/- 2 Ma (Tettelaar, 2004). In terms of the 1365 – 1270 Ma time span for magmatism in the Nain batholith, the anorthositic rocks in the Tikkoatokak centered intrusive complex and the Pearly Gates intrusion are relatively old. It is suggested that the first episode of magma emplacement into the Nain batholith spans a range that includes the Tikkoatokak centered intrusive complex and the Pearly Gates intrusion and thereby ranges from ca. 1365 – 1330 Ma. Other rocks that crystallized at this time include Tessiarsuyungoakh monzonite, Tessiarsuyungoakh ferrodiorite, Fraser Canyon anorthosite, Hare Hill monzonite, Unity gabbronorite and pyroxene diorite, Pants Lake south troctolite, Voisey's Bay troctolite, Apkaume

ferrodiorite and Unity anorthosite (Table 8.2). These plutonic rocks are grouped into episode 1 of the Nain batholith (Fig. 8.22).

The bulk of anorthositic rocks in the Sophie and Kikkertavak centered intrusive complexes show mineral compositions that fall in the range shown by NB noritic anorthosite, and whole rock chemistry that falls in the range shown by NB troctolitic anorthosite. The maximum age for the bulk of these intrusions is 1318 +/- 7 Ma and the minimum age is 1311 +/- 2 Ma. Whole rock chemistry for NB troctolitic anorthosite was compiled from a study by Xue and Morse (1993) on intrusions that they named 'Kikkertavak' and 'Port Manvers Run'. Subsequent dating by Hamilton et al (1994) shows that the Kikkertavak anorthosite contains zircons that crystallized at 1311 +/- 2 Ma. A study by Ryan (2001a) described a study that found zircons in the Port Manvers Run intrusion that crystallized at 1308 +/- 2 Ma. It is suggested that the second phase of magma emplacement in the Nain batholith includes the bulk of the Sophie centered intrusive complex, Kikkertavak intrusion and Port Manvers Run intrusion, and thereby ranges from ca. 1330 – 1310 Ma. Other anorthositic rocks emplaced in this time span include the Pyramid Pass, Paul Island, Ikadlavik Brook and Jonathon intrusions. The Paul Island and Jonathon intrusions are similar to the Kikkertavak and Port Manvers Run intrusions in that they also contain both leuconorite and leucotroctolite (see Wiebe, 1992; Berg et al., 1994). Other plutonic rocks emplaced at this time consist of Barth Island troctolite and ferrodiorite, tholeiitic dikes, Pants Lake north troctolite, Makhavinekh granite, Umiakovik granite and Mushua troctolite (Table 8.3). These plutonic rocks are grouped into episode 2 of the Nain batholith (Fig. 8.23).

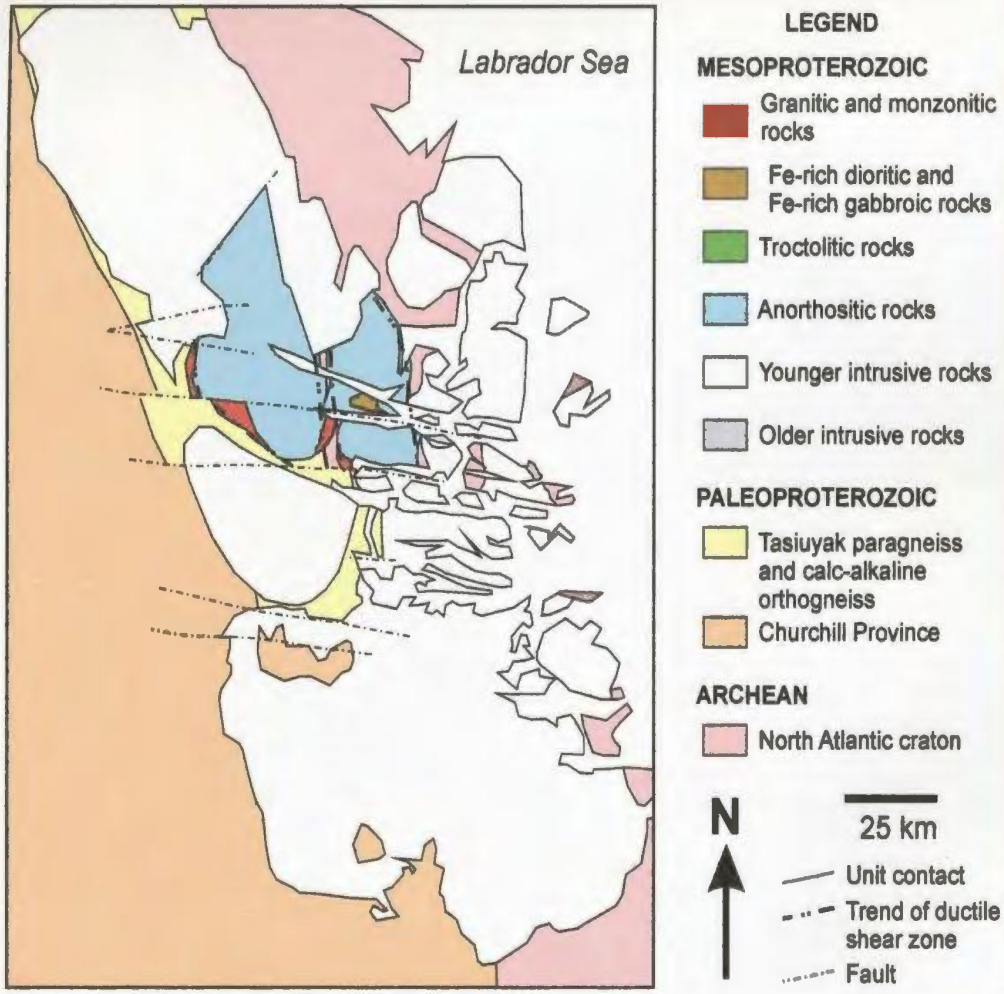

Figure 8.22: Episode 1 (1365 - 1330 Ma) of the Nain batholith showing the anorthositic rocks and lesser abundances of monzonitic, Fe-rich dioritic and troctolitic rocks. Ductile shear zones are predominantly sub-vertical and north-south striking. Note that anorthositic intrusions are also elongate in a north-south direction.

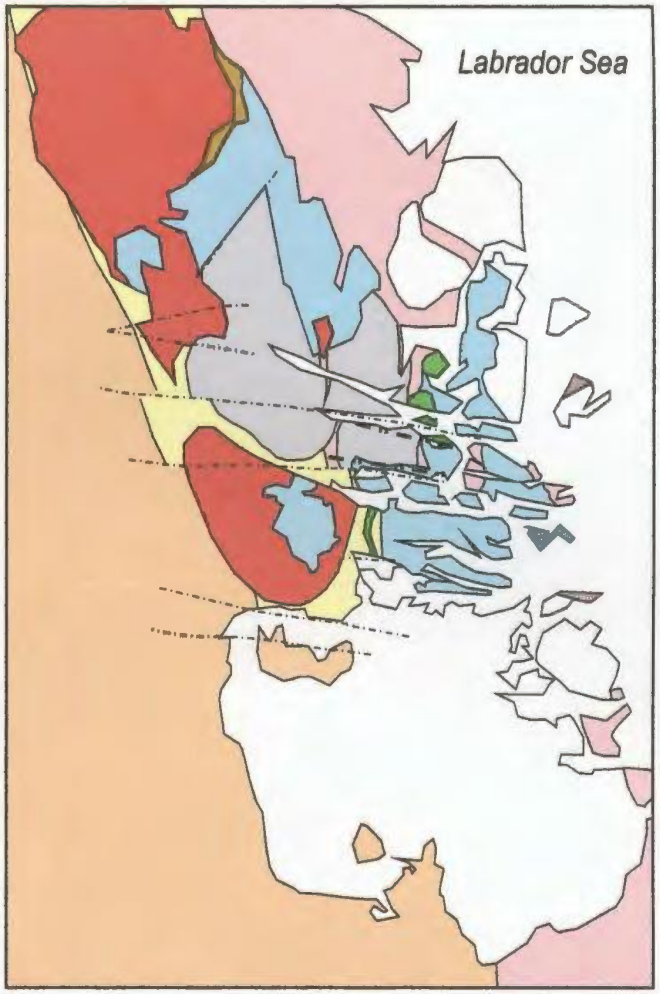

Figure 8.23: Episode 2 (1330 - 1310 Ma) of the Nain batholith showing large abundances of anorthositic and granitic rocks, and lesser abundances of troctolitic and Fe-rich dioritic rocks. Ductile shear zones are moderately south dipping to sub-vertical and east-west striking.

Table 8.3: Mesoproterozoic plutonic rocks of the Nain batholith emplaced during episode 2 (1330 – 1310 Ma)

Intrusion	Rock type	Age (Ma)	Analysis	Reference
Barth Island	troctolite	1330 +/- 1	U-Pb	Gaskill, 2005
Basic dikes I	tholeiite	1328 +/- 2	U-Pb	Cadman et al., 1999
Anaktalik	monzonite	ca. 1326	U-Pb	in Ryan and James, 2003
Pants Lake north	troctolite	1322 +/- 2	U-Pb	Smith et al., 2001
Barth Island	ferrodiorite, monzonite	1322 +/- 2	U-Pb	Hamilton et al., 1994
Makhavinekh	granite	1322 +/- 1	U-Pb	Ryan et al., 1991
Barth Island	monzonite	1322 +/- 2	U-Pb	Hamilton et al., 1994
Ikadlavik Brook	leuconorite	1322 +/- 1	U-Pb	Hamilton et al., 1994
Pyramid Pass	leuconorite, leucotroctolite	1322 +/- 1	U-Pb	Hamilton, 1997
Paul Island	anorthosite	1319 +/- 1	U-Pb	Hamilton et al. 1994
Umiakovik	monzonite	1319 +/- 2	U-Pb	Emslie and Loveridge, 1992
Pikaluyak	Fe-rich gabbroic	1318 +/- 7	U-Pb	this study
Basic dikes II	tholeiite	1316.5 +/- 1.6	U-Pb	Cadman et al., 1999
Umiakovik	granite	1316 +/- 3	U-Pb	Emslie and Loveridge, 1992
Mushua	troctolite	1313	U-Pb	Li et al., 2000
Jonathon Island	ferrodiorite	1312 +/- 3	U-Pb	Hamilton et al., 1994
Kikkertavak	anorthosite, leuconorite	1311 +/- 2	U-Pb	Hamilton et al., 1994
Tabor Island	anorthosite, leuconorite	1311 +/- 2	U-Pb	Hamilton et al., 1994
Jonathon Island	leuconorite, leucotroctolite	1311 +/- 2	U-Pb	Hamilton et al., 1994
Port Manvers Run	leuconorite, leucotroctolite	1308 +/- 2	U-Pb	in Ryan, 2001a

Plutonic rocks emplaced after 1310 Ma comprise: (a) a group of intrusions in the northeastern part of the Nain batholith that is spatially associated with the Kiglapait intrusion, and (b) a group of intrusions in the southern part of the Nain batholith that is spatially associated with the Notakwanon intrusion. Intrusions in the northeastern part of the Nain batholith include Kiglapait troctolite, Newark Island troctolite and gabbronorite, Slambang anorthosite, Tigalak ferrodiorite and Dog Island monzonite (Table 8.4). These intrusions were emplaced between ca. 1310 – 1290 Ma. Intrusions that are spatially associated with the Notakwanon intrusion include Koliktalik Island anorthosite, Goodnews granite and ferrodiorite, Satorsaukulluk ferrodiorite, Cabot Lake ferrodiorite and Sango Bay anorthosite. These intrusions were also emplaced between ca. 1310 –

1290 Ma. The plutonic rocks emplaced between 1310 – 1290 Ma are here grouped into episode 3 of the Nain batholith (Fig. 8.24).

Table 8.4: Mesoproterozoic plutonic rocks of the Nain batholith emplaced during episode 3 (1310 – 1290 Ma)

Intrusion	Rock type	Age (Ma)	Analysis	Reference
Northeastern part				
Kiglapait	troctolite, leucotroctolite	1306 +/- 2	U-Pb	in Miller et al., 1997
Newark Island	troctolite	1305 +/- 5	U-Pb	in Ryan, 1997
Slambang	leuconorite	1305	U-Pb	in Berg et al., 1994
Tigalak	ferrodiorite	1306 +/- 3	U-Pb	Hamilton et al., 1994
Dog Island	monzonite	1296	Pb-Pb	in Miller et al., 1997
Southern part				
Koliktalik Island	anorthosite	1305 +/- 2	U-Pb	Hamilton et al., 1994
Goodnews	granite	1305 +/- 10	U-Pb	in Miller et al., 1997
Satossuakuluk	ferrodiorite, monzonite	1301 +/- 2	U-Pb	Hamilton et al., 1994
Cabot Lake	ferrodiorite	1298 +/- 2	U-Pb	Hamilton et al., 1994
Sango Bay	leucotroctolite	1294 +/- 1	U-Pb	Hamilton et al., 1994
Notakwannon	granite	1292 +/- 4	U-Pb	Ryan et al., 1991

The waning stages of magmatism in the Nain batholith are characterized by the emplacement of the Flowers River peralkaline granite and associated volcanics in the southern-most part of the batholith and basaltic dikes across all intrusive rocks of the batholith (Table 8.5). These intrusions were emplaced between ca. 1290 – 1270 Ma and are grouped into episode 4 (Fig. 8.25). These high-level intrusions record the uplift of the Nain batholith during and shortly after emplacement of the bulk of intrusive rocks. In addition, the basaltic dikes are predominantly sub-vertically oriented and are east-west or north-south striking. These dikes extend the previously recognized periods of north-south and east-west deformation to as late as 1273 +/- 23 Ma.

In summary, episode 1 contains: (a) intrusive rocks that crystallized between 1370 and 1330 Ma, (b) anorthositic rocks with relatively Na-, K-, Ba- and Sr-rich plagioclase,

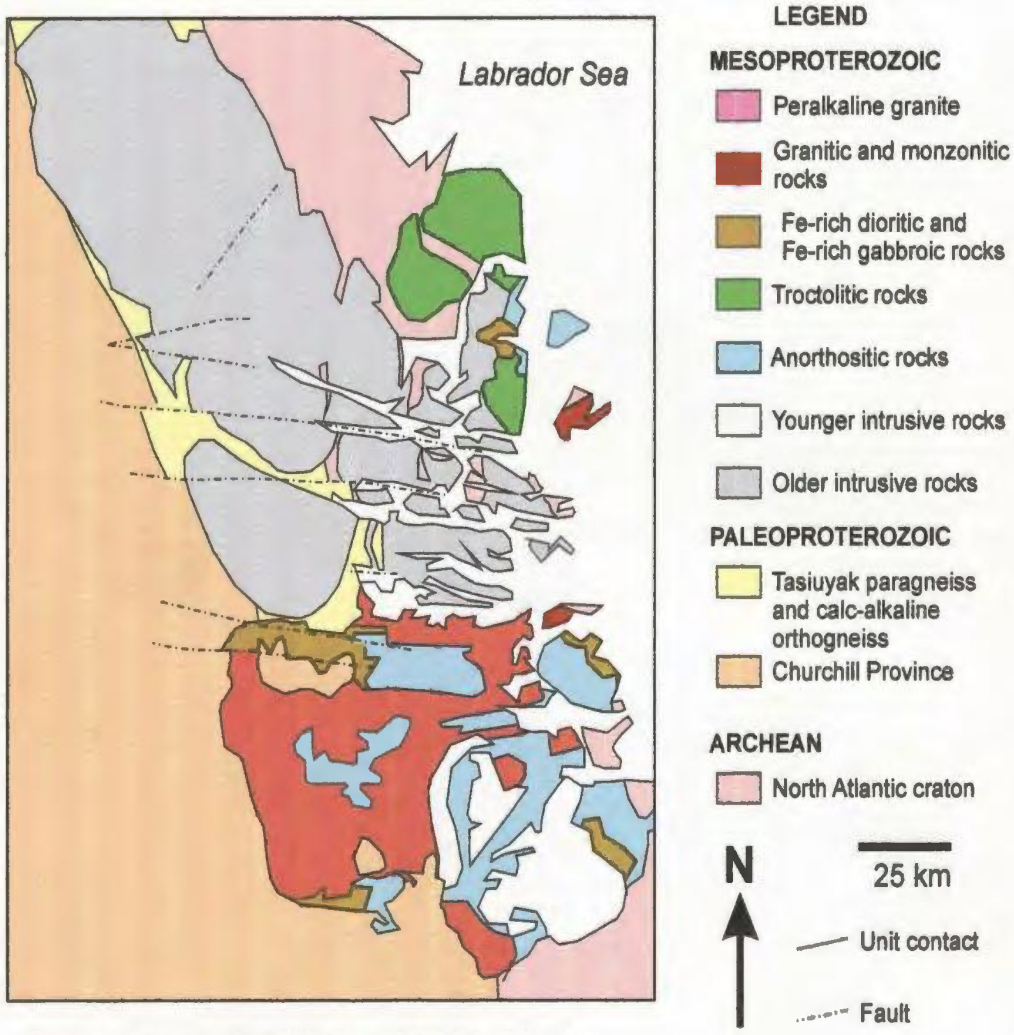

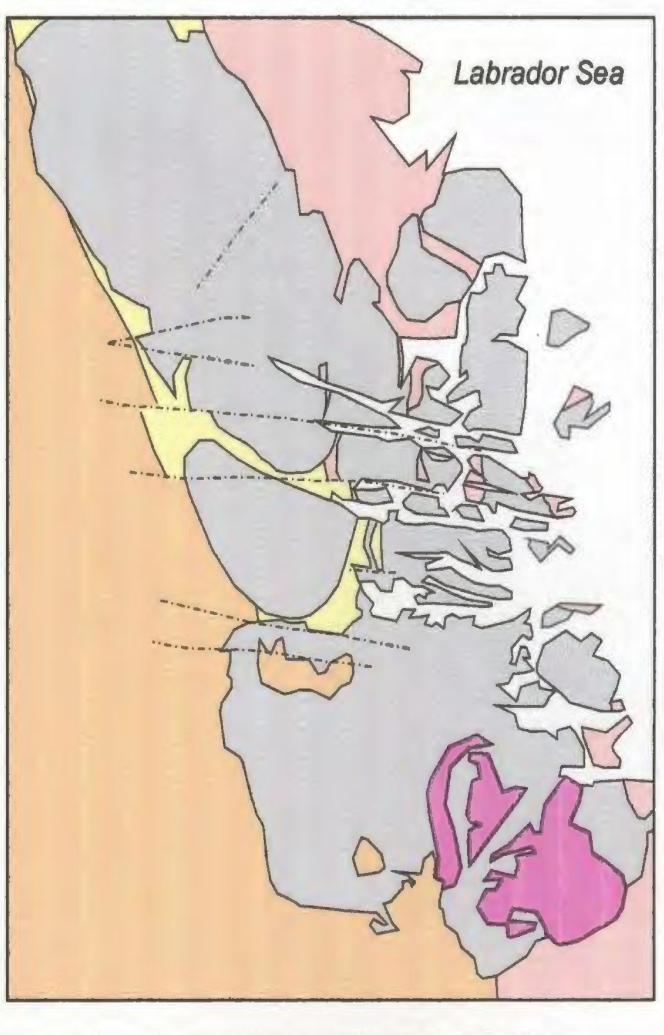

Figure 8.24: Episode 3 (1310 - 1290 Ma) of the Nain batholith showing the emplacement of troctolitic, anorthositic, Fe-rich dioritic and monzonitic rocks in the northeast, and anorthositic, granitic, monzonitic and Fe-rich dioritic rocks in the south.

Figure 8.25: Episode 4 (1290 - 1270 Ma) of the Nain batholith showing the emplacement of peralkaline granite. Basaltic dikes are not shown on this map, but were emplaced into some of the east-west trending faults shown on the figure, and into north-south trending faults as well.

Table 8.5: Mesoproterozoic plutonic rocks of the Nain batholith emplaced during episode 4

Intrusion	Rock type	Age (Ma)	Analysis	Reference
Flowers River	peralkaline granite	1289	U-Pb	in Miller et al., 1997
Nain LP dikes	basalt	1273 +/- 23	Rb-Sr	Carlson et al., 1993

and pyroxene as the primary Fe-Mg silicate, and (c) only minor abundances of other intrusive rocks. Episode 2 contains: (a) intrusive rocks that crystallized between 1330 and 1310 Ma, (b) anorthositic rocks that contain pyroxene and/or olivine, and (c) sub-equal abundances of granitic rocks. Episode 3 contains: (a) intrusive rocks that crystallized between 1310 and 1290 Ma, (b) anorthositic rocks that are similar to those in episode 2, and (c) relatively high abundances of troctolitic rocks (i.e. Kiglapait intrusion). Episode 4 is more of an extrusive episode then an intrusive episode, and contains: (a) intrusive and extrusive rocks that crystallized between 1290 and 1270 Ma, (b) no anorthositic rocks, and (c) peralkaline volcanic and sub-volcanic intrusions, and basaltic dikes.

The origin of this episodic emplacement may be related to episodic heat input from the mantle or episodic crustal deformation. Figures 8.22 to 25 show how the intrusive rocks of the Nain batholith were emplaced in a relatively 'sporadic' manner over a period of ~100 m.y. The term sporadic is here used in contrast to the linear distribution of intrusions that may be expected from plume-related magmatism (see Ryan, 1997). This rather sporadic and long-winded emplacement is inconsistent with a heat input from a single mantle plume. Nor can any of the rock types in the AMCG suite be unequivocally correlated with plume-related magmatism. On the other hand, such sporadic and long-winded emplacement is known from extensional settings (see Tollo et al., 2004), which is consistent with previous ideas that the Nain batholith was emplaced

into a crustal-scale graben (Berg, 1977a) and/or an aborted rift zone (Yu and Morse, 1992).

Chapter 9: Conclusions

This study utilized descriptions of the form, contacts, petrography, textures, structures, mineral chemistry and whole rock chemistry to interpret the tectono-magmatic setting, ascent, emplacement and crystallization of anorthositic intrusions in the Nain batholith. This section lists the major conclusions of the study and provides some directions for future research to test the ideas presented in this thesis.

9.1 Conclusions

The following conclusions have been reached as part of this study:

1. Anorthositic, leucogabbroic granitic (olivine-pyroxene and biotite-hornblende types) and/or true gabbroic (gabbronoritic, troctolitic, Fe-rich gabbroic, Fe-rich dioritic) rocks from composite structures in the study area that consist of: (a) a sub-horizontally oriented core, and (b) a sub-vertically oriented margin. These composite structures are here termed 'centered intrusive complexes'. The various rock types in these complexes were emplaced in a broadly similar time frame (1-10's of m.y.).

2. Strongly deformed rocks in the margins of centered intrusive complexes developed in Mesoproterozoic ductile shear zones that were periodically active during emplacement of the Nain batholith. These shear zones are predominantly sub-vertical and north-south or east-west striking. North-south shear zones strike parallel to Paleoproterozoic structures. On a regional scale, north-south

deformation of plutonic rocks in the Nain batholith occurred between 1351 and 1316 Ma and east-west deformation occurred between 1341 and 1311 Ma. This period of deformation overlaps with regional back-arc magmatism, lithospheric thinning and graben development in western Labrador and adjacent West Greenland.

3. The margins of centered intrusive complexes: (a) are composite, (b) are bound by ductile shear zones, (c) were periodically deformed in ductile shear zones, and (d) are elongate parallel to ductile shear zones. These relations suggest that the ascent and emplacement of anorthositic magma was controlled by ductile shear zones and contrasts with the diapiric emplacement typically ascribed to Proterozoic anorthositic magmas. Control by ductile shear zones also suggests a liquid-state rheology for anorthositic magma during ascent and emplacement. The form of the Tikkoatokak centered intrusive complex suggests that it was emplaced by floor depression.

4. The bulk of the Tikkoatokak centered intrusive complex was emplaced first, the Sophie centered intrusive complex was emplaced second and the Kikkertavak centered intrusive complex was emplaced third. Emplacement of the Tikkoatokak centered intrusive complex was into ductile crust and was structurally controlled by sub-vertical and north-south striking shear zones. Emplacement of the Kikkertavak centered intrusive complex was into brittle crust and was structurally

controlled by sub-vertical and east-west striking shear zones. The margin of the Sophie centered intrusive complex was deformed in both north-south and east-west shear zones. These findings indicate that between emplacement of the Tikkoatokak (>1333 +/- 2 Ma) and the Kikkertavak (ca. 1318 – 1311 Ma) centered intrusive complexes: (a) the rheology of country rock changed from ductile to brittle, and (b) structural control changed from predominantly north-south to east-west shear zones. This change in country rock rheology was most likely related to contemporaneous uplift of the Nain batholith and contrasts with previous studies that suggested this batholith was uplifted shortly after emplacement.

5. The textures, microstructures and mineralogy of anorthositic rocks in the study area indicate: (a) the crystallization of anorthositic rocks involved densification and/or cementation, (b) high-T deformation and/or recrystallization, and (c) redistribution, segregation and aggregation of interstitial melt. All of these processes are consistent with the compaction of cumulus plagioclase frameworks during the crystallization of anorthositic magmas. In addition, it is suggested that partial compaction, deformation and/or recrystallization formed: (a) mottled rocks, (b) layered rocks, (c) foliated rocks, (d) planar pyroxene aggregates, and (e) calcic rims on plagioclase crystals. These findings indicate that the structures of anorthositic rocks formed when the rheology of the magma was mostly solid-state

and contrast with previous work that interpreted textures and structures in terms of liquid-state behavior.

6. Studies of petrography, mineralogy and geochemistry indicate that, over time, the anorthositic magmas became (1) depleted in Si, K and Ba and (2) enriched in Ca and Mg/(Fe+Mg). These characteristics suggest that more crustally-derived and/or evolved anorthositic magmas were emplaced prior to more mantle-derived and/or primitive anorthositic magmas.

7. The emplacement of the Nain batholith (1365 – 1270 Ma) is divided into four episodes. Episode 1 (1365 – 1330 Ma) comprised the emplacement of mostly NB noritic anorthosite, Fe-rich dioritic rocks and monzonitic rocks. Episode 2 (1330 – 1310 Ma) comprised the emplacement of mostly NB noritic anorthosite, NB troctolitic anorthosite and granitic rocks. Episode 3 (1310 – 1290 Ma) comprised the emplacement of mostly troctolitic rocks in the northeastern part of the batholith, and anorthositic and granitic rocks in the southern part of the batholith. Episode 4 (1290 – 1270 Ma) involved the emplacement of basaltic dikes, and peralkaline volcanics and sub-volcanic intrusions. The space-time distribution of intrusive complexes in these episodes suggest that the Nain magmatic event was more likely related to extension of the crust then to impingement of a plume.

9.2 Recommendations for future work

This section describes some tests that may be used to further investigate the conclusions 1 to 6.

1. The ideas of 'cores' and 'margins' may be used to further sub-divide the Nain batholith into centered intrusive complexes. Work done by the Labrador Research Group at Memorial already suggests that there are at least two more centered intrusive complexes, which may be termed 'Ametok' and 'Susie'. Mapping in the margins of these intrusive complexes has shown that they also contain strongly deformed rocks. Detailed U-Pb isotopic studies of the intrusive rocks in these complexes shows that, like those in the study area, they were emplaced over periods of 1 to 10's m.y.
2. A detailed mapping and sampling study of the various north-south and east-west shear zones in the study area would also be interesting. Mapping should be dome at 1:1000 or 1:2000 and would help to further support a model that Proterozoic anorthositic rocks were derived from leucogabbroic parental magmas that were emplaced along crustal-scale weaknesses. The detailed geochronology study would help in investigating the re-setting of zircons in a dynamic magmatic flow environment. The age distribution of igneous zircons may also help delineate peak times of magma transport and emplacement.

3. A detailed structural study of anorthositic rocks in the margins of centered intrusive complexes to help further the hypothesis that they were formed under tectonic stress. This detailed study would also entail looking for structures in the country rock that suggests they were also overprinted in the Mesoproterozoic, and should also look along the margins of the Nain batholith for Mesoproterozoic deformation that was not associated with magma emplacement. This latter finding would be a great help in trying to dispel the idea that all deformation is simply related to magma emplacement.
4. A detailed microprobe and cathodo-luminescence studies of plagioclase crystals in anorthositic rocks would be a good way to examine the zoning patterns. If reverse zoning occurs in textural strain shadows of plagioclase crystals then this supports an origin for reverse zoning by compaction. This would be a novel conclusion on the origins of zoning in igneous rocks and would be quite logical in the face of the abundant compaction that the anorthositic rocks were likely to have underwent.

References

Note: all references labeled NAP refer to: Morse, S.A., (ed), Nain Anorthosite Project, Field report, University of Massachusetts.

Ameglio, L., Vigneresse, J.L., and Bouchez, J.L., 1997. Granite pluton geometry and emplacement mode inferred from combined fabric and gravity data. In: J.L. Bouchez (ed), Granite: from segregation of melt to emplacement fabrics. Kluwer Academic Press, Dordrecht, p. 199-214.

Amelin, Y.V., Li, C., and Naldrett, A.J., 1999. Geochronology of the Voisey's Bay intrusion, Labrador, Canada, by precise U-Pb dating of coexisting baddeleyite, zircon and apatite. Lithos, 47, p. 33-51.

Annen, C., and Sparks, R.S.J., 2002. Effects of repetitive emplacement of basaltic intrusions on thermal evolution and melt generation in the crust. Earth and Planetary Science Letters, 203, p. 937-955.

Ashwal, L.D., Wiebe, R.A., Wooden, J.L., Whitehouse, M.J. and Snyder, D.J., 1992. Pre-Elsonian mafic magmatism in the Nain igneous complex, Labrador: the Bridges layered intrusion. Precambrian Research, 56, p. 73-87.

Ashwal, L. D., 1993. Anorthosites. Springer-Verlag, Berlin, p. 82-217.

Barnichon, J.D., Havenith, H., Hoffer, B., Charlier, R., Jongmans, D. and Duchesne, J.C., 1999. The deformation of the Egersund-Ogna anorthosite massif, south Norway: finite-element modeling of diapirism. Tectonophysics, 303, p. 109-130.

Barros, C.E.M., Barbey, P., and Boullier, A.M., 2001. Role of magma pressure, tectonic stress and crystallization progress in the emplacement of syntectonic granites. The A-type Estrela granite complex (Carajas Mineral Province, Brazil). Tectonophysics, 343, p. 93-109.

Barton Jr., J.M., 1996. The Messina layered intrusion, Limpopo belt, South Africa: an example of in situ contamination of an Archean anorthosite complex by continental crust. Precambrian Research, 78, p. 139-150.

Bates, R.L., and Jackson, J.A., 1984. Dictionary of geological terms. Anchor Books, Doubleday, NewYork.

Bédard, J.H., 2001. Parental magmas of the Nain Plutonic Suite anorthosites and mafic cumulates; a trace element modeling approach. Contributions to Mineralogy and Petrography, 141, p. 747-771.

Berg, J.H., 1972. Geology of the Hettasch Lake area. NAP, p. 49-64.

Berg, J.H., 1973. Further study of the Hettasch intrusion and associated rocks. NAP, p. 107-119

Berg, J.H., 1975. Aphebian metasedimentary and related rocks in the Synder Bay Avakutakh River area, Labrador. NAP, p. 7-19.

Berg, J.H., 1977a. Regional geobarometry in the contact aureoles of the anorthositic Nain Complex, Labrador. Journal of Petrology, 18, p. 399-430.

Berg, J.H., 1977b. Dry granulite mineral assemblages in the contact aureoles of the Nain Complex, Labrador. Contributions to Mineralogy and Petrology, 64, p. 33-52.

Berg, J.H., 1980. Snowflake troctolite in the Hettasch Intrusion, Labrador: evidence for magma-mixing and supercooling in a plutonic environment. Contributions to Mineralogy and Petrology, 72, p. 339-351

Berg, J.H., and Briegel, J.S., 1981. Geology of the Jonathon intrusion and associated rocks. NAP, p. 43-50.

Berg, J.H., Emslie, R.F., Hamilton, M.A., Morse, S.A., Ryan, A.B. and Wiebe, R.A., 1994. Anorthositic, granitoid and related rocks of the Nain Plutonic Suite. Field guide, IGCP #290 - #315 excursion.

Bertrand, J.M., Roddick, J.C., Van Kranendonk, M.J. and Ermanovics, I., 1993. U-Pb geochronology of deformation and metamorphism across a central transect of the early Proterozoic Torngat orogen, North River map area, Labrador. Canadian Journal of Earth Sciences, 30, p. 1470-1489.

Bhattacharya, A., Raith, M., Hoernes, S. and Banerjee, D., 1998. Geochemical evolution of the massif-type anorthosite complex at Bolangir in the Eastern Ghats belt of India. Journal of Petrology, 39, p. 1169-1193.

Bolle, O., Demaiffe, D., and Duchesne, J.C., 2003. Petrogenesis of jotunitic and acidic members of an AMC suite (Rogaland anorthosite province, SW Norway): a Sr and Nd isotopic assessment. Precambrian Research, 124, p. 185-214.

Brand, S., 1974. The geology of the Khingughutik River area. NAP, p. 49-57.

Brown, M., Rushmer, T., and Sawyer, E., 1995. Introduction to special section: mechanisms and consequences of melt segregation from crustal protoliths. Journal of Geophysical Research, 100, p. 15551-15563

Brown, D., Tryggvason, A., 2001. Ascent mechanisms of the Dzhabyk batholith, Southern Urals; constraints from URSEIS reflection seismic profiling. Journal of the Geological Society of London, 158, p. 881-884.

Buchan, K.L., Erns, R.E., Hamilton, M.A., Mertansen, S., Pesonen, L.J., Elming, S-A, 2001. Rodinia: the evidence from integrated palaeomagnetism and U-Pb geochronology. Precambrian Research, 110, p. 9-32.

Buddington, A.F., 1969. Adirondack anorthosite series. In Origin of anorthosite and related rocks, Y.W. Isachsan (ed), New York State Museum Science Service, Memoir 18, Albany, p. 215-231.

Cadman, A.C., Noble, S.R., Tarney, J., Park, R.G., Ryan, A.B. and Royse, K.R., 1999. U-Pb ages of syndeformational dykes associated with the Nain Plutonic Suite, Labrador. Canadian Journal of Earth Sciences, 36, p. 339-348.

Cambray, F.W., Vogel, T.A., and Mills Jr., J.G., 1995. Origin of compositional heterogeneities in tuffs of the Timber Mountain Group: the relationship between magma batches and magma transfer and emplacement in an extensional environment. Journal of Geophysical Research, 100, p. 15793-15805.

Carlson, R.W., Wiebe, R.A. and Kalamarides, R.I., 1993. Isotopic study of basaltic dikes in the Nain Plutonic Suite: evidence for enriched mantle sources. Canadian Journal of Earth Sciences, 30, p. 1141-1146.

Carr, M., 2000. Igpet2000 for Win95/98/NT. Terra Softa Inc., New Jersey.

Christie, R.L., Embry, A.F., and Van Dyck, G.A., (ed), 1981. Lexicon of Canadian stratigraphy. Canadian Society of Petroleum Geologists, 85 p.

Clemens, J.D., and Mawer, C.K., 1992. Granitic magma transport by fracture propagation. Tectonophysics, 204, p. 339-360.

Connelly, J., and Ryan, B., 1994. Late Archean and Proterozoic events in the central Nain craton. In Wardle, R.J., and Hall, J., LITHOPROBE: Eastern Canadian shield onshore-offshore transect (ESCOOT), report of transect meeting, 36, p. 53-61.

Connelly, J.N. and Ryan, B., 1996. Late Archean evolution of the Nain Province, Nain, Labrador: imprint of a collision. Canadian Journal of Earth Sciences, 33, p. 1325-1342.

Connelly, J.N., and Ryan, A.B., 1998. Age and tectonic implication of Paleoproterozoic granitoid intrusions within the Nain Province near Nain, Labrador. Canadian Journal of Earth Sciences, 36, p. 833-853.

Corfu, F., Hanchar, J.M., Hoskin, P.W.O., and Kinny, P., 2003. Atlas of zircon textures. In Reviews in Mineralogy and Geochemistry, 53, p. 468-500.

Cruden, A.R., 1990. Flow and fabric development during the diapiric rise of magma. Journal of Geology, 98, p. 681-698.

Davies, H.M., 1973a. Emplacement sequence of anorthositic rocks in the southeastern portion of the Nain Complex. NAP, p. 59-66

Davies, H.M., 1973b. Geology of Nukasorsuktokh Island. NAP, p. 81-95.

DePaolo, D.J., 1985. Isotopic studies of processes in mafic magma chambers: I. The Kiglapait layered Intrusion, Labrador. Journal of Petrology, 26, p. 925-951.

de Waard, D., 1972. Anorthosite-adamellite contact on Dog Island, Labrador. NAP, p. 63-69.

de Waard, D., and Mulhern, K., 1972. The Barth layered structure. NAP, p. 71-79.

de Waard, D., 1973. Nain Complex: General. In NAP, p. 41-43.

de Waard, D., and Hancock, S., 1973. Gabbroic-granodioritic dike in the Nain anorthosite massif, Labrador. NAP, p. 97-100.

de Waard, D., 1976. Anorthosite-adamellite-troctolite layering in the Barth Island structure of the Nain complex, Labrador. Lithos, 9, p. 833-853.

de Waard, D., Mulhern, K., and Merriam, D.F., 1976. Mineral variation in anorthositic, troctolitic, and adamellitic rocks of the Barth Island Layered Structure in the Nain Anorthosite Complex, Labrador. Mathematical Geology, 8, p. 561-574.

Deer, W.A., Howie, R.A. and Zussman, J., 1992. An introduction to the rock forming minerals. Longman, Harlow, p. 431-454.

Dehls, J.F., Cruden, A.R., and Vigneresse, J.L., 1998. Fracture control of late Achaean pluton emplacement in the northern Slave Province, Canada. Journal of Structural Geology, 20, p. 1145-1154.

Dempster, T.J., Preston, R.J. and Bell, B.R., 1999. The origin of Proterozoic massif-type anorthosites: evidence from interactions between crustal xenoliths and basaltic magma. Journal of the Geological Society of London, 156, p. 41-46.

Deuring, D.E., 1975. Akpaume layered intrusion: Field aspects. NAP, p. 7626

Dick, H.J.B., and Sinton, J.M., 1979. Compositional layering in alpine peridotites: evidence for pressure solution creep in the mantle. Journal of Geology, 87, p. 403-416.

Dubé, B., Dunning, G.R., Lauziere, K., and Roddick, J.C., 1996. New in-sights into the Appalachian orogen from geology and geochronology along the Cape Ray fault zone, southwest Newfoundland. Bulletin of the Geological Society of America, 108, p. 101-116

Duchesne, J.C., and DeMaiffe, D., 1978. Trace elements and anorthosite genesis. Earth and Planetary Science Letters, 38, p. 249-272.

Duchesne, J.C., 1984. Massif anorthosites: another partisan review. In: Brown, W.L. (ed) Feldspar and Feldspathoids. NATO ASI. Kluwer Academic Press, Dordrecht, p. 411-433.

Duchesne, J.C., Liegeois, J.P., Vander Auwera, J. and Longhi, J., 1999. The crustal tongue melting model and the origin of massive anorthosites. Terra Nova, 11, p. 100-105.

Emslie, R.F., 1975. Pyroxene megacrysts from anorthositic rocks: new clues to the sources and evolution of the parent magma. Canadian Mineralogist, 13, p. 138-145.

Emslie, R.F., 1978. Elsonian magmatism in Labrador: age, characteristics and tectonic setting. Canadian Journal of Earth Sciences, 15, p. 438-453.

Emslie, R.F., 1980. Geology and petrology of the Harp Lake complex, central Labrador: an example of Elsonian magmatism. Geological Survey of Canada, Bulletin 293.

Emslie, R.F. and Loveridge, W.D., 1992. Fluorite-bearing early and middle Proterozoic granites, Okak Bay area, Labrador: geochronology, geochemistry and petrogenesis. Lithos, 28, p. 87-109.

Emslie, R.F. and Stirling, J.A.R., 1993. Rapakivi and related granitoids of the Nain Plutonic Suite: Geochemistry, mineral assemblages, and fluid equilibria. Canadian Mineralogist, 31, p. 821-847.

Emslie, R. F., Hamilton, M. A. and Thériault, R. J., 1994. Petrogenesis of a Mid-Proterozoic anorthosite-mangerite-charnockite-granite (AMCG) complex: isotopic and chemical evidence from the Nain Plutonic Suite. Journal of Geology, 102, p. 539-558.

Emslie, R.F., 1996. Troctolitic rocks of the Reid Brook intrusion, Nain Plutonic Suite, Voisey Bay area, Labrador. Geological Survey of Canada, Current Research 1996-C, p. 183-196.

Evans-Lamswood, D.M., Butt, D.P., Jackson, R.S., Lee, D.V., Muggridge, M.G., Wheeler, R.I., and Wilton, D.H.C., 2000. Physical controls associated with the distribution of sulfides in the Voisey's Bay Ni-Cu-Co deposit, Labrador. Economic Geology, 95, p. 749-769.

Ferre, E., Gleizes, G., Djouadi, M.T., and Bouchez, J.L., 1997. Drainage and emplacement of magmas along an inclined transcurrent shear zone: petrophysical evidence from a granite-charnockite pluton (Rahama, Nigeria). In J.L. Bouchez (ed), Granite: from segregation of melt to emplacement fabrics, Kluwer Academic Press, Dordrecht, p. 253-273.

Fram, M.S. and Longhi, J., 1992. Phase equilibria of dikes associated with Proterozoic anorthosite complexes. American Mineralogist, 77, p. 605-616.

Funck, T., Louden, K.E. and Reid, I.D., 2000. Wide-angle seismic imaging of a Mesoproterozoic anorthosite complex: The Nain Plutonic Suite in Labrador, Canada. Journal of Geophysical Research, 105, B11, p. 25693-25707.

Gaskill, O.D., 2005. Geology of the 1.33 – 1.32 Ga Barth Island Ring Complex, near Nain, Labrador. Memorial University of Newfoundland M.Sc. thesis, 257 p.

Gleizes, G., LeBlanc, D., Santana, V., Olivier, P., Bouchez, J.L., 1998. Sigmoidal structure featuring dextral shear during emplacement of the Hercyninan granite complex of Cauterets-Panticosa (Pyrenees). Journal of Structural Geology, 20, p. 1229-1245.

Govindaraju, K., 1989. 1989 compilation of working values and sample description for 272 geostandards. Geostandards Newsletter, 13, 113 p.

Hall, A., 1996. Igneous petrology. Longman, Harlow, p. 483-508.

Hamilton, M.A., Emslie, R.F., and Roddick, J.C., 1994. Detailed emplacement chronology of basic magmas of the Mid-Proterozoic Nain Plutonic Suite, Labrador: insights from U-Pb systematics in zircon and baddeleyite. ICOG VIII conference at Berkeley, program with abstracts, p. 124.

Hamilton, M.A., 1997. New U-Pb geochronological results from the Mesoproterozoic Nain Plutonic Suite, Labrador, and implications for the origin and emplacement of massif anorthosites and related rocks. COPENA conference at NGU, program with abstracts, p. 97.

Hanchar, J.M., and Miller, C.F., 1993. Zircon zonation patterns as revealed by cathodoluminescence and backscattered electron images; implications for interpretation of complex crustal histories. Chemical Geology, 110, p. 1-13.

Harlov, D.E., 2000. Apparent pyrrhotite-chalcopyrite solid solutions in charnockites; the Shevoroy Hills massif, Tamil Nadu, S India and the Bable Sector, SE Norway. Mineralogical Magazine, 64, p. 853-865.

Higgins, M.D., 1991. The origin of laminated and massive anorthosite, Sept Iles layered intrusion, Quebec, Canada. Contributions to Mineralogy and Petrology, 106, p. 340-354.

Hill, J.D., 1982. Geology of the Flowers River-Notakwanon River area, Labrador. Newfoundland Department of Mines and Energy, Report 82-6, 140 p., 2 maps.

Hinchey, J., Kerr, A., Wilton, D., 1999. Magmatic sulphide-oxide mineralization in the Nain Hill area (NTS 14C/12), northern Labrador. Current Research, Newfoundland Department of Mines and Energy, Geological Survey Report 99-1, p. 183-194.

Hollister, L.S., and Crawford, M.L., 1986. Melt-enhanced deformation: a major tectonic process. Geology, 14, p. 558-561.

Hunter, R.H., 1996. Texture development in cumulate rocks. In: Cawthorne, R.G. (ed), Layered Intrusions, Elsevier, Amsterdam, p. 77-101.

Hutton, D.H.W., and Reavy, R.J., 1992. Strike-slip tectonics and granite petrogenesis. Tectonics, 11, p. 960-967.

Irvine, 1982. Terminology for layered intrusions. Journal of Petrology, 23, p. 127-162.

Isachsen, Y.W., and Moxham, R.L., 1969. Chemical variation in plagioclase megacrysts from two vertical sections in the main Adirondack metanorthosite massif. In Origin of anorthosite and related rocks, Y.W. Isachsan (ed), New York State Museum Science Service, Memoir 18, Albany, p. 255-265.

James, D.T., Kamo, S., and Krogh, T.E., 2002. Evolution of 3.1 and 3.0 Ga volcanic belts and a new thermotectonic model for the Hopedale block, North Atlantic craton (Canada). Canadian Journal of Earth Sciences, 39, p. 687-710.

Jenner, G.A., Longerich, H.P., Jackson, S.E., and Fryer, B.J., 1990. ICP-MS; a powerful tool for high-precision trace-element analysis in earth sciences; evidence from analysis of selected U.S.G.S. reference samples. Chemical Geology, 83, p. 133-148.

Kerr, A., 2003. Nickeliferous gabbroic intrusions of the Pants Lake area, Labrador, Canada; implications for the development of magmatic sulfides in magmatic systems. American Journal of Science, 303, p. 221-258.

Kretz, R., 1983. Symbols for rock-forming minerals. American Mineralogist, 68, p. 277 279.

Kroener, A., and Williams, I.S., 1993. Age of metamorphism in the high-grade rocks of Sri Lanka. Journal of Geology, 101, p. 513-521.

Krogh, T.E., and Davis, D.L., 1973. The significance of inherited zircons on the age and origin of igneous rocks – an investigation of the ages of the Labrador adamellites. Carnegie Institute Yearbook, 72, p. 610-613.

Krogh, T.E., 1982. Improved accuracy of U-Pb zircon ages by the creation of more concordant systems using air abrasion technique. Geochimica et Cosmochimica Acta, 46, p. 637-644

Lafrance, B., John, B.E. and Scoates, J.S., 1996. Syn-emplacement recrystallization and deformation microstructures in the Poe Mountain anorthosite, Wyoming. Contributions to Mineralogy and Petrology, 122, p. 431-440.

Lagarde, J.L., Omar, S.A., and Roddaz, B., 1990. Structural characteristics of granitic plutons emplaced during weak regional deformation: examples from the late Carboniferous plutons, Morocco. Journal of Structural Geology, 12, p. 805-821.

Le Maitre, R.W. (ed), 2002. Igneous rocks, a classification and glossary of terms. University Press, Cambridge, UK. 236 p.

Leitch, A., 2003. Magma properties and transport. Unplublised course handout (GLGY 6070), Memorial University of Newfoundland, St John's.

Letteney, C.D., 1969. The anorthosite-charnockite series of the Thirteenth Lake dome, south-central Adirondacks. In Origin of anorthosite and related rocks, Y.W. Isachsan (ed), New York State Museum Science Service, Memoir 18, Albany, p. 329-342.

Li, C., Lightfoot, P.C., Amelin, Y. and Naldrett, A., 2000. Contrasting petrological and geochemical relationships in the Voisey's Bay and Mushua intrusions: implications for ore genesis. Economic Geology, 95, p. 771-799.

Longerich, H.P., Jenner, G.A., Fryer, B.J., and Jackson, S.E., 1990. Inductively Coupled plasma-mass spectrometric analysis of geological samples; a critical evaluation based on case studies. Chemical Geology, 83, p. 105-118.

Longerich, H., 1995. Analysis of Pressed Pellets of Geological Samples using Wavelength-Dispersive X-Ray Fluorescence Spectrometry. X-Ray Spectrometry, 24, p. 123-126

Longhi, J., Fram, M.S., Vander Auwera, J. and Montieth, J.N., 1993. Pressure effects, kinetics, and rheology of anorthositic and related magmas. American Mineralogist, 78, p. 1016-1030.

Longhi, J., Van der Auwera, J. and Fram, M.S., 1999. Some phase equilibrium constraints on the origin of Proterozoic (Massif) anorthosites and related rocks. Journal of Petrology, 40, p. 61-77.

Ludwig, K.R., 1993. UISO; a program for calculation of $^{230}Th - ^{234}U - ^{238}U$ isochron ages. Open-file report – U.S. Geological Survey Report.

Ludwig, K.R., 2003. Isoplot 3.00. Program for Microsoft Excel.

Marsh, B.D., 1981. On the crystallinity, probability of occurrence and rheology of lava and magma. Contributions to Mineralogy and Petrology, 78, p. 85-98.

Marshak, S., and Mitra, G., 1988. Basic methods of structural geology. Prentice Hall, New Jersey, 446 p.

Martignole, J.,Machado, N., Nantel, S., 1993. Timing of intrusion and deformation of the Rivière-Pentecôte anorthosite (Grenville Province). Journal of Geology, 101, p. 652-658.

McBirney, A.R., and Hunter, R.H., 1995. The cumulate paradigm reconsidered. Journal of Geology, 103, p. 114-122.

Mengel, F., and Rivers, T., 1989. Thermotectonic evolution of Proterozoic and reworked Archaean terranes along the Nain – Churchill boundary in the Saglek area, northern Labrador. From Daly, J.S., Cliff, R.A., and Yardley, B.W.D. (eds),

Evolution of Metamorphic belts, Geological Society Special Publication, 43, p. 319-324.

Mengel, F., and Rivers, T., 1997. Metamorphism in the Paleoproterozoic Torngat orogen, Labrador: petrology and P-T-t paths of amphibolite- and granulite-facies rocks across the Komaktorvik shear zone. The Canadian Mineralogist, 35, p. 1137-1160.

Miller, R.B., and Paterson, S.R., 1994. The transition from magmatic to high-T solid state deformation: implications from the Mount Stuart batholith, Washington. Journal of Structural Geology, 16, p. 853-865.

Miller, R.R., Heaman, L.M. and Birkett, T.C., 1997. U-Pb zircon age of the Strange Lake peralkaline complex: implications for Mesoproterozoic peralkaline magmatism in north-central Labrador. Precambrian Research, 81, p. 67-82.

Mitchell, J.N., Scoates, J.S., Frost, C.D., 1995. High-Al gabbros in the Laramie anorthosite complex, Wyoming: implications for the composition of melts parental to Proterozoic anorthosite. Contributions to Mineralogy and Petrology, 119, p. 166-180.

Mitchell, J.N., Scoates, J.S., Frost, C.D. and Kolker, A., 1996. The geochemical evolution of anorthosite residual magmas in the Laramie anorthosite complex, Wyoming. Journal of Petrology, 37, p. 637-660.

Moreau, C., Demaiffe, D., Bellion, Y., and Boullier, A-M., 1994. A tectonic model for the location of Palaeozoic ring complexes in Air (Niger, West Africa). Tectonophysics, 234, p. 129-146.

Morse, S.A., 1969a. The Kiglapait layered intrusion, Labrador. Geological Society of America, Memoir 112, 204 p.

Morse, S.A., 1969b. Layered intrusions and anorthosite genesis. In Origin of anorthosite and related rocks, Y.W. Isachsan (ed), New York State Museum Science Service, Memoir 18, Albany, p. 175-187.

Morse, S.A., 1972a. Plagioclase composition variation. NAP, p. 103-111

Morse, S.A., 1972b. The feldspar/magma density paradox and evidence of crystal settling: layering, lamination, channel scouring. NAP, p. 113-116.

Morse, S.A., and Wheeler, E.P., 1973. Layered anorthosite massifs along Tikkoatokhakh Bay. NAP, p. 129-132.

Morse, S.A., 1981b. Reconnaissance geology of the Bird Lake anorthosite massif, Labrador. NAP, p. 37-41.

Morse, S.A., 1981c. Emplacement history of the Nain complex. NAP, p. 9-15

Morse, S.A. and Nolan, K.M., 1984. Origin of strongly reversed rims on plagioclase in cumulates. Earth and Planetary Science Letters, 68, p. 485-498.

Mukherjee, A., Jana, P., Das, S., 1999. The Banpur-Bagugan and Bolangir anorthosite diapirs of the Eastern Ghats, India; implications for the massif anorthosite problem. International Geology Review, 41, p. 206-241.

Myers, J.S., 1975. Cauldron subsidence and fluidization: mechanisms of intrusion of the Coastal Batholith of Peru into its own volcanic ejecta. Geological Society of America Bulletin, 86, p. 1209-1220.

Myers, J.S., 2000. Unpublished geological map of the Hare Hill area.

Naslund, H.R., and McBirney, A.R., 1996. Mechanisms of formation of igneous layering. In: Cawthorne, R.G. (ed), Layered Intrusions, Elsevier, Amsterdam, p. 1-43.

Neves, S.P., Araujo, A.M.B., Correia, P.B., and Gorki, M., 2003. Magnetic fabrics in the Cabanas granite (NE Brazil); interplay between emplacement and regional fabrics in a dextral transpressive regime. Journal of Structural Geology, 25, p. 441-453.

Nielsen, F.M., Campbell, I.H., McCulloch, M., and Wilson, J.R., 1996. A strontium isotope investigation of the Bjerkreim-Sokndal layered intrusion, southwest Norway. Journal of Petrology, 37, p. 171-193.

Olmsted, J.F., 1969. Petrology of the Mineral Lake intrusion, northwestern Wisconsin. In Origin of anorthosite and related rocks, Y.W. Isachsan (ed), New York State Museum Science Service, Memoir 18, Albany, p. 255-265.

Olson, K.E. and Morse, S.A., 1990. Regional Al-Fe mafic magmas associated with anorthosite-bearing terranes. Nature, 344, p. 760-762.

Owens, B.E., Rockow, M.W., and Dymek, R.F., 1993. Jotunites from the Grenville Province, Quebec: petrological characteristics and implications for massif anorthosite petrogenesis. Lithos, 30, p. 57-80.

Palansky, G.A., 1972. The Bridges area. In NAP, p. 83-89.

Parrish, R.R., 1987. An improved micro-capsule for zircon dissolution in U-Pb geochronology. Chemical Geology; Isotope Geoscience, Section 66, p. 99-102.

Paterson, S.R., Fowler Jr., T.K., Schmidt, K.L., Yoshinobu, A.S., Yuan, E.S., and Miller, R.B., 1998. Interpreting magmatic fabric patterns in plutons. Lithos, 44, p. 53-82.

Paterson, S.R., and Miller, R.B., 1998a. Stoped blocks in plutons: paleoplumb bobs, viscometers, or chronometers? Journal of Structural Geology, 20, p. 1261-1272.

Paterson, S.R., and Miller, R.B., 1998b. Mid-crustal magmatic sheets in the Cascade Mountains, Washington: implications for magmatic ascent. Journal of Structural Geology, 20, p. 1345-1363.

Perchuk, L.L., and Gerya, T.V., 1993. Fluid control on charnockitization. Chemical Geology, 108, p. 175-186.

Petford, N., Cruden, A.R., McCaffrey, K.J.W. and Vigneresse, J-L., 2000. Granite magma formation, transport and emplacement in the earth's crust. Nature, 408, p. 669-673.

Philpotts, A.R., 1990. Principles of igneous and metamorphic petrology. Prentice Hall, New Jersey, p. 12-92.

Philpotts, A.R. and Carroll, M., 1996. Physical properties of partly melted tholeiitic basalt. Geology, 24, p. 1029-1032.

Philpotts, A.R., Carroll, M. and Hill, J.M., 1996. Crystal-mush compaction and the origin of pegmatitic segregation sheets in a thick flood-basalt flow in the Mesozoic Hartford basin, Connecticut. Journal of Petrology, 37, p. 811-836.

Phinney, W.C., 1969. Anorthosite occurrences in Keweenawan rocks of northeastern Minnesota. In Origin of anorthosite and related rocks, Y.W. Isachsan (ed), New York State Museum Science Service, Memoir 18, Albany, p. 135-147.

Piper, J.D.A., 1995. The paleomagnetism of middle Proterozoic dyke swarms of the Gardar Province and Mesozoic dykes in SW Greenland. Geophysical Journal International, 120, p. 339-355.

Rahaman, M.A., van Breemen, O., Bowden, P., and Bennett, J.N., 1984. Age migrations of anorogenic ring complexes in northern Nigeria. Journal of Geology, 92, p. 173-184.

Ranson, W.A., 1975. Geology of the Iglokhsoakhtaliksoakh Lake area, NAP, p. 35-50.

Ranson, W.A., 1981. Anorthosites of diverse magma types in the Puttuaaluk Lake area. Nain complex, Labrador. Canadian Journal of Earth Sciences, 18, p. 26-41.

Rawlings-Hinchey, A.M., Sylvester, P.J., Myers, J.S., Dunning, G.R., and Kosler, J., 2003. Paleoproterozoic crustal genesis; calc-alkaline magmatism in the Torngat orogen, Voisey's Bay area, Labrador. Precambrian Research, 125, p. 55-85.

Rivers, T., Mengel, F., Scott, D.J., Campbell, L.M. and Goulet, N., 1996. Torngat orogen – a Paleoproterozoic example of a narrow doubly vergent collisional orogen. In: Brewer, T.S. (ed), Precambrian Crustal Evolution in the North Atlantic Region, Geological Society Special Publication, 112, p. 117-136.

Rivers, T., 1997.Lithotectonic elements of the Grenville Province; review and tectonic implications. Precambrian Research, 86, p. 117-154.

Rivers, T., and Corrigan, D., 2000. Convergent margin on southeastern Laurentia during the Mesoproterozoic; tectonic implications. Canadian Journal of Earth Sciences, 37, p. 359-383.

Rosenberg, C.L., and Stuenitz, H., 2003. Deformation and recrystallization of plagioclase along a temperature gradient; an example from the Bergell tonalite. Journal of Structural Geology, 25, p. 389-408.

Royce, K.R., Noble, S.R., Tarney, J. and Cadman, A.C., 1999. Country-rock contamination of marginal mafic granulites bordering the Nain Plutonic Suite: implications for mobilization of Sr during high-grade contact metamorphism. Canadian Journal of Earth Sciences, 36, p. 985-997.

Royce, K.R. and Park, R.G., 2000. Emplacement of the Nain Anorthosite: diapiric versus conduit ascent. Canadian Journal of Earth Sciences, 37, p. 1195-1207.

Rubins, C.C., and de Waard, D., 1971. Granulite zones in anorthosite near Nain, Labrador. Akademie van Wettenschappen, Amsterdam, Series BB, 74, p. 263-268.

Rubins, C.C., 1973. Structural, stratigraphic and petrological relations of rocks south of the Barth Island intrusion, Labrador. PhD thesis, University of Vermont, 100 p.

Ryan, B., and Lee., D., 1986. Gneiss-anorthosite-granite relationships in the Anaktalik Brook-Kogaluk River area (NTS 14D/1, 8), Labrador. Current Research, Newfoundland Department of Mines and Energy, 86-1, p. 79-88.

Ryan, B., Lee, D., and Corriveau, L., 1987. Geology of the eastern Churchill Province between Anaktalik Brook and Cabot Lake (NTS 14D/2, 6, 7), Labrador. Newfoundland Department of Mines and Energy, Current Research Report 87-1, p. 155-159.

Ryan, B., 1990. Preliminary geological map of the Nain Plutonic Suite and surrounding rocks (Nain-Nutak, NTS 14 S.W.). Newfoundland Department of Mines and Energy, Geological Survey Branch, Map 90-44, scale 1:500,000.

Ryan, B., 1991a. Makhavinekh Lake pluton, Labrador, Canada: geological setting, subdivisions, mode of emplacement, and a comparison with Finnish rapakivi granites. Precambrian Research, 51, p. 193-225.

Ryan, B., 1991b. New perspectives on the Nain Plutonic Suite and its country rocks. Newfoundland Department of Mines and Energy, Current Research Report 91-1, p. 213-255.

Ryan, B., Krogh, T.E., Heaman, L., Scharer, U., Phillipe, S., and Oliver, G., 1991. On recent geochronological studies in the Nain Province, Churchill Province and Nain Plutonic Suite, north-central Labrador. Newfoundland Department of Mines and Energy, Current Research Report 91-1, 257-261.

Ryan, B., 1996. Commentary on the location of the Nain-Churchill boundary in the Nain area. Newfoundland Department of Mines and Energy, Current Research Report 96-1, 109-129.

Ryan, B., 1997. The Mesoproterozoic Nain Plutonic Suite in Eastern Canada, and the setting of the Voisey's Bay Ni-Cu-Co sulphide deposit. Geoscience Canada, 24, p. 173-188.

Ryan, B., 2000a. Geological investigations in the type locality of the Nain Plutonic Suite (NTS 14C/12). Current Research, Newfoundland Department of Mines and Energy, Geological Survey Report 2000-1, 251-277.

Ryan, B., 2000b. The Nain-Churchill boundary and the Nain Plutonic Suite: a regional perspective on the geologic setting of the Voisey's Bay Ni-Cu-Co deposit. Economic Geology, 95, p. 703-724.

Ryan, B., 2001a. A provisional subdivision of the Nain Plutonic Suite in its type-area, Nain, Labrador (NTS Map Area 14C/12), Current Research, Newfoundland Department of Mines and Energy, Geological Survey Report 2001-1, p. 127-157.

Ryan, B., 2001b. Preliminary geological map of the Nain map sheet (NTS 14C/12), Scale 1;50 000, Map 2001-10, Geological Survey, Department of Mines and Energy, St John's, Open File 014C/12/0136.

Ryan, B. and James, D., 2003. The geology of Labrador between Tikkoatokak Bay and the Quebec border (NTS 14D, north half): a reconnaissance examination. Current Research, Newfoundland Department of Mines and Energy, 03-1, p. 137-165.

Ryan, B. and James, D., 2004. The Mesoproterozoic Nain Plutonic Suite and its country rocks in the Kingurutik Lake-Fraser River area, Labrador (NTS 14D/9 and 16). Current Research, Newfoundland Department of Mines and Energy, 04-1, p. 235-238.

Schiötte, L., Hansen, B.T., Shirey, S.B., and Bridgewater, D., 1993. Petrological and whole rock isotopic characteristics of tectonically juxtaposed Archean gneisses in the Okak area of the Nain Province, Labrador; relevance for terrane models. Precambrian Research, 63, p. 293-323.

Scoates, J.S., 1990. Syn-magmatic deformation of anorthosite: an assessment of the subsolidus evolution of anorthositic rocks in the 1.4 Ga Laramie anorthosite complex, Wyoming. Geological Society of America, Abstract with Programs, 22: A300.

Scoates, J.S., and Chamberlain, K.R., 1995. Baddeleyite (ZrO_2) and zircon ($ZrSiO_4$) from anorthositic rocks of the Laramie anorthosite complex, Wyoming: petrologic consequences and U-Pb ages. American Mineralogist, 80, p. 1317-1327

Scoates, J.S., and Chamberlain, 1997. Orogenic to post-orogenic origin for the 1.76 Ga Horse Creek anorthosite complex, Wyoming, USA. Journal of Geology, 105, p. 331-343.

Scoates, J.S., 2000. The plagioclase-magma density paradox re-examined and the crystallization of Proterozoic anorthosites. Journal of Petrology, 41, p. 627-649.

Scoates, J.S. and Mitchell, J.N., 2000. The evolution of troctolitic and high Al basaltic magmas in Proterozoic anorthosite plutonic suites and implications for the Voisey's Bay massive Ni-Cu sulfide deposit. Economic Geology, 95, p. 677-701.

Scott, D.J., 1998. An overview of the U-Pb geochronology of the Paleoproterozoic Torngat Orogen, northeast of Canada. Precambrian Research, 91, 91-107.

Simmons, K.R., Wiebe, R.A., Snyder, G.A., and Simmons, E.C., 1986. U-Pb zircon age for the Newark Island layered intrusion, Nain anorthosite complex. Geological Society of America, Abstracts and Programs, 18, p. 751.

Simmons, K.R., and Simmons, E.C., 1987. Petrogenetic implications of Pb- and Sr isotopic compositions of rocks from the Nain anorthosite complex, Labrador. Geological Society of America, Abstract with Programs, p. 845.

Smith, R.L., Wilton, D.H.C., Connelly, J.N., and Sparkes, K., 2001. Geology, geochemistry and sulphide mineralization of the basal gabbro sub-division of the Pants Lake intrusion, Labrador. Geological Association of Canada, Abstract with Programs, 26, p. A141.

Smoot, N.C., 1999. Orthogonal intersections in the western Pacific Ocean basin; a case study of the Mid-Pacific Mountains. Geomorphology, 30, p. 323-356.

Spera, F.J., 2000. Physical properties of magma. In Encyclopedia of Volcanoes, H. Sigurdsson (ed)., Academic Press, San Diego, p. 171-190.

Stacey, J.S., and Kramers, J.D., 1975. Approximation of terrestrial lead isotope evolution by a two-stage model. Earth and Planetary Science Letters, 26, p. 207-221.

Streckeisen, A., 1976. To each plutonic rock its proper name. Earth Science Reviews, 12, p. 1-33.

Takeda, Y-T., and Mosaki, O., 2003. Some comments on the rheologically critical melt percentage. Journal of Structural Geology, 25, p. 813-818.

Tettelaar, T.A., 2004. Emplacement history of the Pearly Gates anorthosite pluton and spatially related Tessiarsuyungoakh intrusion, and metamorphic petrology of the adjacent Tasiuyak paragneiss, northern Labrador. M.Sc. thesis, Memorial University of Newfoundland, St John's, NL.

Tollo, R.P., Aleinikoff, J.N., Bartholomew, M.J., and Rankin, D.W., 2004. Neoproterozoic A-type granitoids of the Central and Southern Appalachians; intraplate magmatism associated with episodic rifting of the Rodinian supercontinent. Precambrian Research, 128, p. 3-38.

Upton, B.G.J., 1973. (untitled). NAP, p. 133-143

Upton, B.G.J., Emeleus, C.H., Heaman, L.M., Goodenough, K.M., and Finch, A.A., 2003. Magmatism of the mid-Proterozoic Gardar Province, South Greenland; chronology, petrogenesis and geological setting. Lithos, 68, p. 43-65.

Vander Auwera, J. and Longhi, J., 1994. Experimental study of a jotunite (hypersthene monzodiorite): constraints on the parent magma composition and crystallization conditions (P, T, f_{O2}) of the Bjerkreim-Sokndal layered intrusion (Norway). Contributions to Mineralogy and Petrology, 118, p. 60-78.

Vander Auwera, J., Longhi, J. and Duchesne, J.C., 1998. A liquid line of descent of the jotunite (hypersthene monzodiorite) suite. Journal of Petrology, 3, p. 439-468.

Van der Molen, I., and Paterson, M.S., 1979. Experimental deformation of partially melted granite. Contributions to Mineralogy and Petrology, 98, p. 257-276.

Van Kranendonk, M.J., 1996. Tectonic evolution of the Paleoproterozoic Torngat orogen: evidence from pressure-temperature-deformation paths in the North River map area, Labarador. Tectonics, 15, p. 843-869.

Vauchez, A., and Pacheco Neves, S., 1997. Transcurrent shear zone and magma emplacement in the Neoproterozoic belts of Brazil. In: J.L. Bouchez (ed), Granite: from segregation of melt to emplacement fabrics. Kluwer Academic Press, Dordrecht, p. 275-293.

Vigneresse, J.L., Barbey, P., Cuney, M., 1996. Rheological transitions during partial melting and crystallization with application to felsic magma segregation and transfer. Journal of Petrology, 37, p. 1579-1600.

Wager, L.R., Brown, G.M., and Wadsworth, W.J., 1960. Types of igneous cumulate. Journal of Petrology, 1, p. 73-85.

Wardle, R.J., 1993. Geology of the Naskaupi River Region, Central Labrador (13 NW), Scale 1:500,000. Newfoundland Department of Mines and Energy, Geological Survey Branch, Map 93-16.

Wardle, R.J., Gower, C.F., Ryan, B., Nunn, G.A.G., James, D.T., and Kerr, A., 1997. Geological map of Labrador; 1:1 million scale. Government of Newfoundland and Labrador, Department of Mines and Energy, Geological Survey, Map 97-07.

Wardle, R.J., James, D.T., Scott, D.J., and Hall, J., 2002. The southeastern Churchill Province; synthesis of a Paleoproterozoic transpressional orogen. Canadian Journal of Earth Sciences, 39, p. 639-663.

Wendt, J.I., and Collerson, K.D., 1999. Early Archaean U/Pb fractionation and timing of late Archaean high-grade metamorphism in the Saglek-Hebron segment of the North Atlantic craton. Precambrian Research, 93, p. 281-297.

Wheeler, E.P., 1942. Anorthosite and associated rocks about Nain, Labrador. The Journal of Geology, 50, p. 611-642.

Wheeler, E.P., 1960. Anorthosite-adamellite complex of Nain, Labrador. Bulletin of the Geological Society of America, 71, p. 1765-1782.

Wheeler, E.P., 1969. Minor intrusives associated with the Nain anorthosite. In Origin of anorthosite and related rocks, Y.W. Isachsan (ed), New York State Museum Science Service, Memoir 18, Albany, p. 189-206.

Wheeler, E.P., 1972a. Anorthosite-adamellite-basement relations in the Ikkinikulluit drainage basin. NAP, p. 65-70.

Wheeler, E.P., 1972b. Anorthosite field relations in the outer islands. NAP, p. 31-36

Wheeler, E.P., 1973. Nain complex: contact zones of anorthosite and adamellite. NAP, p. 45-62.

Wiebe, R.A., 1974; Geology of the northern Tunungayuluak Island and vicinity. NAP, p. 37-47.

Wiebe, R.A., 1975. Anorthositic intrusions on and near Tunungayuluak Island, Labrador. NAP, p. 21-26.

Wiebe, R.A., 1978. Anorthosite and associated plutons, southern Nain Complex, Labrador. Canadian Journal of Earth Sciences, 15, 1326-1340.

Wiebe, R.A., 1979. Anorthositic dikes, southern Nain complex, Labrador. American Journal of Science, 279, p. 394-410.

Wiebe, R.A., 1980a. Comingling of contrasted magmas in the plutonic environment: examples from the Nain anorthositic complex. Journal of Geology, 88, p. 197-209.

Wiebe, R.A., 1980b. Emplacement history of the Nain complex. NAP, p. 35-40.

Wiebe, R.A., 1985a. Lower crustal cumulate nodules in Proterozoic dikes of the Nain complex: evidence for the origin of Proterozoic anorthosites. Journal of Petrology, 27, p. 1253-1275.

Wiebe, R.A., 1985b. Proterozoic basalt dykes in the Nain anorthosite complex, Labrador. Canadian Journal of Earth Sciences, 22, p. 1149-1157.

Wiebe, R.A., 1987. Evidence for stratification of basic, silicic, and hybrid magmas in The Newark Island layered intrusion, Nain Labrador. Geology, 15, p. 349-352.

Wiebe, R.A., 1988. Structural and magmatic evolution of a magma chamber: the Newark Island layered intrusion, Nain, Labrador. Journal of Petrology, 29, p. 383-411.

Wiebe, R.A., 1990a. Evidence for unusually feldspathic liquids in the Nain complex, Labrador. American Mineralogist, 75, p. 1-12.

Wiebe, R.A., 1990b. Dioritic rocks in the Nain complex, Labrador. Schweiz. Mineral. Petrogr. Mitt., 70, p. 199-208.

Wiebe, R.A., 1992. Proterozoic anorthosite complexes. In: Condie, K.C. (ed), Proterozoic Crustal Evolution, Elsevier, Amsterdam, p. 215-261.

Wiebe, R.A. and Snyder, D., 1993. Slow, dense replenishments of a basic magma chamber: the layered series of Newark Island layered intrusion, Nain, Labrador. Contributions to Mineralogy and Petrology, 113, p. 59-72.

Woodward, C., 1972. Newark Island layered igneous complex. NAP, p.42-48.

Woussen, G., Dimroth, E., Corriveau, L., Archer, P., 1981. Crystallization and emplacement of the Lac St-Jean anorthosite massif (Quebec, Canada). Petrology, 76, p. 343-350.

Xue, S. and Morse, S.A., 1993. Geochemistry of the Nain massif anorthosite, Labrador: magma diversity in five intrusions. Geochimica et Cosmochimica Acta, 57, p. 3925-3948.

Xue, S. and Morse, S.A., 1994. Chemical characteristics of plagioclase and pyroxene megacrysts and their significance to the petrogenesis of the Nain anorthosites. Geochimica et Cosmochimica Acta, 58, 20, p. 4317-4331.

Yoshinobu, A.S., Okaya, D.A., and Paterson, S.R., 1998. Modeling the thermal evolution of fault-controlled magma emplacement models: implications for the solidification of granitoid plutons. Journal of Structural Geology, 20, p. 1205-1218.

Yu, Y. and Morse, S.A., 1993. $^{40}Ar/^{39}Ar$ chronology of Nain anorthosites, Canada. Canadian Journal of Earth Sciences, 30, p. 1166-1178.

Ziegler, P.A., van Wees, J.D., and Cloetingh, S., 1998. Mechanical controls on collision related compressional intraplate deformation. Tectonophysics, 300, p. 103-129.

Appendix 1: Mean (*) and ranges of mineral compositions in Paleoproterozoic and/or Archean country rocks and Mesoproterozoic plutonic rocks in the study

Sample		00-4-4d	00-22-14	00-27-25	01-14-16	01-14-18	01-16-16	01-16-26	01-29-7a	02-27-5	00-25-12
Unit		Pg	Pg	Pg	Pg	Pg	Pg	Pg	Pg	Pg	Pe
Rock type		hbl ol mgn	hbl gn - mgn	hbl mgn	ol mgn	ox gn	ox ol mgn	bt ox gn	hbl ol mgn	ol gb	px qtz dio
Pl cores (An)*		62	81	60		52		51	62	78	33
Pl rims (An)*		72	86	70		54		51	70	81	39
Opx (En)*			69	74	82	58	85		77		60
Cpx (En)*		44	43	44	47		48	42	46	44	40
Ol (Fo)*					79		83		72	63	
Pl cores	An	60 - 63	75 - 85	59 - 61		50 - 55		49 - 53	60 - 64	70 - 79	32 - 34
	Ab	36 - 39	14 - 25	38 - 41		43 - 48		45 - 50	36 - 39	20 - 23	62 - 64
	Or	0 - 1	0	0 - 1		2		1 - 2	0 - 1	0	3 - 4
Pl rims	An	66 - 81	82 - 88	61 - 79		52 - 63		50 - 52	67 - 74	77 - 84	36 - 37
	Ab	19 - 34	12 - 18	21 - 38		35 - 46		47 - 48	25 - 33	16 - 23	60 - 61
	Or	0 - 1	0	0 - 1		1 - 2		1	0	0	3
Opx	Wo		29 - 34	1	18 - 20	43 - 45	10 - 17		24 - 25		39 - 40
	En		67 - 72	74	81 - 83	57 - 58	83 - 92		76 - 78		59 - 60
	Fs		1	24	1 - 2	0 - 1	0 - 2		1		1 - 2
	wt% Al_2O_3		1.71 - 1.85	2.17	1.36 - 1.84	1.53 - 2.35	2.05 - 2.25		1.77 - 2.19		0.42 - 0.67
Cpx	Wo	11 - 14	11 - 15	10 - 14	6 - 9		7 - 12	10 - 15	8 - 11	47 - 49	15 - 16
	En	44 - 45	42 - 43	43 - 45	46 - 47		46 - 48	41 - 43	45 - 46	43 - 45	40
	Fs	42 - 44	42 - 46	43 - 46	44 - 46		39 - 46	44 - 48	43 - 46	7 - 10	44 - 45
Ol	Fa				20 - 21		15 - 18		26 - 28	37 - 38	
	Fo				79		82 - 85		72 - 74	62 - 63	
Other											

Appendix 1 cont.: Mean (*) and ranges of mineral compositions in Paleoproterozoic and/or Archean country rocks and Mesoproterozoic plutonic rocks in the study

Sample		01-19-5	01-29-7b	02-6-12	02-6-14	02-20-7b	00-24-7	00-24-13	01-37-9	02-5-7	01-12-15a
Unit		Pe	Pe	TY	TY	TY	TLi	TLi	TLb	TLb	TLb
Rock type		px qtz dio	alt px qtz dio	defm cpx ln	defm cpx ln	defm cpx ln	px anor	ln	ln	px anor	lgn
Pl cores (An)*		30	29	55	64	59	43	44	46	42	43
Pl rims (An)*		32	30	63	68	59		48	48	47	44
Opx (En)*				70	72	69		59	60	60	62
Cpx (En)*		35		42				40	40	40	41
Ol (Fo)*											
Pl cores	An	27 - 32	28 - 30	53 - 55	62 - 67	57 - 61	43-44	43-44	45 - 59	41 - 44	42 - 44
	Ab	55 - 68	69 - 71	44 - 45	32 - 63	39 - 41	54-55	53-55	40 - 53	54 - 56	53 - 55
	Or	2 - 18	1 - 2	1 - 2	1 - 2	1	2-3	2	1 - 3	2 - 4	2 - 4
Pl rims	An	15 - 33	29 - 34	54 - 65	64 - 73	58 - 61		43-48	48	45 - 49	42 - 46
	Ab	64 - 85	66 - 70	34 - 44	26 - 34	38 - 41		55-50	50 - 51	49 - 53	48 - 56
	Or	0 - 5	0 - 1	1 - 2	1	1		2	1 - 2	1 - 3	2 - 7
Opx	Wo			1 - 2	1	1		1-2	1	1 - 2	34 - 38
	En			69 - 71	71 - 73	28 - 31		58-60	60	58 - 61	60 - 65
	Fs			28 - 30	26 - 28	68 - 70		40-42	38	37 - 40	1 - 8
	wt% Al_2O_3			1.11 - 1.28	1.45 - 2.26	1.08 - 1.53			1.39 - 1.64	0.66 - 1.33	0.88 - 1.26
Cpx	Wo	18 - 20		47 - 50				14-16	46 - 49	45 - 48	15 - 17
	En	35 - 39		41 - 43				39-41	39 - 41	39 - 41	40 - 41
	Fs	41 - 46		9 - 12				44-45	12 - 15	11 - 16	42 - 45
Ol	Fa										
	Fo										
Other									Or, An ex		

Appendix 1 cont.: Mean (*) and ranges of mineral compositions in Paleoproterozoic and/or Archean country rocks and Mesoproterozoic plutonic rocks in the study

Sample		02-22-7	02-24-23	02-15-14	02-11-15	02-8-6	02-24-19b	01-15-5	02-8-19	02-18-5	02-23-10
Unit		TLb	TLb	TLb	TLb	TLb	TB	TB	TB	TAI	TAI
Rock type		px anor	lgn	lgn	ox anor	defm anor	lgn	anor	defm anor	gn	gn
Pl cores (An)*		44	41	47	45	43	44	43	44	44	43, 36
Pl rims (An)*		45	41	43	46, 95	45	43	42, 70	50, 79	45	41, 34
Opx (En)*		58	57	60			58			44	45
Cpx (En)*		39	39	40	38	39	39	37	27	38	34
Ol (Fo)*											
Pl cores	An	42 - 45	38 - 44	42 - 53	44 - 46	41 - 46	42 - 45	42 - 45	42 - 45	42 - 49	42 - 45
	Ab	53 - 56	54 - 60	46 - 56	51 - 54	52 - 56	52 - 55	52 - 56	53 - 55	50 - 56	54 - 56
	Or	2	2	1 - 3	2 - 3	2 - 5	2	1 - 5	2 - 4	1 - 2	2
Pl rims	An	44 - 45	37 - 44	38 - 45	45 - 95	45 - 46	43 - 44	34 - 72	42 - 57	44 - 47	40 - 42
	Ab	53 - 54	54 - 61	54 - 57	5 - 51	53	53 - 56	18 - 57	41 - 56	52 - 55	56 - 58
	Or	2	2	2 - 8	2 - 3	2	2	1 - 47	1 - 2	1 - 2	2
Opx	Wo	1 - 2	1	2 - 3			2 - 3			1 - 3	2
	En	40 - 42	56 - 58	36 - 38			58			53 - 55	43 - 46
	Fs	57 - 58	41 - 43	59 - 61			38 - 40			43 - 45	52 - 55
	wt% Al_2O_3	0.67 - 0.82	0.72 - 0.78	0.57 - 0.70			0.73 - 0.91			0.78 - 0.81	0.51 - 0.53
Cpx	Wo	47 - 48	43 - 49	45 - 46	47	46 - 50	42 - 45	46 - 47	23 - 26	44 - 47	45 - 48
	En	39 - 40	38 - 39	39 - 41	38	38 - 39	38 - 40	36 - 37	26 - 28	36 - 39	33 - 35
	Fs	12 - 14	12 - 18	14 - 16	15	12 - 15	17 - 18	16 - 17	48 - 49	14 - 20	17 - 22
Ol	Fa										
	Fo										
Other		Or ex		Or			Or ex		An rims		

Appendix 1 cont.: Mean (*) and ranges of mineral compositions in Paleoproterozoic and/or Archean country rocks and Mesoproterozoic plutonic rocks in the study

Sample		02-21-8	02-22-3	02-24-15	02-17-20a	01-30-2b	00-3-2a	01-30-12b	01-30-2a	00-2-4	00-31-27
Unit		TAl	TAl	TAl	TAl	SUb	SUb	SUb	SUb	SUi	SUi
Rock type		gn	lgn	alt lgn	defm bt gn	defm gn	defm gn	defm px dio	defm px dio	alt lgn	alt lgn
Pl cores (An)*		42	42	46	46	45	43	35	38	50	49
Pl rims (An)*		43	42	51	49	50	44	35	39	51	50
Opx (En)*		51	52	56	48	55		52			51
Cpx (En)*		34	36	39	35	38		36		37	35
Ol (Fo)*											
Pl cores	An	41 - 43	40 - 44	43 - 49	46 - 47	44 - 46	38 - 44	34 - 36	38 - 39	49 - 51	48 - 51
	Ab	54 - 57	54 - 59	49 - 55	51 - 52	52 - 53	53 - 61	62 - 64	59 - 60	48 - 49	48 - 51
	Or	2 - 5	1 - 2	2 - 3	2	2	1 - 2	1 - 2	2	1 - 2	1 - 2
Pl rims	An	42 - 45	41 - 44	47 - 56	48 - 50	49 - 51	42 - 45	34 - 36	37 - 39	48 - 57	50 - 51
	Ab	53 - 55	54 - 57	43 - 51	48 - 51	48 - 49	53 - 57	62 - 65	59 - 60	42 - 51	48 - 49
	Or	2 - 3	2 - 4	1 - 2	1 - 2	1 - 2	1 - 2	1 - 2	2	1 - 2	1 - 2
Opx	Wo	1 - 2	2 - 3	2	1 - 3	1 - 2		1 - 3			2
	En	50 - 52	51 - 53	56	48 - 51	53 - 58		50 - 52			51
	Fs	46 - 48	45 - 47	42	48 - 49	41 - 45		45 - 49			48
	wt% Al_2O_3	0.51 - 0.58	0.51	0.72	0.57 - 0.71	0.56 - 0.61		0.35 - 0.73			0.13
Cpx	Wo	46 - 48	45 - 46	44 - 47	46 - 48	45 - 49		43 - 46		42 - 48	43 - 46
	En	34 - 35	35 - 37	38 - 41	34 - 36	36 - 39		36 - 37		35 - 39	34 - 36
	Fs	17 - 20	17 - 19	12 - 18	16 - 19	12 - 18		18 - 20		15 - 20	20 - 21
Ol	Fa										
	Fo										
Other			Or ex								

Appendix 1 cont.: Mean (*) and ranges of mineral compositions in Paleoproterozoic and/or Archean country rocks and Mesoproterozoic plutonic rocks in the study

Sample		01-30-29	00-26-16i	00-22-5	00-25-5b	01-32-9b	00-29-12a	00-29-8	00-29-10	00-25-9d	00-21-16
Unit		SUi	SUi	SUi	SUi	SA	SP	SP	SP	SHlb	SHlb
Rock type		alt anor	alt opx anor	alt px anor	defm anor	defm ox gn	alt Fe-gb	ol Fe-gb	Fe-gb	defm gn	ol gn
Pl cores (An)*		49	53	54	45	48	51	49	52	52	59
Pl rims (An)*		49	54	58		50	51	50	52		57
Opx (En)*						59	32	31	36	59	57
Cpx (En)*		41				40	26	24	28	40	37
Ol (Fo)*									16		45
Pl cores	An	48 - 50	51 - 54	53 - 55	41 - 53	46 - 49	47 - 55	48 - 50	51 - 54	50 - 53	54 - 61
	Ab	48 - 50	45 - 47	43 - 45	45 - 57	49 - 52	43 - 51	49 - 50	44 - 47	46 - 49	37 - 43
	Or	2	2	1 - 2	2 - 4	2	2	2	2	1	2
Pl rims	An	49	52 - 58	57 - 59		47 - 51	49 - 53	49 - 50	52		56 - 58
	Ab	49	41 - 46	39 - 41		47 - 51	46 - 49	48 - 49	46		40 - 42
	Or	2	1 - 2	1 - 2		1 - 2	1 - 2	1 - 2	1 - 2		2
Opx	Wo					2	3 - 13	2	2 - 7	1	1 - 2
	En					58 - 60	32 - 33	30 - 31	35 - 37	57 - 60	56 - 58
	Fs					39 - 40	55 - 64	68	58 - 62	39 - 43	41 - 43
	wt% Al_2O_3					0.76 - 0.80	0.20 - 1.04	0.36 - 0.41	0.35 - 0.37	0.68 - 0.93	0.35 - 0.76
Cpx	Wo	48 - 49				47 - 49	39 - 46	42 - 45	44 - 45	44 - 45	43 - 45
	En	40 - 41				39 - 41	25 - 27	24	28	39 - 40	37 - 38
	Fs	9 - 12				11 - 13	28 - 34	31 - 34	27 - 28	16 - 17	18 - 20
Ol	Fa								83 - 88		53 - 55
	Fo								10 - 16		44 - 46
Other											

Appendix 1 cont.: Mean (*) and ranges of mineral compositions in Paleoproterozoic and/or Archean country rocks and Mesoproterozoic plutonic rocks in the study

Sample		01-24-14	00-22-11	00-1-10	00-7-19	01-20-15	01-31-2	00-3-6	01-34-4	00-2-13	00-20-6b
Unit		SHli	SHli	SHli	SHli	SHli	SHui	SHui	SHui	SHui	SHui
Rock type		cpx ln	cpx ln	ox ln	alt ln	anor	ox lgn	ox lgn	lgn	alt anor	alt lgn
Pl cores (An)*		51	55	52	53	56	49	49	52	52	52
Pl rims (An)*		52	52	51	54	58	53	51	59	54	52
Opx (En)*		63	58	59	61		47	47	54		
Cpx (En)*		41	39	39	39		35	34	36	39	32
Ol (Fo)*											
Pl cores	An	48 - 53	54 - 57	49 - 54	53 - 54	53 - 61	47 - 52	48 - 50	51 - 53	49 - 55	51 - 52
	Ab	45 - 50	41 - 44	44 - 48	44 - 45	38 - 45	47 - 51	48 - 49	45 - 47	44 - 49	46 - 48
	Or	1 - 2	2 - 3	1 - 3	2	1 - 2	2	2	2	1 - 2	1 - 2
Pl rims	An	50 - 57	50 - 54	50 - 54	53 - 57	54 - 62	52 - 54	50 - 53	52 - 71	50 - 60	51 - 52
	Ab	42 - 49	44 - 48	45 - 49	42 - 46	37 - 45	45 - 47	46 - 48	21 - 47	38 - 48	47 - 48
	Or	1 - 2	2	1 - 3	1 - 2	1 - 2	1 - 2	1	1	1 - 2	1
Opx	Wo	1	1 - 3	1	1 - 2		2	1 - 6	2		
	En	62 - 64	56 - 59	55 - 60	61		47	46 - 48	54		
	Fs	36 - 37	40 - 43	40 - 44	38		51	49 - 53	45		
	wt% Al_2O_3	0.60 - 0.62	0.51 - 0.83	0.48 - 0.53	0.41 - 0.65		0.72	0.33 - 0.47	1.06		
Cpx	Wo	42 - 45	44 - 45	41 - 47	45 - 46		43 - 48	41 - 47	46 - 48	44 - 46	46 - 47
	En	40 - 42	39	38 - 39	39 - 40		35 - 36	33 - 34	34 - 38	38 - 41	32
	Fs	13 - 17	16 - 17	16 - 20	14 - 16		17 - 22	19 - 25	15 - 18	15 - 16	21
Ol	Fa										
	Fo										
Other											

Appendix 1 cont.: Mean (*) and ranges of mineral compositions in Paleoproterozoic and/or Archean country rocks and Mesoproterozoic plutonic rocks in the study

Sample		00-22-2	00-26-16ii	01-33-31	00-30-19	01-31-16	00-3-2e	02-30-3a	02-30-1	02-28-2a	02-30-3b
Unit		SHui	SHub	SHub	SHub	SHub	SHub	KA	KAd	KAd	KSi
Rock type		alt anor	lgn	gn	ox gn	defm bt ox gn	ox gn	alt ox lgn	Fe-dio	Fe-dio	ln
Pl cores (An)*		53	53	50	44	45	48	45	30	34	50
Pl rims (An)*		53	54	51	45	47	49	48	30	37	50
Opx (En)*			59	45	36	33			29		64
Cpx (En)*		36	39	34	28	28	32	36	25	33	37
Ol (Fo)*											
Pl cores	An	51 - 56	53 - 54	46 - 53	41 - 48	43 - 50	48	44 - 48	29 - 30	32 - 37	47 - 53
	Ab	43 - 48	44 - 47	45 - 52	50 - 56	49 - 55	50 - 51	50 - 54	67 - 68	61 - 65	46 - 51
	Or	1 - 2	1 - 2	2	2 - 3	1 - 2	1	1 - 3	3	2 - 3	2
Pl rims	An	52 - 54	53 - 54	48 - 54	43 - 46	43 - 51	49 - 50	46 - 49	27 - 32	35 - 38	46 - 53
	Ab	45 - 46	44 - 46	44 - 50	51 - 55	48 - 55	49 - 50	49 - 52	65 - 70	60 - 62	46 - 53
	Or	1 - 2	1 - 2	1 - 2	2	1 - 2	1	1 - 2	2 - 5	2 - 3	1 - 2
Opx	Wo		1 - 2	1 - 2	2	2 - 4			3 - 7		3 - 5
	En		58 - 60	44 - 46	35 - 37	31 - 35			29 - 30		63 - 65
	Fs		40	52 - 54	62 - 63	62 - 67			63 - 67		32 - 33
	wt% Al_2O_3		0.23 - 0.30	0.41 - 0.50	0.22 - 0.36	0.36 - 0.71			0.37 - 0.41		0.73 - 1.86
Cpx	Wo	44 - 45	44 - 47	45 - 48	44 - 46	46 - 50	45 - 46	39 - 48	37 - 47	45 - 47	45 - 48
	En	35 - 36	38 - 39	32 - 35	27 - 28	26 - 29	32	34 - 38	24 - 25	30 - 35	35 - 38
	Fs	19 - 20	15 - 17	18 - 23	27 - 28	27 - 28	23	18 - 23	28 - 37	19 - 24	16 - 19
Ol	Fa										
	Fo										
Other									Or exsoln	Calcite	

Appendix 1 cont.: Mean (*) and ranges of mineral compositions in Paleoproterozoic and/or Archean country rocks and Mesoproterozoic plutonic rocks in the study

Sample		01-13-21b	01-13-21a	02-25-10b	00-5-13b	02-24-19a	00-5-12	01-23-13a	01-18-20	01-23-6
Unit		KSi	KSi	Ksi peg	KSb	KSb	KSb	KSb	KSb	KSb
Rock type		In	opx anor	anor + gran	cpx tr	ltr	gn	gn	alt mgn	lgn
Pl cores (An)*		52	52	47	54	64	45	56		51
Pl rims (An)*		54	54	16	75	59	46	62		54
Opx (En)*						67	56	71	64	59
Cpx (En)*					44	41	39	44	42	41, 38
Ol (Fo)*						56				
Pl cores	An	50 - 54	50 - 56	43 - 51	54	57 - 67	44 - 46	55 - 57		49 - 55
	Ab	45 - 48	42 - 48	48 - 54	43 - 44	30 - 41	51 - 53	42 - 44		43 - 48
	Or	1 - 2	2	1 - 4	2 - 3	1	2 - 3	1		2 - 3
Pl rims	An	50 - 57	51 - 56	15 - 18	73 - 78	55 - 66	45 - 46	57 - 80		52 - 75
	Ab	42 - 47	42 - 47	81 - 86	22 - 26	33 - 44	52 - 53	20 - 42		25 - 46
	Or	1 - 2	2	0 - 1	1	1 - 2	2	0 - 1		1 - 2
Opx	Wo					1	1 - 2	0 - 4	1 - 4	1 - 2
	En					65 - 68	55 - 58	67 - 77	63 - 68	58 - 61
	Fs					31 - 34	42 - 45	23 - 35	32 - 38	39 - 42
	wt% Al_2O_3					0.72 - 0.87	0.88 - 1.23	1.18 - 1.39	0.97 - 1.69	0.61 - 1.04
Cpx	Wo				42 - 44	12 - 14	41 - 45	41 - 47	40 - 46	39 - 47
	En				44	40 - 43	39 - 40	42 - 45	41 - 43	37 - 42
	Fs				12 - 14	45 - 47	16 - 18	10 - 15	12 - 17	14 - 19
Ol	Fa					42 - 46				
	Fo					54 - 58				
Other									vl Fe-Ti ox	

Appendix 1 cont.: Mean (*) and ranges of mineral compositions in Paleoproterozoic and/or Archean country rocks and Mesoproterozoic plutonic rocks in the study

Sample		01-23-12	01-23-13b	02-10-12	02-25-18
Unit		KSb	KSb	KSb	KSb
Rock type		defm ox lgn	defm lgn	gn	defm gn
Pl cores (An)*		50	48	45	49
Pl rims (An)*		51	54	42	49
Opx (En)*			65	51	65
Cpx (En)*		41	42	37	42
Ol (Fo)*					
Pl cores	An	50 - 51	46 - 54	44 - 46	49
	Ab	47 - 48	47 - 51	51 - 54	49 - 50
	Or	1 - 3	2 - 3	2 - 3	2
Pl rims	An	48 - 62	48 - 58	41 - 44	48 - 50
	Ab	35 - 50	40 - 50	54 - 56	49 - 50
	Or	2	1 - 2	3	2
Opx	Wo		1 - 11	1 - 6	1 - 3
	En		62 - 67	49 - 54	64 - 66
	Fs		29 - 35	44 - 50	32 - 33
	wt% Al_2O_3		0.71 - 1.14	0.50 - 0.67	1.01 - 1.22
Cpx	Wo	40 - 47	38 - 47	13 - 19	43 - 48
	En	38 - 43	41 - 45	36 - 40	41 - 44
	Fs	15 - 18	12 - 17	44 - 48	10 - 14
Ol	Fa				
	Fo				
Other					

Appendix 2

All major elements were analyzed by X-Ray Fluorescence (XRF), whereas trace elements were analyzed by XRF or Inductively Coupled Plasma-Mass Spectrometry (ICP-MS).

XRF analytical procedures

Operating conditions for the XRF can be found in "Analysis of Pressed Pellets of Geological Samples using Wavelength-Dispersive X-Ray Fluorescence Spectrometry" by Longerich (1995).

ICP sinter analysis

ICP-MS analysis was done using the method of internal standardization to correct for matrix and drift effects. A pure quartz reagent blank (BLANK) and one or more certified geological reference standards (usually gabbro MRG-1 (CCRMP) and basalt BR-688 (NIST SRM 668)) were prepared and analyzed with each sample. Reagent blank concentrations are generally insignificant and were not subtracted from the sample concentrations. Several samples were prepared and analyzed in duplicate in order to determine precision.

Appendix 2: Whole rock major element oxides (wt%) and trace elements (ppm) for Paleoproterozoic and/or Archean country rocks and Mesoproterozoic plutonic rocks in the study area.

Sample	01-16-26	01-30-12b	02-22-8b	00-27-25	02-27-5	02-22-8a	01-16-16
Analysis	ICP-MS	ICP-MS	XRF	ICP-MS	XRF	XRF	ICP-MS
Unit	Pg	Pg	Pg	Pg	Pg	Pg	Pg
Rock type	bt ox gn	gn	hbl gn	hbl mgn	ol gb	hbl ol mgn	ox ol mgn
SiO_2	48.08	46.91	45.94	48.87	44.03	45.76	44.14
TiO_2	0.78	0.51	0.39	0.51	0.45	0.39	0.44
Al_2O_3	14.57	10.08	15.31	5.01	16.92	3.05	1.73
FeOt	11.44	12.58	10.63	11.69	11.71	11.9	12.98
MnO	0.2	0.21	0.17	0.2	0.23	0.2	0.19
MgO	6.84	17.15	13.81	16.45	10.71	27.97	30.53
CaO	13.24	9.54	10.73	13.57	13.09	7.31	8.26
Na_2O	2.32	0.77	0.53	0.47	1.04	0.46	0.13
K_2O	0.28	0.13	0.41	0.05	0.03	0.41	
P_2O_5	0.08	0.01	0.03	0.03	0.02	0.01	0
S	26	23	107	34	93	304	34
Cl	243	1542		1628	<55		544
Ni			475		146	1651	
Cr	229	1462	419	1875	188	1785	1758
V	255	211	173	166	134	113	116
Sc	28	38	27	41	26	19	11
Cu			10		21	10	
Zn			49		40	72	
As			<17		<17	<17	
Ga			13		13	7	
Rb	2	0	8	0	<1	24	<1
Ba	164	85	45	188	38	243	0
Sr	130	89	53	33	386	60	40
Nb		1	2	0	<0.9	2	0
Zr		22	26	55	4	37	15
Y		13	6	11	5	6	7
Ce	48	5	<53	35	<53	<53	5
Pb		1	8	1	<5	5	0
Th		0	<4	0	<4	<4	0
U		0	<5	0	<5	<5	0

Appendix 2 cont.: Whole rock major element oxides (wt%) and trace elements (ppm) for Paleoproterozoic and/or Archean country rocks and Mesoproterozoic plutonic rocks in the study area.

Sample	01-29-7a	02-23-4	00-4-6b	02-6-12i	02-6-12ii	02-6-14
Analysis	ICP-MS	XRF	ICP-MS	XRF	XRF	XRF
Unit	Pg	Pe	Pe	TY	TY	TY
Rock type	hbl ol mgn	alt px qtz dio	qtz dio	defm cpx ln	defm cpx ln + px aggr	defm cpx ln
SiO_2	45.33	64.29	63.35	52.08	51.79	51.26
TiO_2	0.35	1.02	0.45	0.28	0.47	0.26
Al_2O_3	8.15	15.15	16.11	22.65	19.4	23.45
FeOt	12.96	5.69	5.05	4.84	5.53	4.59
MnO	0.19	0.08	0.07	0.08	0.1	0.08
MgO	22.53	2.48	2.97	5.08	5.89	5.63
CaO	7.33	5	5.3	9.74	11.84	9.69
Na_2O	0.9	3.56	3.92	3.31	3.13	2.88
K_2O	0.1	0.62	0.36	0.22	0.23	0.29
P_2O_5	0.02	0.19	0.14	0.04	0.05	0.03
S	22	699	14	120	138	76
Cl		61	928	59	66	<53
Ni		89		62	61	36
Cr	2008	80	80	159	160	293
V	174	116	90	56	92	46
Sc	22	13	14	12	20	14
Cu		59		39	20	6
Zn		25		14	15	13
As		<17		<16	<16	<16
Ga		20		20	18	18
Rb	0	2	1	<0.9	1	1
Ba	33	659	452	161	168	151
Sr	32	430	430	672	593	552
Nb		7	2	1	2	<0.9
Zr		107	44	9	30	8
Y		5	7	<0.9	<0.9	<0.9
Ce	5	58	23	<50	<50	<50
Pb	<1	5	5	5	<5	<5
Th		<4	0	<4	<4	<4
U		<5	0	<5	<5	<5

Appendix 2 cont.: Whole rock major element oxides (wt%) and trace elements (ppm) for Paleoproterozoic and/or Archean country rocks and Mesoproterozoic plutonic rocks in the study area.

Sample	02-20-30	02-5-7	02-22-7	02-24-23	02-15-14	02-11-15	02-8-6
Analysis	XRF	XRF	XRF	XRF	XRF	XRF	XRF
Unit	TY	TLb	TLb	TLb	TLb	TLb	TLb
Rock type	defm cpx ln	px anor	px anor	lgn	lgn	ox anor	defm anor
SiO_2	52.97	55.27	54.54	52.98	54.65	47.41	54.63
TiO_2	0.12	0.45	0.89	2.1	0.65	3.24	0.95
Al_2O_3	24.48	23.09	24.36	18.84	21.45	22.44	24.79
FeOt	2.92	3.39	2.57	7.33	4.97	8.01	1.89
MnO	0.05	0.05	0.03	0.11	0.07	0.05	0.02
MgO	3.13	2.19	0.94	3.72	3.46	0.3	0.41
CaO	9.91	8.14	8.73	8	7.32	9.69	8.8
Na_2O	3.82	4.64	5	4.12	4.33	4.36	5.05
K_2O	0.51	0.7	0.79	0.66	0.74	0.56	0.71
P_2O_5	0.02	0.02	0.15	0.07	0.15	1.59	0.18
S	45	131	101	913	239	176	146
Cl	136	115	89	125	120	119	111
Ni	44	14	8	31	40	10	<4
Cr	108	41	12	27	64	11	<9
V	34	22	35	119	42	201	38
Sc	15	10	<9	9	<9	15	<10
Cu	6	8	8	45	28	28	13
Zn	18	12	6	24	21	34	<2
As	<17	<16	<17	<17	<17	<17	<16
Ga	19	22	24	24	22	24	25
Rb	9	1	3	4	2	<1	1
Ba	147	505	520	725	586	564	537
Sr	584	797	810	725	726	963	915
Nb	2	<0.9	3	3	<0.9	10	1
Zr	<1.5	<1.5	23	41	14	47	<1.5
Y	4	<0.9	1	3	<0.9	20	<0.9
Ce	<53	<50	<53	<55	<53	94	55
Pb	13	<5	<5	<5	<5	6	<5
Th	<4	<4	<4	<4	<4	<4	<4
U	<5	<5	<5	<5	<5	<5	<5

Appendix 2 cont.: Whole rock major element oxides (wt%) and trace elements (ppm) for Paleoproterozoic and/or Archean country rocks and Mesoproterozoic plutonic rocks in the study area.

Sample	02-21-10	02-24-19b	02-8-13	02-7-17ii	02-7-17i	02-8-19	02-23-10i
Analysis	XRF	XRF	XRF	XRF	XRF	XRF	XRF
Unit	TLb	TB	TB	TB	TB	TB	TAl
Rock type	defm anor	lgn	px anor	alt qtz lgn	px anor	defm anor	gn
SiO_2	56.40	53.63	53.94	56.00	55.32	56.30	49.73
TiO_2	0.47	1.23	0.31	0.11	0.11	0.08	3.44
Al_2O_3	24.72	19.19	23.51	23.68	26.01	26.01	17.2
FeOt	1.72	7.24	3.80	2.32	0.67	0.53	10.68
MnO	0.02	0.11	0.05	0.04	0.01	0.01	0.13
MgO	0.68	4.76	3.14	1.56	0.27	0.09	2.79
CaO	6.81	7.16	8.63	8.41	8.98	8.76	8.15
Na_2O	5.85	3.85	4.34	4.66	5.15	5.33	3.67
K_2O	1.75	0.66	0.30	0.52	0.78	0.71	0.79
P_2O_5	0.11	0.13	0.04	0.03	0.02	0.02	0.25
S	164	489	64	252	117	52	965
Cl	277	78	<53	123	223	<53	116
Ni	6	51	40	23	<4	2	26
Cr	<9	136	100	55	23	4	37
V	23	78	55	10	10	7	200
Sc	7	9	<10	<10	10	7	26
Cu	8	20	4	17	6	6	42
Zn	6	33	9	12	<2	<2	58
As	<17	<17	<16	<16	<16	<17	<17
Ga	23	21	22	25	23	27	24
Rb	17	2	<0.9	2	4	1	5
Ba	415	577	302	482	468	444	682
Sr	811	655	788	790	861	985	640
Nb	2	4	<0.9	<0.9	<0.9	<0.9	16
Zr	15	49	<1.5	38	<1.5	<1.5	107
Y	<0.9	3	<0.9	<0.9	<0.9	<0.9	11
Ce	<53	<55	<50	63	<50	<53	19
Pb	8	<5	<5	<5	<5	<5	7
Th	<4	<4	<4	<4	<4	<4	<4
U	<5	<5	<5	<5	<5	<5	<5

Appendix 2 cont.: Whole rock major element oxides (wt%) and trace elements (ppm) for Paleoproterozoic and/or Archean country rocks and Mesoproterozoic plutonic rocks in the study area.

Sample	02-15-23	02-21-8	02-17-20a	01-30-2b	00-2-4	01-32-9a	01-32-9b
Analysis	XRF	XRF	XRF	ICP-MS	ICP-MS	ICP-MS	ICP-MS
Unit	TAI	TAI	TAI	SUb	SUi	SA	SA
Rock type	gn	gn	defm bt gn	defm gn	alt lgn	cpx ln	defm ox gn
SiO_2	44.07	43.66	47.66	52.27	52.83	53.04	45.34
TiO_2	3.36	4.86	1.45	0.83	0.29	0.21	3.30
Al_2O_3	13.99	11.57	12.18	17.79	22.85	21.17	15.63
FeOt	18.81	17.28	15.86	10.31	4.59	5.62	15.94
MnO	0.23	0.25	0.27	0.18	0.07	0.1	0.17
MgO	2.95	4.97	6.81	5.16	3.52	5.75	4.80
CaO	8.15	9.02	10.59	7.77	10.31	8.55	9.85
Na_2O	2.93	2.5	2.18	3.3	3.85	3.44	2.71
K_2O	0.57	0.44	0.35	0.22	0.35	0.25	0.17
P_2O_5	1.53	2.17	0.12	0.22	0.01	0.01	0.02
S	344	168	326	27	12	17	15
Cl	145	214	196	2413	1448	770	328
Ni	10	18	73				
Cr	<9	28	52	111	18	181	21
V	163	260	419	56	57	32	396
Sc	24	32	48	17	15	12	30
Cu	38	31	76				
Zn	146	91	94				
As	<17	<17	<17				
Ga	30	18	19				
Rb	1	2	2	1	1	0	1
Ba	1050	739	130	562	379	335	167
Sr	695	535	141	676	720	852	553
Nb	22	23	5	5	0	0	0
Zr	78	110	48	24	11	4	10
Y	49	45	28	14	4	1	4
Ce	216	161	<53	22	7	5	2
Pb	11	10	10	2	1	2	2
Th	<4	<4	<4	0	0	1	0
U	<5	<5	<5	0	0	0	0

Appendix 2 cont.: Whole rock major element oxides (wt%) and trace elements (ppm) for Paleoproterozoic and/or Archean country rocks and Mesoproterozoic plutonic rocks in the study area.

Sample	00-29-12b	01-31-8	00-25-9d	01-24-14	00-22-11	01-31-2	01-33-31
Analysis	ICP-MS	ICP-MS	ICP-MS	ICP-MS	ICP-MS	ICP-MS	ICP-MS
Unit	SP	SP	SHlb	SHlb	SHlb	SHui	SHui
Rock type	Fe-gb	Fe-gb	defm gn	cpx ln	cpx ln	ox lgn	ox gn
SiO_2	49.38	48.68	48.20	51.61	52.87	51.45	50.89
TiO_2	2.81	2.82	1.11	0.58	0.33	1.34	1.75
Al_2O_3	14.40	13.51	14.69	23.84	21.19	22.98	19.68
FeOt	15.07	15.44	13.27	4.82	6.24	5.52	8.11
MnO	0.23	0.23	0.20	0.06	0.10	0.08	0.13
MgO	2.94	2.98	7.02	2.47	4.76	1.85	3.10
CaO	7.58	7.82	10.01	10.12	8.72	10.10	9.19
Na_2O	3.58	3.43	2.41	3.79	3.39	3.86	3.46
K_2O	0.57	0.53	0.09	0.34	0.40	0.40	0.44
P_2O_5	0.84	0.92	0.01	0.02	0.06	0.12	0.35
S	19	15	35	33	13	75	14
Cl	1474	1115	1447	3709	2541	1042	1197
Ni							
Cr	14	14	144	93	84	108	67
V	143	148	311	97	60	82	99
Sc	29	37	32	5	9	12	19
Cu							
Zn							
As							
Ga							
Rb	1	1	0	1	2	1	1
Ba	952	1013	120	414	372	537	636
Sr	537	512	178	902	593	620	603
Nb	41	40	1	0	1	5	11
Zr	34	78	31	7	16	23	17
Y	53	61	17	3	4	8	18
Ce	109	161	7	6	11	20	44
Pb	5	5	1	2	2	3	4
Th	0	0	0	0	0	0	0
U	0	0	0	0	0	0	0

Appendix 2 cont.: Whole rock major element oxides (wt%) and trace elements (ppm) for Paleoproterozoic and/or Archean country rocks and Mesoproterozoic plutonic rocks in the study area.

Sample	01-28-5b	01-34-1	02-30-3a	02-36-10	02-30-1	02-28-2a	02-28-12
Analysis	ICP-MS	ICP-MS	XRF	XRF	XRF	XRF	XRF
Unit	SHub	SHub	KA	KA xen	KAd	KAd	KAd
Rock type	gn	ox gn	alt ox lgn	alt ln	Fe-dio	Fe-dio	Fe-dio
SiO_2	48.81	41.75	53.68	50.40	47.80	44.60	47.11
TiO_2	1.49	4.84	0.38	0.11	3.91	3.55	2.57
Al_2O_3	15.06	12.10	23.66	22.48	12.41	14.31	13.79
FeOt	12.41	17.65	3.37	6.75	16.83	16.84	17.47
MnO	0.18	0.23	0.05	0.12	0.25	0.21	0.29
MgO	7.65	6.02	1.58	6.00	2.97	3.53	1.97
CaO	9.05	10.49	8.76	8.88	7.36	8.49	6.82
Na_2O	2.44	2.12	4.61	3.20	3.33	3.41	3.64
K_2O	0.22	0.18	0.43	0.25	1.06	0.39	1.35
P_2O_5	0.25	2.01	0.04	0.02	1.26	1.32	0.83
S	27	15	307	435	144	647	2118
Cl		975	81	412	155	189	73
Ni			21	149	5	10	10
Cr	87	<9	9	11	<9	<9	<9
V	275	436	34	5	95	206	20
Sc	35	34	12	4	32	31	23
Cu			40	39	29	37	37
Zn			11	44	98	108	127
As			<17	<17	<17	<17	<17
Ga			24	19	24	26	20
Rb	1	1	<1.0	<1.0	4	<1.0	<1.0
Ba	281	333	433	214	1914	955	4440
Sr	564	457	839	589	599	698	692
Nb	4	7	<0.9	<0.9	19	2	23
Zr	21	44	8	<1.5	150	5	1525
Y	9	32	<0.9	<0.9	42	20	41
Ce	23	80	<55	<55	141	<55	85
Pb	2	2	<5	<5	5	6	7
Th	0	0	<4	<4	<4	<4	<4
U	0	0	<5	<5	<5	<5	<5

Appendix 2 cont.: Whole rock major element oxides (wt%) and trace elements (ppm) for Paleoproterozoic and/or Archean country rocks and Mesoproterozoic plutonic rocks in the study area.

Sample	02-30-3b	01-13-21b	01-13-21a	02-25-10a	02-25-10b	02-31-8ii	02-31-8i
Analysis	XRF	ICP-MS	ICP-MS	XRF	XRF	XRF	XRF
Unit	KSi	KSi	KSi	KSi	KSi	KSd	KSd
Rock type	ln	ln	opx anor	alt px anor	anor + gran	Fe-dio	lgn lens
SiO_2	53.86	52.92	53.39	53.19	55.93	47.03	52.7
TiO_2	0.34	0.24	0.17	0.56	0.38	3.62	0.53
Al_2O_3	23.5	23.95	27.04	23	23.44	13.21	22.6
FeOt	3.69	3.53	1.13	4.57	3.1	16.55	5.33
MnO	0.06	0.06	0.01	0.06	0.05	0.28	0.11
MgO	2.89	3.2	0.51	2.14	1.54	3.64	3.04
CaO	9.07	9.73	10.76	9.09	8.21	7.85	8.98
Na_2O	4.17	3.9	4.45	4.06	4.57	2.93	4.01
K_2O	0.41	0.3	0.42	0.53	0.61	0.41	0.35
P_2O_5	0.05	0.02	0.02	0.07	0.16	1.13	0.14
S	122	27	20	482	343	378	101
Cl	<52	849	1390	193	323	133	75
Ni	24			19	35	15	10
Cr	68	87	11	27	11	32	72
V	26	44	11	61	30	181	38
Sc	9	16	14	9	13	26	10
Cu	23			16	59	44	21
Zn	11			17	8	99	36
As	<17			<17	<17	<17	<16
Ga	22			21	21	25	21
Rb	2	1	3	3	4	<1.0	1
Ba	372	267	291	433	591	1228	597
Sr	769	618	694	727	749	642	722
Nb	1	0	1	2	2	45	5
Zr	19	9	22	34	56	974	129
Y	<0.9	2	3	3	5	52	6
Ce	<55	5	12	<55	<55	265	<53
Pb	<5	1	1	6	6	11	6
Th	<4	0	0	<4	<4	<4	<4
U	<5	0	0	<5	<5	<5	<5

Appendix 2 cont.: Whole rock major element oxides (wt%) and trace elements (ppm) for Paleoproterozoic and/or Archean country rocks and Mesoproterozoic plutonic rocks in the study area.

Sample	02-24-19a	00-5-12	01-23-13a	01-23-6	02-10-12	02-25-18
Analysis	XRF	ICP-MS	ICP-MS	ICP-MS	XRF	XRF
Unit	KSb	KSb	KSb	KSb	KSb	KSb
Rock type	ltr	gn	gn	defm lgn	gn	defm gn
SiO_2	48.95	52.92	47.60	53.27	46.66	47.85
TiO_2	0.43	0.45	0.45	0.27	3.71	0.09
Al_2O_3	24.15	16.96	10.75	25.69	14.75	14.65
FeOt	6.17	9.52	11.94	2.57	13.67	13.77
MnO	0.08	0.16	0.21	0.03	0.17	0.18
MgO	4.50	6.89	14.09	1.47	4.47	7.42
CaO	10.45	7.57	11.73	10.3	9.39	10.01
Na_2O	3.22	3.20	1.06	4.23	2.97	2.51
K_2O	0.22	0.48	0.10	0.37	0.56	0.14
P_2O_5	0.07	0.02	0.01	0.03	0.98	0.04
S	234	11	34	22	1074	261
Cl	61		1580	735	110	<52
Ni	59				15	185
Cr	20	135	1325	34	<9	147
V	38	81	203	26	361	278
Sc	7	29	38	13	23	38
Cu	16				42	32
Zn	16				49	78
As	<17				<17	18
Ga	18				23	22
Rb	1	1	0	1	4	<1.0
Ba	152	627	77	362	527	312
Sr	526	482	126	742	566	329
Nb	2	0	0	1	5	<0.9
Zr	24	16	16	17	72	27
Y	2	7	9	2	14	17
Ce	<55	14	5	7	<53	<55
Pb	<5	2	1	2	10	7
Th	<4	0	0	0	<4	<4
U	<5	0	0	0	<5	<5

Appendix 3: CIPW norms for Paleoproterozoic and/or Archean country rocks and Mesoproterozoic plutonic rocks.

Sample	01-16-26	01-30-12b	02-22-8b	00-27-25	02-27-5	02-22-8a	01-16-16	01-29-7a	02-23-4	00-4-6b
Unit	Pg	Pg	Pg	Pg	Pg	Pg	Pg	Pg	Pe	Pe
Rock type	bt ox gn	gn	hbl gn	hbl mgn	ol gb	hbl ol mgn	ox ol mgn	hbl ol mgn	alt px qtz di	qtz di
qtz									23.28	19.86
or	1.65	0.77	2.42	0.3	0.18	2.42		0.59	3.66	2.13
ab	18.87	6.52	4.48	3.98	7.91	3.89	1.1	7.62	30.12	33.17
an	28.51	23.66	38.18	11.41	41.41	5.05	4.14	17.9	23.53	25.3
ne	0.41				0.48					
crn										
di	30.49	19.14	12.06	45.14	19.21	24.92	29.47	14.77	0.03	0.07
hy		22.33	19.45	21.55		12.34	5.55	13.96	15.07	16.02
ol	16.22	24.48	20.54	13.44	28.14	48.07	57.31	42.31		
ilm	1.48	0.97	0.74	0.97	0.85	0.74	0.84	0.66	1.94	0.85
ap	0.19	0.02	0.07	0.07	0.05	0.02	-	0.05	0.44	0.32
Gabbroic components										
Pl	0.50	0.31	0.45	0.16	0.51	0.09	0.05	0.26	0.78	0.78
Ol	0.17	0.25	0.22	0.14	0.29	0.51	0.59	0.44	0.00	0.00
Px	0.32	0.43	0.33	0.70	0.20	0.40	0.36	0.30	0.22	0.22

Appendix 3 cont.: CIPW norms for Paleoproterozoic and/or Archean country rocks and Mesoproterozoic plutonic rocks.

Sample	02-6-12i	02-6-12ii	02-6-14	02-20-30	02-5-7	02-22-7	02-24-23	02-15-14	02-11-15
Unit	TY	TY	TY	TY	TLb	TLb	TLb	TLb	TLb
Rock type	defm cpx ln	defm cpx ln + px aggr	defm cpx ln	defm cpx ln	px an	px an	lgn	lgn	ox an
qtz	0.13		0.62	0.75	2.44	1.38	1.14	2.49	
or	1.3	1.36	1.71	3.01	4.14	4.67	3.9	4.37	3.31
ab	28.01	26.49	24.37	32.32	39.26	42.31	34.86	36.64	36.89
an	46.3	38.21	47.88	48.14	40.11	41.69	30.96	35.33	37.68
ne									
crn			0.85					0.58	0.85
di	1.44	16.49		0.73	0.12	0.53	6.86		
hy	20.52	11.39	22.17	12.7	10.97	5.38	16.05	16.8	5.38
ol		3.49							3.7
ilm	0.53	0.89	0.49	0.23	0.85	1.69	3.99	1.23	6.15
ap	0.09	0.12	0.07	0.05	0.05	0.35	0.16	0.35	3.68
Gabbroic components									
Pl	0.77	0.67	0.77	0.86	0.88	0.93	0.74	0.81	0.89
Ol	0.00	0.04	0.00	0.00	0.00	0.00	0.00	0.00	0.04
Px	0.23	0.29	0.23	0.14	0.12	0.07	0.26	0.19	0.06

Appendix 3 cont.: CIPW norms for Paleoproterozoic and/or Archean country rocks and Mesoproterozoic plutonic rocks.

Sample	02-8-6	02-21-10	02-24-19b	02-8-13	02-7-17ii	02-7-17i	02-8-19	02-23-10i	02-15-23	02-21-8
Unit	TLb	TLb	TB	TB	TB	TB	TB	TAl	TAl	TAl
Rock type	defm an	defm an	lgn	px an	alt qtz lgn	px an	defm an	gn	gn	gn
qtz	2.7		1.75	1.5	4.75	2.3	3.34	0.29		
or	4.2	10.34	3.9	1.77	3.07	4.61	4.2	4.67	3.37	2.6
ab	42.73	49.5	32.58	36.72	39.43	43.58	45.1	31.05	24.79	21.15
an	42.48	33.07	33.13	42.55	41.53	44.42	43.33	28.12	23.34	19.05
ne										
crn	0.15	1.08		0.45	0.23	0.41	0.59			
di			1.27					9.04	6.13	9.75
hy	2.96	1.3	22.69	14.38	8.04	1.74	1.08	16.53	14.74	24.87
ol		2.09							14.29	5.04
ilm	1.8	0.89	2.34	0.59	0.21	0.21	0.15	6.53	6.38	9.23
ap	0.42	0.25	0.3	0.09	0.07	0.05	0.05	0.58	3.54	5.03
Gabbroic components										
Pl	0.97	0.96	0.73	0.85	0.91	0.98	0.99	0.70	0.58	0.50
Ol	0.00	0.02	0.00	0.00	0.00	0.00	0.00	0.00	0.17	0.06
Px	0.03	0.02	0.27	0.15	0.09	0.02	0.01	0.30	0.25	0.43

Appendix 3 cont.: CIPW norms for Paleoproterozoic and/or Archean country rocks and Mesoproterozoic plutonic rocks.

Sample	02-17-20a	01-30-2b	00-2-4	01-32-9a	01-32-9b	00-29-12b	01-31-8	00-25-9d	01-34-1	01-28-5b
Unit	TAl	SUb	SUi	SA	SA	SP	SP	SHlb	SHub	SHub
Rock type	defm bt gn	defm gn	alt lgn	cpx ln	defm ox gn	Fe-g	Fe-g	defm gn	ox gn	gn
qtz		1.23		0.75						
or	2.07	1.3	2.07	1.48	1	3.37	3.13	0.53	1.06	1.3
ab	18.45	27.92	32.58	29.11	22.93	30.29	29.02	20.39	17.94	20.65
an	22.42	33.08	44.03	41.58	29.98	21.54	19.9	29	22.97	29.49
ne										
crn										
di	24.67	3.37	5.82	0.63	15.89	9.08	11.07	17.2	13.42	11.43
hy	12.45	29.06	12.57	24.17	3.29	24.97	25.42	16.2	13.75	23.54
ol	14.39		1.03		18.53	0.86	0.33	11.56	14.41	7.75
ilm	2.75	1.58	0.55	0.4	6.27	5.34	5.36	2.11	9.19	2.83
ap	0.28	0.51	0.02	0.02	0.05	1.95	2.13	0.02	4.66	0.58
Gabbroic components										
Pl	0.44	0.65	0.80	0.74	0.58	0.60	0.57	0.52	0.50	0.54
Ol	0.16	0.00	0.01	0.00	0.20	0.01	0.00	0.12	0.17	0.08
Px	0.40	0.35	0.19	0.26	0.21	0.39	0.43	0.35	0.33	0.38

Appendix 3 cont.: CIPW norms for Paleoproterozoic and/or Archean country rocks and Mesoproterozoic plutonic rocks.

Sample	01-24-14	00-22-11	01-31-2	01-33-31	02-30-3a	02-36-10	02-30-1	02-28-2a	02-28-12	02-30-3b
Unit	SHlb	SHlb	SHui	SHui	KA	KA xen	KAd	KAd	KAd	KSi
Rock type	cpx ln	cpx ln	ox lgn	ox gn	alt ox lgn	alt ln	Fe-di	Fe-di	Fe-di	ln
qtz		1.27	0.84	1.58	1.76					1.66
or	2.01	2.36	2.36	2.6	2.54	1.48	6.26	2.66	7.98	2.42
ab	32.07	28.69	32.66	29.28	39.01	27.08	28.18	29.87	30.8	35.29
an	47.03	41.42	44.2	36.87	42.6	43.92	15.78	23.48	17.3	44.19
ne										
crn						0.85				
di	2.54	1.19	4.32	5.35	0.5		10.75	6.83	9.67	0.39
hy	12.75	22.36	10.5	17.27	9.34	17.07	23.03	3.46	7.42	13.33
ol	0.1					7.56	2.84	16.8	15.86	
ilm	1.1	0.63	2.54	3.32	0.72	0.21	7.43	6.51	4.88	0.65
ap	0.05	0.14	0.28	0.83	0.09	0.05	2.92	4.26	1.92	0.12
Gabbroic components										
Pl	0.84	0.75	0.84	0.75	0.89	0.74	0.55	0.66	0.59	0.85
Ol	0.00	0.00	0.00	0.00	0.00	0.08	0.04	0.21	0.20	0.00
Px	0.16	0.25	0.16	0.25	0.11	0.18	0.42	0.13	0.21	0.15

Appendix 3 cont.: CIPW norms for Paleoproterozoic and/or Archean country rocks and Mesoproterozoic plutonic rocks.

Sample	01-13-21b	01-13-21a	02-25-10a	02-25-10b	02-31-8ii	02-31-8i	02-24-19a	00-5-12	01-23-13a
Unit	KSi	KSi	KSi	KSi peg	MSd	MSd	KSb	KSb	KSb
Rock type	ln	opx an	alt px an	an + gran	Fe-di	lgn lens	ltr	gn	gn
qtz	0.96	1.46	1.98	5.23	0.14	0.72			
or	1.77	2.48	3.13	3.6	2.42	2.07	1.3	2.84	0.59
ab	33	37.65	34.35	38.67	24.79	33.93	27.25	27.08	8.97
an	46.96	52.57	42.97	39.68	21.68	42.63	50.79	30.5	24.28
ne									
crn				0.72					
di	0.97	0.57	1.4		8.45	0.83	0.49	5.73	27.57
hy	13.69	2.8	12.21	8.99	29.68	16.27	5.46	30.5	15.39
ol							11.98	0.63	20.27
ilm	0.46	0.32	1.06	0.72	6.88	1.01	0.82	0.85	0.85
ap	0.05	0.05	0.16	0.37	2.62	0.32	0.16	0.05	0.02
Gabbroic components									
Pl	0.85	0.96	0.85	0.90	0.55	0.82	0.81	0.61	0.34
Ol	0.00	0.00	0.00	0.00	0.00	0.00	0.12	0.01	0.21
Px	0.15	0.04	0.15	0.10	0.45	0.18	0.06	0.38	0.45

Appendix 3 cont.: CIPW norms for Paleoproterozoic and/or Archean country rocks and Mesoproterozoic plutonic rocks.

Sample	01-23-6	02-10-12	02-25-18
Unit	KSb	KSb	KSb
Rock type	gn	defm gn	defm lgn
qtz			1.29
or	3.31	0.83	2.19
ab	25.13	21.24	35.79
an	25.26	28.29	50.02
ne			
crn			
di	12.58	17.65	0.74
hy	14.86	9.02	7.62
ol	6.88	19.36	
ilm	7.05	0.17	0.51
ap	2.27	0.09	0.07
Gabbroic components			
Pl	0.59	0.52	0.91
Ol	0.08	0.20	0.00
Px	0.32	0.28	0.09

Appendix 4

Isotope Dilution-Thermal Ionization Mass Spectrometer (ID-TIMS) analyses were performed at Memorial University of Newfoundland, Canada. Handpicked zircons were abraded and then washed in dilute nitric acid and ultra-pure acetone. Single grains of zircons were then placed into 0.35 ml Teflon vials together with 30 µl HF and a mixed ^{205}Pb-^{235}U spike. Eight of these Teflon vials were then placed in a Parr Container for 2 days at 210°C (Parrish, 1987).

After two days in the oven, the Teflon vials were cooled down and the contents were dried out on a hot plate. Once dried, 10 drops of HCl 3.1N was added to each vial. All the vials were put back inside the Parr Container and left in the oven at 210 °C overnight. The vials were then cooled down. Separation of Pb and U was performed with micro-columns and ion-exchange resin AG1X8 following the technique described in Dubé et al. (1996).